An integrated molecular cell biology and agent-based simulation approach to dissecting microRNA regulatory networks

German Leonov

PhD

University of York

Biology

September 2015

Abstract

Discoveries in the world of non-coding RNAs made during the turn of the last century challenge the flow of information described by Francis Crick in his description of the *central dogma of molecular biology* – the information encoded by the DNA no longer solely requires a protein intermediate to control the fate of a living cell. Dozens of mechanisms involving RNA-protein, protein-protein and RNA-RNA interactions have been described that govern regulation of information controlled at the level of replication, transcription and translation. The networks that emerge from these interactions support unique, context dependent regulation of gene expression, are dynamic in nature, and provide multiple layers of complexity underlying the biological system. Advancements in molecular biology allow researchers to dissect complex interactions between components of gene regulatory networks, interpretation of which is only feasible using automated computer-aided approaches. Inevitably, uncovering novel mechanisms involved in biological systems benefits from an integrated approach between experimental biology and computational modelling.

This thesis investigates the function of a group of non-coding RNAs, microRNAs, that regulate gene expression at a post-transcriptional level. Firstly, Argonaute-2, the crucial effector of microRNA function, is revealed as a novel direct target of microRNA-132. The functional role of this regulation is explored in primary lymphatic endothelial cells during cell activation. Secondly, the regulation of two microRNA-132 targets – Argonaute-2, required for microRNA-mediated gene regulation, and E1A-associated Protein p300, necessary for microRNA-132 transcription – are incorporated into an agent-based model. Following the CoSMoS process, a rigorous methodology for model development, the documented regulatory network is captured in a model that is able to simulate the expected behaviour of the *real-world* problem domain. Finally, using the gathered data on microRNA-132 regulation and cell activation, the model is used to evaluate the domain knowledge of microRNA-mediated gene silencing *in silico*, proposing testable hypothesis for *in vitro* experimentation.

List of Contents

Abstract **2**

List of Contents **3**

List of Tables **9**

List of Figures **11**

Acknowledgements **16**

Declaration **17**

1 Introduction **18**

1.1 Motivation 18

1.2 Mammalian miRNA biology 20

1.2.1 miRNA biogenesis 20

1.2.1.1 Transcriptional regulation of miRNAs 21

1.2.1.2 Nuclear processing 22

1.2.1.3 Transport 22

1.2.1.4 Cytoplasmic processing 23

1.2.2 miRNA-mediated gene silencing 23

1.2.2.1 AGO-family proteins 24

1.2.2.2 RISC formation 28

1.2.2.3 Processing bodies 28
1.2.2.4 Translational repression and target degradation 29
1.2.3 miRNA-mediated regulation 30
1.2.4 miRNA networks 32
1.2.5 miRNAs in LECs 34
1.2.5.1 miRNAs important for endothelial cell function 34
1.2.5.2 miRNAs expressed in LECs involved in tumour growth . 35
1.2.5.3 miR-132 biology 35
1.3 Modelling and Simulation 38
1.3.1 Mathematical modelling 38
1.3.2 Agent-based modelling 39
1.3.3 Modelling miRNA regulatory networks 40
1.3.4 Modelling process 41
1.4 Thesis aim 43

2 Materials and methods **44**

2.1 Cell and molecular biology approaches 44
2.1.1 Cell culture 44
2.1.1.1 LECs 44
2.1.1.2 HeLa cell line 45
2.1.2 Treatments 46
2.1.2.1 PMA 46
2.1.2.2 siRNA, mimics and inhibitors transfections 46
2.1.2.3 Lentiviral transductions 47
2.1.3 Molecular biology techniques 48
2.1.3.1 Tissue homogenisation 48
2.1.3.2 RNA extraction 48
2.1.3.3 cDNA synthesis 49

2.1.3.4 Real-time qRT-PCR 50
2.1.3.5 Protein extraction and quantification 52
2.1.3.6 Western blotting 53
2.1.4 Cell viability assay 57
2.1.5 Statistical analysis of biological data 57
2.2 Modelling and simulation of biological systems 58
2.2.1 Biological domain and simulation specification 58
2.2.1.1 Model specification 58
2.2.1.2 Notation in *state* and *activity diagrams* 60
2.2.1.3 Justification and model validation 61
2.2.1.4 Parametrisation 61
2.2.2 Model development 62
2.2.2.1 Modelling system 62
2.2.2.2 Version control and distribution 62
2.2.2.3 Code profiling and testing 63
2.2.3 Statistical analysis and calibration 64
2.2.3.1 Simulation output 64
2.2.3.2 Aleatory uncertainty analysis 65
2.2.3.3 Calibration 65
2.2.3.4 Single parameter exploration 66
2.2.3.5 Global exploration of parameter space 67

3 Direct regulation of AGO2 by miR-132 – *in vitro* and *ex vivo* investigation 68
3.1 miRNA target prediction 68
3.2 miR-132/AGO2 binding and silencing activity 72
3.3 miR-132 overexpression 74
3.3.1 pri-miR-132 lentiviral transduction 74
3.3.2 miRIDIAN mimics transfection 75

3.4 Endogenous miR-132 activation 79
3.5 miR-132 inhibition in activated LECs 82
3.5.1 miRIDIAN inhibitors transfection 82
3.5.2 LNA-based inhibitors transfection 84
3.6 Effect of AGO2 regulation 88
3.6.1 siRNA-mediated knockdown 88
3.6.2 AGO2^{-UTR} lentiviral overexpression in activated LECs 90
3.6.3 AGO2^{-UTR} lentiviral overexpression in miR-132 overexpressing LECs 95
3.7 TIE2 regulation in activated LECs 99
3.7.1 miR-132 overexpression affects TIE2 99
3.7.2 miR-132 inhibition effect on TIE2 101
3.7.3 TIE2 rescue by AGO2^{-UTR} overexpression 103
3.8 LEC viability during miR-132/AGO2 regulation 105
3.9 miR-132 -/- knockout mice 107
3.10 Summary and Discussion 110
3.10.1 Role for miR-132 mediated suppression of AGO2 111
3.10.2 Loss of function experiments using antisense miRNAs 112
3.10.3 miR-132 activity controlled by its targets AGO2 and EP300 112
3.10.4 AGO2 loss, not upregulation, affects miRNA abundance 115
3.10.5 TIE2 expression regulated by AGO2 abundance? 116

4 Development of an *in silico* model of miR-132 mediated silencing 117
4.1 Domain model 118
4.2 Platform model 135
4.2.1 Supporting evidence 149
4.2.2 Parametrisation 152
4.3 Executable model 155
4.4 Calibration 156

4.4.1 Aleatory uncertainty analysis 156
4.4.2 Single parameter perturbation 159
4.4.3 Global analysis of parameter space 162
4.5 Baseline model 166
4.6 Discussion – the miR-132 silencing model development 170
4.6.1 Reflecting on the development process 170
4.6.2 Reflecting on Repast Simphony 171
4.6.3 Reflecting on the baseline model 173

5 Explorative simulation of miR-132 activity and function *in silico* 174
5.1 PMA activation 175
5.2 Experimentation *in silico* during PMA-activity 179
5.2.1 Baseline LEC stimulation 179
5.2.2 miR-132 enhanced transcription 183
5.2.3 Non-regulated *AGO2* mRNA 185
5.2.4 Non-regulated *EP300* mRNA 187
5.3 Discussion 189
5.3.1 Simulating miR-132 expression in response to PMA treatment . . . 189
5.3.2 miR-132 controlled recovery of EP300 activity 190
5.3.3 AGO2 regulation by miR-132 during cell activation 191

6 Discussion and future work 194
6.1 Summary 194
6.2 AGO2 expression is necessary, but not sufficient, for the prolonged expression of miR-132 197
6.3 Fine-tuning confers robustness to miRNA function, and consequently to gene expression 200
6.4 AGO2 loading during LEC activation 202

6.5 Reflection on the development of an agent-based model development on an intracellular scale integrated with experimental data acquisition 204
6.6 Expansion of the miRNA-regulatory network 205
6.7 Conclusion 207

Appendices **208**

Appendix A Biological data **209**
A.1 EP300 antibody optimisation 210
A.2 HDLEC morphology 212
A.3 Expression by experimental replicate 214

Appendix B Model development **216**
B.1 Class inheritance 216

Appendix C Simulation results **218**
C.1 Visual model output of the miR-132 silencing model 219
C.2 RISC loading – baseline 221
C.3 RISC loading – during enhanced miR-132 expression 222
C.4 RISC loading – during enhanced miR-132 expression with a non-regulated *AGO2* mRNA 223
C.5 RISC loading – during enhanced miR-132 expression with a non-regulated *EP300* mRNA 224
C.6 Two-sample Kolmogorov-Smirnov tests 225

Abbreviations **227**

References **231**

List of Tables

2.1 Transfected nucleic acid products and used concentrations. 46

2.2 Real-time qRT-PCR primers and assays. 51

2.3 Antibodies used for western blot detections. 56

3.1 Predicted miR-132 targets using the EIMMO prediction analysis tool showing enriched GOs 69

3.2 RBPs predicted by multiple online algorithms as targets of miR-132. 70

4.1 Evidence supporting the domain state diagram for Ribosome 123

4.2 Evidence supporting the domain state diagram for Promoter 123

4.3 Evidence supporting the domain state diagram for *AGO2* mRNA 125

4.4 Evidence supporting the domain state diagram for *EP300* mRNA 125

4.5 Evidence supporting the domain state diagram for miR-132 127

4.6 Evidence supporting the domain state diagram for miR-221 127

4.7 Evidence supporting the domain state diagram for AGO2 protein 129

4.8 Evidence supporting the domain state diagram for EP300 protein 131

4.9 Evidence supporting the domain state diagram for CREB protein 131

4.10 Summary of changes made from the domain to the platform model. 136

4.11 Model parameters (part I) 153

4.12 Model parameters (part II) 154

4.13 Global parameter sensitivity analysis (part I) 164

4.14 Global parameter sensitivity analysis (part II) 165

5.1 Variable values b and η used for generating the profile of the PMA activation functions for each of the affected parameters. 177

C.1 K-S test – LEC baseline compared to enhanced baseline 225

C.2 K-S test – Enhanced baseline with AGO2 compared to AGO2^{-UTR} 226

C.3 K-S test – Enhanced baseline with EP300 compared to EP300^{-UTR} 226

List of Figures

1.1 Canonical pathway of miRNA biogenesis 21

1.2 Alignment of human AGO1-4 26

1.3 Human AGO1 and AGO2 crystal structures 27

1.4 Suggested model of miRNA-mediated silencing of target mRNA 30

2.1 *LYVE1* mRNA levels in HFFs compared to LECs 45

2.2 Model development cycle as defined by the CoSMoS process (Andrews et al., 2010a). 59

2.3 Generalised work flow for manual model calibration 64

3.1 miR-132 target screen of RBPs 69

3.2 AGO2 sequence alignment with miR-132. 71

3.3 Luciferase assay of miR-132 binding to the AGO2 3'UTR in HeLas 73

3.4 Silencing activity during miR-132 overexpression in HeLas 73

3.5 Lentiviral overexpression of pri-miR-132 in LECs 74

3.6 miR-132 mimics overexpression in HeLas 75

3.7 Titration of miR-132 mimics in LECs 76

3.8 Overexpression of miR-132 mimics in LECs - miR-132, pri-miR-126, miR-126, miR-221, *AGO2* mRNA and protein, RASA1 and EP300 protein . . . 78

3.9 PMA titration - miR-132 time course in LECs 79

3.10 PMA-induced CREB phosphorylation time course in LECs 80

3.11 Effect of PMA on mature and primary miR-132, *AGO2* and *EP300* mRNA, and AGO2 protein in LECs 81
3.12 Inhibition of miR-132 in PMA activated LECs using miRIDIAN inhibitors - miR-132, *AGO2* and *EP300* mRNA, and AGO2 protein 83
3.13 Inhibition of miR-132 in PMA activated LECs using LNA-based inhibitors - miR-132, *AGO2* mRNA, AGO2 and RASA1 protein 86
3.14 Inhibition of miR-132 in PMA activated LECs using LNA-based inhibitors - miR-126, miR-146a, miR-221 and pri-miR-126 87
3.15 Knockdown of AGO2 in LECs - miR-132, miR-126, miR-221, *AGO2* mRNA and protein, RASA1 protein 89
3.16 Titration of AGO2 lentiviral overexpression in LECs 90
3.17 AGO2^{-UTR} lentiviral overexpression in activated LECs - *AGO2* mRNA and protein, RASA1 protein 91
3.18 AGO2^{-UTR} lentiviral overexpression in activated LECs - miR-132, miR-126, miR-146a, miR-221 92
3.19 AGO2^{-UTR} lentiviral overexpression in activated LECs - *ANG2*, *IL6*, *SPRED1*, *TIE2*, *VEGFR1*, *VEGFR3* mRNA 94
3.20 AGO2^{-UTR} lentiviral overexpression in miR-132 overexpressing LECs - *AGO2* and *SPRED1* mRNA, AGO2 and RASA1 protein 96
3.21 AGO2^{-UTR} lentiviral overexpression in miR-132 overexpressing LECs - miR-132, miR-126, miR-221 98
3.22 Overexpression of miR-132 mimics in LECs - *TIE2* mRNA and protein . . 100
3.23 Inhibition of miR-132 in PMA activated LECs using LNA-based inhibitors - *TIE2* mRNA and protein 102
3.24 AGO2^{-UTR} lentiviral overexpression in miR-132 overexpressing LECs and PMA activated LECs - TIE2 protein 104
3.25 LEC viability (MTT assays) during miR-132/AGO2 regulation 106

3.26 Expression of miR-132, AGO2 mRNA and protein, and RASA1 protein in wild type (C57BL/6) and miR-132 -/- KO mice 108
3.27 Immunoblots comparing C57BL/6 and miR-132 -/- KO mouse brain samples - AGO2 protein and different loading controls 109

4.1 Domain model - expected behaviour diagram 120
4.2 Domain model - state diagrams - ribosome, promoter 122
4.3 Domain model - state diagrams - *AGO2* mRNA, *EP300* mRNA 124
4.4 Domain model - state diagrams - miR-132, miR-221 126
4.5 Domain model - state diagrams - AGO2 protein 128
4.6 Domain model - state diagrams - EP300 protein, CREB protein 130
4.7 Domain model - combined activity diagram - part 1 132
4.8 Domain model - combined activity diagram - part 2 133
4.9 Domain model - combined activity diagram - part 3 134
4.10 Platform model - state diagrams - ribosome, promoter 138
4.11 Platform model - state diagrams - *AGO2* mRNA, *EP300* mRNA, miR-132, miR-221 139
4.12 Platform model - state diagrams - AGO2 protein 140
4.13 Platform model - state diagrams - EP300 protein, CREB protein 141
4.14 Platform model - activity diagrams - ribosome 142
4.15 Platform model - activity diagrams - promoter 143
4.16 Platform model - activity diagrams - *AGO2* mRNA, *EP300* mRNA 144
4.17 Platform model - activity diagrams - miR-132, miR-221 145
4.18 Platform model - activity diagrams - AGO2 protein 146
4.19 Platform model - activity diagrams - EP300 protein 147
4.20 Platform model - activity diagrams - CREB protein 148
4.21 Aleatory analysis of the miR-132 silencing model 158
4.22 Example OAT analysis graph - the effect of altering pCREB-EP300 availability 161

4.23 OAT analysis - abundance of miR-132 and miR-221 and their loading onto AGO2 when altering pCREB-EP300 complex availability 162
4.24 Baseline and miR-132 enhanced expression effect on the abundance of miR-132, miR-221 and RISC loading of miRNAs 168
4.25 Baseline and miR-132 enhanced expression effect on the expression of AGO2 and EP300 mRNA and protein 169

5.1 PMA treatment activation functions 178
5.2 Simulation of miR-132 mediated silencing of AGO2 and EP300 in LECs during PMA-activation 182
5.3 Simulation of miR-132 mediated silencing of AGO2 and EP300 in LECs during PMA-activation with enhanced miR-132 transcription activity 184
5.4 Simulation of miR-132 mediated silencing of AGO2^{-UTR} and EP300 in LECs during PMA-activation with enhanced miR-132 transcription activity 186
5.5 Simulation of miR-132 mediated silencing of EP300^{-UTR} and EP300 in LECs during PMA-activation with enhanced miR-132 transcription activity 188

6.1 Summary – AGO2 stabilises miRNA expression during LEC activation . . 199

A.1 EP300 antibody optimisation – immunoblot 211
A.2 LECs morphology during PMA activation and miR-132 inhibition 213
A.3 Inhibition of miR-132 in PMA activated LECs using LNA-based inhibitors - AGO2 protein expression by individual replicates 214
A.4 AGO2^{-UTR} lentiviral overexpression in miR-132 overexpressing LECs - AGO2 protein expression by individual replicates 215

B.1 Class inheritance diagram of the miR-132 model 217

C.1 Visual simulation output of the miR-132 silencing model 220

C.2 RISC loading distribution during miR-132 mediated silencing of AGO2 and EP300 in PMA-activated LECs 221

C.3 RISC loading distribution during miR-132 mediated silencing of AGO2 and EP300 in PMA-activated LECs with enhanced miR-132 transcriptional activity 222

C.4 RISC loading distribution during miR-132 mediated silencing of AGO2^{-UTR} and EP300 in PMA-activated LECs with enhanced miR-132 transcriptional activity 223

C.5 RISC loading distribution during miR-132 mediated silencing of AGO2 and EP300^{-UTR} in PMA-activated LECs with enhanced miR-132 transcriptional activity 224

Acknowledgements

Having completed a Bachelor's degree in Molecular Biology, I was presented with the opportunity to apply for a highly interdisciplinary programme, that promised the young researchers to undertake a combination of any scientific fields. Following my ambition to work at the cutting-edge of science, I was determined to challenge myself to take on an interdisciplinary project that combined hands-on experimental biology with computational modelling. The conducted work for this thesis was made possible by the underlying support-network of people, to whom I would like to express my sincere gratitude:

To my supervisor *Dimitris Lagos* and co-supervisor *Jon Timmis*, for the opportunity to take on this captivating, diverse and challenging project, and providing helpful and insightful observations in support of my work.

To the former and current members of the *York RNA Group* and the *York Computational Immunology Lab*, with whom I have had the pleasure to work with.

To the colleagues from the York Center for Complex Systems Analysis, and with special thanks to *Reidun Twarock*, who motivated and inspired my interest in becoming an interdisciplinary scientist.

To *James Alexander Ceran Geraets*, for being an outstanding friend and a perceptive conversationalist and researcher, throughout our time in York.

To my parents, *Aleksandr* and *Ljudmila*, for their unconditional support of my life, namely, educational choices, all the way from the other side of Europe.

To my son, *Feliks Patrick Tiberius*, born in February 2015, keeping me awake on countless occasions, most likely to ensure that there was plenty of time in the day, or night, to think about my thesis.

To my wife, *Hannah Elizabeth Laura Leonova*, for her love, patience and support during the difficult and the *more* difficult periods over the lifetime of this degree; notably, to *Sue* and *Pat*, Hannah's parents, who provided support day in and day out, to allow me to carry this work past the finish line.

Declaration

I declare that this thesis is a presentation of original work and I am the sole author. This work has not previously been presented for an award at this, or any other, University. All sources are acknowledged as References.

Findings contained in Chapter 3 have been published by **Leonov et al. (2015)** subsequent to the submission of the thesis for examination.

Chapter 1

Introduction

1.1 Motivation

Since their discovery two decades ago by Lee et al. (1993) and recognition as a class of tiny regulatory RNAs, termed microRNAs (miRNAs) (Lagos-Quintana et al., 2001; Lau et al., 2001; Lee and Ambros, 2001), the miRNA field has been rapidly expanding, with ~2500 sequences documented in the publicly available miRNA database (Kozomara and Griffiths-Jones, 2014). Their involvement in nearly all aspects of cell biology has generated a more dynamic understanding of gene regulation. Although many pathways of miRNA-gene target regulatory models have been described, a large proportion of research is still needed to establish context-dependent miRNA biogenesis and function. The field of miRNA biology has benefited through the use of several computational tools, which aid with the identification of potential miRNA target genes. Together with advancements in sequencing technologies and single-cell *-omics* analysis approaches, the general mechanisms of miRNA-mediated gene silencing are being established.

It has been shown that the effect of a single miRNA in miRNA-mediated gene regulation is commonly mild. However, a single miRNA can alter the expression of multiple target genes. Moreover, several miRNAs can target the same target gene, resulting in a combinatorial effect on gene expression regulation. These interactions form complex networks that

during regular cell function confer robustness to gene expression programmes (Ebert and Sharp, 2012; Nazarov et al., 2013; Stark et al., 2005). The exact miRNA expression pattern varies between cell types and even between different cell activation states. This gives rise to context-specific gene regulatory networks, which modulate gene expression programmes in a spatially and temporally resolved manner.

The traditional approach to the discovery of novel miRNA targets involves the investigation of predicted targets using computational tools, the characterisation of the interaction of the miRNA and the targeted region of the gene, and typically an investigation into the functional impact of the interaction described in a model biological system. Although some temporal information is gathered in these experiments, the cost and limitations of molecular biology techniques make it challenging to collect high resolution continuous data that would give a comprehensive understanding of the dynamics of miRNA-mediated silencing.

Just over a decade ago, Kitano (2002) described the need for complex system approaches for understanding biological systems: whilst individual studies focus on understanding key functionalities of single biological components, the integration of vast amounts of high-throughput data that supports a network of regulatory functions for those biological components are, in fact, highly dynamic and intrinsically complex. The discovery of regulatory patterns governing biological processes and their constituents, the study of system dynamics, and *in silico* predictions through simulating biological systems can therefore be made possible through a combined approach between computational modelling and wet-lab experimental approaches. Following these principles, we employ the traditional approach to novel miRNA target discovery followed by an in-depth investigation of the regulatory mechanism by a miRNA on its targets. Through the use of modelling and simulation, we intend to demonstrate that the development of a computational model capturing the miRNA-target interaction furthers our understanding of the biological system. Notably, the information gained from the simulation suggests further experiments to explain phenomena revealed through simulating a biological system.

1.2 Mammalian miRNA biology

MiRNAs are a class of highly-conserved short non-coding RNAs that regulate gene expression at the post-transcriptional level (Bartel, 2009). The ~23 nucleotides long miRNAs are associated with Argonaute (AGO) family proteins. Nucleotides 2-7 of the 5' region on a miRNA, known as the 'seed' site, determines the specificity for the mRNA transcript, commonly located at the 3'untranslated region (UTR). Following target recognition and binding, AGO proteins recruit other factors in order to silence the target gene expression (Huntzinger and Izaurralde, 2011). There are characteristic differences in the biogenesis, evolutionary origin and structure of mammalian and plant miRNAs (Axtell et al., 2011), with only the mammalian miRNA biology being covered in this chapter.

1.2.1 miRNA biogenesis

With over a half of the protein-coding genome subject to miRNA regulation (Friedman et al., 2009), dysfunction in miRNA-mediated biogenesis and silencing components results in embryonic developmental abnormalities and lethality (Bernstein et al., 2003; Chong et al., 2010; Liu et al., 2004; Wang et al., 2007), indicating an essential role for miRNAs in cell biology. This section describes the biogenesis (the canonical miRNA pathway summarised in Figure 1.1) and function of miRNAs, the involved functional complexes and introduces the relevant miRNAs investigated in this thesis.

The biogenesis of the majority of miRNAs follows a canonical pathway, although non-canonical processing pathways have been identified (Babiarz et al., 2008; Cheloufi et al., 2010; Chong et al., 2010). The canonical pathway involves primary miRNA (pri-miR) transcription by RNA polymerase II (Lee et al., 2004) or III (Borchert et al., 2006), followed by two main processing steps: first, the pri-miR is processed by the Microprocessor complex in the nucleus comprised of DROSHA and DiGeorge Syndrome Critical Region 8 (DGCR8), and the produced precursor miRNA (pre-miR) is cleaved in the cytoplasm by the

DICER-TAR RNA Binding Protein (TRBP) complex into a short RNA duplex, ready for AGO loading. The transcription, processing, transport and function of miRNAs are subject to context-dependent regulation.

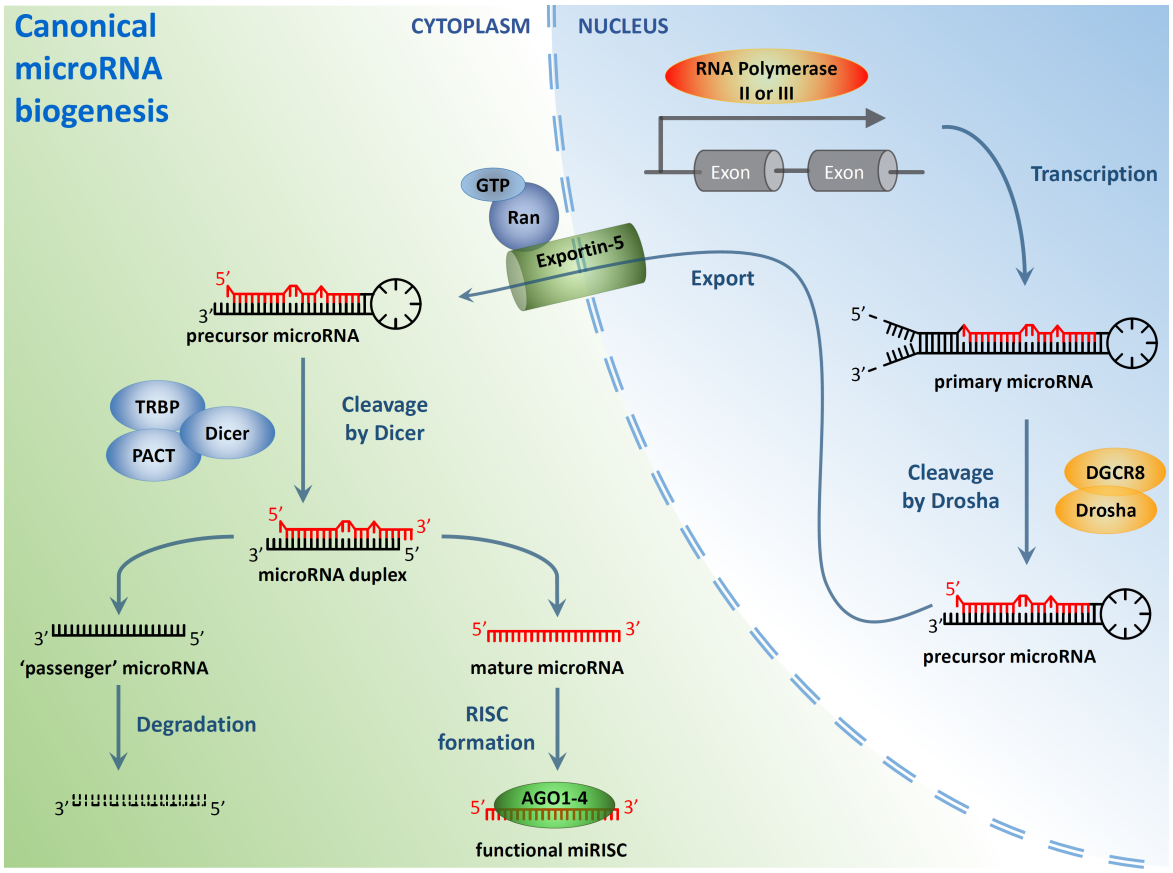

Figure 1.1: Overview of the canonical pathway of miRNA biogenesis.

1.2.1.1 Transcriptional regulation of miRNAs

miRNAs have been found both in intergenic and intragenic regions of the genome. The transcriptional start sites (TSSs) and the RNA polymerase responsible for the transcription have been reported for a fraction of miRNAs (Ozsolak et al., 2008). RNA polymerase II is suggested to be the predominant transcriber of the majority of miRNAs (Lee et al., 2004), but the exact TSS positions for many miRNAs remains a complex issue with many features of miRNA promoters being identified (Corcoran et al., 2009). Some miRNAs are transcribed together with other miRNAs as part of a single polycistronic unit (Lee et al., 2002; Altuvia

et al., 2005). Such miRNAs belong to the same cluster and are produced together (Nohata et al., 2012; Remenyi et al., 2010), but can be post-transcriptionally regulated. The produced pri-miRs are from several hundred base pairs to several kilobases in length (Saini et al., 2007).

1.2.1.2 Nuclear processing

The pri-miR is typically processed by the DROSHA-DGCR8 Microprocessor complex into a short-lived intermediate precursor, pre-miR. The pre-miR is ~65 nucleotides in length, consisting of a single terminal loop structure with 5' and 3' overhangs. DROSHA is a type III ribonuclease, which is able to cleave double-stranded RNAs in the nucleus (Lee et al., 2003). For efficient nuclear processing DROSHA is translocated to the nucleus upon its activation (Tang et al., 2011). DGCR8 has been shown to be essential for DROSHA-mediated miRNA processing (Gregory et al., 2004), and both proteins are involved in an autoregulatory loop with each other to control the Microprocessor activity in mammals (Han et al., 2004, 2009). Interestingly, not all miRNAs require nuclear processing by DROSHA: several groups of miRNAs have been shown to be products of intron splicing that produce < 500 nucleotide long hairpins, known as "mirtrons", with shorter primary transcripts, not suitable for DROSHA processing (Okamura et al., 2007; Ruby et al., 2007; Babiarz et al., 2008); instead, they are processed as a result of splicing into DICER compatible substrates.

1.2.1.3 Transport

The pre-miR is exported from the nucleus by Exportin 5 (EXP5) in a guanosine triphosphate (GTP)-dependent manner (Bohnsack et al., 2004). Upon export, the EXP5-RanGTP complex is hydrolysed allowing the release of the double-stranded pre-miR and causing the disassembly of the EXP5-RanGTP nucleopore complex (Okada et al., 2009). A non-canonical miRNA has been shown to be exported via an alternative route by Exportin 1 (EXP1) that recognises the 5' m^7G-cap on a pre-miR (Xie et al., 2013).

1.2.1.4 Cytoplasmic processing

The exported pre-miR is recognised by DICER, another type III ribonuclease resident in the cytoplasm. DICER processing requires the recognition of the terminal loop of the pre-miR (Tsutsumi et al., 2011). The result of DICER processing is a miRNA duplex with 2-nucleotide 3' overhangs, which in humans is loaded into AGO-family proteins without preference (Siomi and Siomi, 2008; Su et al., 2009). Only one strand is selected during AGO-loading, termed as the *mature* strand, whereas the other strand is rapidly degraded (*passenger* strand, commonly marked with an asterisk after the miRNA name).

The human *DICER1* mRNA is a target of the *let-7* miRNA family and is subject to autoregulation due to DICER's involvement in miRNA processing (Forman et al., 2008; Tokumaru et al., 2008). Other genes, such as *LIN28* are targeted by the *let-7* miRNAs, where LIN28 associates with the terminal loop of the pre-miR and prevents DICER-mediated processing (Heo et al., 2008; Newman et al., 2008). Other proteins involved in pre-miR processing have also been identified, such as TRBP and Protein Activator of PKR (PACT). Both of the aforementioned proteins associate with DICER and have been shown to regulate pre-miR binding specificity and processing (Lee and Doudna, 2012; Lee et al., 2013). TRBP has been shown to be actively regulated by phosphorylation at S142 and S152 (Paroo et al., 2009; Nakamura et al., 2015), whilst PACT has been shown to be regulated at a transcriptional level by Specificity Protein 1 (SP1) (Fasciano et al., 2007).

Alternative pathways that skip DICER-processing have been suggested in humans, where DICER is unable to recognise a shorter miRNA precursor (Cifuentes et al., 2010). Instead, AGO2 associates with the pre-miR, and processes and cleaves the pre-miR into the mature miRNA with the aid of a poly-A specific ribonuclease (Yoda et al., 2013).

1.2.2 miRNA-mediated gene silencing

Processed mature miRNAs are loaded into AGO to form the RNA-induced silencing complex (RISC). Many other proteins are involved in the formation, stabilisation and the func-

tion of the RISC, with AGO playing a key role in small RNA-mediated gene silencing.

1.2.2.1 AGO-family proteins

There are four AGO family members in the mammalian genome, with *AGO2* located on the human chromosome 8q24.3 and the other 3 AGOs positioned together on the human chromosome 1p34.3. The amino acid conservation between AGO1-4 is over 80% (Figure 1.2). Predominant expression of AGO1 and AGO2 has been found in HeLa and HEK 293T cells (Meister et al., 2004; Petri et al., 2011), with AGO3 and AGO4 being magnitudes lower in abundance; similar results were shown for Ago1 and Ago2 dominance over Ago3 and Ago4 in different mouse tissues (Valdmanis et al., 2012). Unlike in mammals, 10 different AGO family protein have been reported in *Arabidopsis thaliana* (Qi et al., 2005) and 2 in *Drosophila melanogaster* (Okamura et al., 2004), with distinct, context dependent roles in small RNA mediated silencing.

Over the last few years, the crystal structures of human AGO2 ($2.3\mathring{A}$) (Schirle and MacRae, 2012) and AGO1 ($2.1\mathring{A}$) (Faehnle et al., 2013) were obtained in complex with miR-20a and *let-7*, respectively (Figure 1.3), displaying many structural similarities and structural domain conservation of the 4 main regions (N-terminal, PAZ, PIWI and Mid domains). Early in the millennium, of the 4 AGOs, only AGO2 was shown to function as a catalytically active endonuclease (Liu et al., 2004; Meister et al., 2004). Moreover, recent studies have suggested, that some of the AGO family proteins have overlapping roles – AGO1 and AGO3 have been shown to play redundant role during small interfering RNA (siRNA) mediated gene suppression *in vivo*, not requiring the participation of AGO2 to suppress gene expression (Ruda et al., 2014). To much surprise, Faehnle et al. (2013) demonstrated that the cleavage activity of AGO2 can be transferred onto AGO1 and AGO3 by making chimeric proteins – domain swaps of domain N and PIWI onto AGO1, a domain swap of domain N onto AGO3, or 2 point mutations of AGO1 (alignment position 698 and 829 in Figure 1.2), indicated that slicer activity is possible in AGO1 and AGO3. This was

proposed to be due to the interplay of the AGO domains to create a catalytic center similar to that of the endogenous AGO2, mediated by the PL3 loop (Faehnle et al., 2013) (alignment position 692-699 in Figure 1.2).

AGO proteins associate with miRNAs to perform their function in silencing target genes. Due to the limited availability of AGO, miRNAs must compete for AGO-loading (Lund et al., 2011; Janas et al., 2012). Several studies demonstrated that miRNAs, through their interaction with AGO, have increased stability (Diederichs and Haber, 2007; O'Carroll et al., 2007) and can also act to maintain the abundance of AGO protein expression (Elkayam et al., 2012). The regulation of AGO2 activity has been demonstrated by post-transcriptional modifications through:

hydroxylation required for Heat Shock Protein 90 (HSP90) binding for miRNA loading onto AGO2 (Wu et al., 2011)

phosphorylation at S387 determining AGO2 localisation to processing bodies and its silencing activity (Zeng et al., 2008)

phosphorylation at Y529 reducing affinity of miRNA binding to AGO2 (Rüdel et al., 2011)

ubiquitylation targeting AGO2 for degradation (Gibbings et al., 2012)

Finally, AGO2 has been found to be upregulated by Epidermal Growth Factor Receptor (EGFR) and Mitogen-Activated Protein Kinase (MAPK) signalling (Adams et al., 2009). Therefore, many mechanisms exist in regulating AGO2 activity in mammals, with AGO2 being the predominant functional and the most studied member of the AGO family.

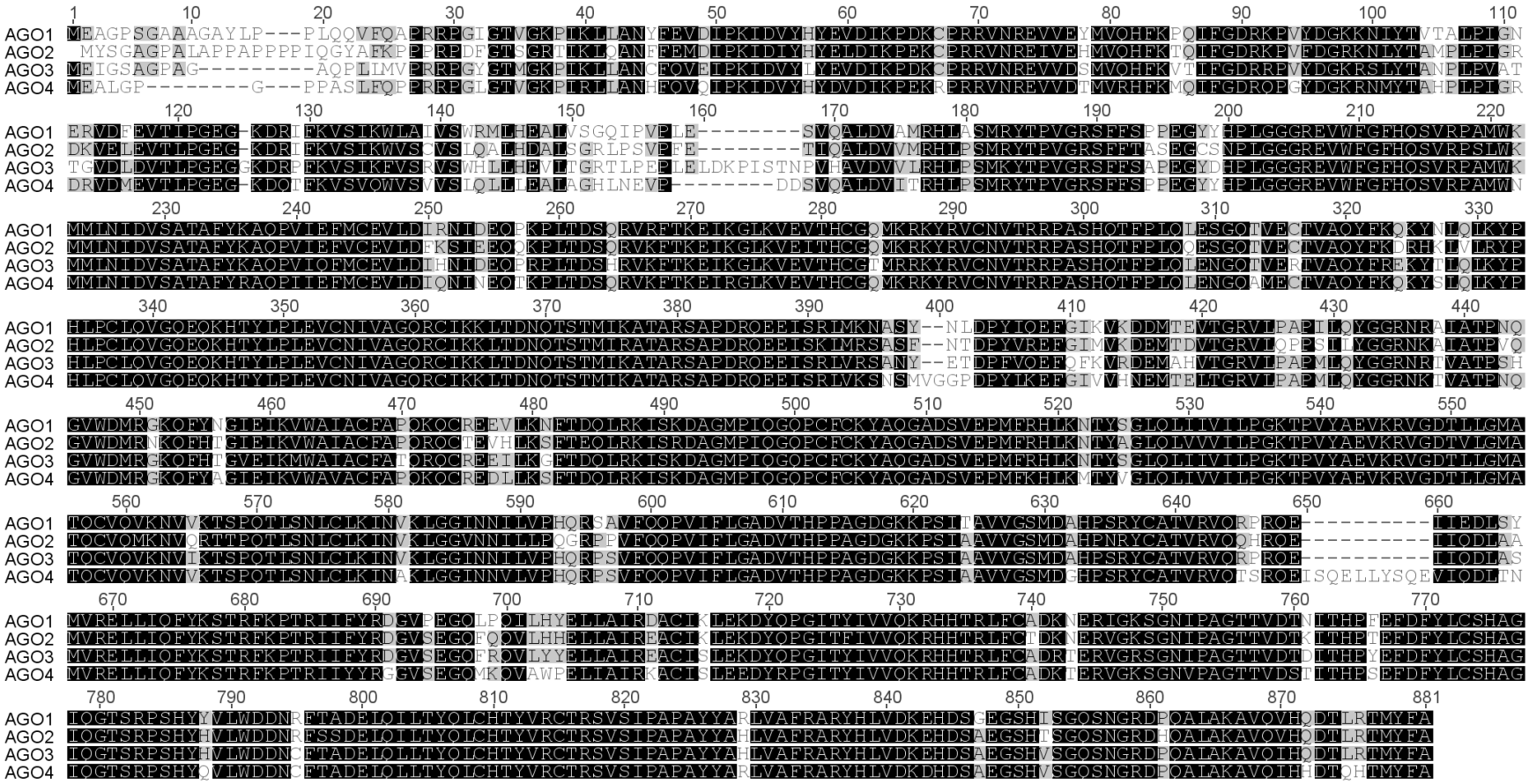

Figure 1.2: The alignment of the human AGO1-4 proteins. Highly conserved regions are highlighted in black.

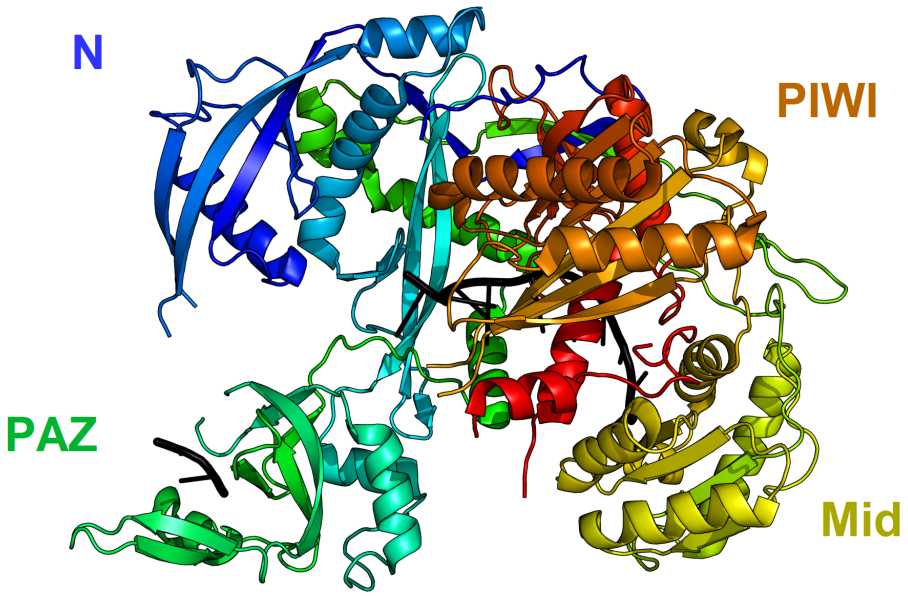

(a) human AGO1

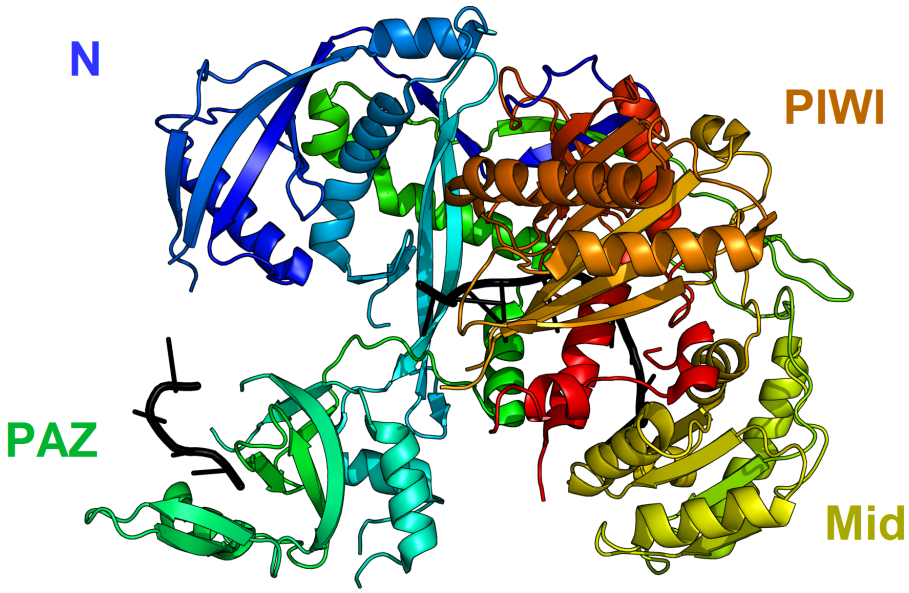

(b) human AGO2

Figure 1.3: The crystal structures of the human AGO1 protein (4KRF) with superimposed *let-7* (*black*) and AGO2 protein (4F3T) with superimposed miR-20a (*black*). The domains N, PAZ, Mid and PIWI are labelled and approximately highlighted based on the atom colour scheme.

1.2.2.2 RISC formation

The maturation of a functional RISC complex occurs in two distinguishable steps: the adenosine triphosphate (ATP)-dependent loading of the miRNA and the ATP-independent removal of the passenger strand (Kawamata et al., 2009; Yoda et al., 2010). The loading of a miRNA duplex can occur in the presence or absence of DICER (Murchison et al., 2005). The catalytically active AGO - AGO2 - has endonuclease activity and is able to cleave the passenger strand that is perfectly complimentary to the guide strand (Rand et al., 2005). However, most mammalian miRNAs contain kinks and mismatches. Moreover, other AGO proteins do not possess catalytic activity (Liu et al., 2004; Meister et al., 2004), and generally act through the more common mechanism of passenger strand removal - unwinding of the RNA duplex. Mismatches in the seed region and the 12-15 nucleotide region (Kawamata et al., 2009) promotes the unwinding of the RNA duplex and thereby promotes RISC maturation. The guide strand is typically selected favouring 5' terminus, with a preference for a uracil in position 1 of the mature miRNA sequence (Hu et al., 2009). The mature RISC requires further recruitment of inhibitory factors to the miRNA:mRNA duplex to initiate silencing.

1.2.2.3 Processing bodies

Processing bodies are cytoplasmic foci where a large concentration of translation inhibiting proteins are localised, together with mRNA decapping complexes, exonucleases and other constituents involved in miRNA-mediated decay (Kedersha and Anderson, 2007). They are dynamic entities, that have been suggested to form as a consequence of miRNA-mediated gene silencing (Eulalio et al., 2007), and can form as a result of mRNA deadenylation (Zheng et al., 2008). They are identifiable by their protein composition (Kedersha and Anderson, 2007) and are the sites for stalled and actively degraded mRNAs.

1.2.2.4 Translational repression and target degradation

The binding partner of AGO2, GW182, is essential for efficient miRNA-mediated silencing (Eulalio et al., 2008) and is localised to processing bodies (Behm-Ansmant et al., 2006). There has been mounting evidence that GW182 (3 paralogues in humans called TNRC6A-C) functions as the key adaptor protein for recruitment and binding of translation inhibitory factors, that facilitate the deadenylation of the poly-A tail (Braun et al., 2011; Piao et al., 2010) and subsequent mRNA decapping (Rehwinkel et al., 2005). As a result, it is suggested that through these mechanisms of destabilisation the mRNAs becomes a target for XRN1 driven mRNA degradation in a 5' to 3' manner. The proposed model for mRNA silencing together with the participating proteins is described in Figure 1.4. Indeed, mRNA destabilisation has been proposed to play the dominant role miRNA mediated silencing in mammals (Eichhorn et al., 2014) when the majority of target mRNA suppression is observed; moreover, mRNA destabilisation by miRNAs is reflected in their overall role to act as fine-tuners of gene regulation as measured by their mostly mild impact on the proteome (Baek et al., 2008).

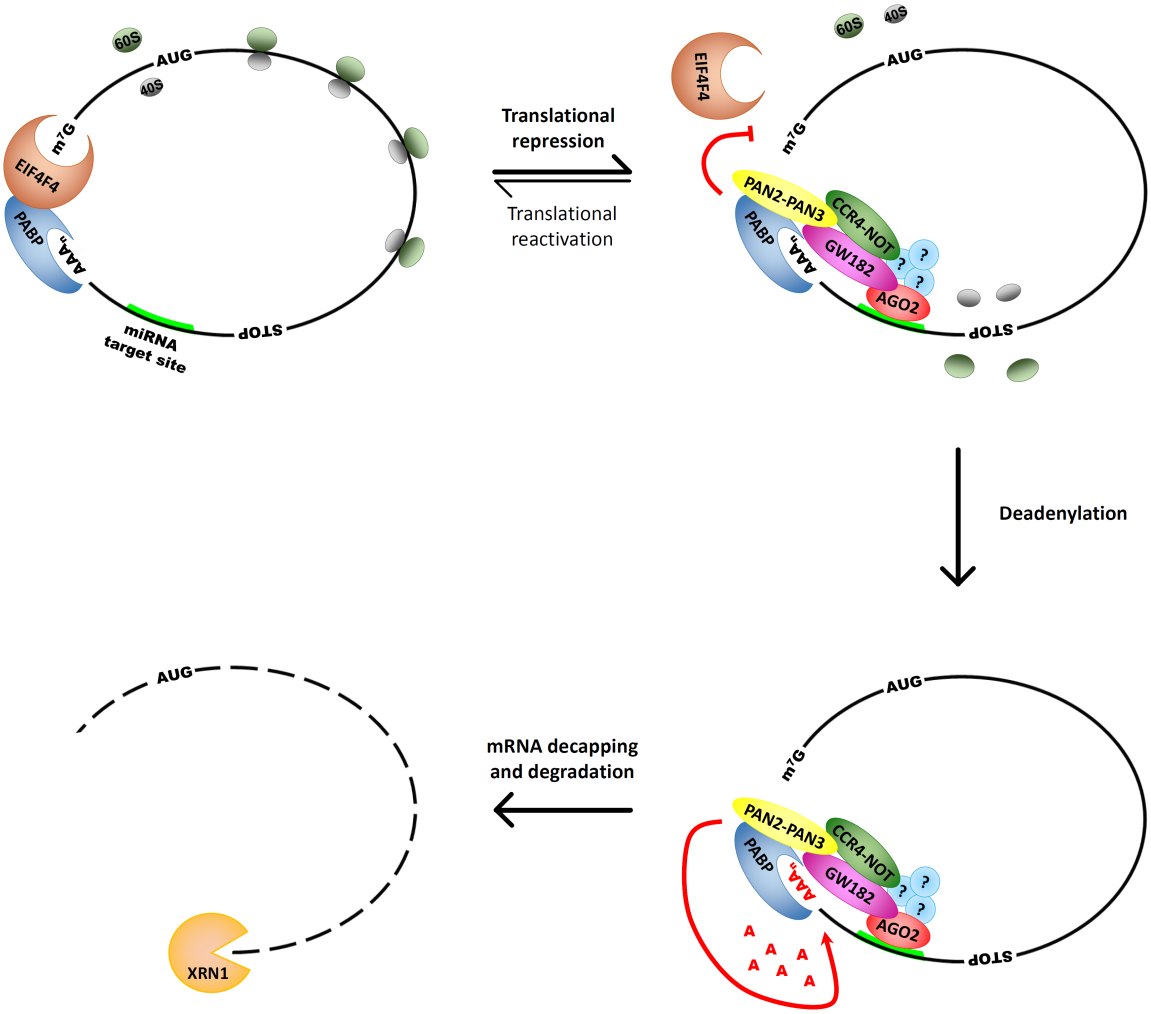

Figure 1.4: A proposed model describing mRNA silencing by a miRNA-loaded RISC. Upon miRISC binding to the miRNA target site, several adaptor proteins are recruited necessary for the recruitment of mRNA deadenylation and decapping complexes. (reviewed in (Fabian and Sonenberg, 2012)).

1.2.3 miRNA-mediated regulation

The post-transcriptional regulation of a miRNA target requires miRNA-target base-pairing and site accessibility. The conservation of a the seed region of the miRNA demonstrated over a third of human genes are targeted by miRNAs (Lewis et al., 2005; Friedman et al., 2009). The direct association of the the miRNA with the target mRNA forms a miRNA-mRNA duplex. The pairing of the seed site, nucleotides 2-8 of the miRNA, is necessary for target binding and specificity, however mismatches at the 1st nucleotide position of the miRNA is

tolerated to allow miRNA binding to the mRNA target site (Wee et al., 2012). Additional mutants of the miRNA-target pair have been studied suggesting a model for miRNA association, where the seed region binds to the target mRNA first, with the additional binding sequence at nucleotide positions 13-16 binding subsequently to increase the miRNA-mRNA complex stability (Wee et al., 2012).

Initially, approaches for identifying miRNA targets have been largely based on seed region base pairing (Rehmsmeier et al., 2004; Krek et al., 2005; Miranda et al., 2006; Betel et al., 2008). Other factors such as evolutionary conservation of the target sequence (Friedman et al., 2009; Obermayer and Levine, 2014) and target site accessibility were considered (Kertesz et al., 2007). Each of the aforementioned algorithms operate on independent web servers providing users with the option to search for predicted targets, but yield a large proportion of false-positive results (Yue et al., 2009). By comparing the expression profiles of miRNAs and their candidate mRNA targets using a microarray or sequencing data sets, MirZ (Hausser et al., 2009) offered a way for reducing some of the false-positive results. The combined analysis from multiple algorithms can be used to predict miRNA-target relations, however the accuracy of such predictions remain still limited. More accurate target identification would involve AGO2 immunoprecipitation, or a combined approach to wide-scale protein expression and miRNA and mRNA gene expression analysis in order to improve positive target discovery rates (Yue et al., 2009). The latter analysis technique – utilising chromatography separation and tandem mass spectrometry for protein quantification, sequencing of the miRNA and mRNA expression – has been used in more recent studies by Clarke et al. (2012) and Li et al. (2015). Despite the involved expense of the combined *-omics* techniques limiting the amount of studies published containing genome- and proteome-wide data sets, such data sets yield results that are directly relevant to the studied model system and are ideal for computational model development of miRNA-gene regulatory networks, with different techniques in molecular biology benefiting different stages of data analysis, target identification (Yao et al., 2015) and understanding of miRNA-mediated

gene regulation (Baek et al., 2008; Eichhorn et al., 2014).

1.2.4 miRNA networks

High-throughput data that is obtained from gene, miRNA and protein profiling experiments provides essential information for the investigation of regulatory networks involved in the studied biological system. The high quantity of gathered data from biological experiments requires a computer-aided approach to process and analyse data. As a single miRNA can negatively regulate multiple gene targets by complimentary binding, it affects multiple cellular processes at once, linking it into a wider network of processes regulated through a complex network of feed-back and feed-forward loops controlling mRNA and protein expression (Shalgi et al., 2007; Sengupta and Bandyopadhyay, 2013).

The perturbation of the miRNA-mediated silencing on gene expression has down-stream effects: the direct target of the miRNA is perturbed, followed by the effect of initial target-perturbation which may be involved in the regulation of multiple gene transcriptional events leading to a phenotypic change in cell biology. For example, miR-132 regulates the transcription of RASA1 (Anand et al., 2010), which in turn allows for the activation of Ras, triggering the endothelial cells to form vessels. In such cases, miRNAs have temporally separated effects on their targets, and simply considering direct miRNA-target impact on differential gene expression would be insufficient to identify miRNA-target regulation patterns. To address the propagation of miRNA-mediated regulation utilising genome-wide studies, a network propagation based method has been proposed (Wang et al., 2014).

On the other hand, multiple miRNAs can potentially regulate 2 distinct regions of a single mRNA target, giving rise to cooperative miRNA regulation. Through the use of modelling and simulation of two miRNA binding to a single mRNA, Schmitz et al. (2014) have proposed a model of potential miRNA-mRNA triplexes. The synergistic regulation of miRNA targets would contribute to the idea that miRNAs act as fine-tuners of global gene expression in the context of a gene regulatory network, and nearby miRNA target sites have

been suggested to allow silencing complexes to interact in a cooperative manner (Sæ trom et al., 2007).

The complex nature of disease development and progression involves a large set of involved genes and miRNAs, and has been extensively used in understanding cancer regulatory networks (Zhang et al., 2014b; Ding et al., 2015). A lot of the aforementioned studies investigating miRNA-gene regulatory networks utilise the power of web servers that contain information about gene regulatory patterns (Kanehisa et al., 2014) and enable them to perform gene ontology enrichment analysis (Ashburner et al., 2000). The availability of online tools provides multiple platforms for the identification and studying of miRNA targets and their involvement in gene regulatory networks; modelling that aims to investigates the dynamics of such networks is described in the following section on Modelling and Simulation.

1.2.5 miRNAs in LECs

Lymphatic Endothelial Cells (LECs) can be identified by their expressed lineage specific markers – Lymphatic Vessel Endothelial Hyaluronan Receptor (LYVE1) (Banerji et al., 1999), Podoplanin (PDPN) (Breiteneder-Geleff et al., 1999), Prospero Homeobox protein 1 (PROX1) (Wigle and Oliver, 1999) and Vascular Endothelial Growth Factor Receptor 3 (VEGFR3) (Veikkola et al., 2001) – and differentiate as a result of Vascular Endothelial Growth Factor C (VEGFC) induced signalling (Karkkainen et al., 2004). They form an extensive network of the lymphatic vasculature, lining the vessels with a single cell layer that has loose junctions to allow fluid and cell uptake and trafficking in a unidirectional manner. The lymphatic vasculature functions as a trafficking platform for immune cells and a drainage system for collecting and diverting excess interstitial fluid (Karkkainen et al., 2004). LECs play an important role in lymphangiogenesis and in the recruitment of immune cells (Johnson and Jackson, 2010). From a disease perspective, the lymphatic vasculature is exploited by cancers as a pathway for metastasis (Alitalo, 2011). The involvement of miRNAs in the interactions of maintaining the normal function of LECs has been a focus of recent studies and its implication in cell biology is summarised in this section.

1.2.5.1 miRNAs important for endothelial cell function

Many miRNAs have been described to function as regulators of gene expression programmes in LECs. Studies have demonstrated the involvement of endothelial cell expressed miRNAs in the positive (Anand et al., 2010; Chen and Gorski, 2008; Kuehbacher et al., 2007; Nicoli et al., 2012) and negative (Poliseno et al., 2006; Sabatel et al., 2011) regulation of vascular angiogenesis.

Other miRNAs, such as miR-126, are abundantly expressed in endothelial cells and also play a pivotal role in controlling endothelial cell migration, proliferation and angiogenesis (Fish et al., 2008; Wang et al., 2008). Several miRNAs are involved in controlling LEC phenotype by regulating the expression of lineage specific marker PROX1 (Kazenwadel

et al., 2010; Pedrioli et al., 2010).

1.2.5.2 miRNAs expressed in LECs involved in tumour growth

The miRNAs present in endothelial cells are important for LEC function, and the dysregulation of these miRNAs result in uncontrolled cell proliferation and vessel growth. Vascular Endothelial Growth Factor (VEGF), a positive regulator of angiogenesis has been shown to be under the regulation of miR-15b and miR-16 in cells subject to hypoxic environment during tumour angiogenesis (Hua et al., 2006). The miR-17-92 cluster targets anti-angiogenic factors to enhance neovascularisation and growth of vessels in tumours (Dews et al., 2006). Interestingly, miR-126, also shown to suppress the expression of VEGF (Fish et al., 2008; Zhu et al., 2011), has been a major focus for a large amount of cancer studies where it was mostly found to be down regulated (Ebrahimi et al., 2014). The role of miR-221 in endothelial cells has been shown to both oppose (Poliseno et al., 2006) and promote angiogenesis (Nicoli et al., 2012), and in addition in cancer cell lines it has been found to target p27, a cell cycle inhibitor, promoting the proliferation of tumour cells (le Sage et al., 2007), suggesting a diverse role for miR-221 in context dependent regulation.

1.2.5.3 miR-132 biology

The miR-132/212 cluster is co-transcribed as a primary transcript from the intergenic region of chromosome 17p13.3. The sequence of the 3'-arm of the miR-132 duplex (miR-132-3p) has confirmed miRNA target sites for several genes described below. Although miR-212 is co-transcribed with miR-132, sharing the seed sequence and potential predicted targets, its expression is relatively low compared to miR-132 (Lagos et al., 2010).

The expression of miR-132 in LECs is low, compared to other miRNAs, such as miR-126 and miR-21 (Lagos et al., 2010). Vo et al. (2005) were first to note that miR-132 expression can be induced by Brain-Derived Neutrophic Factor (BDNF). The upregulation of miR-132 was shown to be a consequence of cAMP-Response Element Binding protein (CREB)

phosphorylation at Ser-133 (Gonzalez and Montminy, 1989). The function of miR-132 was demonstrated in neurons by Vo et al. (2005) by targeting Rho GTPase Activating Protein 32 (p250GAP). Subsequently, it was shown that miR-132, although important in neuronal development and function (Impey et al., 2010; Wayman et al., 2008), was not critical for development in mice (Remenyi et al., 2010). The latter authors also demonstrated that phorbol myristate acetate (PMA) and lipopolysaccharide (LPS), just like BDNF are both able to stimulate miR-132 expression.

Several other targets have been since demonstrated to be suppressed by miR-132 up-regulation. The cycling of miR-132 expression was observed during light-exposure driven regulation of CREB, which downstream activated miR-132 transcription (Vo et al., 2005), where through the combined activity with miR-219 it functioned to regulate the circadian rhythm in a light-dependent manner targeting Period Circadian Clock 1 (Per1) gene expression (Cheng et al., 2007). In addition, Alvarez-Saavedra et al. (2011) demonstrated that in the mouse suprachiasmatic nucleus (SCN), miR-132 regulates chromatin remodelling by direct targeting of Lysine (K)-Specific Demethylase 5A (Jarid1a), Methyl CpG Binding Protein 2 (Mecp2), E1A-associated Protein p300 (Ep300) and modulates translation control through its direct targeting of Polyadenylate-binding Protein-Interacting Protein 2 (Paip2) and B-cell Translocation Gene 2 (Btg2). These studies revealed that miR-132 fine-tunes the expression of many targets involved in pathways that govern mammalian circadian rhythms.

During cell activation, miR-132 has found its role as a regulator of EP300 (Lagos et al., 2010), a transcriptional co-activator that binds the phosphorylated form of CREB to activate miR-132 transcription. In the context of a viral infection, the inflammatory response genes are regulated through the activity of the pCREB-EP300 transcription complex, where miR-132 acts to modulate the innate immune response based on miR-132 abundance over its time-course of expression (Lagos et al., 2010). In addition, Acetylcholinesterase (AChE) has been demonstrated as a target of miR-132 (Shaked et al., 2009), with the ability to attenuate inflammation during cell activation.

The function of miR-132 has also been demonstrated in the regulation of heart function, where miR-132 suppression of Forkhead Box O3 (FOXO3) was necessary to modulate recovery from cardiac hypertrophy (Ucar et al., 2012). In addition miR-21, miR-212 and miR-129 have previously been demonstrated to be involved in cardiomyocyte function, suggesting an important role for miRNA-mediated regulation (Thum et al., 2007). As miR-212 is co-expressed with miR-132, both miRNAs may play a role in cardiomyocyte function. Finally, the development of vasculature has been shown to be under the control of miR-132, where it targets RASA1 (encoding p120RasGap) and thereby enables Ras activity to promote endothelial cell proliferation and angiogenesis (Anand et al., 2010).

1.3 Modelling and Simulation

The interactions that exist between molecules in the cell take place from less than a second time scale, are dynamic in nature, and result in complex systemic behaviour. The intracellular molecular interactions that result in the non-linear behaviour can be best understood using computational modelling (Wolkenhauer et al., 2005). Capturing regulation of molecular processes at the subcellular level allows to identify the regulatory properties of the participating molecular components, the impact of their interactions, and provides information about the abundance of molecules that drive cellular responses.

1.3.1 Mathematical modelling

A biological system can be captured following a deterministic or a stochastic modelling approach (Gillespie, 1977). A deterministic component of a model can be described using an Ordinary Differential Equation (ODE), or a Partial Differential Equation (PDE) where the component needs to be spatially separated into discrete locations. In case of a subcellular model, molecules can be described as a system of coupled ODEs or PDEs. These type of approaches are useful for simulating system level dynamics where the abundance of participating components are present in a high abundance (Khan et al., 2003). However, in order to better capture reactions where a low abundance of components can have system-wide effects (such as miRNA-mediated control of a low-expressed mRNA translation resulting in magnitudes larger abundance of protein molecules), a stochastic approach needs to be considered due to the random perturbations that can occur during these regulatory steps (Sreenath et al., 2008). Kinetics of stochastic biochemical networks can be captured using Stochastic Differential Equations (SDEs) (Alves et al., 2006), where each molecule can be considered as an independent entity and separated in both time and space.

Models that utilise stochastic approaches require a deeper understanding of the underlying biology and assume that the numerous parameters that describe the model system of

biology do not change during the simulation time. The power of stochastic simulations lies in the more accurate representation of a biological system, with an increasing cost to computational time with the increase in parameter and component count: a subcellular model describing biochemical reaction networks can capture thousands of individual entities simulated over continuous time and space.

1.3.2 Agent-based modelling

Although mathematical models of complex biochemical networks have been used in modelling biological phenomena, they require an large set of parameters determining each of the kinetic reactions. Whilst this may be feasible for small-scale models of biological processes, mathematical models are limited by the availability of kinetic information for large-scale models (Acerbi et al., 2012). Moreover, the small abundance of some of the molecule components, such as the abundance of miRNAs (Lee et al., 2008) and specifically – abundance of miR-132 in LECs (Lagos et al., 2010), can significantly affect system dynamics (Pogson et al., 2006).

In order to resolve some of the aforementioned issues with mathematical modelling, an agent-based model (ABM) framework can be used. In ABMs, each entity, or *agent*, is provided a set of simple rules which describe its behaviour in an environment. There are several features to an agent that make ABMs a powerful tool for capturing biological phenomena (An et al., 2009):

1. Each *agent* is an autonomously acting entity which responds to environmental cues

2. Each *agent* contains its own set of parameters allowing heterogeneity on the scale of a single entity (e.g. no cell in biology is identical)

3. Some of the system parameters can be abstracted, allowing qualitative hypothesis testing of a domain, where knowledge is incomplete

4. The modularity of an ABM allows to build systems that span multiple scales of detail, providing an appropriate abstraction for each organisational level of biology (e.g. organ, cellular, molecular level) that are easily extensible (e.g. addition of a new type of cell as an agent with its own behaviour)

5. The interactions between *agents* are inherently resolved in a spatio-temporal manner (e.g. allowing for time-delayed effects) and the resulting behaviour is implicitly stochastic

6. The heterogeneous distribution of entities and their individual properties as defined by their parameters are more naturally resembling the heterogeneity present in biological systems

ABMs have been successfully used in biology to capture complex biological phenomena in immunology (Read et al., 2012; Alden et al., 2012; Moore et al., 2013), cancer development (Pappalardo et al., 2011), mRNA transport (Azimi et al., 2014) and more recently in molecular interaction networks (Williams, 2014). To date, only a single ABM has been described by Ripoli et al. (2009) that involves two negative feedback loops between miR-221 and miR-222, and their target CD117 in endothelial cells.

1.3.3 Modelling miRNA regulatory networks

Whilst only a single example of a miRNA-regulatory network has been found using an ABM approach (Ripoli et al., 2009), there has been a myriad of studies investigating the function of miRNAs in cell biology. The methods involved in investigating miRNA-regulatory networks range from analytical methods that predict target regulation and infer networks (Gennarino et al., 2012; Sengupta and Bandyopadhyay, 2013; Weber et al., 2013; Aure et al., 2015), study general miRNA role and function (Sæ trom et al., 2007; Zinovyev et al., 2013; Obermayer and Levine, 2014; Schmitz et al., 2014) to specific miRNA-mRNA target modelling (Schuetz et al., 2012).

Most relevant to the work presented in this thesis, Schuetz et al. (2012) combine an ABM approach with a set of 17 ODEs to describe a model of tumour growth. In Schuetz et al. (2012) model, the molecular interaction network model of miR-451, Liver Kinase B1 (LBK1) and 5'-AMP-activated Protein Kinase Catalytic Subunit α-1 (AMPK1), previously published by Godlewski et al. (2010), is incorporated into a cell-based agent system, where the subcellular network interactions described by ODEs determine the function of the cell agent. Whilst this is a novel model involving a miRNA in an ABM, the subcellular level of interactions are not represented as a network, making the interactome subject to possible system dynamics inaccuracies (Pogson et al., 2006). Moreover, their work has not presented a fully calibrated system, with no statistical evaluation of the model parameter space, although conclusions from the *in silico* simulation were proposed. Additionally, no methods describing the development rationale of the ABM were provided, highlighting the continued need to establish good model development, validation and verification standard in the field of computational biology.

1.3.4 Modelling process

Computational models that capture biology can only be as accurate as our understanding of the biological system. Importantly, computational models should be used to aid the understanding of a specific biological process, integrated into a wet-lab and simulation coupled approach. The need for such development life cycle in studying biological systems was drawn attention to by Kitano (2002), who suggested that modelling and experimental work should progress hand in hand, allowing models to be used as predictive tools for further experimental studies in biology.

Designing a biological experiment involves several key stages: the understanding of the problem domain and its constituents, the design of an experiment that would address a hypothesis, the necessary tools required to perform the experiment, and the appreciation for limitations of the experimental approach including the sources of error. Similar to this ap-

proach, a computational model requires the understanding of the domain it is modelling, driven by a defined hypothesis that the model is expected to address, which in turn is limited by the constituents involved in the setup of the model, imposing limitations on what the model can tell us about the biological system. In line with these principles, the Complex Systems Modelling and Simulation (CoSMoS) process has been developed (Andrews et al., 2010a), providing a framework for designing, developing and exploring complex systems. The stages of the project development are described in detail under Modelling and simulation of biological systems (Section 2.2). The CoSMoS modelling process has proven to be an effective and transparent framework for the developing of several other complex biological processes (Read et al., 2012; Alden et al., 2012; Moore et al., 2013), and has been used to coordinate the research investigating miR-132 regulation of AGO2 and EP300 in LECs.

1.4 Thesis aim

The aim of this work is to characterise the interaction between miR-132 and human AGO2 by perturbing the expression of miR-132 and AGO2 in Human Dermal Lymphatic Endothelial Cells (HDLECs) (Chapter 3). The regulation of AGO2 and EP300 (Lagos et al., 2010), both targets of miR-132, is captured in an ABM (Chapter 4) in order to understand the emergent properties of this regulatory network (Chapter 5).

Chapter 2

Materials and methods

2.1 Cell and molecular biology approaches

2.1.1 Cell culture

Cells were cultured in a humid environment at 37°C, 5% CO_2. Cryopreserved cells stored in 1:10 dimethyl sulfoxide (DMSO) (Sigma-Aldrich)-fetal calf serum (FCS) (Sigma-Aldrich) were thawed in a water bath (37°C) and added to a Ø$10\,\mathrm{cm}$ plate containing $8\,\mathrm{ml}$ of appropriate pre-heated media. After 5 to $6\,\mathrm{h}$ the cells were washed with phosphate-buffered saline (PBS) and the appropriate fresh media was replenished.

2.1.1.1 LECs

HDLECs were purchased from Promocell (C-12219), grown in Endothelial Cell Growth Medium MV ready-to-use (Promocell, C-22020) and supplemented with $10\,\mathrm{ng\,ml^{-1}}$ Recombinant Human VEGF-C (R&D Systems, 2179-VC-025). Supplemented media was changed every 24 to $48\,\mathrm{h}$.

A single vial containing ~5×10^5 HDLECs were grown from passage 0 and cryopreserved in liquid N_2 at passages 2, 3, and 5 in a $1\,\mathrm{ml}$ volume at $5 \times 10^5\,\mathrm{cells\,ml^{-1}}$. Cells were frozen at -80°C, $24\,\mathrm{h}$ prior to cryopreservation. Passage 5 cells were used for all experi-

ments. Passage 2 and 3 cells were expanded to passage 5 for later experiments when needed. The HDLECs were tested for LYVE1 expression as a determinant of LEC lineage (Banerji et al., 1999), showing that LYVE1 was highly expressed in HDLECs compared to Human Foreskin Fibroblasts (HFFs) (Figure 2.1). The LEC marker confirmation was performed by Daniel Yee (University of York, UK).

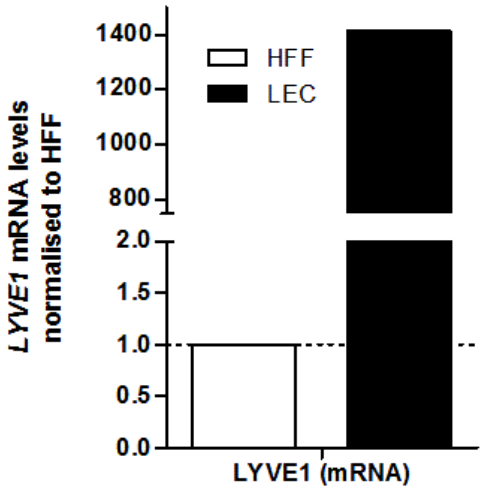

Figure 2.1: Comparison of the expression of *LYVE1* mRNA in HFFs and LECs ($n = 1$).

Sub-confluent cells (80-90%) were split between 2-4 plates dependant on cell count. The cells were washed with PBS, and incubated for $5\,\mathrm{min}$ at 37°C with $4\,\mathrm{ml}$ pre-warmed 1:5 trypsin-EDTA (Invitrogen) and PBS mix. Trypsin-EDTA was neutralised with $4\,\mathrm{ml}$ of media, and the cells were pelleted by centrifugation for $5\,\mathrm{min}$ at $260\,g$. Resuspended HDLECs were seeded at 5×10^5 per Ø$10\,\mathrm{cm}$ plate (BD Falcon™).

2.1.1.2 HeLa cell line

HeLa cells were cultured in Dulbecco's Modified Eagle Medium (DMEM) (Invitrogen), supplemented with 10% FCS and 1% of $100\,\mu\mathrm{g\,ml^{-1}}$ penicillin G and $100\,\mu\mathrm{g\,ml^{-1}}$ streptomycin (Invitrogen). Cells were split 1:4 every 48 to $72\,\mathrm{h}$ grown in Ø$10\,\mathrm{cm}$ plates.

2.1.2 Treatments

For all treatments cells were seeded in 6-well plates (BD Falcon™) at 6×10^4 cells per well and grown for $16\,\mathrm{h}$ before any treatment.

2.1.2.1 PMA

A $5\,\mathrm{mM}$ stock of PMA (Sigma) was prepared in DMSO. Next, aliquots of $5\,\mu\mathrm{M}$ PMA diluted in basal LEC media (without supplements) were stored. Aliquots of 1:1000 DMSO in basal media were prepared as a control. HDLECs were treated with $25\,\mathrm{nM}$ PMA or the DMSO control unless stated otherwise. Stand alone PMA treatments were done $16\,\mathrm{h}$ after plating, and $48\,\mathrm{h}$ after transfections or transductions described below.

2.1.2.2 siRNA, mimics and inhibitors transfections

The transfection mix was prepared using Opti-MEM (Invitrogen), *Trans*IT-siQUEST (Mirus) and the respective nucleic acid (see Table 2.1), following the manufacturer's instructions. The final volume of the transfection mix in each well was $800\,\mu\mathrm{l}$. 5 to $6\,\mathrm{h}$ post-transfection $1\,\mathrm{ml}$ of LEC media was added. $24\,\mathrm{h}$ after the transfection the cells were washed with PBS and replenished with fresh media.

Table 2.1: Transfected nucleic acid products and used concentrations.

Product	Concentration	Name	Target
siRNA	25 nM	SMARTpool ON-TARGETplus siRNA	NTC AGO2 EP300
mimic		miRIDIAN microRNA mimic	NTC miR-132
inhibitor	100 nM	miRIDIAN microRNA hairpin inhibitor	NTC miR-132
LNA inhibitor	50 nM	miRCURY LNA™ microRNA inhibitor	NTC miR-132

2.1.2.3 Lentiviral transductions

The used lentiviral constructs were provided by Dimitris Lagos, produced as described in Lagos et al. (2010). The miR-132/miR-212 cluster and AGO2^{-UTR} were amplified from genomic DNA and cDNA respectively and subcloned into the *pSIN* lentiviral vector using the *NotI* and *BamHI* restriction enzymes. For lentiviral transduction, virions were produced as described in Lagos et al. (2008).

Prepared lentiviral constructs were incubated with cells for $6\,\mathrm{h}$ in a total volume of $800\,\mu\mathrm{l}$ per well. Unless stated otherwise, the amount of lentivirus added per well was $20\,\mu\mathrm{l}$ for AGO2 and $400\,\mu\mathrm{l}$ for miR-132 overexpression experiments. Cells infected with miR-132 and AGO2^{-UTR} constructs were harvested after $48\,\mathrm{h}$ or $30\,\mathrm{h}$, respectively.

2.1.3 Molecular biology techniques

2.1.3.1 Tissue homogenisation

Mouse brain and spleen tissue used for RNA and protein analysis were provided by Mark Coles' group (University of York, UK) from 6-8 weeks old C57BL/6 and miR-132 -/- KO mice (Magill et al., 2010). The extracted brain tissue was supplied frozen in one piece. Each brain tissue sample was cut over dry ice into similar sized chunks ($<30\,\mathrm{mg}$) for RNA and protein extraction. The prepared samples were homogenised on a TissueLyser LT (Qiagen) device for $3\,\mathrm{min}$ at $50\,\mathrm{Hz}$ in $1\,\mathrm{ml}$ of appropriate solution using two beads per tube. QIAzol Lysis Reagent (Qiagen) was used for homogenising tissue for RNA analysis and radio-immunoprecipitation assay (RIPA) lysis buffer (for recipe see Protein extraction and quantification Section below) was used for homogenising tissue for protein analysis.

2.1.3.2 RNA extraction

A dedicated RNA extraction workspace was used for all RNA extractions. RNaseZap RNase (Ambion) was used to wipe down the workspace surfaces and pipettes prior to sample processing. The miRNeasy Mini Kit (Qiagen) was used for all total RNA extractions. Extra RNAse-free Microfuge tubes (Ambion) were purchased for carrying out the extraction protocol and storing the samples.

The cells in each well were lysed using $700\,\mu\mathrm{l}$ of QIAzol, collected into $1.5\,\mathrm{ml}$ Eppendorf tubes and frozen at -80°C for at least a few hours. The lysed cell samples were processed according to the manufacturer's instructions and eluted in $30\,\mu\mathrm{l}$ of RNAse-free H_2O. The DNAse I digestion step was only carried out for mouse tissue samples.

The extracted RNA quality was measured on the NanoDrop ND 1000 (Thermo) using $1\,\mu\mathrm{l}$ of eluted RNA. Samples with an absorbency measure of $>$2.0 for A260/A280 were used for further analysis, suggesting that the sample contains a higher proportion of RNA (purity). Most samples had a recommended A260/A230 value in the range of 1.8-2.0. Due to low yield of RNA as a result of treatment conditions and cell viability, some samples showed

lower A260/A230 values; this was the case with samples where the yield of nucleic acids from extraction were very low ($<20\,\mathrm{ng\,\mu l^{-1}}$ and the 230 peak which measures presence of contaminants such as phenol gave a higher signal than the 260 peak (indicates nucleic acid presence)). Subsequent to cDNA synthesis and quantitative reverse transcription polymerase chain reaction (qRT-PCR) the results replicated previously collected experiments and could be reliably used.

2.1.3.3 cDNA synthesis

The extracted RNA concentration used for polyadenylated and random hexamer cDNA synthesis was typically ~$100\,\mathrm{ng\,\mu l^{-1}}$. Mouse sample RNA was diluted to a similar concentration range. For miRNA cDNA synthesis the RNA was further diluted to 1 to $5\,\mathrm{ng\,\mu l^{-1}}$.

The cDNA synthesis of polyadenylated RNA was done by incubating $1\,\mu$l of RNA for $6\,\mathrm{min}$ at 70°C with $1\,\mu$l of $5\,\mu$M oligo(dt) and $1\,\mu$l of $10\,\mu$M dNTP made up to $12\,\mu$l of total volume with ddH_2O per reaction mix. Samples were chilled on ice before adding a mix of $4\,\mu$l of 5x First-Strand Buffer (Invitrogen), $2\,\mu$l of 0.1 M DTT (Invitrogen), $1\,\mu$l of RNaseOUT (40 units, Invitrogen) and $1\,\mu$l of SuperScript II (200 units, Invitrogen). Samples were incubated at 40°C for $1\,\mathrm{h}$ and finally heated at 70°C for $10\,\mathrm{min}$ to inactivate SuperScript II.

To reverse transcribe primary miRNA transcripts, $1\,\mu$l of RNA was incubated at 65°C for $6\,\mathrm{min}$ with $1\,\mu$l of $50\,\mathrm{ng\,\mu l^{-1}}$ random hexamers and $1\,\mu$l of $10\,\mu$M dNTP made up to $10\,\mu$l of total volume with ddH_2O per reaction mix. Samples were chilled on ice before adding a mix of $2\,\mu$l of 10x First-Strand Buffer (Invitrogen), $4\,\mu$l of $25\,\mathrm{mM}$ $MgCl_2$ (Invitrogen), $2\,\mu$l of 0.1 M DTT (Invitrogen), $1\,\mu$l of RNaseOUT (40 units, Invitrogen) and $1\,\mu$l of SuperScript III (200 units, Invitrogen). Samples were incubated at 25°C for $10\,\mathrm{min}$, 50°C for $50\,\mathrm{min}$ and finally heated at 85°C for $5\,\mathrm{min}$ to inactivate SuperScript III.

miRNA cDNA synthesis was performed using the TaqMan® miRNA Reverse Transcription Kit (Applied Biosystems). Following manufacturer's instructions, a master mix was prepared using the supplied $4.16\,\mu$l of ddH_2O, $1.5\,\mu$l of cDNA synthesis buffer, $0.15\,\mu$l of

dNTP mix, $0.19\,\mu l$ of RNAse inhibitor and $1\,\mu l$ of Reverse Transcriptase, giving a final volume of $7\,\mu l$ per reaction. $5\,\mu l$ of diluted RNA (1 to $5\,ng\,\mu l^{-1}$) was mixed together with $2\,\mu l$ of miRNA specific reverse transcription primers. Samples were then chilled on ice for $5\,min$, followed by an incubation at 16°C for $30\,min$, 42°C for $30\,min$ and finally heated at 85°C for $5\,min$ to inactivate the reverse transcriptase.

Prepared cDNAs were chilled on ice and stored at -20°C.

2.1.3.4 Real-time qRT-PCR

Expression levels of target sequences were quantified by qRT-PCR press using SYBR Green (Applied Biosystems) and TaqMan primers (Applied Biosystems), detailed in Table 2.2, designed with the aid of the online service Universal ProbeLibrary Assay Design Center (Roche). Primers were used at 300 nM final concentration with typically $1\,\mu l$ of neat cDNA in a final volume of $20\,\mu l$ per reaction. The MicroAmp Optical 96-well Reaction and MicroAmp Fast Optical 96-Well Reaction (Applied Biosystems) plates were used on the Thermal Cycler 7500 System (Applied Biosystems) and the StepOnePlus™ Real-Time PCR System (Applied Biosystems), respectively. The plates were sealed using the MicroAmp Optical Adhesive Film (Applied Biosystems) and briefly pulsed to $300\,g$ prior to the qRT-PCR. The default program for 40 cycles of amplification was used. GAPDH was used as a loading control for target gene mRNAs, pri-miR-126 and pri-miR-132. RNU6 was used as a loading control for all mature miRNAs. The relative change in target expression was quantified using the comparative CT method.

Table 2.2: Real-time qRT-PCR primers and assays. Asterisk (*) indicates that these are mouse-specific primers. TaqMan primer sequences marked as not applicable (N/A) as they are supplied with the product data sheet.

Target	Assay	Forward primer	Reverse primer
ANG1	SYBR	5'-CAGGAGGATGGTGGTTTGATG-3'	5'-TGGTTTTGTCCCGCAGTATAGAA-3'
ANG2		5'-TTCCTCCTGCCAGAGATGGA-3'	5'-TGCACAGCATTGGACACGTA-3'
GAPDH		5'-GGAGTCAACGGATTTGGTCGTA-3'	5'-GGCAACAATATCCACTTTACCAGAGT-3'
IL6		5'-TGACAAACAAATTCGGTACATCCT-3'	5'-AGTGCCTCTTTGCTGCTTTCAC-3'
Hprt*		5'-GTTGGATACAGGCCAGACTTTGTTG-3'	5'-GATTCAACCTTGCGCTCATCTTAGGC-3'
MMP9		5'-TTGACAGCGACAAGAAGTGG-3'	5'-GCCATTCACGTCGTCCTTAT-3'
pri-miR-126		5'-TATCAGCCAAGAAGGCAGAA-3'	5'-CGTGGCGTCTTCCAGAAT-3'
SPRED1		5'-GGCGACTTCTGACAACGATAA-3'	5'-CATCCACCACTTGAGTCATCTC-3'
TIE2		5'-GATTTTGGATTGTCCCGAGGTCAAG-3'	5'-CACCAATATCTGGGCAAATGATGG-3'
TNFα		5'-CTGGCCCAGGCAGTCAGAT-3'	5'-AGCTGCCCCTCAGCTTGAG-3'
VEGFA		5'-CTACCTCCACCATGCCAAGT-3'	5'-GCAGTAGCTGCGCTGATAGA-3'
AGO2	TaqMan	N/A	
Ago2*			
EP300			
miR-16			
miR-21			
miR-30c			
miR-126			
miR-132			
miR-146a			
miR-221			
pri-miR-132			
RNU6			

2.1.3.5 Protein extraction and quantification

RIPA lysis buffer was used for all protein extractions, supplemented with phosphatase and protease inhibitor cocktails (Sigma) that were only added immediately before lysis. The recipe is detailed below:

RIPA lysis buffer:

25 mM Tris•HCl, pH 7.2

150 mM NaCl

0.5% (w/v) Triton X-100 (Sigma)

1% (w/v) sodium deoxycholate

0.1% (w/v) sodium dodecyl sulphate (SDS)

0.1% (w/v) ethylenediaminetetraacetic acid (EDTA), pH 8.0

The cultured cells were washed with PBS (37°C) and all of the PBS was removed using a P1000 pipette by tilting the plate under an small angle. The plate was transferred onto ice. Typically, 30 µl of RIPA lysis buffer was added per well and spread using a cell scraper. Next, the plate was placed under an angle and the cell scrapper was used to collect the cell lysate at the bottom of the well. The lysate was then transferred to a 0.5 ml Eppendorf tube and kept on ice. The lysates were centrifuged at 10 000 *g* for 10 min to pellet the cellular debris. The supernatant was transferred to a new Eppendorf tube and stored at -80°C.

Mouse samples that were homogenised in RIPA lysis buffer (see the Tissue homogenisation Section above) were centrifuged at 10 000 *g* for 10 min two times. After the first centrifugation the sample separated into three distinct phases: the upper white few mm thick lipid layer, the middle predominantly aqueous protein lysate layer, and the bottom layer containing intracellular and extracellular debris, and the two metal beads used during homogenisation. 800 µl of the lysate was transferred to a new Eppendorf in order to avoid carryover of debris and lipids. After the second centrifugation the remaining debris was pelleted and a final volume of 700 µl of protein lysate was kept and stored at -80°C.

Protein concentration was measured using the Pierce BCA Protein Assay kit (Thermo Scientific). The standard curve was prepared by serial diluting (6 times) the Albumin Standard ampoules provided with the kit that contained $2\,\mathrm{mg\,ml^{-1}}$ of bovine serum albumin (BSA). A 1:4 dilution of HDLEC and HeLa protein lysates and 1:40 dilution of mouse brain protein lysates was prepared in ddH_2O. The samples were pipetted into a 96-well Maxisorp Multiwell plate (Sigma) in duplicate, and incubated at 37°C for $90\,\mathrm{min}$ with $200\,\mu\mathrm{l}$ of BCA reagent mix per well, prepared according to the manufacturer's instructions. The absorption was measured at $562\,\mathrm{nm}$ and the protein concentrations calculated against the standard curve.

2.1.3.6 Western blotting

Protein lysates were prepared in 4x SDS-polyacrylamide gel electrophoresis (SDS) sample loading buffer (recipe below) and topped up with ddH_2O to the same final volume. Cultured cell lysates and mouse sample lysates were prepared at $1\,\mu\mathrm{g\,\mu l^{-1}}$ and $2\,\mu\mathrm{g\,\mu l^{-1}}$ of protein, respectively.

SDS-PAGE sample loading buffer:

$250\,\mathrm{mM}$ Tris•HCl, pH 6.8

8% (w/v) SDS

10% (v/v) glycerol

5% (v/v) β-mecaptoethanol

0.05% (w/v) bromophenol blue

The proteins were separated on $0.75\,\mathrm{mm}$ thick 8% polyacrylamide gel in SDS-PAGE running buffer (National Diagnostics) using the Mini-PROTEAN Tetra Handcast Systems (Bio-Rad), typically for $1.5\,\mathrm{h}$ at $120\,\mathrm{V}$. The recipe for the stacking and the resolving gel is detailed below:

4% stacking gel:

3 ml dH_2O

0.67 ml 30% (w/v) acrylimide

1.25 ml 1.5 M Tris, pH 6.8

50 ml 10% (w/v) SDS

50 ml 10% (w/v) ammonium persulfate (APS)

5 ml TEMED

8% resolving gel:

3.7 ml dH_2O

2.13 ml 30% (w/v) acrylimide

2 ml 1.5 M Tris, pH 8.8

80 ml 10% (w/v) SDS

80 ml 10% (w/v) APS

8 ml TEMED

Prepared protein samples for SDS-PAGE were denatured by heating at 95°C for 5 min, prior to loading. Empty lanes were loaded with 1x SDS-PAGE sample loading buffer. Fermentas Protein Ladder Pageruler Plus Prestained (Thermo Scientific) was diluted 1:1 with the 1x SDS-PAGE sample loading buffer. Each lane was loaded with 12 µl of sample.

Protein was transferred onto a polyvinylidene fluoride (PVDF) membrane (Millipore) at 0.2 A and a maximum of 25 V for 75 min using a semi-dry transfer apparatus (Bio-Rad) and transfer buffer (National Diagnostics). Prior to transfer the PVDF membrane was activated by immersing in methanol for 1 min, followed by dH_2O for 1 min and transfer buffer for 5 min. Membranes were blocked in 5% (w/v) BSA-TBS/T (see TBS/T recipe below) for 1 h at room temperature on a gently rocking platform.

10x TBS, pH 8.0

87.65 g Tris

12.2 g NaCl

dissolved in final volume of 1 l dH_2O

adjusted to pH 8.0 using 1 M HCl

TBS/T

900 ml dH_2O

100 ml 10xTBS

0.1% (v/v) Tween-20 (Sigma)

After blocking the PVDF membranes were placed in 50 ml Falcon tubes and incubated at 4°C with 10 ml of 1° antibody (see Table 2.3 for used antibodies) overnight on a gentle roller. Following the 1° antibody incubation the membranes were washed three times for 5 min each time in TBS/T on a gently rocking platform. Next, the membranes were incubated at room temperature in the appropriate horse-radish peroxidase conjugated 2° antibody for 1 h on a gently rocking platform, followed by the three TBS/T washes. Finally, the membranes were incubated for 5 min in the ECL Western Blotting reagent (GE Healthcare) in the dark. The chemiluminescence signal was detected on the Hyperfilm ECL (GE Healthcare). After detection the membranes were washed three times as before and re-used for more target detections: the membranes were blocked again in 5% (w/v) BSA-TBS/T or, if necessary, stripped using a stripping buffer (Thermo Scientific) at 37°C for 30 min on a shaking platform. After stripping the membranes were washed several times with dH_2O, followed by three 5 min washes with TBS/T. Used membranes were briefly placed on Whatman paper to soak up excess liquid, wrapped in cling film and stored flat at -20°C.

The films were scanned in at 600 DPI and the signal of each band was quantified using ImageJ. Each target band signal was normalised to the corresponding lane loading control (β-actin or GAPDH).

Table 2.3: Antibodies used for western blot detections.

Supplier	Antibody	Target	Dilution	Buffer
Cell Signalling	D84G10	AGO1	1/1000	5% (w/v) BSA-TBS/T
	C34C6	AGO2	1/1000	
	48H2	CREB	1/1000	
	87G3	phoshpo-CREB (Ser^{133})	1/1000	
	AB33	TIE2	1/500	
	4221S	phoshpo-TIE2 (Tyr^{992})	1/500	
Santa Cruz	B4F8	RASA1	1/500	
Sigma	F3165	FLAG M2	1/1000	5% (w/v) milk-TBS/T
Abcam	AC-15	β-actin	1/5000	
	6C5	GAPDH	1/5000	
	3G230	EP300	1/500	
Dako	P0447	mouse IgG	1/5000	
	P0448	rabbit IgG	1/5000	

2.1.4 Cell viability assay

HDLECs were plated in 12-well plates (BD Falcon™) at 1.5×10^4 cells per well and grown for $16\,\mathrm{h}$ before any treatment. Cell viability was measured using the Colorimetric Cell Viability Kit IV (PromoKine) at the desired time point after treatment. All of the media from the wells was collected (per treatment condition) and used to prepare $40\,\mu\mathrm{l}$ of the MTT reagent in $360\,\mu\mathrm{l}$ of media (37°C) per well. $400\,\mu\mathrm{l}$ of the MTT mix was returned to each corresponding well and incubated at 37°C for $4\,\mathrm{h}$. After the incubation with the MTT reagent, $800\,\mu\mathrm{l}$ of DMSO was added per well and mixed by pipetting up and down several times. After $5\,\mathrm{min}$ $300\,\mu\mathrm{l}$ of the contents of each well was transferred in triplicate to a 96-well Maxisorp Multiwell plate, and the absorbency was measured at $570\,\mathrm{nm}$ to obtain the signal and at $630\,\mathrm{nm}$ to obtain the background readings. The normalised absorbency signal was obtained by subtracting the background from the signal absorbency values.

2.1.5 Statistical analysis of biological data

Where applicable (sample $n \geq 3$), the significance of the difference between experimental conditions was determined by calculating the *p*-value using a two-tailed *t*-test. The difference was considered significant if $p < 0.05$ (indicated by *), $p < 0.01$ (indicated by **) or $p < 0.001$ (indicated by ***).

2.2 Modelling and simulation of biological systems

The tools and packages for developing, testing, and evaluating the models have been well-established within the York Computational Immunology Lab (YCIL) group[1]. To ensure good software development practices the standard protocols and applications have been documented by Dr. Kieran Alden (University of York, UK) and made available on the YCIL intranet[2]. The steps involved and the software used in developing this model are outlined within this section below.

2.2.1 Biological domain and simulation specification

"Essentially, all models are wrong, but some are useful." ~ George E. P. Box

The biological domain in the context of the research question was explicitly defined using the strategy described below. This allowed to establish the scope of the problem and suggest possible hypothesis that could be tested by the model. The systematic approach for developing models of biological systems was based on the CoSMoS process (Andrews et al., 2010a,b), a conceptual framework for engineering complex systems. The CoSMoS process schematic is described in Figure 2.2 which was used as a roadmap for model development.

2.2.1.1 Model specification

Once the problem domain, *i.e.* the biological context, was agreed upon with the domain expert, it was captured in diagrams using the Unified Modeling Language (UML). The biological problem and the way system components[3] interact was captured in *pseudo*-UML *expected behaviour diagram*. This diagram represents the top-level mechanism and the emergent behaviour that was expected of the model. The behaviour of each component was

[1] https://www.york.ac.uk/computational-immunology/

[2] https://www.york.ac.uk/computational-immunology/intranet/

[3] Defined as an abstracted object of the *real* world domain that is able to function based on input and output information; e.g. a component in an ABM is an agent

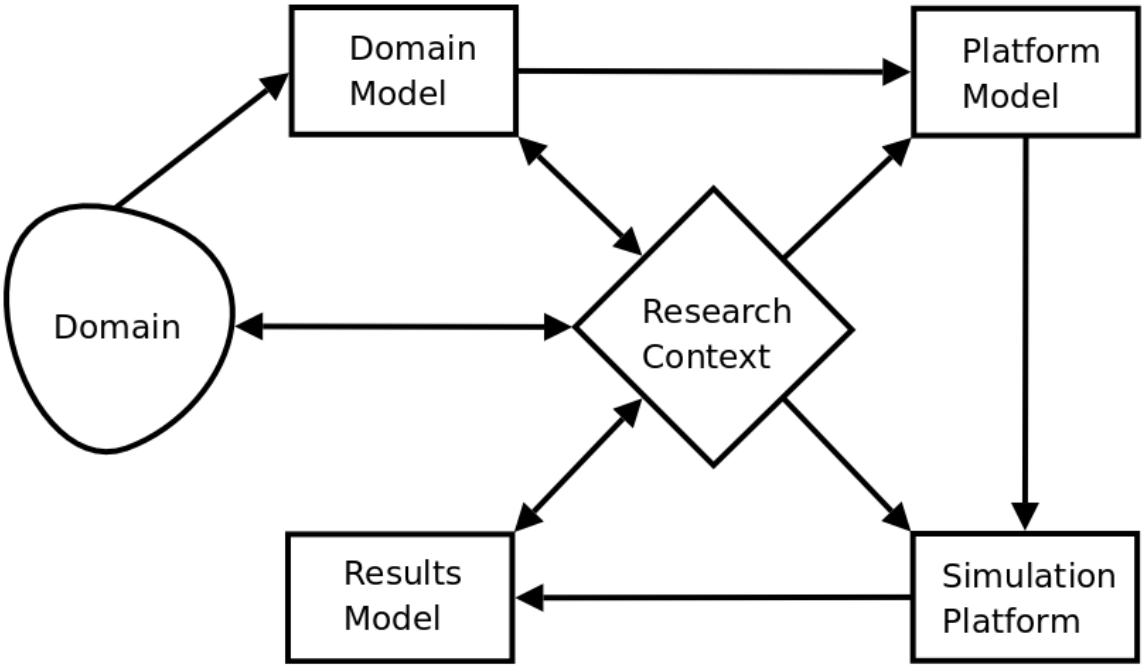

Figure 2.2: Model development cycle as defined by the CoSMoS process (Andrews et al., 2010a).

then described in *UML state diagrams*. The actions and activities of the system components were captured in *UML activity diagrams*. The diagrams allowed the representation of concurrent actions that many components in biological systems often exhibit, such as when several proteins need to interact before a product can be synthesised. The afore-mentioned diagrams captured the necessary components to describe the biological domain within the context of the scientific question and constitute the *domain model*.

The specifications for the implementation of an executable model were captured in the *platform model*. Explicit parameter names and transitions conditions were used in the *state* and *activity diagrams* for the *platform model*. Some concepts in the *domain model* were further abstracted. Figure 2.2 suggests that the information flow is directed from the problem domain towards the *platform model*, however decisions made when abstracting knowledge from the *domain model* and appropriating it to the *platform model* suggested gaps in knowledge in the *domain model*. This resulted in revisiting the problem domain and updating the *domain model* and consequently the *platform model*. Although the workflow shown in

Figure 2.2 is goal-oriented towards completing the full cycle of model development, the *Research Context* interface allows the revision of earlier modelling steps when necessary.

2.2.1.2 Notation in *state* and *activity diagrams*

The *state* and *activity diagrams* are captured using standard UML notation. However, there are some non-standard notations. For clarity, the full key to the diagrams is described below:

Rounded rectangle *State diagrams*: Contains the *state* of the component; an encapsulated rounded rectangle within another *state* suggests a *sub-state*

Solid circle Starting point of the component - from a model perspective, this is where the component is instantiated

Solid circle with an inner white line End point of the component - from a model perspective, this is where the component is removed

Arrow Displays the direction of the *state* or *activity* transition

Text next to an arrow Describes the condition for the *state* or *activity* transition (together with the Arrow, it is commonly known as a *"guard"*); text enclosed in "[...]" refers to specific conditions or parameters; text following a forward-slash "/ ..." instructs a parameter change upon the transition; text following "& ..." suggests that the condition above within the same transition must be met simultaneously; ">", "<", "==", "! =" refer to "greater than", "smaller than", "equivalent to" and "not equivalent to", respectively, and are used as part of a condition description

Diamond *Activity diagrams*: Arrows feeding into a diamond suggest a point where multiple activities converge; Arrows pointing out of a diamond allow one of the activities to take place depending on which transition condition is met

Thick solid line *Activity diagrams*: Arrows feeding into the thick solid line are prerequisite conditions that need to be met for the emerging Arrow(s) activity to be triggered

Dotted line Indicates that states on either side of the line act in parallel

2.2.1.3 Justification and model validation

The information gathered when studying the biological domain and performing wet-lab experiments was used in justifying decisions made in the development of the domain and platform models, and later also used part of validating the model against the *real* world domain. Every component and interaction was documented and justifications were drawn based on existing data from the lab and supporting evidence from literature.

2.2.1.4 Parametrisation

Finding values for each of the parameters in the model was done alongside the argumentation. Based on the *platform model* specification of parameters, a table was prepared with approximate real world values and possible ranges using the sources in the argumentation structure. Some of the parameters were chosen to form the baseline values against which other model parameters would be calibrated (described under Statistical analysis and calibration).

2.2.2 Model development

The model was developed in the Java programming language using the latest JRE and JDK (JVM version 1.7.0).

2.2.2.1 Modelling system

The model was developed using the Eclipse IDE (Kepler) which was supplied with Repast Simphony (version 2.2) (North et al., 2013). Repast Simphony is an agent-based modelling environment which was built based on its predecessor Repast 3 (North et al., 2006).

Based on the platform model specification a system architecture was developed and a class structure was implemented (Figure B.1). Next, the model main class that builds the simulation environment was implemented. The agent classes were developed sequentially with basic functionality. Finally, more complex functionality with other agents was developed and refined. The model underwent several iterations to improve and refine readability, and the code was appropriately documented. The Doxygen (van Heesch, 2012) tool was used to compile the documentation.

2.2.2.2 Version control and distribution

Git (Torvalds and Hamano, 2005) was used as the version control system of choice, integrated within the Eclipse IDE. During the model implementation at the end of each revision cycle the state of the model was described in the *commit* notes, including known bugs and suggested revisions. The source code was synchronised after each *commit* with the BitBucket repository[4]. The implemented model can be distributed as a stand-alone installer and executed on any system with Java version 1.7 or later.

Due to many pitfalls discovered after developing a model using Repast Simphony (described in detail in Section 4.6.2), the developed model has been packaged up[5] for cluster

[4]https://bitbucket.org/gl524/mirnet.git

[5]https://bitbucket.org/gl524/mirnet/src/58bd98b6932968ffb83946dd36f5cad1aa7a7aaa/model_package/

execution together with necessary modifications to Repast Simphony and cluster execution scripts. The Graphical User Interface (GUI) based installer supported on devices running Java 7 or higher is also available in the same directory.

2.2.2.3 Code profiling and testing

The JVM Monitor (Eclipse Foundation, 2012) integrated with Eclipse IDE was used to establish central processing unit (CPU) intensive parts of the model. The profiler was useful at revealing other built-in Repast Simphony implementation pitfalls.

Exploratory testing was employed when developing the model. After every *commit* cycle the updated and related code was reviewed and tested. The system components in the model were loosely coupled allowing each of the individual components to be rigorously tested during implementation. Effort was made to test individual system components as well as perform integrated system testing. Although test-driven development was not employed in the development of this model, the YCIL model development cycle should support effective test-driven development in the future.

2.2.3 Statistical analysis and calibration

Statistical analysis and evaluation of the model is a cyclic process that aims to understand how the model behaves during various parameter perturbations. An overview of this process is captured in Figure 2.3 The steps involved are described below using the *Spartan* toolkit (Alden et al., 2013). Statistical analysis of the differences between treatments *in silico* was performed using the 2-sample Kolmogorov-Smirnov (K-S) test described in further detail under Section C.6.

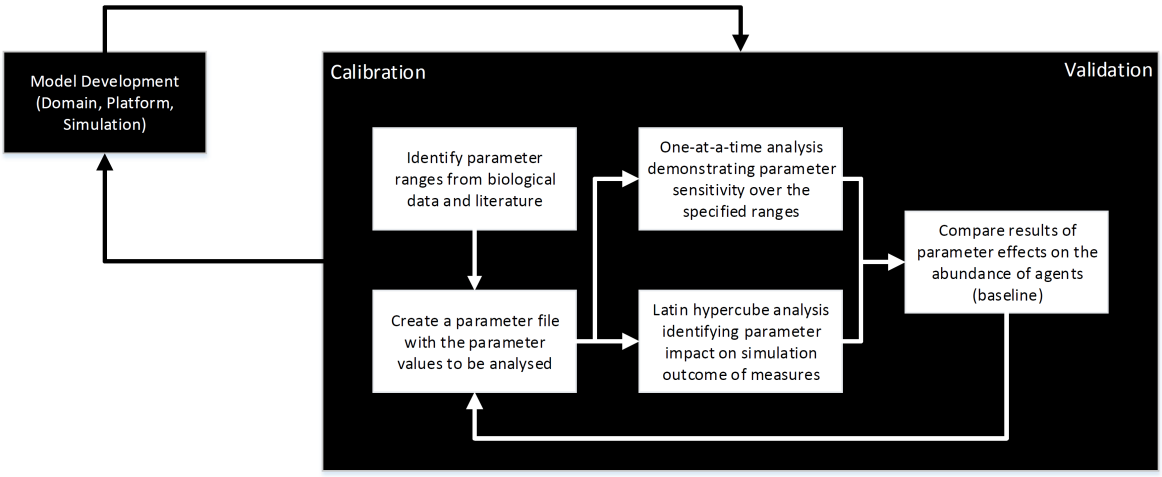

Figure 2.3: The work flow involved in calibrating a model to a baseline model subsequent to domain, platform and executable model development. The calibration utilises two main parameter space analysis techniques and the output is compared to a biological data set of expected outcomes (also referred to as ”measures”), i.e. molecular abundance of miR-132. The parameter set that matches all the measures can then be used as a baseline model to drive hypothesis by performing *in silico* experimentation and further develop the model.

2.2.3.1 Simulation output

Stochastic simulations produce different output under the same starting conditions and using the same parameter values. In computational simulations the stochastic nature of the model output is defined by a Random Number Generator (RNG). In order to obtain exact replicate simulation output the RNG must make the same choices each time it is used. Within a simulation this can be set using a *seed* value that the RNG uses to compute the next value for a function call. The simulation *seed* value in Repast Simphony is computed using the

Mersenne Twister algorithm (Matsumoto and Nishimura, 1998). The *seed* must be set at the start of the simulation by explicitly defining a static environment variable. This ensures that the same *seed* value can be supplied in the parameter file when the exact simulation run needs to be reproduced or tested. Simulations that differ by the *seed* parameter can be statistically evaluated.

2.2.3.2 Aleatory uncertainty analysis

The impact of stochastic behaviour in a simulation needs to be understood before any further analysis can be performed. As mentioned earlier, the output of any two non-deterministic simulations that only differ by a *seed* will produce different output, creating uncertainty in the simulation response outcome (Helton, 2008). In order to reduce uncertainty that is due to the RNG alone, many simulation runs need to be performed. The method for estimating the minimum amount of simulation runs required to reduce the uncertainty of the simulation output, also known as aleatory analysis, has been previously described (Read et al., 2012). Aleatory analysis is done by evaluating the uncertainty in an increasing amount of simulation runs, measuring the output variation of having a specific amount of simulation runs using the A-Test score (Vargha and Delaney, 2000). The simulation can enter the calibration cycle after completing the aleatory analysis, where each new combination of simulation parameters will be used to execute a simulation with a different *seed* the amount of times required to keep the uncertainty of simulation output to an accepted minimum.

2.2.3.3 Calibration

Depending on the amount of parameters that need to be calibrated and the complexity of the model, calibration of a stochastic simulation is currently one of the most time-consuming processes in computational modelling. The parameters that are specified in the model are derived from two main sources:

- parameter values based on published or unpublished experimental data

- parameter values introduced at the *platform model* development stage that represent an element of the real-world domain or an abstraction

Some parameters of the model are considered to be exact values that should not be altered by calibration, whilst others, especially the parameters introduced during the *platform model* development, need to calibrated within a predefined range. Having parameter values that are considered to be closely representing the real-world domain can reduce the time required to establish the less known parameter values, as each parameter requiring calibration adds another level of complexity to the calibration process.

During calibration the simulation output is matched against the experimental data that the model is aiming to reproduce. The parameter set combination that produces a simulation outcome that qualitatively resembles the experimental data formulates the *baseline*. The *baseline* parameter values that result in the expected experimental system behaviour can further be used for *in silico* experimentation. The two techniques described below are used to achieve the behaviour of the model system that resembles *real* world phenomena by studying the effect of altering parameters under controlled conditions.

2.2.3.4 Single parameter exploration

Perturbation of a single parameter at a time is needed to understand the magnitude effect that each parameter has on the system outcome. This is done using the *one-at-a-time* (OAT) analysis technique.

By choosing a large range of values for each parameter of interest it is possible to identify the parameter settings that significantly affect the simulation outcome as measured by the A-Test score. Small changes to a single parameter that result in big differences in the simulation outcome indicate that the parameter is highly sensitive to change. Such information can suggest that the value of the parameter needs to be accurately measured, or that the value range where the parameter is perturbed destabilises the system, changing the behaviour of the model. Further rounds of OAT sampling can be used to establish the turning

point for the sensitive parameters using narrower ranges with tighter increments to evaluate the effect on the simulation outcome.

The gathered information from OAT analysis is useful for redefining some of the parameter *baseline* values for the following calibration and analysis rounds. The final round of OAT sampling, where most of the *baseline* parameter values have been established, can be used to understand how the resulting model behaviour compares to the *real-world* system.

2.2.3.5 Global exploration of parameter space

Subsequent to the OAT analysis, the sensitivity of the simulation in response to multiple parameter perturbations can be studied using the *Latin Hypercube* (LHC) sampling technique. The LHC analysis produces a correlation coefficient between the tested *parameter* and the resulting outcome *measure*. Highly correlated or anti-correlated *parameter-measure* pairs indicates that during the LHC sampling and analysis the effect that resulted in the outcome *measure* was predominantly caused by the single *parameter* alone; other parameters, although varied in a specified range, are unlikely to be the cause for the observable outcome. The LHC sampling technique is useful in aiding the calibration process by indicating which parameters are most likely to cause large perturbations to the simulation response. Some of these finding may also suggest the driving forces that regulate or maintain specific real-world phenomena. Each correlation coefficient is assigned a *p-value* to indicate significance of the correlation.

Chapter 3

Direct regulation of AGO2 by miR-132 – *in vitro* and *ex vivo* investigation

In LECs the expression of miR-132 is relatively low (Lagos et al., 2010), however it has been shown to play a role in the anti-inflammatory response during KSHV infection (Lagos et al., 2010) by targeting EP300 and by mediating angiogenesis through the regulation of p120RasGap (RASA1) (Anand et al., 2010). In both aforementioned studies, miR-132 was upregulated up to 10-fold, sufficient for miR-132 mediated functional regulation in activated LECs. Therefore, LEC activation was required in order to investigate endogenous miR-132 regulation of AGO2. In this chapter I demonstrate the direct targeting of AGO2 by miR-132 through the overexpression of miR-132 and induction of the miRNA endogenously. Furthermore, I aim to investigate how miR-132 and AGO2 modulation affects other functions within LECs in the context of cell activation.

3.1 miRNA target prediction

The pilot study for identifying the potential novel targets for miR-132 was carried out by Dimitris Lagos (University of York, UK) by performing an overexpression of miR-132 using a lentiviral construct (see Figure 3.1). The targets were chosen based on the EIMMO

prediction analysis tool (Gaidatzis et al., 2007) which suggested that RNA-binding proteins (RBPs) were among the highly correlated miR-132 targets (see Table 3.1). I identified that several of the RBPs were predicted by multiple online target prediction tools (see Table 3.2) as potential targets of miR-132. The mature miR-132 sequence was then aligned against one of the selected candidate targets, AGO2 (see Figure 3.2).

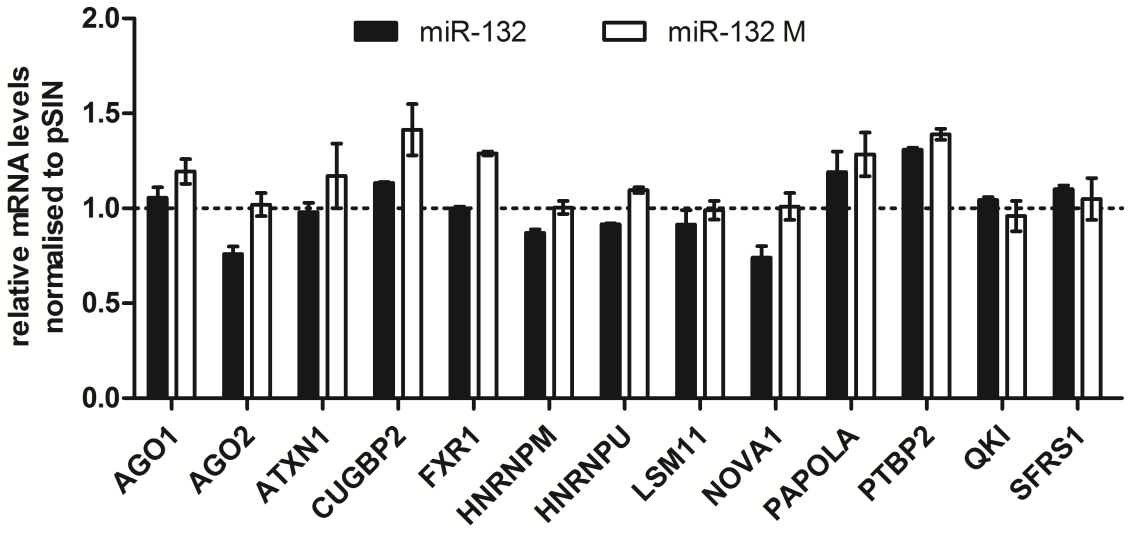

Figure 3.1: RBP target screen after $48\,\mathrm{h}$ of miR-132 or miR-132 mutant (M) lentiviral overexpression ($n = 2$, mean $\pm$ standard error margin (S.E.M.)).

Table 3.1: Predicted miR-132 targets using the EIMMO prediction analysis tool showing enriched Gene Ontologies (GOs) (Gaidatzis et al., 2007).

GO Term (Molecular Process)	**Bonferonni corrected *p*-value**
DNA binding	1.23×10^{-5}
transcription factor activity	1.63×10^{-5}
DNA (cytosine-5-)-methyltransferase activity	2.92×10^{-4}
RNA binding	2.39×10^{-3}
protein serine/threonine kinase activity	6.93×10^{-3}
voltage-gated sodium channel activity	1.54×10^{-2}
AF-2 domain binding	3.16×10^{-2}
transferase activity	4.46×10^{-2}

Table 3.2: RBPs predicted by multiple online algorithms as targets of miR-132.

Gene Symbol	**Prediction algorithm**					
	miRanda	miRDB	PICTAR	PITA	Targetscan	MiRZ
AGO1	**Yes**	No	No	**Yes**	**Yes**	**Yes**
AGO2	**Yes**	No	**Yes**	**Yes**	**Yes**	**Yes**
ATXN1	**Yes**	No	No	No	**Yes**	**Yes**
CUGBP2	**Yes**	No	No	**Yes**	**Yes**	**Yes**
FXR1	No	No	No	**Yes**	**Yes**	**Yes**
HNRNPM	**Yes**	No	No	**Yes**	**Yes**	**Yes**
HNRNPU	No	**Yes**	**Yes**	**Yes**	**Yes**	No
LSM11	**Yes**	No	No	**Yes**	**Yes**	**Yes**
NOVA1	**Yes**	**Yes**	**Yes**	**Yes**	**Yes**	**Yes**
PAPOLA	**Yes**	No	**Yes**	**Yes**	**Yes**	**Yes**
PTBP2	**Yes**	**Yes**	**Yes**	**Yes**	**Yes**	**Yes**
QKI	**Yes**	No	**Yes**	**Yes**	**Yes**	**Yes**
SFRS1	**Yes**	No	No	**Yes**	**Yes**	**Yes**

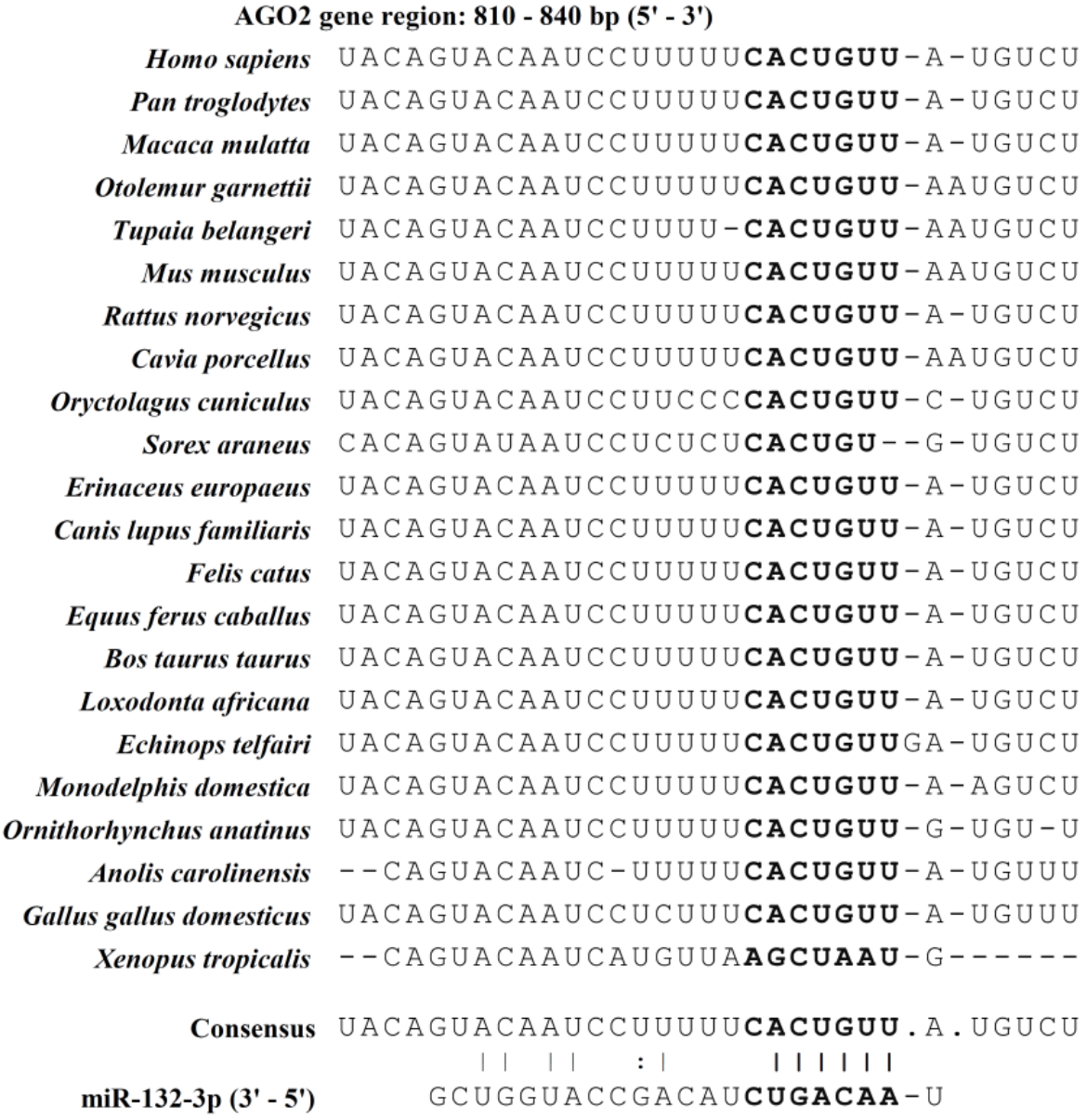

Figure 3.2: AGO2 sequence alignment with miR-132 across different species. Seed sequence is highlighted in bold.

3.2 miR-132/AGO2 binding and silencing activity

Based on target prediction and miR-132/AGO2 alignment (Figure 3.2), miR-132-3p was predicted to target only one sequence in the 3'UTR of AGO2. In order to demonstrate that miR-132 indeed binds the specific 3'UTR site of AGO2, the AGO2 miR-132 binding site at positions 2-4 of miR-132 was mutated from GUU to AAA:

WT: 5′-GUACAAUCCUUUUUCACUGUUU-3′

Mut: 5′-GUACAAUCCUUUUUCACUAAAU-3′

The concentration of miR-132 mimics appropriate for miR-132 mediated AGO2 regulation were determined by titration and presented later in Section 3.3.2. The wild-type AGO2 full length 3'UTR, the mutated AGO2 3'UTR and a positive control EP300 full length 3'UTR were expressed (40 nM) as part of a luciferase gene construct in HeLas. The introduction of miR-132 mimics (20 nM) suppressed the activity of the luciferase reporter in wild type AGO2 3'UTR and wild type EP300 3'UTR reporters, but not when AGO2 3'UTR was mutated (Figure 3.3). The level of luciferase signal suppression was approximately 35% for AGO2 and 45% for EP300. These experiments in HeLas were performed by Kunal Shah (Barts Cancer Institute, UK).

In order to determine if the suppression of AGO2 would alter the silencing activity of AGO2, Kunal Shah (Barts Cancer Institute, UK) also performed a silencing activity assay. In this experiment, a constitutively active luciferase promoter is regulated by either a single fully complementary *let-7* binding site located in the 3'UTR of the luciferase gene (*si*), or 7 times repeat of mismatched *let-7* binding sites (*mi7*). If AGO2 is regulated by miR-132, the activity of AGO2 to silence the luciferase gene by miRNA-mediated silencing should decrease. This was observed both when knocking down AGO2 directly, or by miR-132 overexpression (Figure 3.4), confirming that miR-132 targets AGO2, affecting miRNA mediated silencing.

The results showed that miR-132 suppresses the predicted region on the AGO2 3'UTR, allowing to investigate miR-132 regulation of AGO2 in HDLECs.

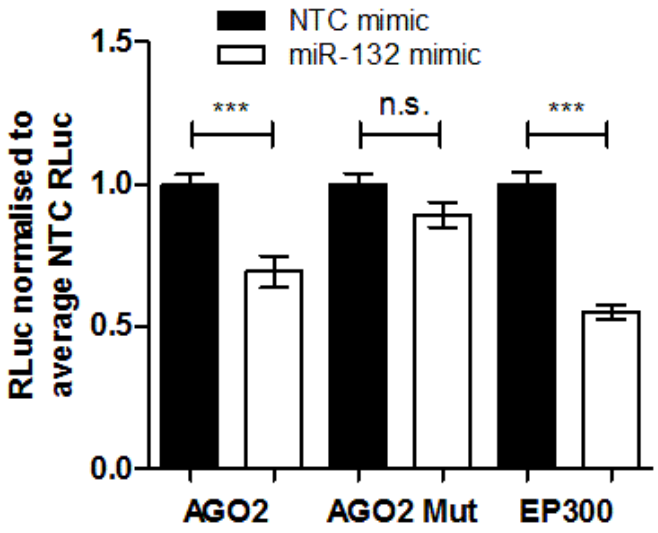

Figure 3.3: Luciferase activity assay in HeLas demonstrating that miR-132 overexpression reduces luciferase activity by suppressing EP300 3'UTR and AGO2 3'UTR, but not a mutated AGO2 3'UTR ($n = 3$, mean $\pm$ S.E.M.).

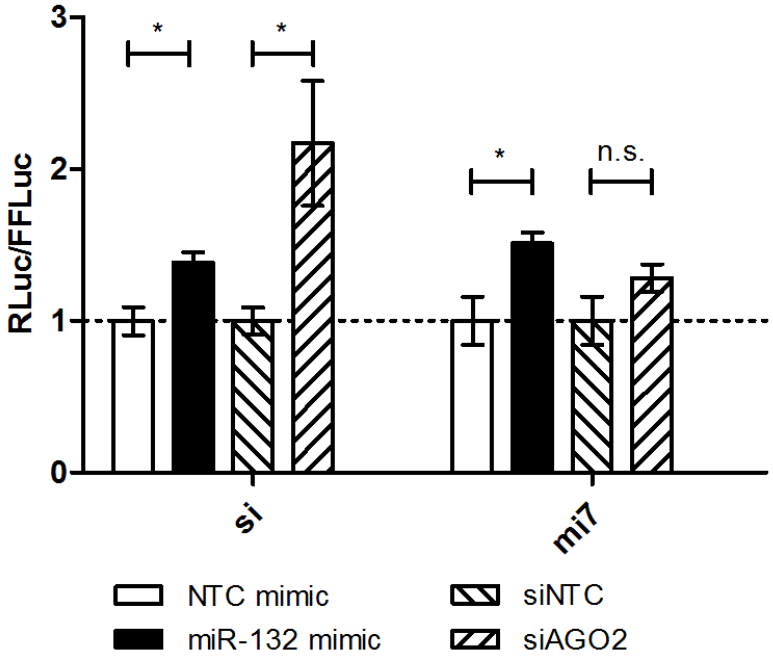

Figure 3.4: Silencing activity reporter assay demonstrating the *let-7* target site silencing activity in HeLas ($n = 3$, mean $\pm$ S.E.M.).

3.3 miR-132 overexpression

Several approaches were taken to demonstrate the regulation of AGO2 by miR-132 in LECs: the transduction of lentiviral vector with a constitutively active promoter expressing pri-miR-132, the transfection of miR-132 mimics (miRIDIAN) and the endogenous activation of miR-132 through the activation of LECs. In this section the first two methods of exogenous miR-132 introduction are presented.

3.3.1 pri-miR-132 lentiviral transduction

The transduction of lentiviral expression vectors differs from the mimics transfection – the constitutively active promoter produces a full length primary miR-132 transcript, which is subject to processing steps, that require miRNA biogenesis machinery within the cell, prior to its loading onto AGO. Following the initial screen that looked at potential miR-132 predicted targets at the mRNA level (Figure 3.1), the protein expression was determined using lentiviral overexpression of a wild type pri-miR-132 and a mutated pri-miR-132 (Lagos et al., 2010). After processing, the mutated miR-132 was unable to suppress AGO2 protein expression compared to the wild type miR-132 (Figure 3.5).

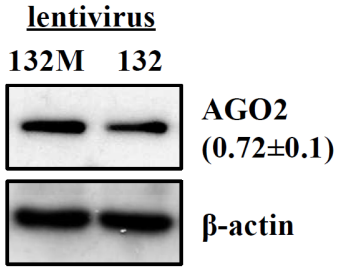

Figure 3.5: Lentiviral overexpression of pri-miR-132 (132) and mutated pri-miR-132 (132M) in LECs for 72 hours: effect on AGO2 protein expression ($n = 2$, mean $\pm$ S.E.M.)..

3.3.2 miRIDIAN mimics transfection

During miR-132 mimics transfection the mimics are taken up by the cell, with only a small fraction of it loaded onto AGO to form functional RISC (Thomson et al., 2013). HeLa cells were used for the initial miR-132 mimics transfections, in order to investigate the level of AGO2 suppression. As a result of miR-132 overexpression, AGO2 was significantly downregulated at the mRNA level (Figure 3.6a). As a consequence of the loss of AGO2 mRNA, the protein output was also decreased for AGO2 (Figure 3.6b), but not AGO1.

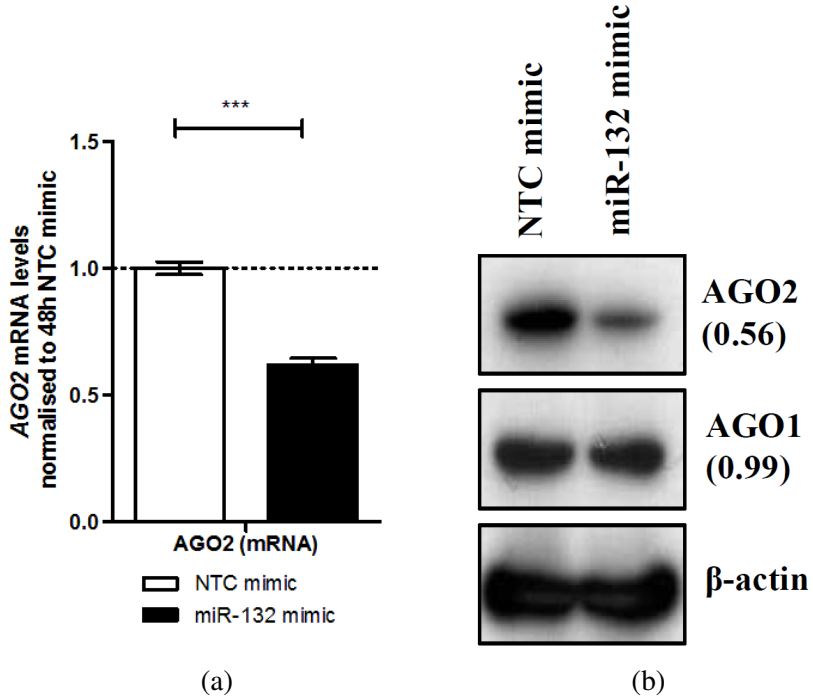

(a) (b)

Figure 3.6: Overexpression of miR-132 miRIDIAN mimics in HeLas for 48 hours: relative levels of *AGO2* mRNA, AGO1 protein and AGO2 protein ($n = 3$, mean $\pm$ S.E.M.; 1 replicate for (b)).

For LECs, the aim was to choose a concentration of miR-132 mimics to be used for further experiments where AGO2 and a positive control were suppressed, without using an excess amount of transfected miR-132 in order to reduce off-target effects and cut costs. Thereby, miR-132 mimics were transfected into LECs across a range of concentrations in order to determine the effective range of miR-132-induced regulation of its targets. Both AGO2 and the previously published target RASA1 (Anand et al., 2010) were downregulated

when using > 12.5 nM concentration of transfected miR-132 mimics (Figure 3.7). The concentration of 25 nM was chosen for further experiments performed in LECs.

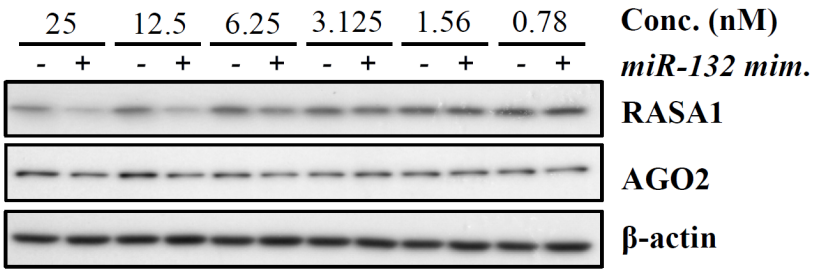

(a)

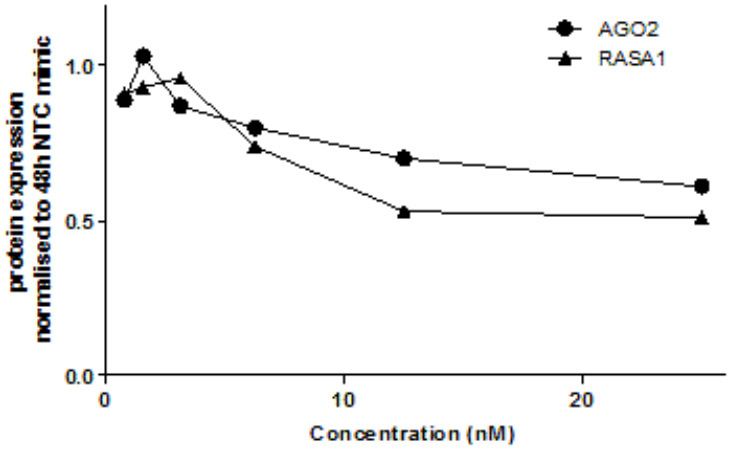

(b)

Figure 3.7: Titration of miR-132 mimics in LECs for 48 hours ($n = 1$).

Similar to the results of miR-132 overexpression in HeLas (Figure 3.6), the LECs showed a similar downregulation of *AGO2* mRNA and protein (Figures 3.8a-3.8b). EP300 and RASA1 served as positive controls, however only 2 successful replicates were completed to this stage for EP300 protein detection, with a large deviation from the mean in the measured response, making it an unreliable control. The optimisation to improve EP300 detection in LECs is presented in section A.1 – EP300 antibody optimisation.

Indeed, the transfection of miR-132 into LECs resulted in a large abundance of detectable miR-132 (Figure 3.8c). Since miR-132 overexpression decreased the amount of AGO2 in LECs, it was expected that the loss of AGO2 would globally affect the abun-

dance of other miRNAs (Winter and Diederichs, 2011) and result in decreased processing (Diederichs and Haber, 2007). The measured expression of two miRNAs, miR-126 and miR-221 – both highly expressed (Lagos et al., 2010) and essential for LECs role in angiogenesis (Fish et al., 2008; Zhu et al., 2011; Nicoli et al., 2012; Poliseno et al., 2006) – showed a decrease (Figure 3.8c), most likely due to the decrease in AGO2 protein expression. Additionally, the expression of the primary miR-126 transcript remained unchanged (Figure 3.8d), resulting in a drop of the mature to primary miR-126 ratio. Notably, this confirms that miR-132 mediated loss of AGO2 does not affect the transcription of the primary miR-126, but rather reduces the abundance of the mature miR-126 through the mechanism of miRNA loaded RISC complex associated stability or AGO2-related miRNA processing.

The overexpression of miR-132 in LECs demonstrated that AGO2 expression can be regulated to a similar extent as the already confirmed targets EP300 (Lagos et al., 2010) and RASA1 (Anand et al., 2010), and that the regulation of AGO2 impacts on the abundance of other miRNAs, miR-126 and miR-221. To further our understanding of endothelial cell function during this regulation the following section describes the effect of endogenous miR-132 induction in the context of LEC activation.

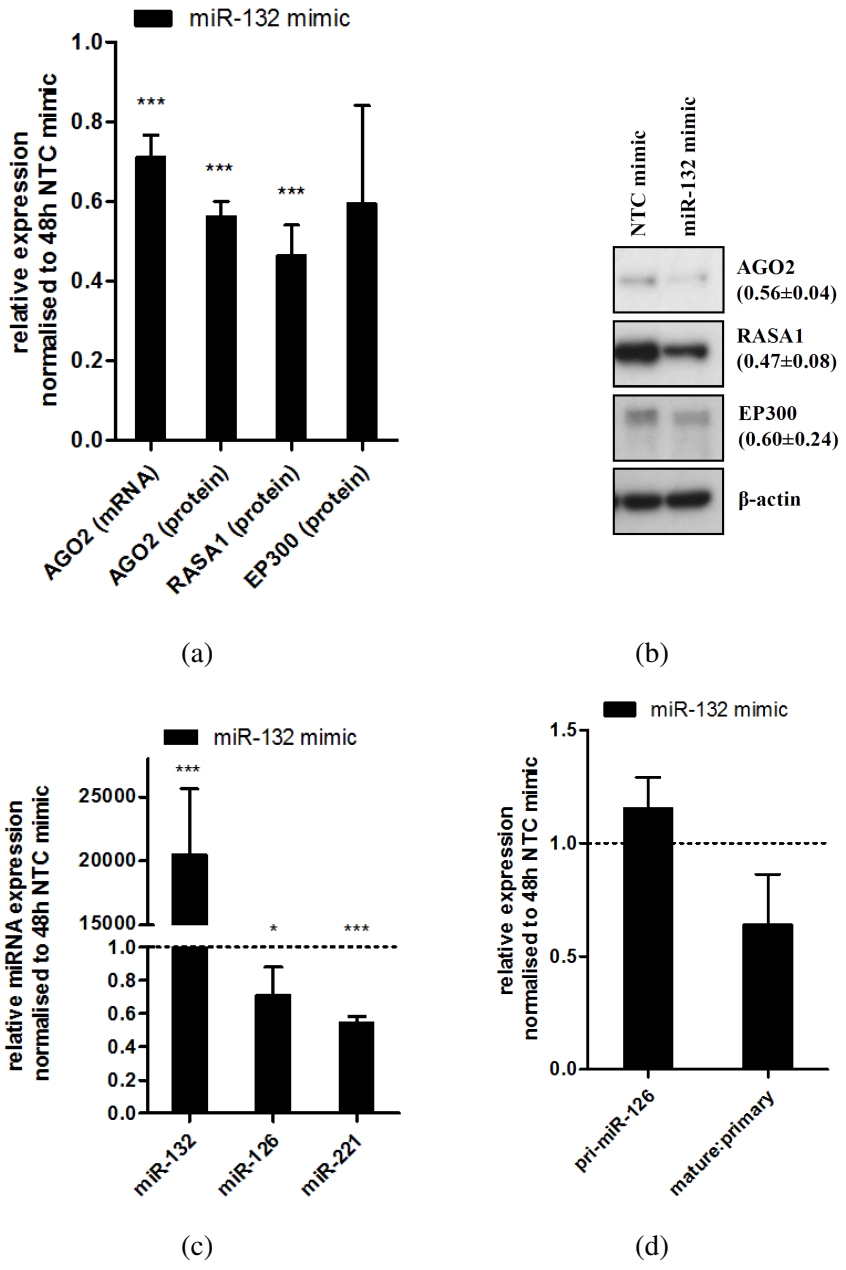

Figure 3.8: Overexpression of miR-132 mimics in LECs for 48 hours: relative levels of *AGO2* mRNA and protein, and RASA1 and EP300 protein (a, b), miR-126, miR-132 and miR-221 expression (c), with pri-miR-126 expression and mature:primary miR-126 ratio (d) ($n = 3$, mean $\pm$ S.E.M.; 2 replicates for EP300 protein (b) and pri-miR-126 (d); 5 replicates for AGO2 protein (b)).

3.4 Endogenous miR-132 activation

The activation of endogenous miR-132 expression can be achieved by PMA in neurons (Remenyi et al., 2010; Vo et al., 2005). PMA is a small molecule drug that potently activates protein kinase C signalling, which results in cell activation and promotes angiogenesis in LECs (Montesano and Orci, 1987). In order to determine the PMA concentration necessary to activate miR-132 transcription in LECs, a titration of PMA was performed over a time period of 48 hours. LECs, when exposed to 10 to 200 nM concentration of PMA, express a similar amount of miR-132 over the 48 hour period (Figure 3.9). For all following experiments 25 nM concentration was used to induce miR-132 expression in LECs.

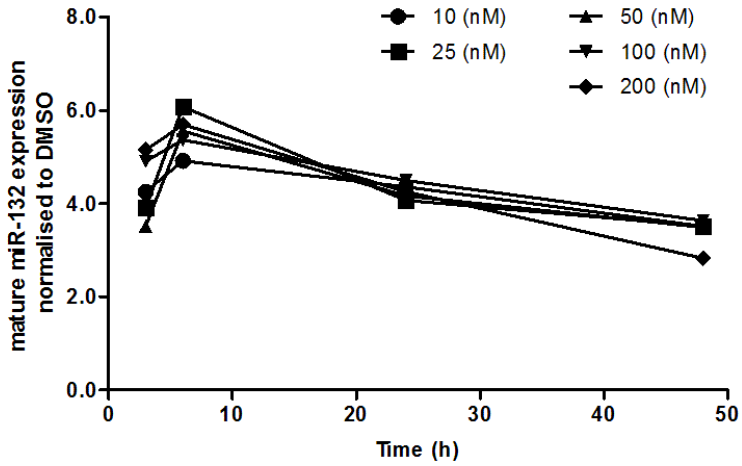

Figure 3.9: The level of mature miR-132 in LECs over a 48 hour period across different PMA concentrations ($n = 1$).

As a result of PMA treatment in LECs, Figure 3.10 shows that the resulting CREB phosphorylation is rapid (peak 30 min), with pCREB levels returned to baseline by 24 hours. The phosphorylation of CREB is necessary for the induction of miR-132 (Remenyi et al., 2010), and the recruitment of EP300 (Mayr and Montminy, 2001). The activation of LECs by PMA increase mature miR-132 expression and sustains it over the course of 24 hours (Figure 3.11a). Mature miR-132 is upregulated 5-fold, however the transcriptionally activated pri-miR-132 expression returns to baseline at the 24 hour time point (Figure 3.11b). The rel-

ative expression profile of pri-miR-132 fits the expression profile of pCREB (Figure 3.10), supporting Remenyi et al. (2010); Vo et al. (2005) findings that miR-132 is upregulated by PMA through transcriptional activation.

In addition, *AGO2* mRNA is significantly upregulated in the first 6 hours after PMA treatment (Figure 3.11c), with no change in *EP300* mRNA (Figure 3.11d). This results in a significantly increased level of AGO2 protein expression at 6 hours post-PMA treatment (Figure 3.13c-3.13d).

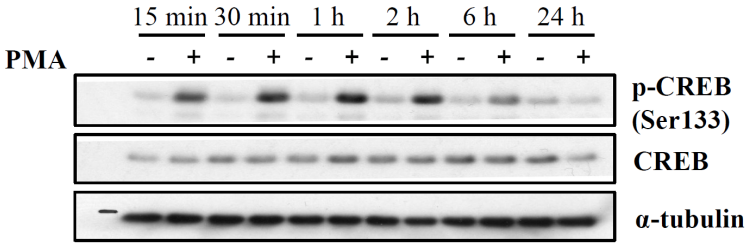

(a)

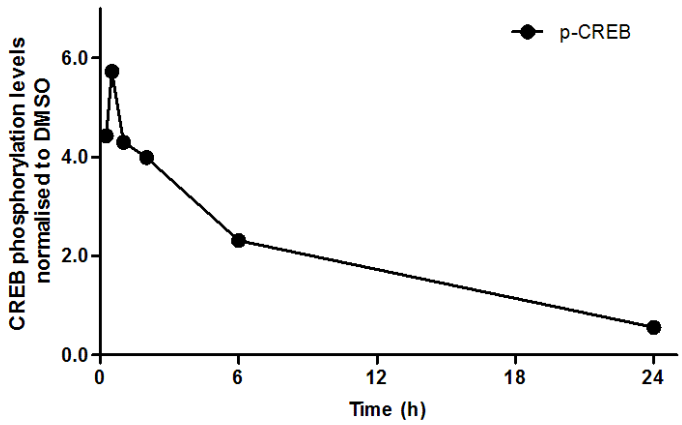

(b)

Figure 3.10: PMA triggered activation of CREB phosphorylation over 24 hours in LECs (immunoblot (a) and densitometry (b)) ($n = 1$).

The fact that PMA activation of LECs affects the expression of *AGO2* mRNA as well as miR-132 creates a regulatory feedback loop, assuming miR-132 levels reach high enough expression to impact on AGO2 protein expression. In order to further understand this regulation, miR-132 would need to be inhibited to compare the effect of PMA activation during miR-132 upregulation and inhibition.

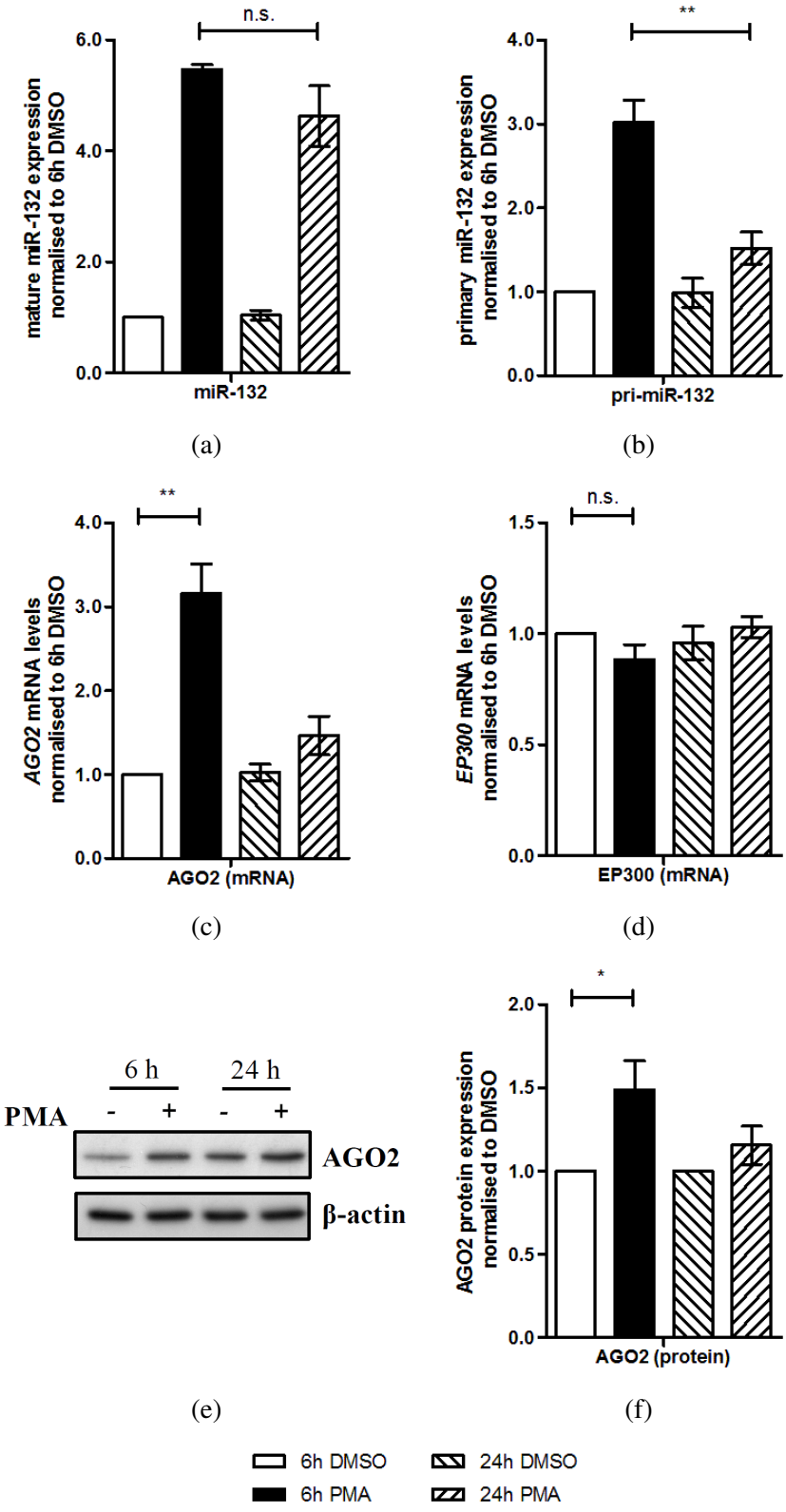

Figure 3.11: PMA triggered activation of LECs: relative levels of mature (a) and primary miR-132 (b), *AGO2* (c) and *EP300* mRNA (d), and AGO2 protein (immunoblot (e), densitometry (f)) 24 and 48 hours post-treatment ($n = 3$, mean $\pm$ S.E.M.).

3.5 miR-132 inhibition in activated LECs

The activation of LECs results in the simultaneous upregulation of miR-132 and AGO2. In order to distinguish the effect of miR-132 induced regulation on AGO2 expression during LEC activation, miR-132 was inhibited using 2 different miR-132 inhibitors - hairpin based miRIDIAN inhibitors and LNA-based inhibitors.

3.5.1 miRIDIAN inhibitors transfection

The hairpin miRIDIAN inhibitors of miR-132 significantly reduced the miR-132 expression in LECs, but failed to reduce miR-132 expression in activated LECs (Figure 3.12a). As recorded previously in Figure 3.11c, the level of *AGO2* mRNA upregulation 24 hours after PMA treatment was not significant. There was no regulation occurring during any treatment condition at the mRNA level for EP300 (Figure 3.12c). The expression of AGO2 protein 24 hours post-PMA treatment remained significantly increased (Figure 3.12d-3.12e).

Since the expression of miR-132 could not be effectively suppressed by miR-132 hairpin inhibitors, none of the miR-132-linked regulatory effects could be observed nor interpreted. Therefore, a more stable form of inhibitors needed to be tested for the same treatment conditions.

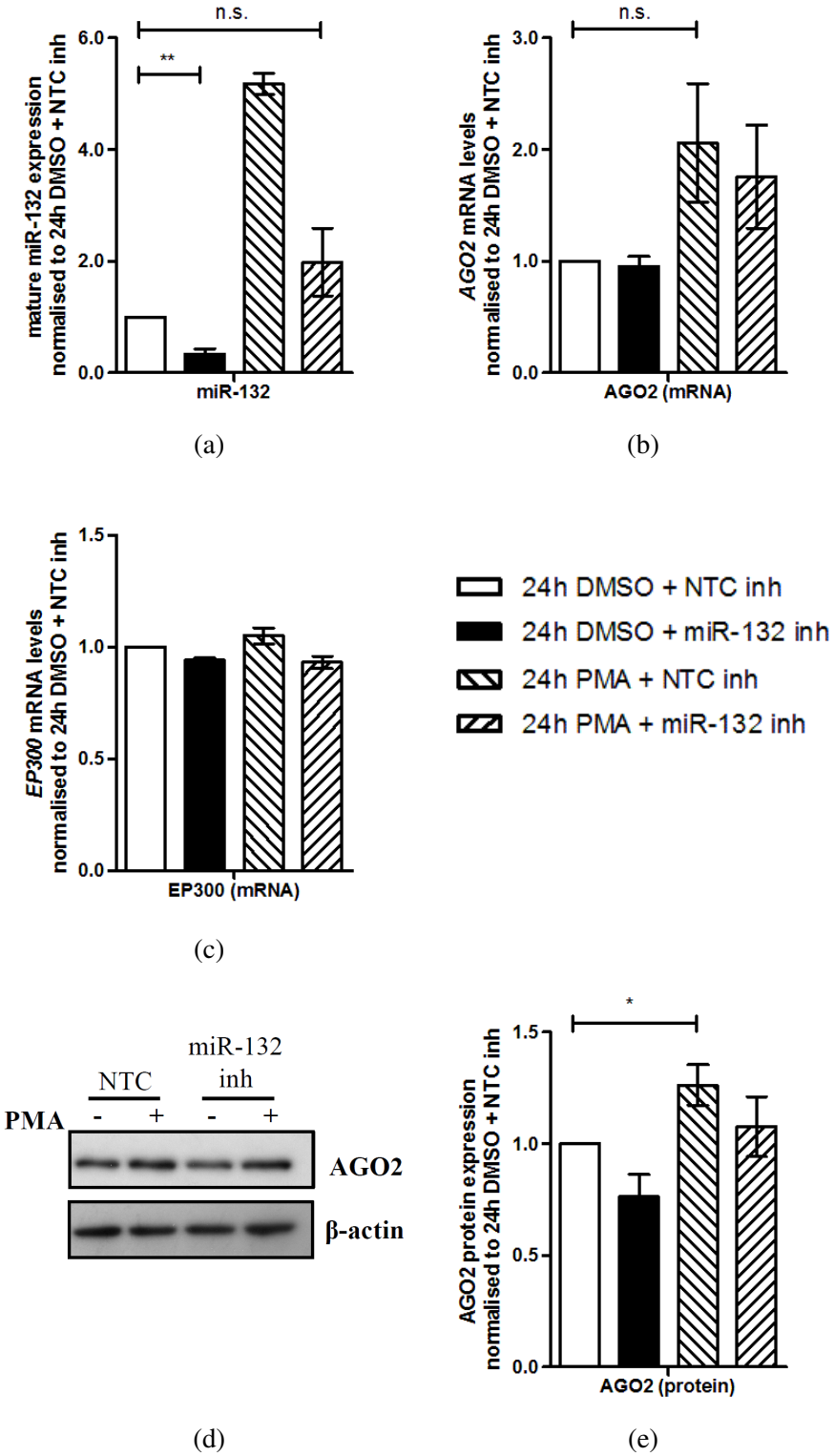

Figure 3.12: Inhibition (miRIDIAN) of miR-132 in PMA-activated LECs: relative levels of mature miR-132 (a), *AGO2* (b) and *EP300* mRNA (c), and AGO2 protein (immunoblot (d), densitometry (e)) 24 hours post-treatment($n = 3$, mean $\pm$ S.E.M.; only 2 replicates for (c)).

3.5.2 LNA-based inhibitors transfection

Using the LNA-based miR-132 inhibitors it was possible to suppress miR-132 expression in both PMA-activated LECs as well as the untreated (DMSO) control LECs (Figure 3.13a). Inhibiting miR-132 without activation resulted in a mild but significant upregulation of *AGO2* mRNA, and the activation of LECs maintained above baseline expression of *AGO2* mRNA 24 hours post-PMA treatment (Figure 3.13b). Similar to previous findings, AGO2 protein expression was increased as a result of PMA 24 hours post-treatment, however the inhibition of miR-132 in PMA-activated LECs did not reach significant change compared to the effects of the PMA alone (Figure 3.13d). Nevertheless, AGO2 protein expression followed a trend where miR-132 inhibition in activated LECs derepressed AGO2 protein expression in each individual replicate condition (Figure A.3).

The aim of miR-132 inhibition was to observe and record the effect of miR-132 during PMA-activation of LECs, however PMA-activation was the bigger contributing factor to modulating the expression levels of miR-132 targets. Therefore, it was difficult to observe small differences between replicate conditions, which can be attributed to two observations:

1. PMA induced upregulation of miR-132 had high variance (variance $\sigma^2 = 2.39$, mean $\mu = 4.95$) between the replicate conditions (Figure 3.13a)

2. AGO2 protein expression was significantly affected by PMA treatment, with increased variance (variance $\sigma^2 = 0.43$, mean $\mu = 1.96$) when miR-132 was inhibited

Based on the observed trend on AGO2 expression (Figure 3.13d), we tested the expression of miR-126, miR-221 and miR-146a (Taganov et al., 2006), miRNAs important for LEC function as described in section 1.2.5.1. Since AGO2 regulation was not observed to a significant extent during miR-132 inhibition in activated LECs, it was expected that most of the impact on other miRNAs will be due to the effects of PMA: miR-126 expression did not change significantly (Figure 3.14a), miR-146a was significantly upregulated (Figure 3.14b) and miR-221 was significantly downregulated (Figure 3.14c) in response to PMA. Unex-

pectedly, the transcription of primary miR-126 was decreased in response to the combined effect of miR-132 inhibition and PMA treatment.

Since the positive control (RASA1) which should have been affected by miR-132 inhibition in activated LECs did not reach significance between 2 treatment conditions in PMA activated LECs, it did not refute the hypothesis that endogenously upregulated miR-132 regulates AGO2 expression in LECs, suggesting that an alternative experimental approach is needed to further investigate miR-132 mediated regulation of its targets in LECs.

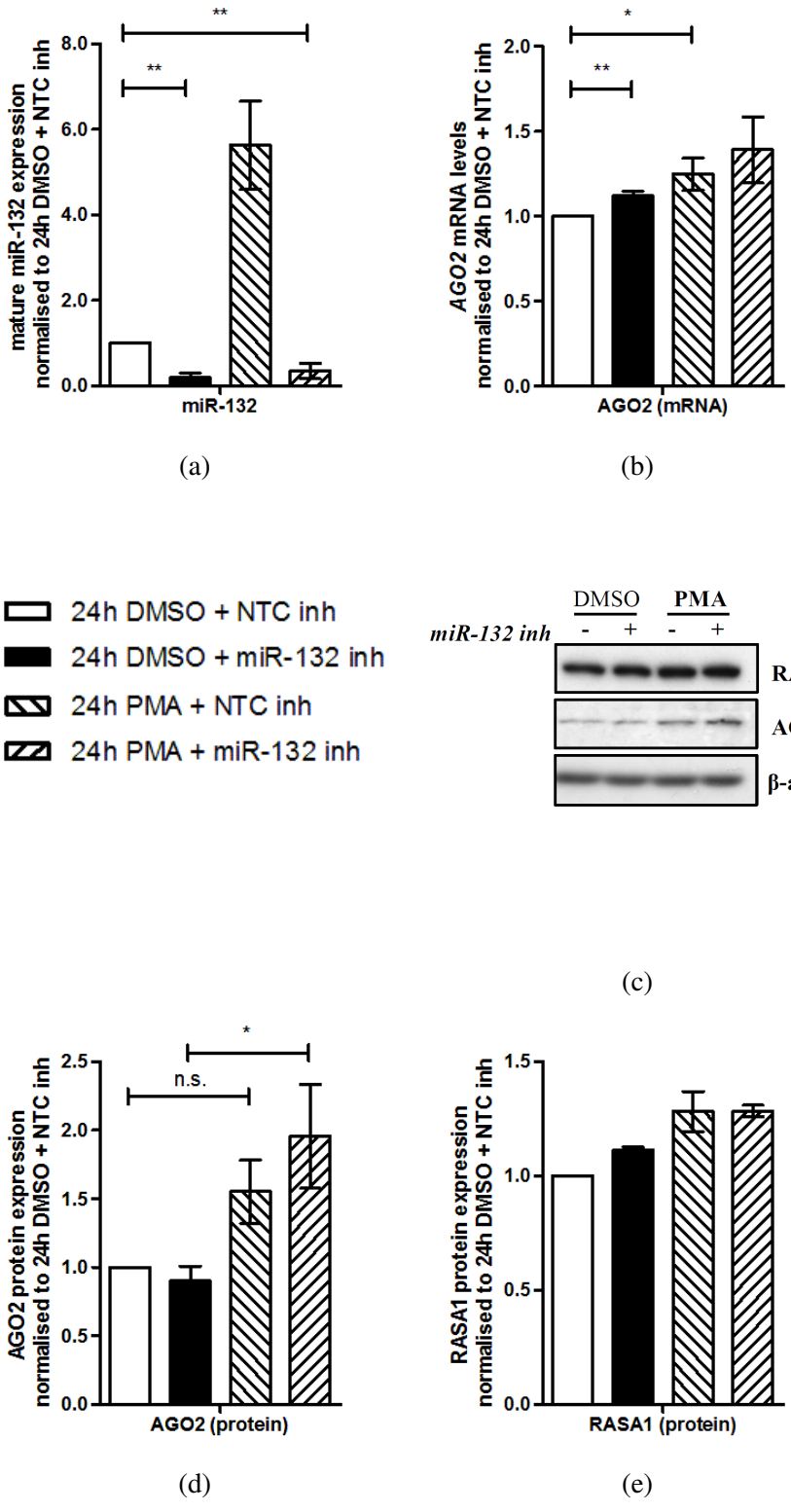

Figure 3.13: Inhibition (LNA) of miR-132 in PMA-activated LECs: relative levels of mature miR-132 (a), *AGO2* mRNA (b), AGO2 (c) and RASA1 protein (d) 24 hours post-treatment ($n = 4$, mean $\pm$ S.E.M.; only 2 replicates for (e)).

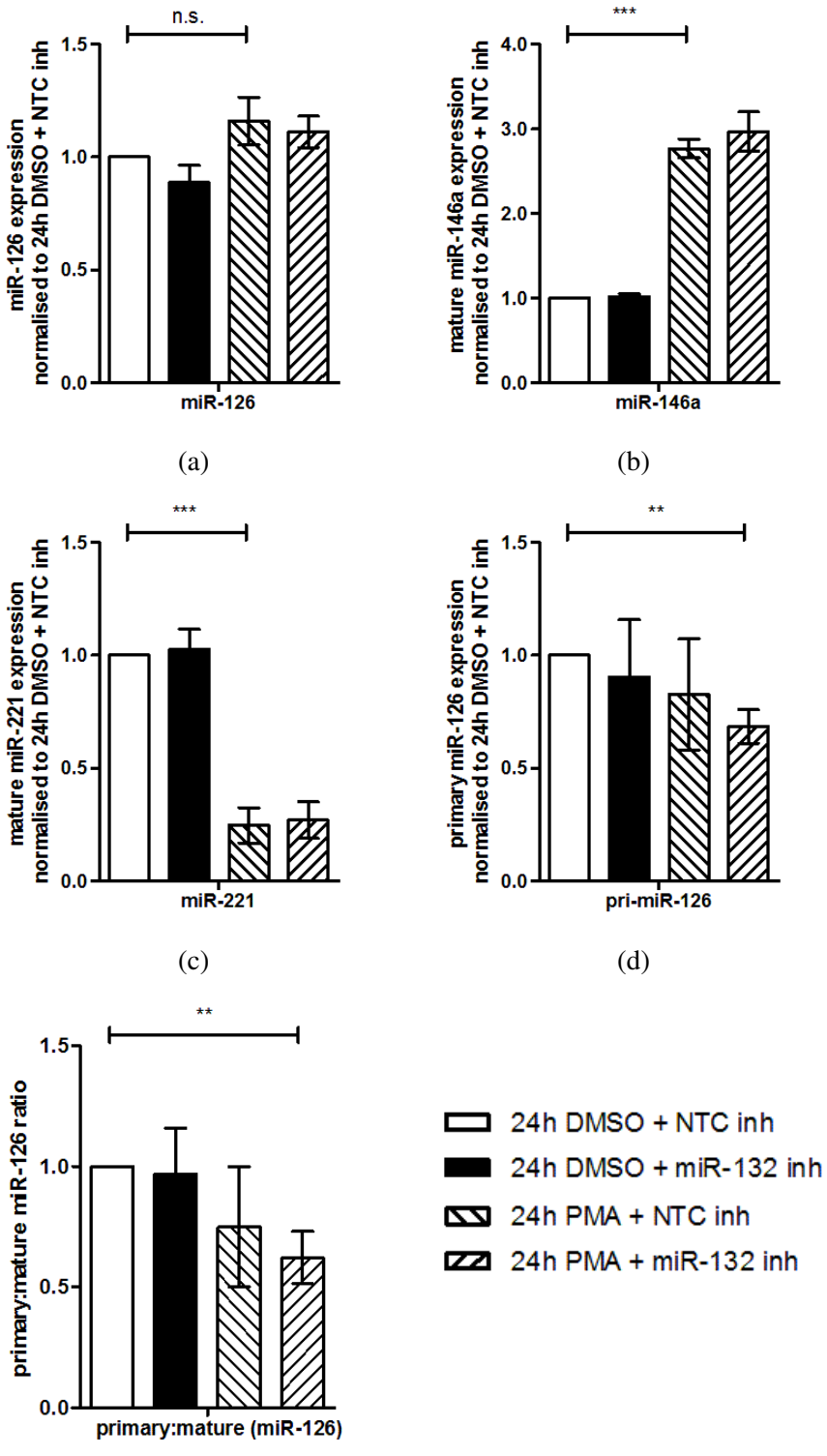

Figure 3.14: Inhibition (LNA) of miR-132 in PMA-activated LECs: relative levels of mature miR-126 (a), miR-146a (b), miR-221 (c) and pri-miR-126 (d), and the mature:primary miR-126 relative expression (e) 24 hours post-treatment ($n = 3$, mean $\pm$ S.E.M.; 2 replicates for (d and e); 4 replicates for (a)).

3.6 Effect of AGO2 regulation

Keeping in mind that miR-132 overexpression demonstrated that AGO2 can be regulated by miR-132, the functional role of AGO2 was the focus of the next set of experiments. The aim was to demonstrate that small changes in AGO2 expression affected its function to modulate miRNA abundance.

3.6.1 siRNA-mediated knockdown

Downregulation of AGO2 can be achieved by siRNA-mediated knockdown, which should results in a significant loss of AGO2 protein and thereby reduce miRNA abundance in response to AGO2 depletion (Winter and Diederichs, 2011). The addition of siAGO2 for 48 hours resulted in a loss of *AGO2* mRNA and protein without affecting RASA1 protein expression (Figure 3.15a-3.15b. Consequently, the depletion of AGO2 negatively impacted on miR-126, miR-132 and miR-221 abundance. These results confirmed that AGO2 is needed to maintain high levels of miRNA abundance (Winter and Diederichs, 2011).

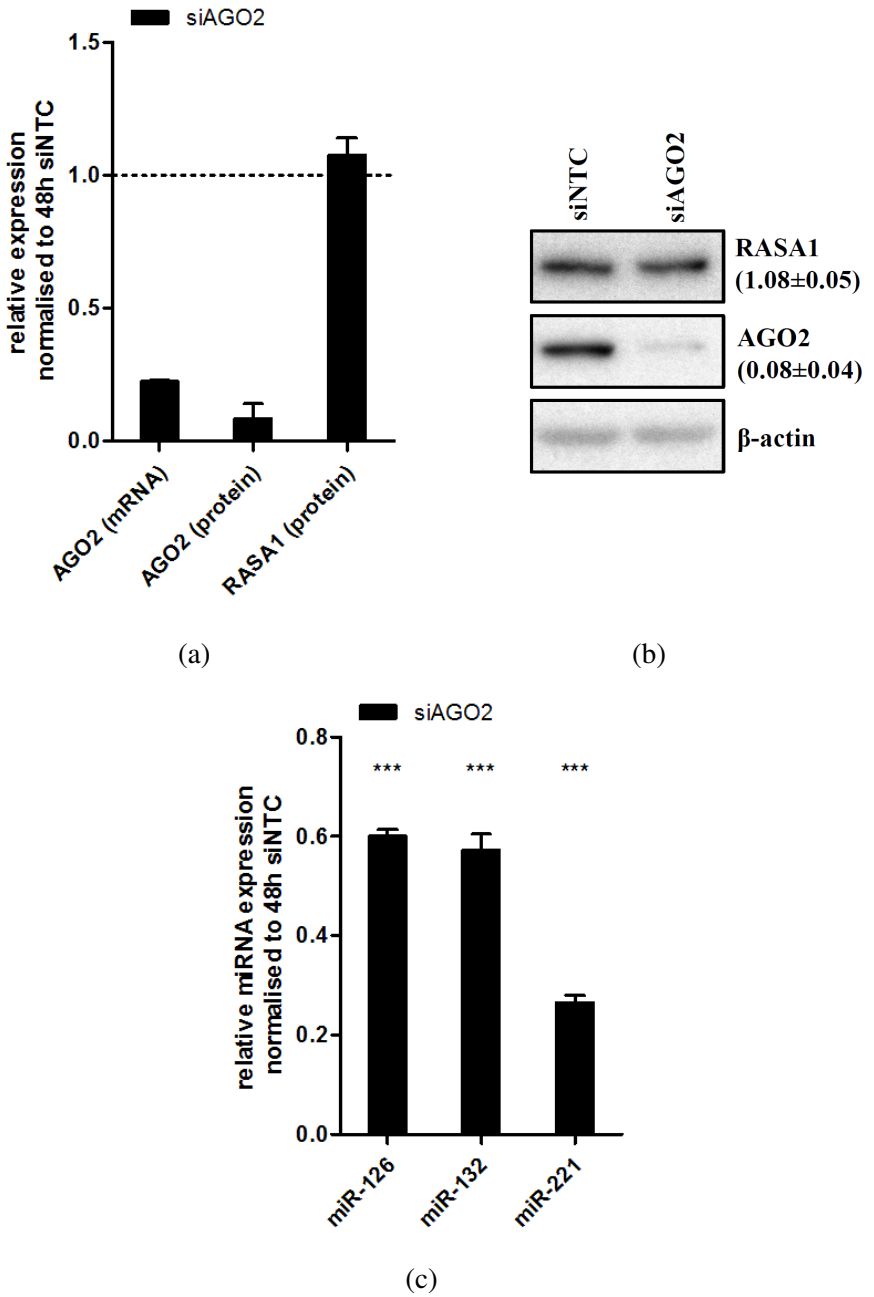

Figure 3.15: Knockdown of AGO2 in LECs for 48 hours: relative levels of *AGO2* mRNA and protein, and RASA1 protein (a, b), and miR-126, miR-132 and miR-221 expression (c) ($n = 4$, mean $\pm$ S.E.M.; only 2 replicates for (a, b)).

3.6.2 AGO2^{-UTR} lentiviral overexpression in activated LECs

Knowing that loss of AGO2 was sufficient to reduce miRNA abundance in LECs, the reverse had to be tested: does upregulating AGO2 increase miRNA abundance? Importantly, assuming that miR-132 expression during cell activation could impact on AGO2 expression (presented in a representative immunoblot in Figure 3.13c), AGO2 protein expression would need to be modulated by less than 5-fold. By accurately but mildly overexpressing AGO2 using a lentiviral construct with the full length AGO2 protein fused with M2-FLAG and lacking AGO2 3'UTR (cannot be targeted by miR-132), I aimed to investigate the effect of AGO2 upregulation in the context of activated endothelial cells and during overexpression miR-132.

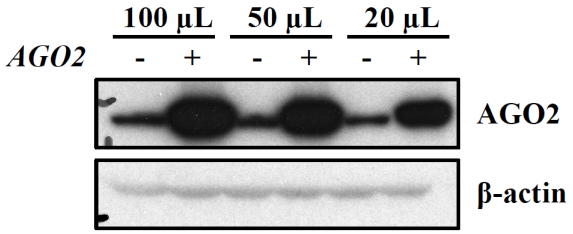

Figure 3.16: Titration of AGO2 lentiviral overexpression in LECs for 48 hours ($n = 1$).

The titration of the AGO2 lentiviral mix used to transduce LECs suggested that 20 µl is sufficient to give a mild overexpression of AGO2 protein (Figure 3.16) and was used for all following AGO2^{-UTR} overexpression experiments.

The overexpression of *AGO2* mRNA was successful (Figure 3.17a), resulting in a mild upregulation of AGO2 protein expression in activated and DMSO control conditions where AGO2 lentivirus was expressed (Figure 3.17b-3.17c). Interestingly, AGO2 overexpression or PMA alone also resulted in an increased expression of RASA1 protein expression (Figure 3.17d).

From the 4 miRNAs that were measured, miR-132, miR-126 and miR-146a were positively regulated by PMA, but not by AGO2^{-UTR} overexpression (Figure 3.18). On the other hand, miR-221 showed an increase in miR-221 levels in response to AGO2^{-UTR} over-

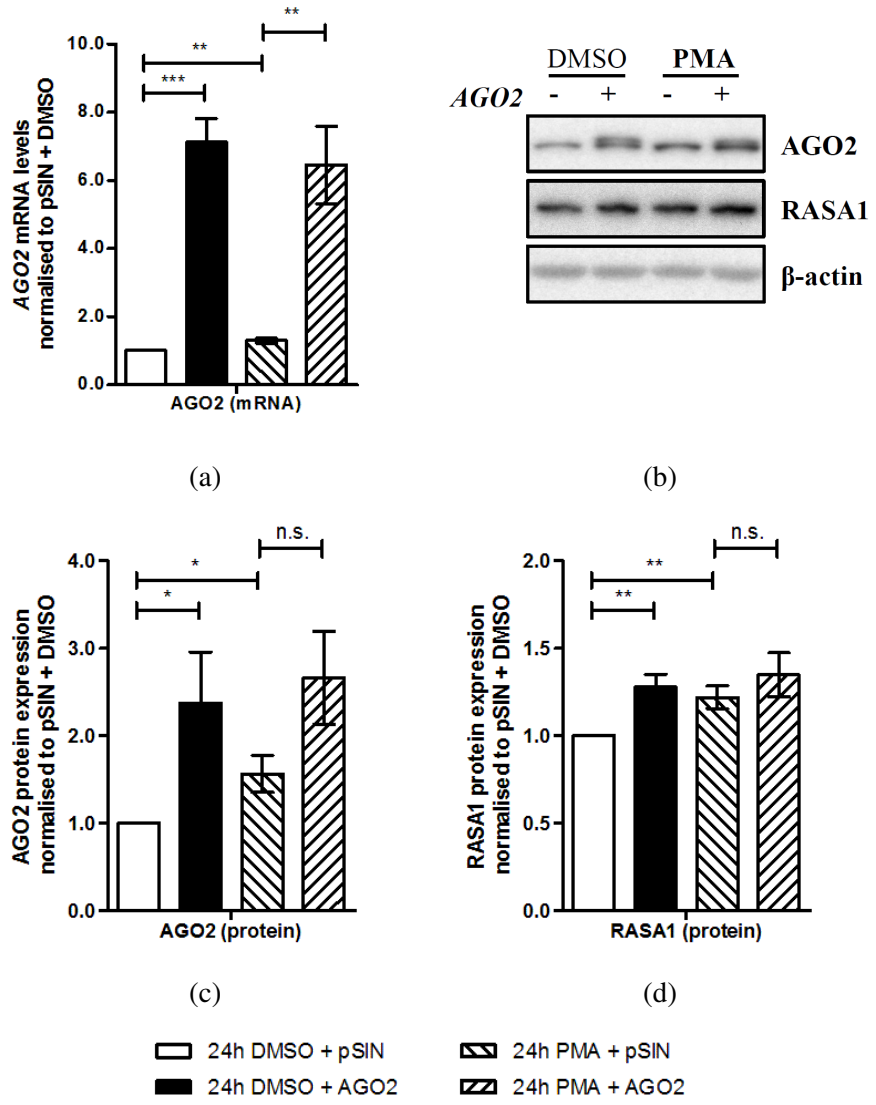

(a) (b) (c) (d)

Figure 3.17: Overexpression of AGO2^{-UTR} for 30 hours followed by LEC activation for 24 hours: relative levels of *AGO2* mRNA (a), and AGO2 and RASA1 protein (immunoblot (b), densitometry (c and d, respectively)) ($n = 3$, mean $\pm$ S.E.M.; 4 replicates for (a)).

expression and a decrease in response to PMA treatment (Figure 3.18d). Previously, PMA treatment did not reach a significant increase in inducing miR-126 expression (Figure 3.14a). This may be explained by the fact that PMA induced regulation was stronger in these sets of experiments: miR-132 was induced almost 8-fold (Figure 3.18a) compared to the LNA-inhibition experiments (Figure 3.13a).

The overexpression of AGO2^{-UTR} by ~2.5-fold (Figure 3.17c) did not show any con-

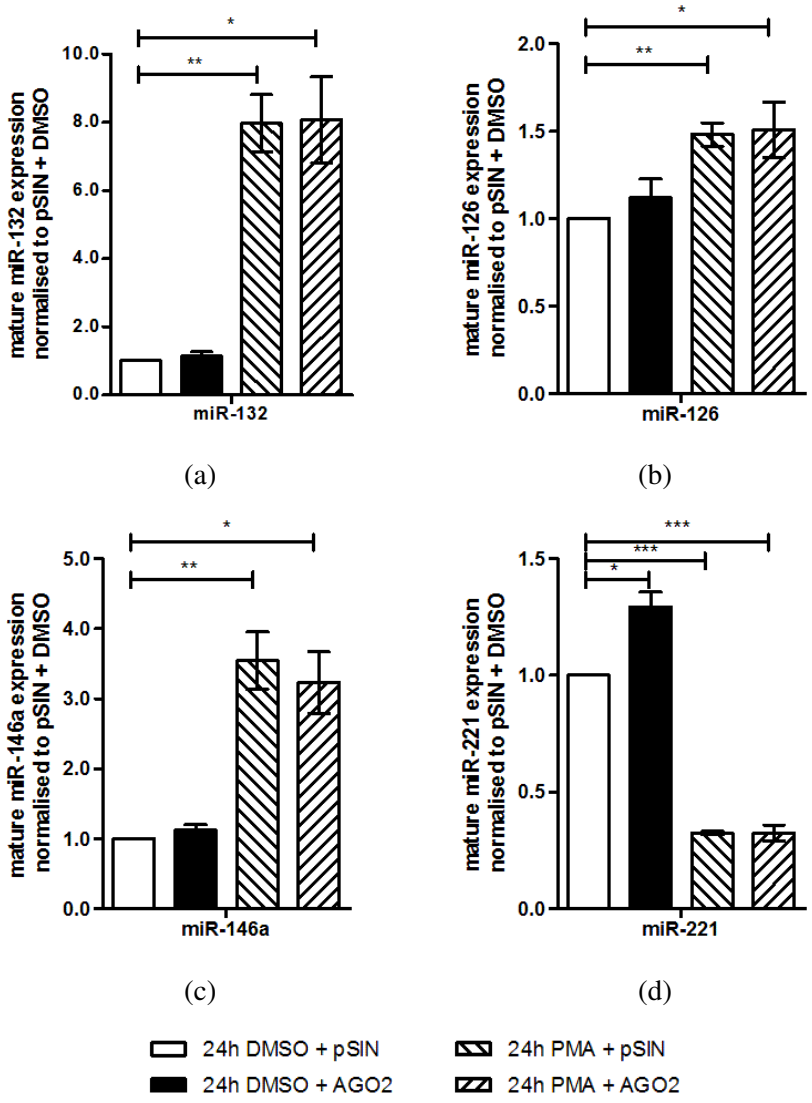

Figure 3.18: Overexpression of AGO2^{-UTR} for 30 hours followed by LEC activation for 24 hours: relative levels of miR-132 (a), miR-126 (b), miR-146a (c) and miR-221 (d) ($n = 4$, mean $\pm$ S.E.M.).

sistent noticeable regulatory effects on miRNA expression other than on miR-126 (Figure 3.18b). However, PMA induced effects on miRNA expression was significant in all cases (Figure 3.18). In order to determine if AGO2^{-UTR} overexpression and PMA had any effect on LEC gene expression, several mRNA candidates were chosen: Angiopoietin 2 (ANG2), Tyrosine kinase with Ig and EGF homology domains-2 (TIE2), Vascular Endothelial Growth Factor Receptor 1 (VEGFR1) and VEGFR3 (associated with LEC lin-

eage differentiation and function (Zheng et al., 2014; Hamaguchi et al., 2006; Olsson et al., 2006; Pan et al., 2009)), Interleukin 6 (IL6) (under the regulation of miR-132/EP300 feedback loop (Vanden Berghe et al., 1999)) and Sprouty-Related, EVH1 Domain Containing 1 (SPRED1) (a target of miR-126 and essential for LEC function (Fish et al., 2008)). In all cases PMA-induced LEC activation lead to an upregulation of all aforementioned mRNAs (Figure 3.19). Interestingly, AGO2 overexpression significantly affected TIE2 expression (Figure 3.19d). PMA induced LEC activation during AGO2^{-UTR} overexpression found that miR-221 and TIE2 are both responsive to AGO2 abundance. The regulation of TIE2 in the context of AGO2 regulation by miR-132 was further investigated (section 3.7.1).

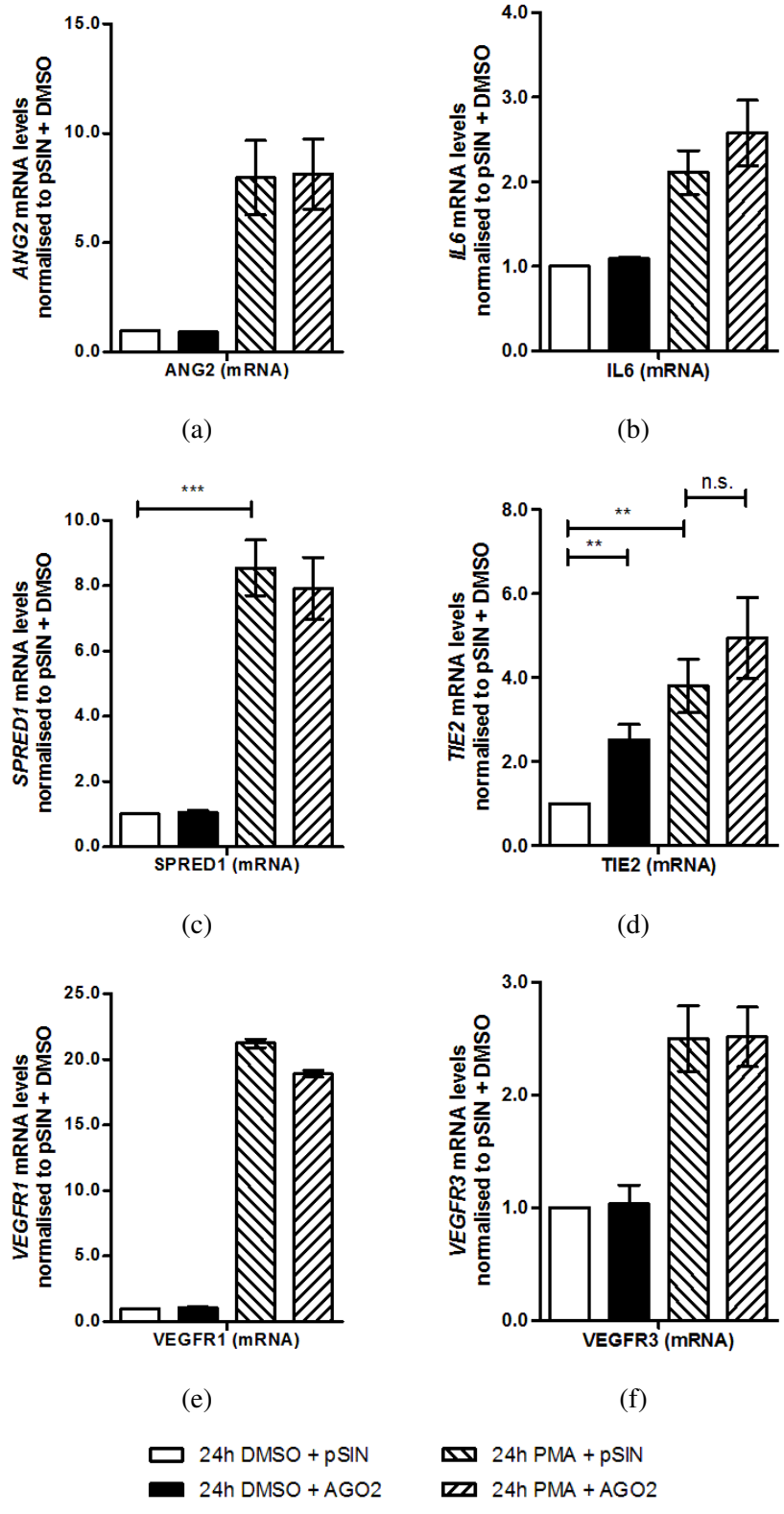

Figure 3.19: Overexpression of AGO2^{-UTR} for 30 hours followed by LEC activation for 24 hours: relative levels of *ANG2* (a), *IL6* (b), *SPRED1* (c), *TIE2* (d), *VEGFR1* (e) and *VEGFR3* (f) mRNA ($n = 3$, mean $\pm$ S.E.M.; 2 replicates for (a, b, e, f)).

3.6.3 AGO2^{-UTR} lentiviral overexpression in miR-132 overexpressing LECs

Another way of demonstrating that AGO2 regulation affects miRNA abundance is to use an AGO2 that cannot be targeted by miR-132, such as the lentiviral overexpression vector with AGO2^{-UTR}. The overexpression AGO2^{-UTR} in this set of experiments resulted in a much larger variance (variance $\sigma^2 = 57.79$, mean $\mu = 9.02$) of the overexpressed AGO2 mRNA (Figure 3.20a) and protein (Figure 3.20d,3.20c). This meant that statistical significance could not be *achieved* for AGO2 expression, although the lowest relative fold overexpression of AGO2 mRNA was 3.52 and highest 19.77. Despite the variance in the data, AGO2 was overexpressed. There was no notable change found in *SPRED1* mRNA expression (Figure 3.20b). RASA1 protein expression was downregulated by miR-132 overexpression as expected (Anand et al., 2010). Importantly, as seen in Figure 3.20c, the overexpressed AGO^{-UTR} (indicated by FLAG row) did not change, however there was a loss in total AGO2 protein expression (indicated by AGO2 row) as a result of miR-132 overexpression. Since the overexpressed AGO2 levels did not change in response to miR-132 overexpression, the loss of total AGO2 expression must be due to the endogenous AGO2 protein expression downregulation by miR-132. This effect could be observed in each replicate condition (Figure A.4).

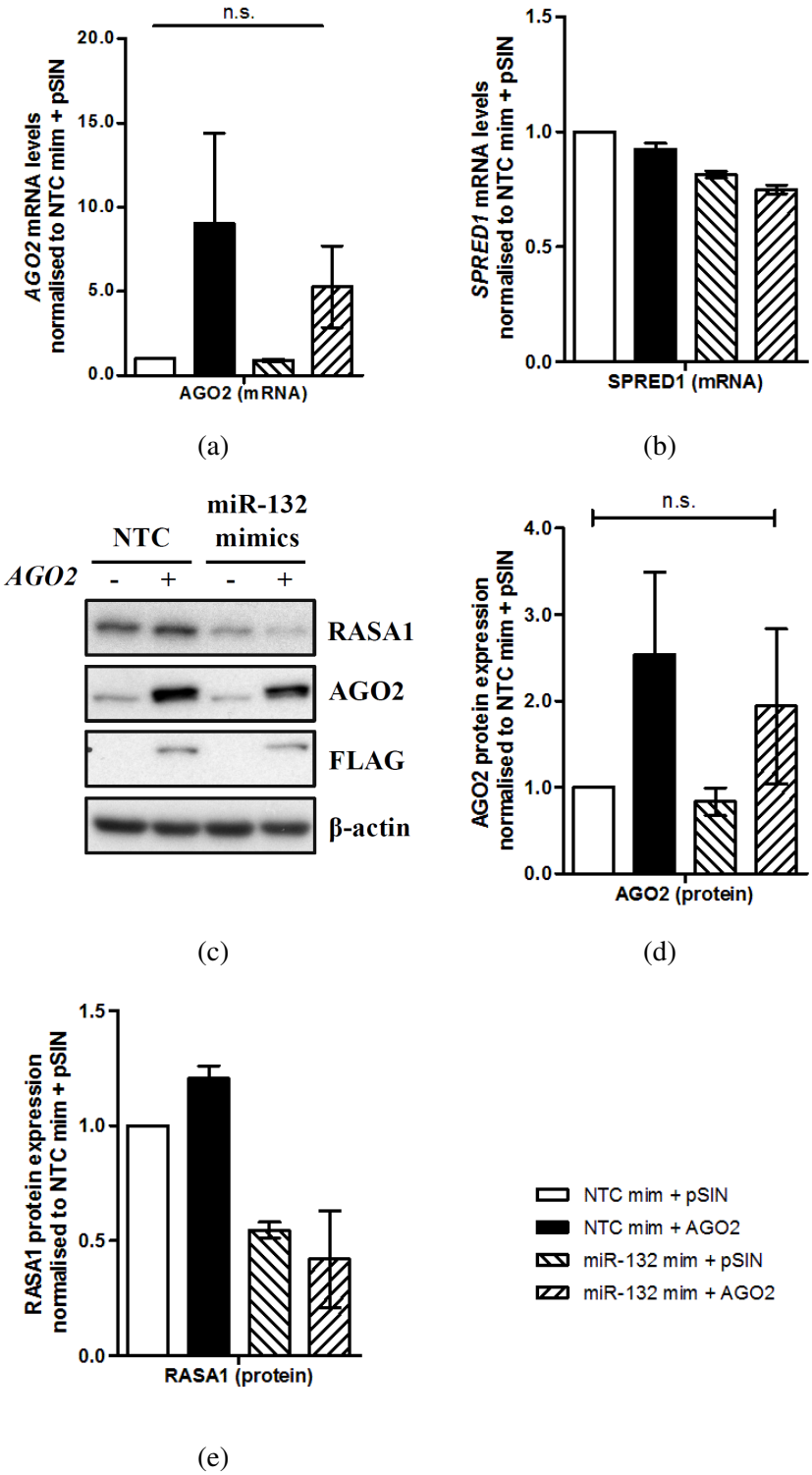

Figure 3.20: Overexpression of miR-132 mimics for 30 hours followed by AGO2^{-UTR} lentiviral overexpression for 24 hours: relative levels of *AGO2* (a) and *SPRED1* (b) mRNA, AGO2 and RASA1 protein (immunoblot (c), densitometry (d and e, respectively)) ($n = 3$, mean $\pm$ S.E.M.; only 2 replicates for (b and e)).

Unexpectedly, AGO2^{-UTR} overexpression resulted in a drop of mature miR-132 expression (Figure 3.21a), whereas no such drop was observed in miR-126 or miR-221 expression (Figures 3.21b-3.21c). For miR-126, the overexpression of miR-132 resulted in a drop of miR-126 abundance, which was partially rescued by overexpressing a non-targeted form of AGO2 (Figure 3.21b). It was only a partial recovery of miR-126 abundance, since the level of AGO2^{-UTR} overexpression was not sufficient to overcome the effect of miR-132 overexpression on miR-126 abundance.

The overexpression of AGO2, despite its large variance between experimental replicates, resulted in more tightly controlled responses in miRNA abundance. This suggests that despite the large differences in AGO2 overexpression, the overexpression of AGO2 protein elicits small effects on miRNA abundance in these AGO2^{-UTR} experimental conditions (Figures 3.18d, 3.21b).

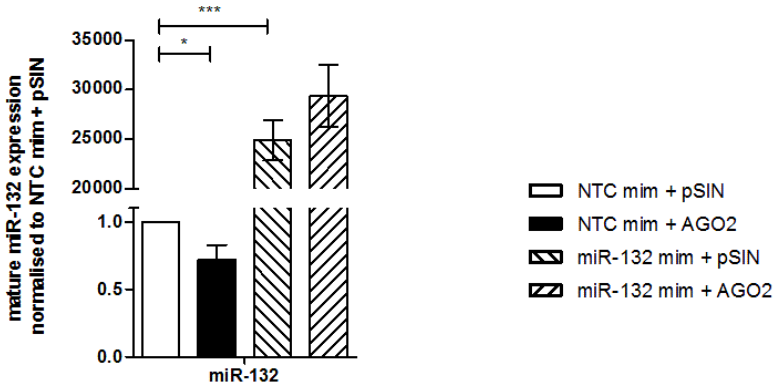

(a)

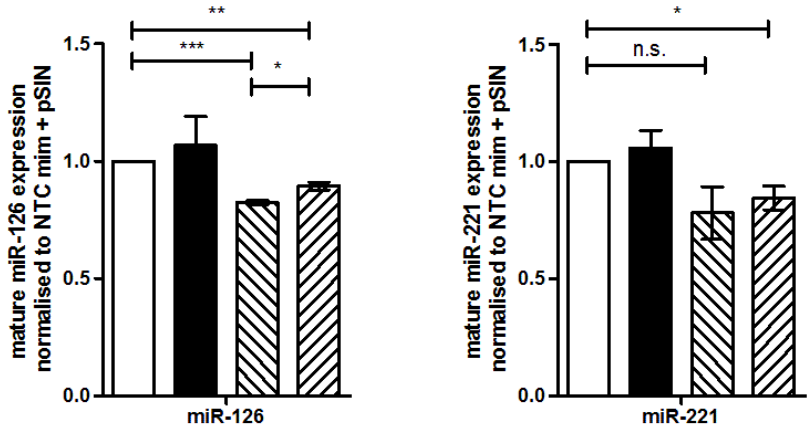

(b) (c)

Figure 3.21: Overexpression of miR-132 mimics for 30 hours followed by AGO2^{-UTR} lentiviral overexpression for 24 hours: relative levels of miR-132 (a), miR-126 (b) and miR-221 (c) ($n = 3$, mean $\pm$ S.E.M.).

3.7 TIE2 regulation in activated LECs

Based on the finding that TIE2 was significantly upregulated by an increased abundance of AGO2 protein (Figure 3.19d), as well as positively regulated by PMA induced LEC activation, the previously collected results were revisited and tested for TIE2 expression. Online miRNA prediction tools such as TargetScan could not identify TIE2 as a potential miR-132 target. The aim was to determine if there was a link between TIE2 expression, AGO2 abundance and its regulation by miR-132, rather than TIE2 being a direct target of miR-132.

3.7.1 miR-132 overexpression affects TIE2

In compliance with AGO2 upregulation resulting in an increased expression of TIE2 mRNA (Figure 3.19d), the downregulation of AGO2 by miR-132 mimics also resulted in a drop of both *TIE2* mRNA and TIE2 protein expression (Figure 3.22).

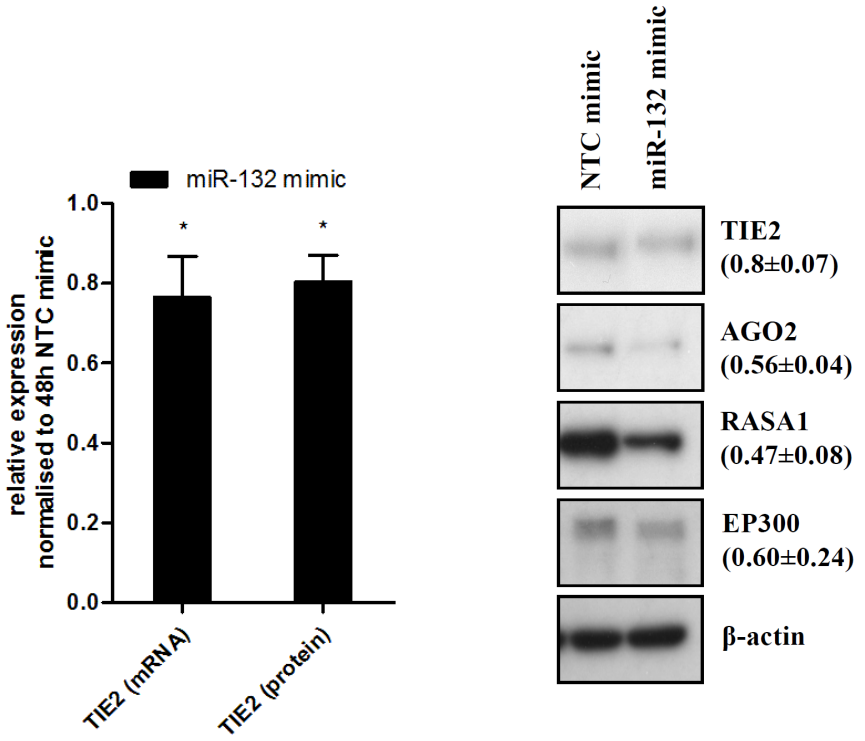

(a) (b)

Figure 3.22: Overexpression of miR-132 mimics in LECs for 48 hours: relative levels of *TIE2* mRNA and protein (a - mRNA and densitometry, b - immunoblot comparing TIE2 downregulation by miR-132 mimics relative to other miR-132 targets) ($n = 3$, mean $\pm$ S.E.M.).

3.7.2 miR-132 inhibition effect on TIE2

The activation of LECs by PMA did not show a significant effect on *TIE2* mRNA (Figure 3.23a), but reduced the expression of TIE2 protein in response to LEC activation (Figures 3.23b-3.23c). Since AGO2 was upregulated by PMA induced LEC activation (Figure 3.13d), it was expected that TIE2 protein expression would also increase as noted during AGO2 overexpression (Figure 3.19d). However, PMA induced LEC activation seemed to have a predominant effect on TIE2 expression and the increase in TIE2 due to the increase in AGO2 could not be observed. This meant that AGO2 had to be overexpressed using a lentiviral transduction in order to avoid the side effect of PMA on TIE2 protein abundance.

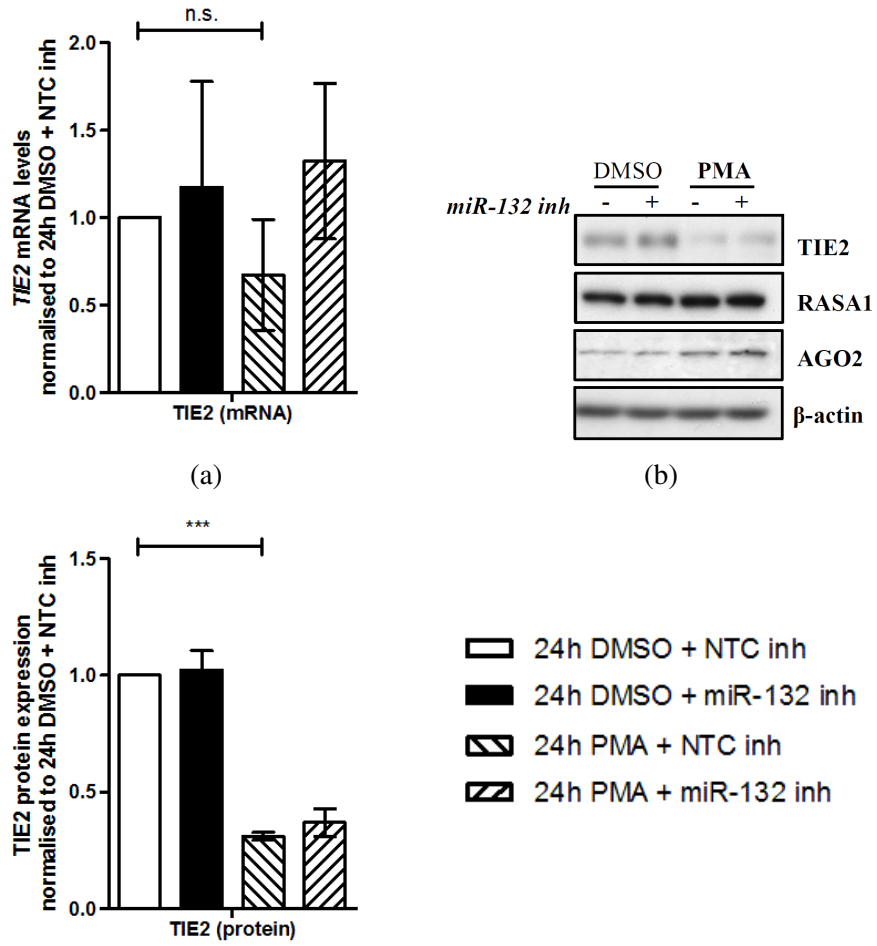

Figure 3.23: Inhibition (LNA) of miR-132 in PMA-activated LECs: relative levels of *TIE2* mRNA (a) and protein (b - immunoblot comparing TIE2 regulation to AGO2 and RASA1, c - densitometry) ($n = 3$, mean $\pm$ S.E.M.).

3.7.3 TIE2 rescue by AGO2^{-UTR} overexpression

Up until now it was established that AGO2 overexpression increase TIE2 protein expression (Figure 3.19d), and miR-132 mediated downregulation of AGO2 decreases TIE2 expression (Figure 3.22). The aim was to see if the overexpression of AGO2 could rescue TIE2 expression in both activated LECs and during miR-132 overexpression.

It was unclear what occured during PMA induced LEC activation in regards to *TIE2* mRNA levels due to the differences in *TIE2* mRNA expression between Figure 3.19d and Figure 3.23a. As previously found in Figure 3.23c, PMA negatively affected TIE2 protein abundance, which was reproduced again in Figures 3.24a-3.24b. No significant effect was consistently observed on TIE2 protein expression as a result of AGO2^{-UTR} overexpression, although as evident from the immunoblot (Figure 3.24a), TIE2 can potentially be upregulated during AGO2 overexpression in activated LECs.

The attempt to rescue TIE2 protein expression using AGO2^{-UTR} lentiviral overexpression resulted in more unexpected outcomes: TIE2 protein expression was upregulated as a result of miR-132 mimics alone, and further downregulated by the introduction of AGO2^{-UTR} in miR-132 overexpressing LECs (Figures 3.24c-3.24d). This is contradictory to previous results where AGO2 overexpression was found to increase TIE2 abundance at the mRNA level (Figure 3.19d), and that loss of AGO2 would result in loss of TIE protein abundance (Figure 3.22).

Based on the conflicting results observed during AGO2 overexpression experiments when measuring TIE2 expression, it was only possible to conclude that increase in AGO2 abundance did not result in increased TIE2 protein expression. However, the loss of AGO2 alone significantly impacted on *TIE2* mRNA and protein abundance (Figure 3.22). This concurs with the idea that the increase in AGO2 abundance has less profound effects in LECs compared to the loss of AGO2 abundance.

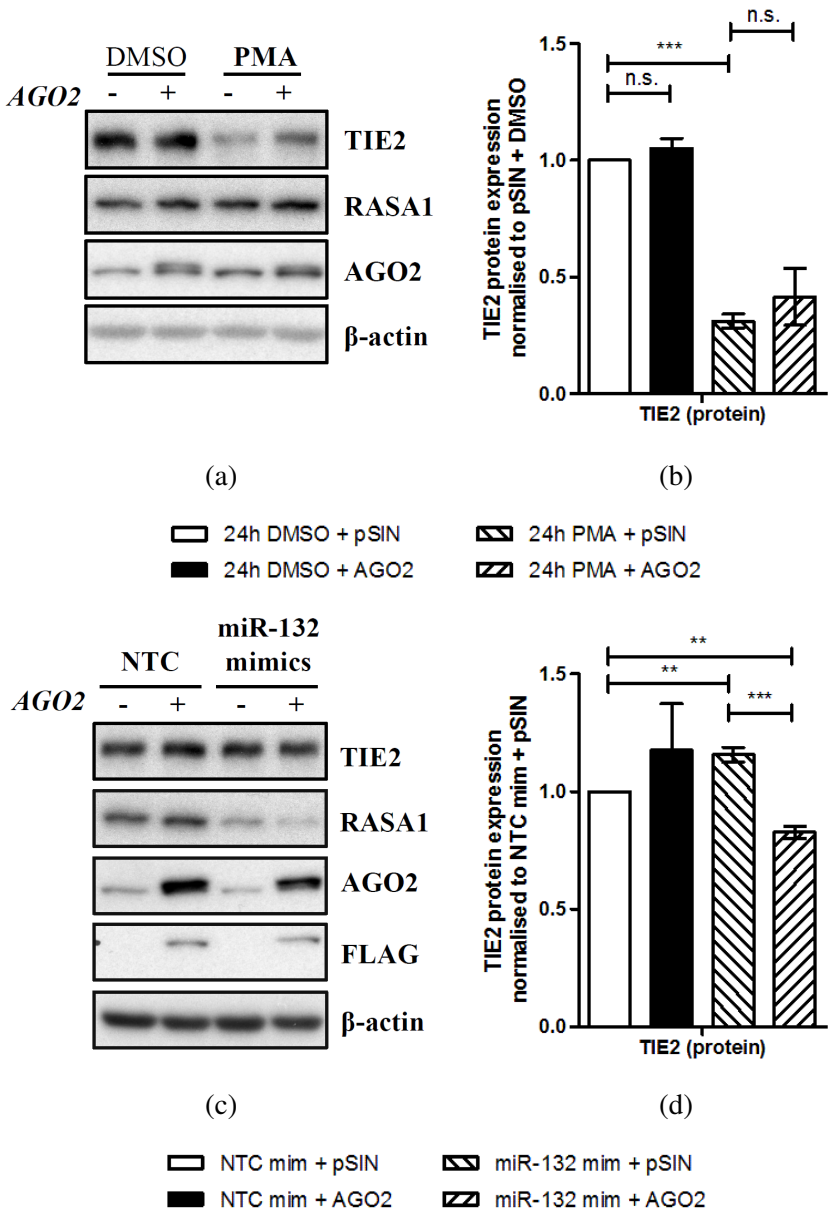

Figure 3.24: Overexpression of AGO2^{-UTR} for 30 hours followed by LEC activation for 24 hours: relative expression of TIE2 protein (a - immunoblot, b - densitometry) ($n = 3$, mean $\pm$ S.E.M.). Overexpression of miR-132 mimics for 30 hours followed by AGO2^{-UTR} lentiviral overexpression for 24 hours: relative expression of TIE2 protein (c - immunoblot, d - densitometry) ($n = 3$, mean $\pm$ S.E.M.).

3.8 LEC viability during miR-132/AGO2 regulation

It has been long known that LEC activation by PMA leads to increased growth and proliferation (Montesano and Orci, 1987), and the increase in miR-132 expression could be the facilitator of angiogenesis through its ability to downregulate RASA1 (Anand et al., 2010). Here I aimed to reproduce these findings in LECs to shed light on how the AGO2 and miR-132 regulation observed in Chapter 3 could affect LEC viability during the different treatment conditions. MTT assays were performed to determine the relative level of live cells present between treatment conditions.

First, PMA treatment did not show any effect on cell viability after 24 or 54 hours of PMA treatment (Figure 3.25a). It was clear, however, that LECs appeared healthier over the period of 24-54 hours (Figure 3.25a). Following these results, the inhibition of the low abundantly expressed miR-132 in LECs (Lagos et al., 2010) did not result in an increase in cell viability (Figure 3.25b). Only the overexpression of miR-132 increased LEC viability (Figure 3.25c), and this was not due to the result of AGO2 downregultion (Figure 3.25d), but most likely due to miR-132 downregulating RASA1 to activate LEC angiogenic function (Anand et al., 2010).

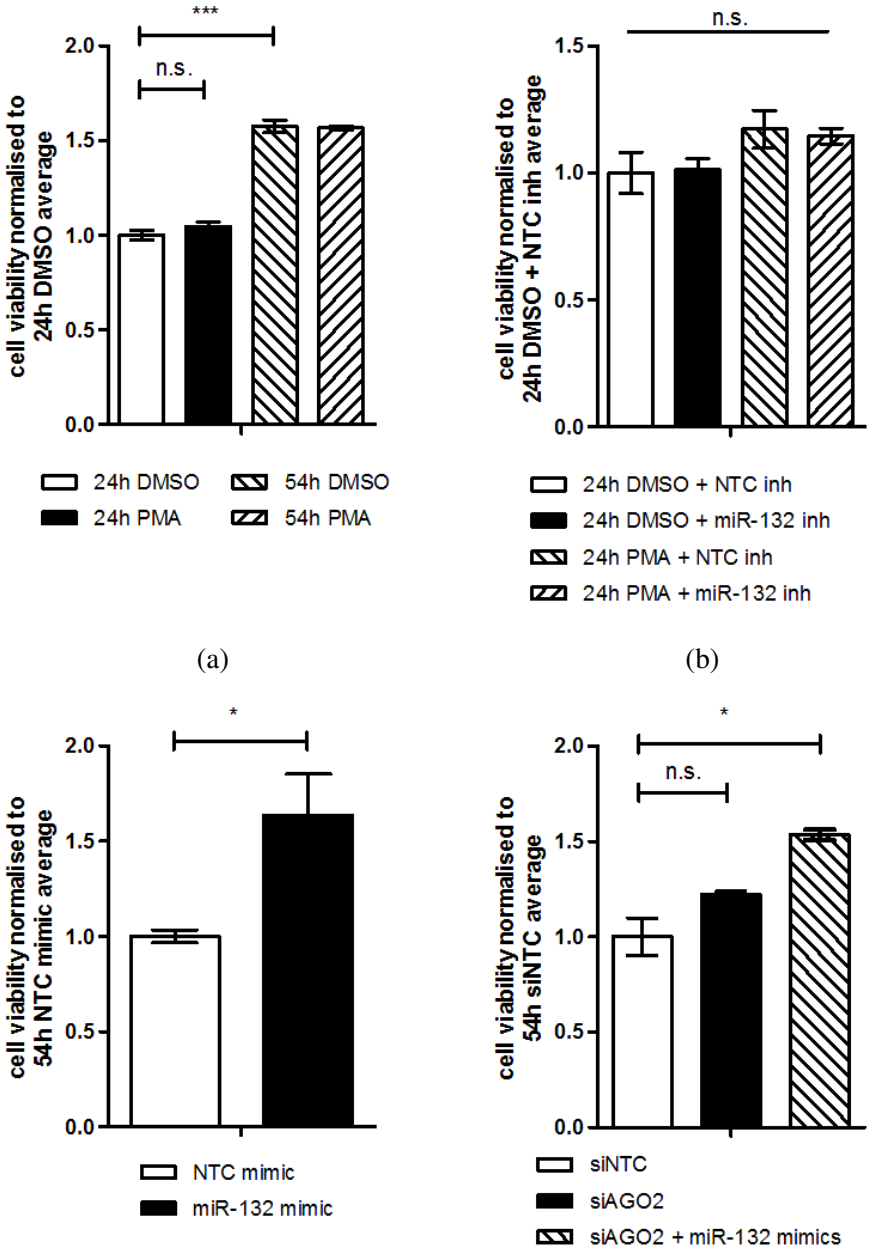

Figure 3.25: MTT assay showing LEC viability during PMA activation (a), miR-132 inhibition in PMA-activated (b), miR-132 overexpression (c) and AGO2 knockdown during miR-132 overexpression (d) ($n = 3$, mean $\pm$ S.E.M.; 6 replicates for (c)).

3.9 miR-132 -/- knockout mice

Following the *in vitro* investigations, it was interesting to determine if miR-132 has regulatory functions *in vivo*. First, the expression of miR-132 was compared between spleen and brain, where it was found that C57BL/6 (WT) mice express 2 magnitudes higher level of miR-132 in the brain than in the spleen (Figure 3.26a). There was no significant difference in the expression of *AGO2* mRNA (Figure 3.26b), AGO2 protein (Figures 3.26c, 3.27a, 3.27c, 3.27d), or RASA1 (Figures 3.26d, 3.27a) between WT and miR-132 KO mouse samples in their corresponding tissues.

Considering that the low expression of miR-132 in the spleen would be unlikely to contribute significantly to target regulation, it was expected that miR-132 would at least show a difference in AGO2 or RASA protein expression between the WT and miR-132 KO mice, however this was not observed.

There was also an attempt made to compare the expression of AGO2 between the spleen and brain tissue where miR-132 levels in wild type mice drastically differ (Figure 3.26a), but this lead to more experiments in search for a normalisation control for protein loading between tissues. Of the three tested loading controls – α-tubulin, β-actin and GAPDH – none of them showed an equal loading distribution when comparing brain and spleen sample lanes (Figure 3.27b) and could only be used to normalise WT vs miR-132 KO conditions within each tissue.

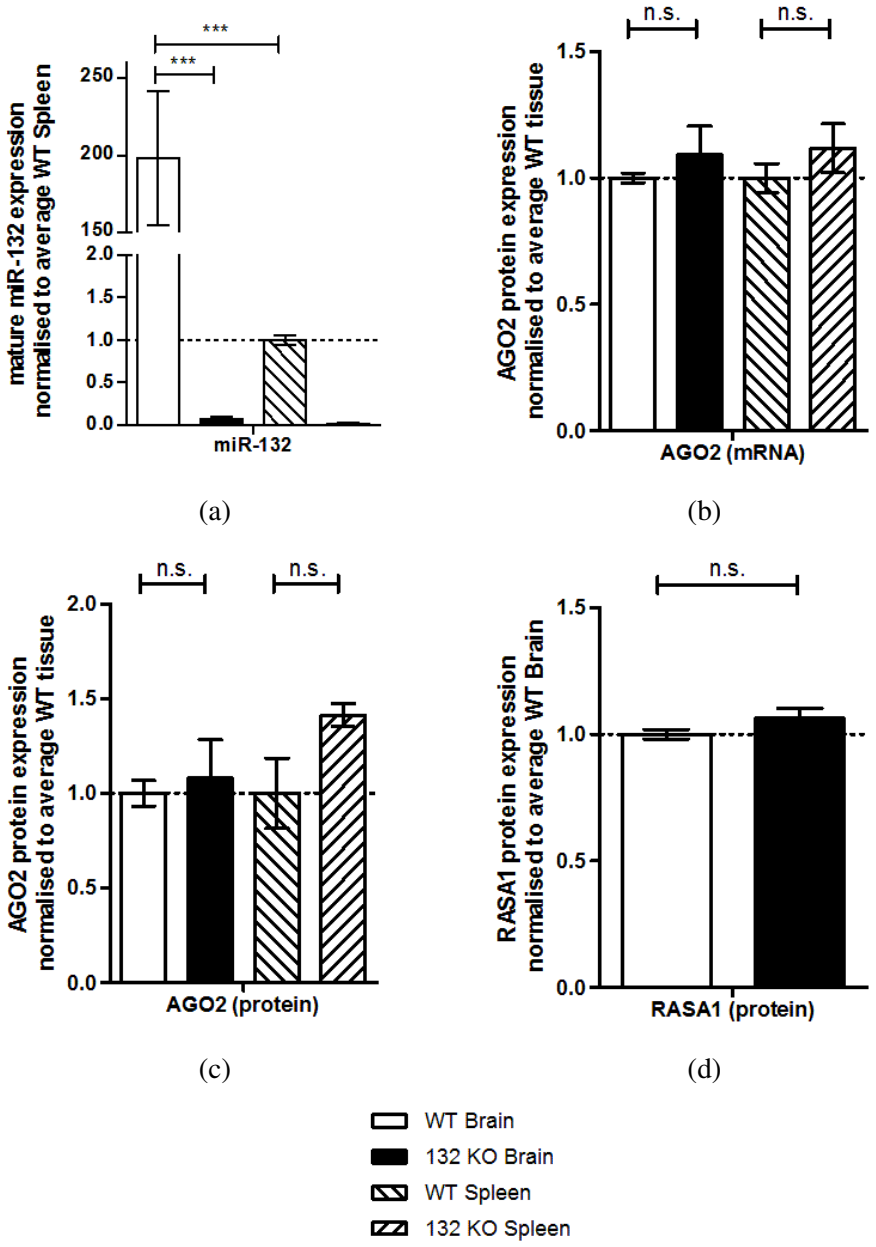

Figure 3.26: The levels of miR-132 (a), *AGO2* mRNA (b), AGO2 protein (c) and RASA1 protein (d) in wild type (C57BL/6) and miR-132 double genomic knockout mice (age 6-8 weeks), in spleen and brain tissues ($n = 8$, mean $\pm$ S.E.M.; 3 replicates for (b), 5 replicates for (c) spleen, 3 replicates for (d))

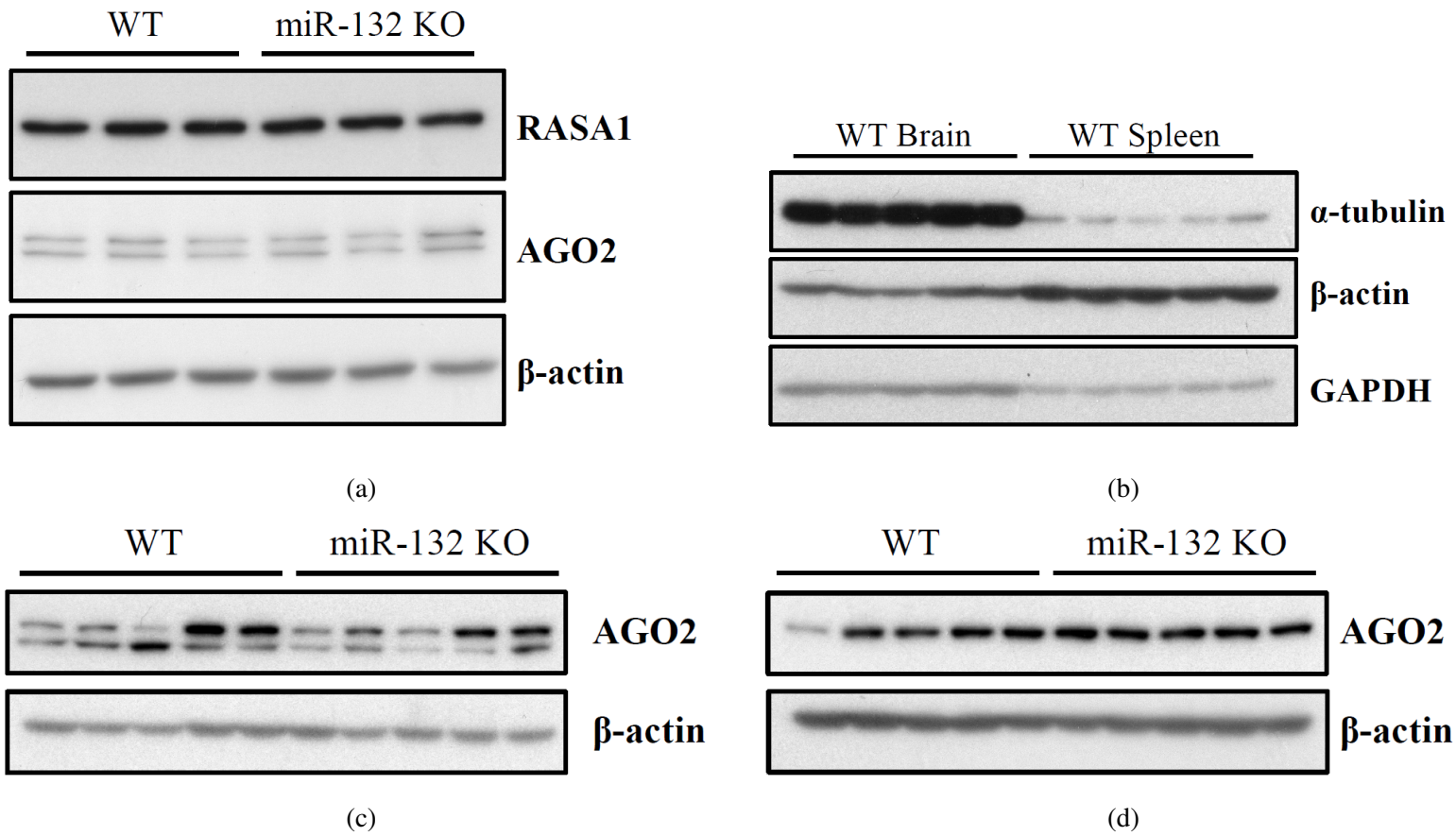

Figure 3.27: Immunoblots comparing C57BL/6 and miR-132 -/- KO mouse brain samples - AGO2 and RASA1 protein in brain (a), AGO2 protein in brain (c) and spleen (d), and different loading controls (b).

3.10 Summary and Discussion

The work presented in this chapter focused around validating the interaction of miR-132 with a potential candidate target – AGO2. Having confirmed miR-132 direct binding to the predicted miR-132 site on the AGO2 3'UTR (Figure 3.3), the following experiments demonstrated:

- AGO2 is downregulated by miR-132 overexpression in HeLas and LECs (Section 3.3)
- miR-132 mediated regulation of AGO2 affects miRNA-mediated silencing (Figure 3.4)
- miR-132 overexpression affects AGO2 function in LECs by affecting miR-126 and miR-221 abundance (Figure 3.8)
- miR-132 is transcriptionally induced by PMA in LECs through the phosphorylation of CREB (Figure 3.10)
- endogenous induction of miR-132 by PMA can be inhibited using LNA-based inhibitors (Figure 3.13a)
  - but not miRIDIAN hairpin based inhibitors (Figure 3.12a)
  - which relieves AGO2 protein suppression by miR-132 (Figure 3.13d)
- AGO2^{-UTR} (cannot be targeted by miR-132) overexpression
  - upregulates miR-221 abundance (Figure 3.18d)
  - can recover miR-132 overexpression induced loss of miR-126 (Figure 3.21b)
- TIE2 protein and mRNA levels indirectly affected by miR-132 overexpression (Figure 3.22)
- AGO2 and RASA1 (miR-132 positive control (Anand et al., 2010)) protein expression is unchanged between miR-132 -/- KO and C57BL/6 mice (Figure 3.26)

3.10.1 Role for miR-132 mediated suppression of AGO2

In the work presented here, a low expressed miRNA in LECs (~10^2 copies per cell), miR-132 (Lagos et al., 2010), was shown to directly target AGO2 and was able to mediate AGO2 regulation during LEC activation. However, this is not the first miRNA that has been shown to target AGO2: miR-99a, a regulator of AGO2 in hepatocellular carcinoma cell line, was found to be downregulated in several liver cancers (Zhang et al., 2014a). The downregulation of miRNAs has been previously reported as a common feature among liver cancer. Zhang et al. (2014a) show that the loss of AGO2 leads to a drop in miR-21, a miRNA targeting a tumour suppressor, Phosphatase and Tensin Homolog (PTEN) (Meng et al., 2007). The downregulation of miR-21 expression is associated with cancer progression and increased proliferation (Zhang et al., 2014a). In this context, loss of miR-99a regulation of AGO2 resulted in increased AGO2 protein expression, enabling miR-21 to suppress PTEN and enhance carcinogenesis, and demonstrating that miR-99a mediated AGO2 regulation was necessary to reduce cell proliferation and thereby oncogenesis. Moreover, the regulation of AGO2 by miR-184 epidermal keratinocytes during cell activation by Interleukin 22 (IL22) was shown by Roberts et al. (2013). Shortly after, a publication by Tattikota et al. (2014) confirmed miR-184 mediated regulation of AGO2 in pancreatic β cells, where AGO2 regulation was positively correlated with cell proliferation, complementing the possible function for AGO2 in the control of cell proliferation Zhang et al. (2014a).

Conversely, Anand et al. (2010) demonstrated that miR-132 positively controls cell proliferation and angiogenesis in endothelial cells by regulating Ras activity through the suppression of RASA1. Based on the finding that miR-132 is a direct target of AGO2 (Chapter 3), the loss of AGO2 in endothelial cells would result in decreased proliferation of cells, contrary to the findings made by Tattikota et al. (2014); Zhang et al. (2014a). This suggests a possibility of context-dependent regulation of cell proliferation by AGO2. Moreover, it is important to consider the expression profiles of the miRNAs that regulate AGO2: based on Lagos et al. (2010), the estimated abundance of miR-99a and miR-184 in LECs is $> 10^4$

and $< 10^1$ copies per cell, respectively. Interestingly, the target sites on AGO2 for miR-184, miR-99a and miR-132 are non-overlapping. Should all three miRNAs operate to suppress AGO2 in LECs, this would create a complex regulatory network modulating AGO2 expression. A study investigating the engagement of these differentially expressed miRNAs in the regulation of AGO2 would expand our understanding of context-dependent miRNA-mediated target regulation.

3.10.2 Loss of function experiments using antisense miRNAs

MiRNA hairpin based inhibitors used to inhibit miR-132 levels showed different efficiencies between untreated and PMA-activated LECs (Figure 3.12a). It was unexpected that PMA induced miR-132 expression would not be suppressed below baseline level. Stenvang et al. (2012) assessed the inhibition of miRNAs using hairpin inhibitors and LNA-based inhibitors, demonstrating that LNA-based inhibitors (Petersen and Wengel, 2003) provide higher efficiency for miRNA inhibition, with increased specificity for on-target effects (Obad et al., 2011). By inhibiting miR-132 in PMA activated LECs, we indeed observed a significant loss of miR-132 (Figure 3.13a), allowing to proceed with the loss of function experiments.

The alternative to the LNA and hairpin based inhibitors would be to test miRNA sponges, which instead of blocking miRNA loaded RISC, create a decoy site for endogenous miRNA binding (Ebert et al., 2007). As such, it would be interesting to use sponge technology, for example, to sequester multiple miRNAs that could potentially bind and target other AGO2 miRNA binding sites (Meng et al., 2007; Roberts et al., 2013), reducing any possible off target effects.

3.10.3 miR-132 activity controlled by its targets AGO2 and EP300

The expression of miR-132 is negatively regulated during its activation by downregulating EP300 (Lagos et al., 2010), however the final product, mir-132-3p, remains expressed above

steady-state levels after activation. This implies that miR-132 abundance is stabilised, most likely as a result of the ability of AGO2 to stabilise miRNAs (Diederichs and Haber, 2007; Winter and Diederichs, 2011); AGO loading of this low-expressed miRNA must occur soon after its synthesis following a canonical biogenesis pathway (Meister, 2013) in order for the stability of the miRNA to be increased.

Although miR-132 was observed to be inducible as a result of LEC activation by PMA, several other miRNAs were affected – miR-146a was significantly upregulated whilst miR-221 was significantly downregulated. Considering that only 1 in 10 miRNAs could be loaded onto an AGO2 protein at any given moment (Janas et al., 2012), the cell would need to accommodate the change in miRNA abundance in response to transcriptional activation due to LEC activation. PMA-induced activation of AGO2 transcription can function to allow newly synthesised miRNAs to be incorporated into functional complexes. This way the accelerated synthesis of miRNAs that are upregulated during LEC activation can elicit their function by binding and being stabilised by AGO2 – suggesting a coupled activation of both the functional regulators, miRNAs, and the effector complex, AGO2.

Unlike *AGO2* mRNA (Figure 3.11c), *EP300* mRNA (Figure 3.11d) was not transcriptionally induced during LEC activation by PMA. EP300 acts as a co-activator to facilitate miR-132 transcriptional induction, and therefore the transcription of EP300 should remain unaffected by LEC activation to allow for miR-132 to post-transcriptionally regulate the protein required for its own biogenesis. As a consequence, EP300 downregulation by miR-132 reduces its function to activate cytokine production during LEC activation (Lagos et al., 2010). The increased sustained expression of miR-132 even 24 hours after LEC activation is potentially able to both maintain EP300 expression at a steady-state level of expression (Lagos et al., 2010), as well as control the silencing activity of AGO2 that was induced to accommodate the increase in LEC activation responsive miRNAs.

In other systems, such as neurons, miR-132 is highly expressed and its regulatory function is necessary to maintain neuron cell identity and function (Vo et al., 2005; Remenyi

et al., 2010). However the gene expression programmes active in neurons will be vastly different from cells of the lymphatic endothelium, with different targets and miRNA:target ratios available to miR-132. The relative abundance of miR-132 to its targets will determine miR-132 activity as it will be competing for its targets, eliciting different effects on different targets depending on miRNA:target ratio (Mukherji et al., 2011; Bosson et al., 2014). The additional targets of miR-132, such as AGO2, will decrease this ratio. However, the level of AGO2 expression present in brain cannot be depleted, as its silencing function is necessary for miRNA function; since miR-132 is able to directly target AGO2, this suggests that the broad range of targets that have been discovered for miR-132 (Cheng et al., 2007; Lagos et al., 2010; Anand et al., 2010; Alvarez-Saavedra et al., 2011; Ucar et al., 2012; Mehta et al., 2015b) titrate the effect of miR-132 impact on AGO2 in a context-dependent manner.

In LECs, EP300 and AGO2 act together in an enclosed regulatory loop with miR-132 during endothelial cells activation to control miRNA mediated silencing, effects which are unlikely to occur in unstimulated LECs, where miR-132 expression is naturally low. Although an attempt was made to compare high and low miR-132 expressing tissues *in vivo* using C57BL/6 mice (Figure 3.9), it was not possible to use standard loading controls to normalise and compare AGO2 expression between spleen and brain tissues (Figure 3.27b), where the expression of miR-132 in WT mice differs by two magnitudes (Figure 3.26a). de Kok et al. (2005) demonstrated that Hypoxanthine Phosphoribosyltransferase (HPRT) may be yet the best control between different types of tissue samples, however their estimated error of up to 2-fold differences in expression from HPRT normalisation would leave many miRNA-target regulatory comparisons inconclusive, as miRNA effect on target regulation is often within a 2-fold range; a different method – using multiple loading controls or normalising to total protein expression (Eaton et al., 2013), cell count based or total RNA normalisation – comparing cell types with large differences in miR-132 expression, could benefit this approach. AGO2, necessary for miRNA-mediated silencing, is present in cells with both high and low miR-132 expression, and therefore it would be interesting to see how

miR-132 activity and ability to silence AGO2 is managed considering the large difference in gene expression programmes between different cell types.

3.10.4 AGO2 loss, not upregulation, affects miRNA abundance

It has been shown that miRNAs are stabilised by the presence of AGO1-4 (Winter and Diederichs, 2011). Winter and Diederichs (2011) demonstrated that by overexpressing a AGO1, AGO2 or AGO3 and *let-7* simultaneously they could stabilise the overexpressed *let-7* miRNA pool. During the AGO2 overexpression performed in LECs, where AGO2 is overexpressed only by a few fold above its steady state, it was difficult to detect noticeable changes even in the highly expressed miRNAs in LECs, such miR-126 and miR-221 (Figures 3.18, 3.21), although some cases were observed. Based on the experiments performed in LECs, the loss of AGO2 below the steady state expression level had profound effects on miRNA abundance (Figures 3.15c, 3.8c). These findings suggested, that AGO2 is present in cells at an optimal expression level, where the decrease, rather than the increase in AGO2 would cause several changes to cell function. Because AGO2 is the limiting factor in stabilising miRNAs in cells (Janas et al., 2012), it should effect low and high expressed miRNAs to a different extent. Although miR-132 is a low expressed miRNA in LECs, its function becomes apparent during LEC activation regulating RASA1 to promote angiogenesis (Anand et al., 2010). In contrast, miR-126 is a highly expressed miRNA in LECs, responsible for regulating SPRED1 expression in order to maintain the LEC phenotype (Fish et al., 2008). However, in both cases AGO2 expression is required to maintain miRNA regulatory functionality, whereas the increase in AGO2 expression would only attenuate the potential for miRNA mediated regulation if no change in miRNA transcription follows AGO2 upregulation. An interesting study would be to investigate (1) the threshold level when changing miRNA abundance affects its target expression and (2) identify what proportion of the miRNA is loaded onto RISC, importantly distinguishing between low and high expressed miRNAs in LECs.

3.10.5 TIE2 expression regulated by AGO2 abundance?

During several experiments where AGO2 abundance was regulated either through cell activation, miR-132 or AGO2 overexpression, TIE2 was sensitive to the changes that correlated with AGO2 expression. TIE2 is a receptor that can positively regulate angiogenesis by being activated via its extracellular domain through Angiopoietin 1 (ANG1) ligand binding, or negatively regulated during ANG2 association (Maisonpierre et al., 1997). In this study, PMA-induced activation of LECs resulted in the upregulation of the competitive antagonist of ANG1 for TIE2 signalling (Figure 3.19a), and downregulation of TIE2 protein expression (Figure 3.23c). The drop in TIE2 protein expression can be explained by TIE2 endodomain cleavage (Reusch et al., 2001) in response to PMA induced ANG2 upregulation (Singh et al., 2012). However, it remains unclear why AGO2 abundance positively correlated with TIE2 protein abundance. AGO2 overexpression alone was sufficient to upregulate TIE2 expression only at the mRNA level (Figure 3.19d), but without any effect on miR-132 expression (Figure 3.18a) or TIE2 protein abundance (Figure 3.24b), suggesting that miR-132 may not be involved in regulating TIE2 abundance directly acting through an unknown mechanism. Furthermore, miR-132 overexpression indicated an increase in cell viability (Figure 3.25), which would contradict the role of TIE2 in regulating LEC proliferation and blood vessel formation Morisada et al. (2005). Therefore the regulation of TIE2 by miR-132 may be coincidental and the mechanism of indirect TIE2 regulation by miR-132 remains unclear.

Chapter 4

Development of an *in silico* model of miR-132 mediated silencing

The impact of miRNA-mediated gene regulation on target gene expression is typically small, with each miRNA predicted to target multiple target mRNAs within a cell. As a result, miRNAs have become predominantly viewed as fine-tuners of gene expression. However, despite the small changes in gene expression elicited by miRNAs, they have been shown to have important functional roles described previously in Section 1.2.5.3. The regulatory potential of miRNAs within gene regulatory networks (described in detail in Section 1.2.4) becomes evident when we consider the abundance of miRNAs and their candidate target mRNAs: whilst the majority of mRNAs are present in the low 2-digit range of molecular abundance (Schwanhäusser et al., 2011), the abundance of functional miRNAs can exceed median mRNA copy number by a factor of 10, such as in the case of miR-132 (Lagos et al., 2010). Given this stoichiometry, each miRNA-mediated silencing event can contribute to moderating the protein output in a temporally resolved manner.

Using the strengths of agent-based modelling to our advantage (see Section 1.3.2) we aim to gain insight into the dynamic regulation of miR-132 target genes based on the available *in vitro* LEC data presented in Chapter 3 complemented by available published litera-

ture. The development of the model is described within this Chapter, following the CoSMoS process (described in Section 2.2).

4.1 Domain model

The purpose of the domain model is to capture the information relevant to the biological problem (Andrews et al., 2010a,b): biological processes and actors are captured at appropriate levels of abstraction, in order to help scope the purpose, and subsequent development of, a computer based model or equations.

Based on the work presented in Chapter 3, AGO2 was identified as one of the targets of miR-132 in LECs. AGO2 is one of the proteins required for effective miRNA-mediated silencing. EP300, another miR-132 target previously identified by Lagos et al. (2010), is a co-transcriptional activator; when bound to an active form of CREB during LEC activation (described in Section 3.4), EP300 is able to activate the transcription of miR-132. Therefore, two negative feedback loops are regulated through the function of a single entity - miR-132 - targeting *AGO2* and *EP300* mRNA, preventing ribosomes from translating the mRNAs into functional proteins. In order to determine the functional impact of miR-132 suppression on AGO2, in Chapter 3, the expression of another miRNA, miR-221, was measured. It is known that loss of AGO2 results in a loss of global miRNA expression (Winter and Diederichs, 2011), therefore miR-221 was included as part of the problem domain for developing the miR-132 silencing model.

The interactions between these *components*[1] form the regulatory network to describe miR-132 function in the context of miRNA-mediated gene silencing of AGO2 and EP300. The expected behaviour diagram (Figure 4.1) describes how these components interact, and how their behaviour changes over a period of 48 hours based on the available data from Chapter 3. The rationale for the inclusion of each of the components described above and

[1] Defined as an abstracted object of the *real* world domain that is able to function based on input and output information; e.g. a component in an ABM is an agent

included in Figure 4.1 is summarised below:

AGO2 protein Functions as a mediator of miRNA-mediated silencing when associated with a miRNA.

EP300 protein Functions as a co-activator of miR-132 transcription after its association with activated CREB protein.

CREB protein Upon cell activation, the phosphorylation of CREB (pCREB) is necessary for its translocation to the nucleus, where after the association with EP300, will function as an activator of miR-132 transcription.

RISC The RISC comprises of an AGO2 protein associated with a miRNA and necessary co-factors that drive miRNA-mediated silencing.

miR-132 The key regulator of the interaction network. When in complex with the AGO2 protein, it determines target specificity for the AGO2 protein to bind to the *EP300* mRNA or *AGO2* mRNA.

miR-221 A secondary miRNA in the model, that acts as a competitor with miR-132 for AGO2 protein loading. This miRNA does not have target mRNAs in this model.

***AGO2* mRNA** The mRNA that is a direct target of miR-132-associated RISC. It is a prerequisite for AGO2 protein synthesis.

***EP300* mRNA** The mRNA that is a direct target of miR-132-associated RISC. It is a prerequisite for EP300 protein synthesis.

Promoter A transcription start site for mRNA and miRNAs production. Although constitutively active, it requires the pCREB-EP300 complex localisation to the nucleus and the binding to the promoter to drive miR-132 transcription. Based on information in Chapter 3, *AGO2* mRNA and miR-221 transcription is also affected by cell activation. Different genes have different transcription rates, which in case of mRNAs may affect the dynamics of miR-132 mediated regulation.

Ribosome Requires the association with an mRNA. Produces the corresponding protein, releasing the mRNA after protein synthesis. Longer mRNAs take longer to translate into protein - functions as a time delay.

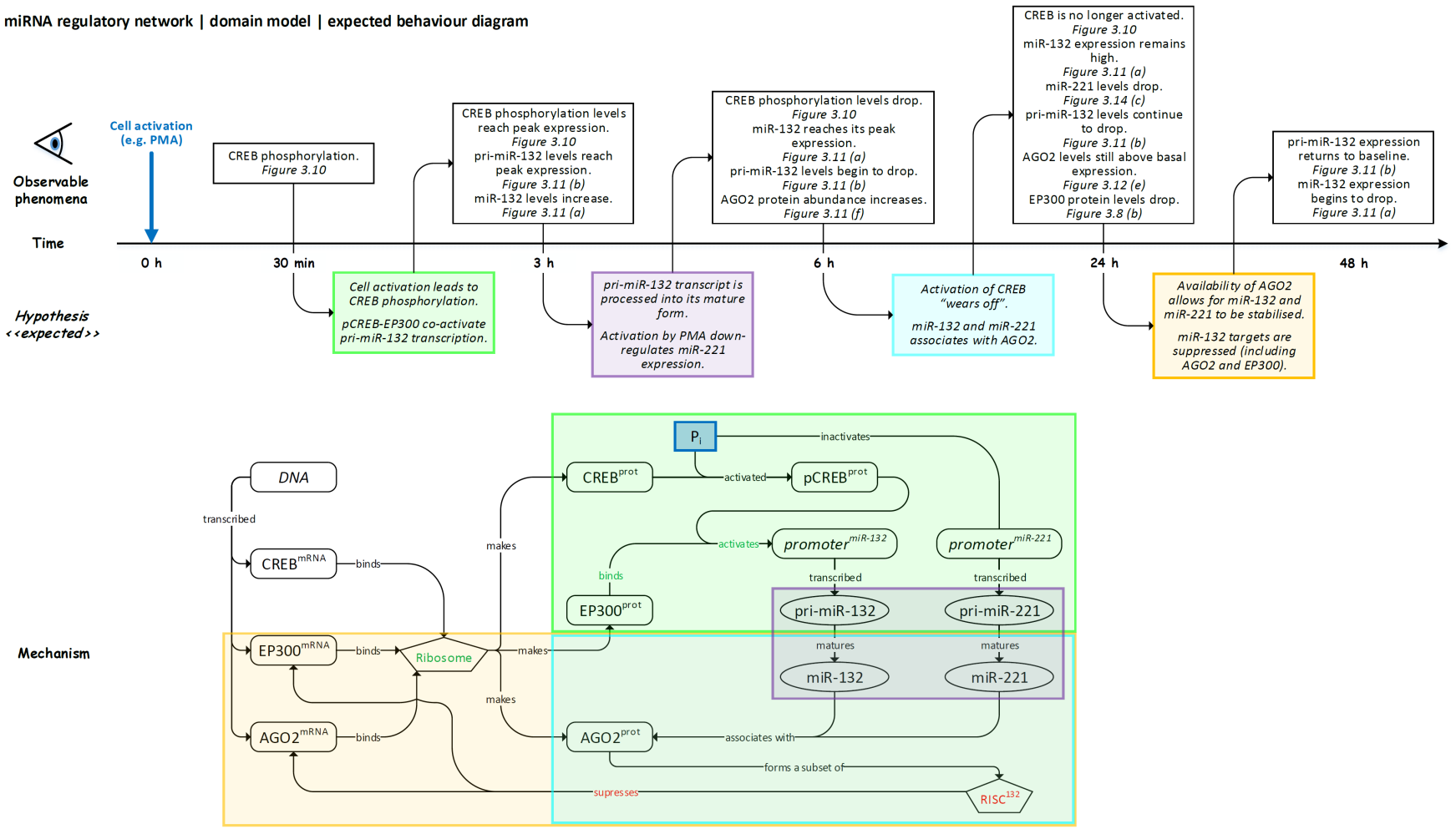

Figure 4.1: Expected behaviour diagram of the domain model. The *mechanism* describes the regulatory functionality of the interaction network. The *cell activation* event is a network perturbation which is described by the *observed phenomena* as recorded in Chapter 3 (relevant figures in italics under each phenomena), and the propagation of this event is explained by the *expected* behaviour under the timeline. The colours of the *expected* behaviour boxes are linked to the mechanistic components through which these events manifest.

The documentation and specification of the functional role of the abovementioned components was captured in the domain model *state* and *activity* diagrams. The key to the Notation in *state* and *activity diagrams* is described in Section 2.2.1.2. The evidence supporting transitions is provided either from literature, supporting data from Chapter 3 or based on assumptions made in collaboration with the domain expert. The diagrams below present the domain model *state* and *activity* diagrams; the sequence of presented diagrams (Figures 4.2-4.6) are supported by a table of evidence following each diagram figure, with the captions in the figures detailing the purpose of each of the model components. The *activity* diagram following the *state* diagrams combines the activity of the components into an integrated *activity* diagram (Figures 4.7-4.9).

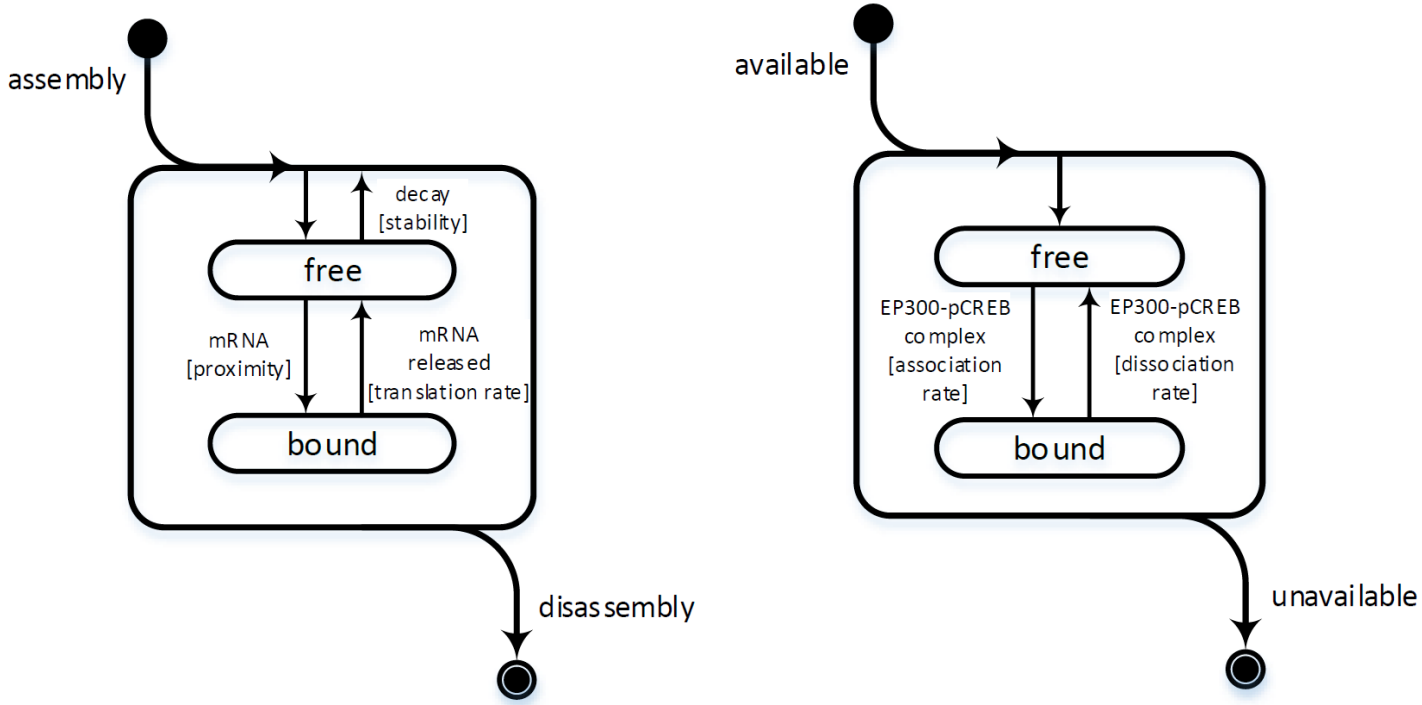

(a) ribosome state diagram

(b) promoter state diagram

Figure 4.2: State diagrams of the domain model for ribosome and promoter with supporting evidence in Tables 4.1 and 4.2, respectively. The ribosome exists in 2 states – the mRNA bound and unbound state, where the mRNA associates with a free ribosome, and upon the completion of translation is dissociated, freeing up the ribosome for the next mRNA. The promoter is part of the DNA, and in the context of this model is bound or unbound by an activator complex EP300-pCREB, which drives miR-132 transcription.

Table 4.1: Evidence supporting the domain state diagram for Ribosome

Domain model – *state* diagram – Ribosome		
State	**Associated transition**	**Evidence**
free	assembly	Lafontaine and Tollervey (2001)
	disassembly	
	mRNA released [translation rate]	Reid and Nicchitta (2015)
bound	mRNA [proximity]	

Table 4.2: Evidence supporting the domain state diagram for Promoter

Domain model – state diagram – Promoter		
State	**Associated transition**	**Evidence**
free	available	Domain expert assumption
	unavailable	
	EP300-pCREB complex [dissociation rate]	Zhang et al. (2005)
bound	EP300-pCREB complex [association rate]	

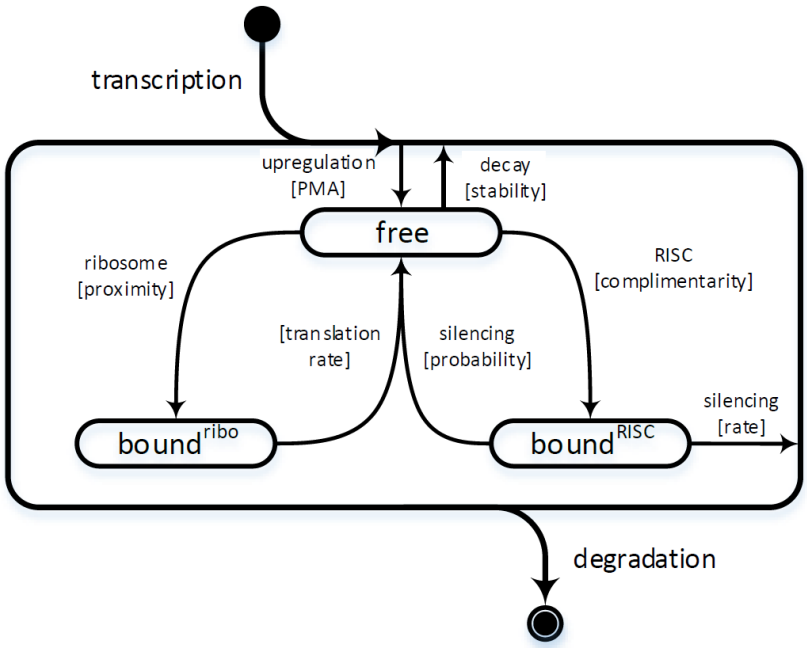

(a) *AGO2* mRNA state diagram

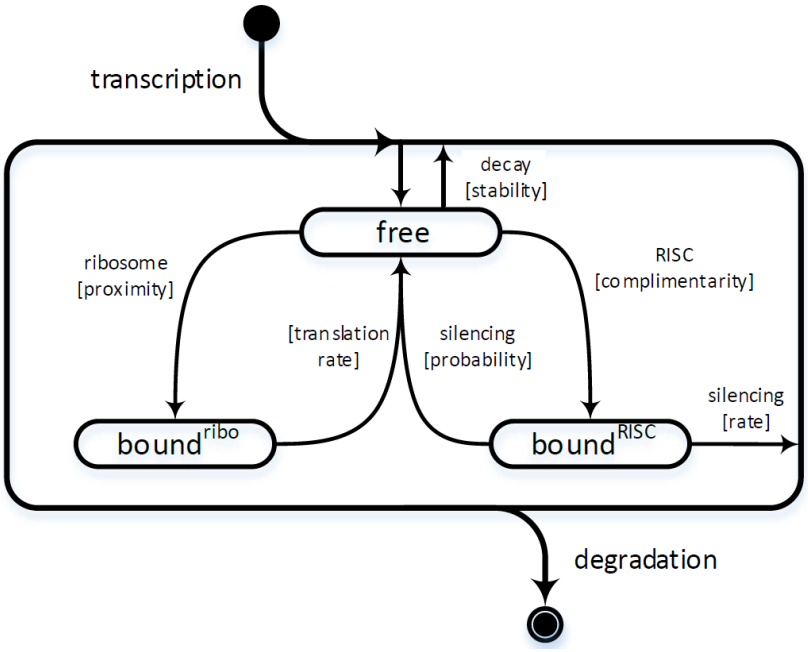

(b) *EP300* mRNA state diagram

Figure 4.3: State diagrams of the domain model for *AGO2* mRNA and *EP300* mRNA with supporting evidence in Tables 4.3 and 4.4, respectively. Both mRNAs have 3 states – free, bound by ribosome or bound by a RISC complex with the complimentary miRNA (miR-132). Following translation the mRNA is free of that ribosome. Following RISC binding, the mRNA can be silenced and degraded with a certain probability, otherwise it is released into its free form. Although both mRNAs are transcribed at a certain rate, *AGO2* mRNA transcription is affected by PMA activation.

Table 4.3: Evidence supporting the domain state diagram for *AGO2* mRNA

Domain model – *state* diagram – *AGO2* mRNA		
State	**Associated transition**	**Evidence**
free	transcription	Schwanhäusser et al. (2011)
	upregulation [PMA]	Figure 3.11c
	degradation	Schwanhäusser et al. (2011)
	[translation rate]	Lackner et al. (2007)
	silencing [probability]	Figure 3.3
bound^{RISC}	RISC [complementarity]	Figure 3.2
	silencing [rate]	Domain expert assumption
bound^{ribo}	ribosome [proximity]	Reid and Nicchitta (2015)

Table 4.4: Evidence supporting the domain state diagram for *EP300* mRNA

Domain model – *state* diagram – *EP300* mRNA		
State	**Associated transition**	**Evidence**
free	transcription	Schwanhäusser et al. (2011)
	degradation	Schwanhäusser et al. (2011)
	[translation rate]	Lackner et al. (2007)
	silencing [probability]	Figure 3.3
bound^{RISC}	RISC [complementarity]	Lagos et al. (2010)
	silencing [rate]	Domain expert assumption
bound^{ribo}	ribosome [proximity]	Reid and Nicchitta (2015)

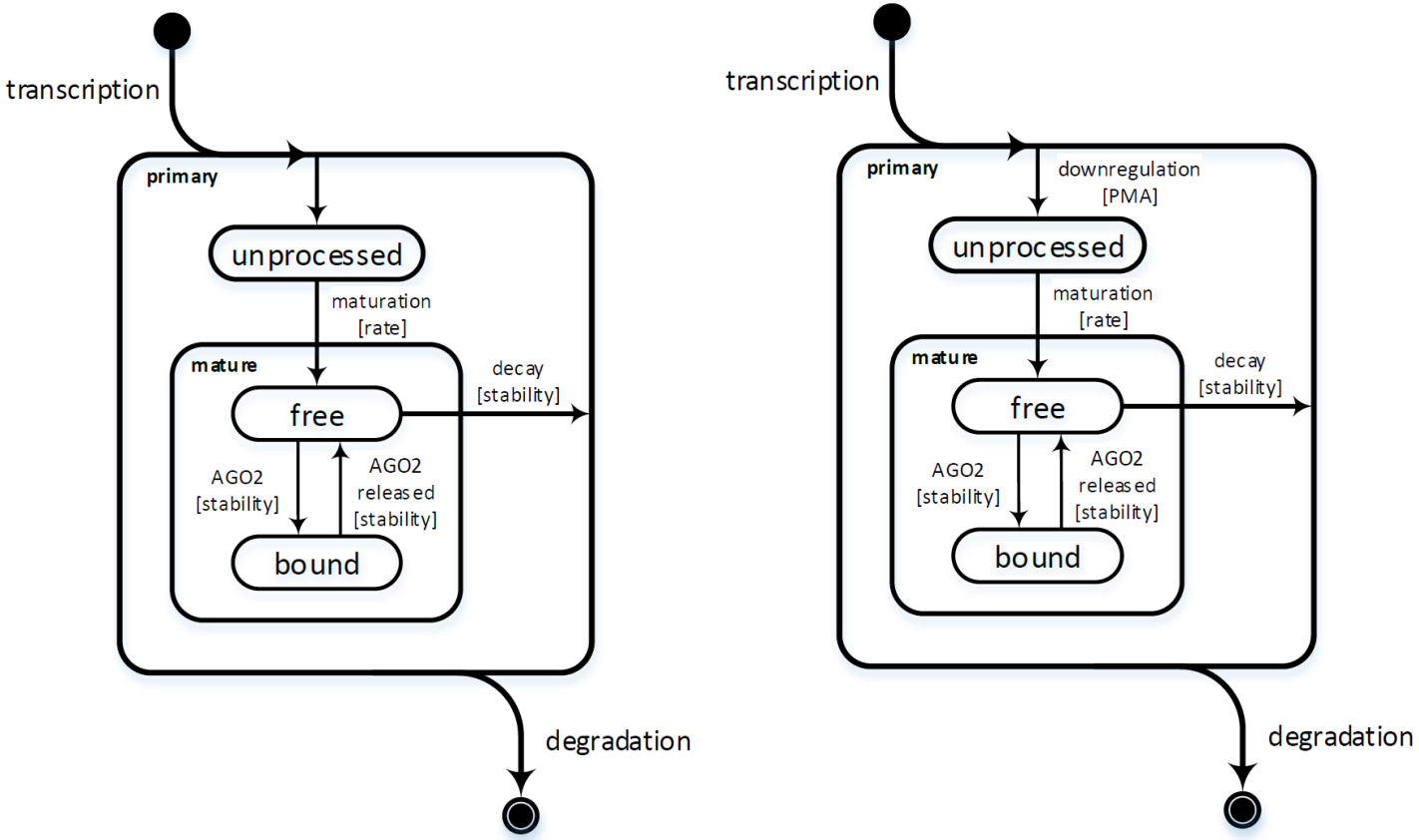

(a) miR-132 state diagram

(b) miR-221 state diagram

Figure 4.4: State diagrams of the domain model for miR-132 and miR-221 with supporting evidence in Tables 4.5 and 4.6, respectively. Both miRNAs are transcribed as primary transcripts in the *unprocessed* state, which will mature and become available for AGO2 binding. Based on the mature miRNA state – free or bound – it will have different stability affecting its lifespan. Although both miRNAs are transcribed from the promoter, miR-221 transcription is affected by PMA activation.

Table 4.5: Evidence supporting the domain state diagram for miR-132

Domain model – *state* diagram – miR-132		
State	**Associated transition**	**Evidence**
primary – unprocessed	transcription	Vo et al. (2005)
mature – free	maturation [rate]	Faller et al. (2010); Ota et al. (2013)
	degradation	Winter and Diederichs (2011)
	AGO2 released [stability]	
mature – bound	AGO2 [stability]	

Table 4.6: Evidence supporting the domain state diagram for miR-221

Domain model – *state* diagram – miR-221		
State	**Associated transition**	**Evidence**
primary – unprocessed	transcription	Schwanhäusser et al. (2011)
	downregulation [PMA]	Figure 3.14c
mature – free	maturation [rate]	Faller et al. (2010); Ota et al. (2013)
	degradation	Winter and Diederichs (2011)
	AGO2 released [stability]	
mature – bound	AGO2 [stability]	

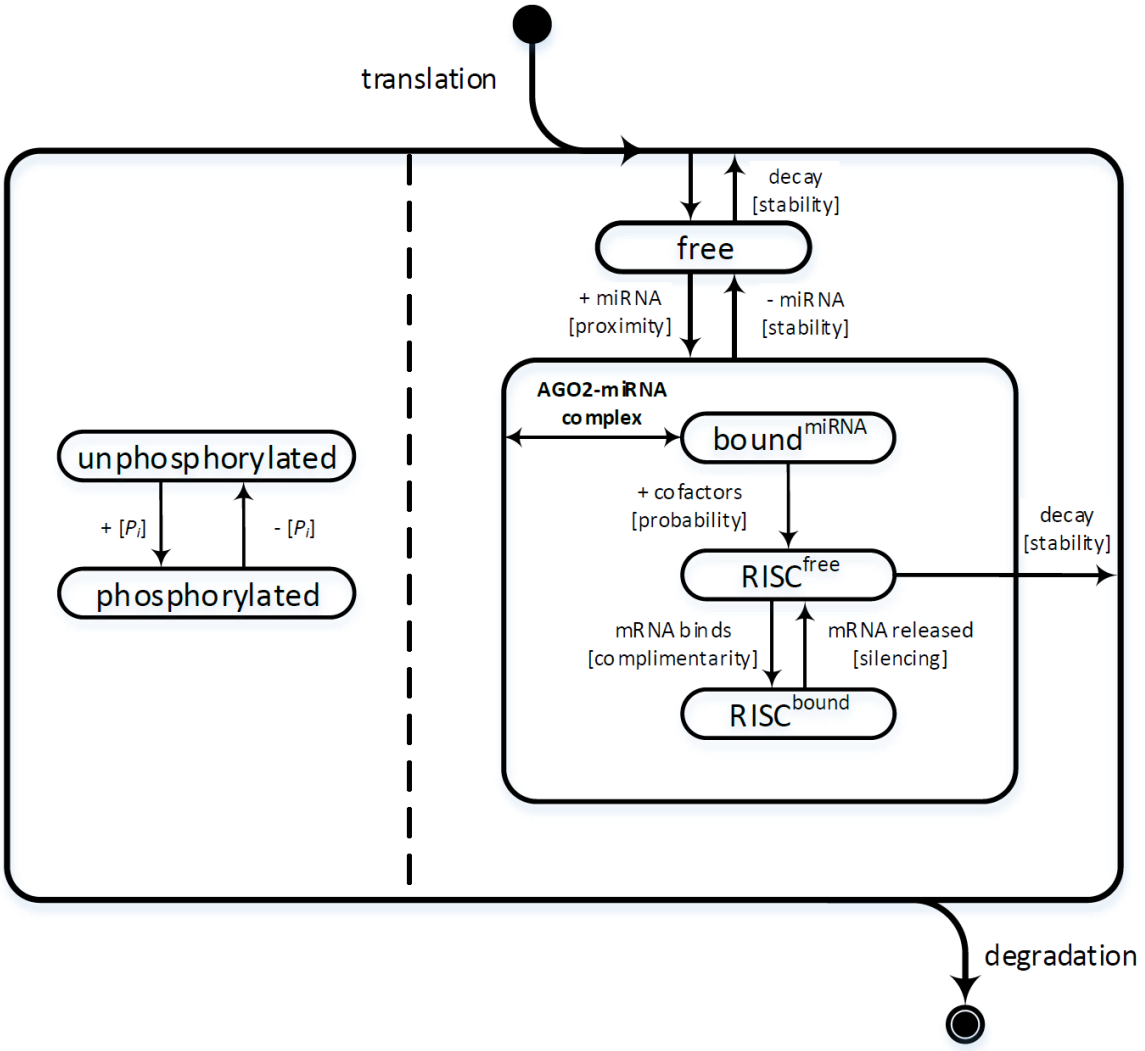

Figure 4.5: State diagram of the domain model for AGO2 protein with supporting evidence in Table 4.7. AGO2 is translated as a *free* protein and is able to bind a miRNA. The association is potentially reversible. Upon miRNA binding, additional cofactors will contribute to the function of the AGO2-miRNA complex, which will allow it to bind a potential mRNA based on miRNA-mRNA complementarity and silence it. The complex may potentially be re-used to suppress another mRNA target. AGO2, has a limited lifespan and may degrade upon its lifespan expiration. The activity of AGO2 is positively controlled by a post-translational modification and could occur at any time during its lifetime.

Table 4.7: Evidence supporting the domain state diagram for AGO2 protein

Domain model – *state* diagram – AGO2 protein		
State	**Associated transition**	**Evidence**
free	translation	Lackner et al. (2007)
	degradation	Weinmann et al. (2009)
	$-$ miRNA [stability]	Domain expert assumption
bound^{miRNA}	$+$ miRNA [proximity]	Section 1.2
RISC^{free}	miRNA released [silencing]	Stalder et al. (2013)
	$+$ cofactors [probability]	Domain expert assumption
	degradation	Weinmann et al. (2009)
RISC^{bound}	mRNA binds [complementarity]	Section 1.2.3
unphosphorylated	$-$ [P$_i$]	Zeng et al. (2008)
phosphorylated	$+$ [P$_i$]	

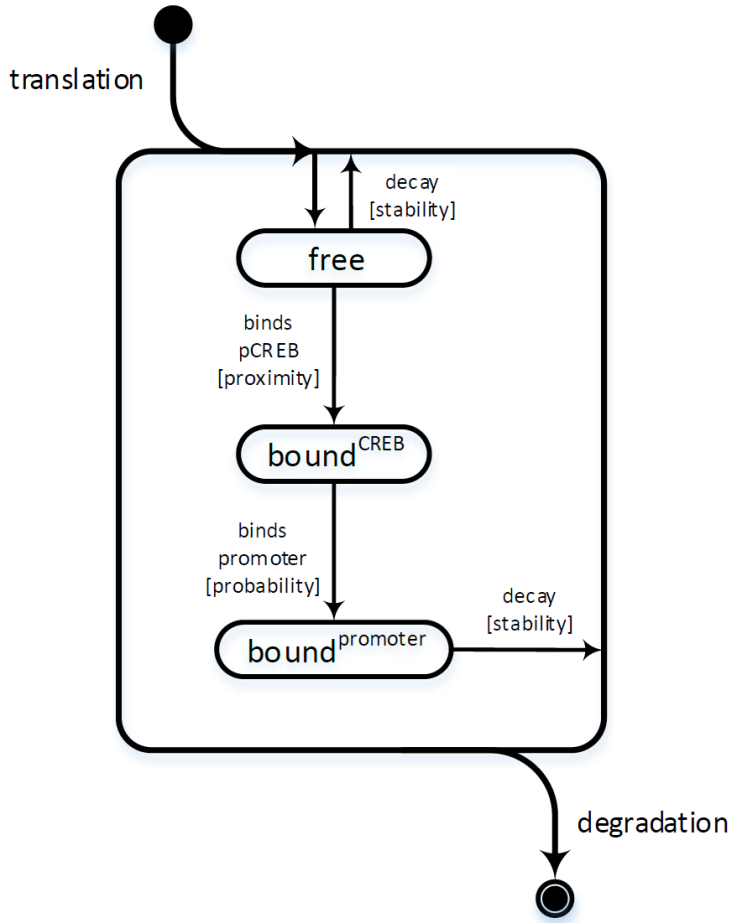

(a) Protein EP300 state diagram

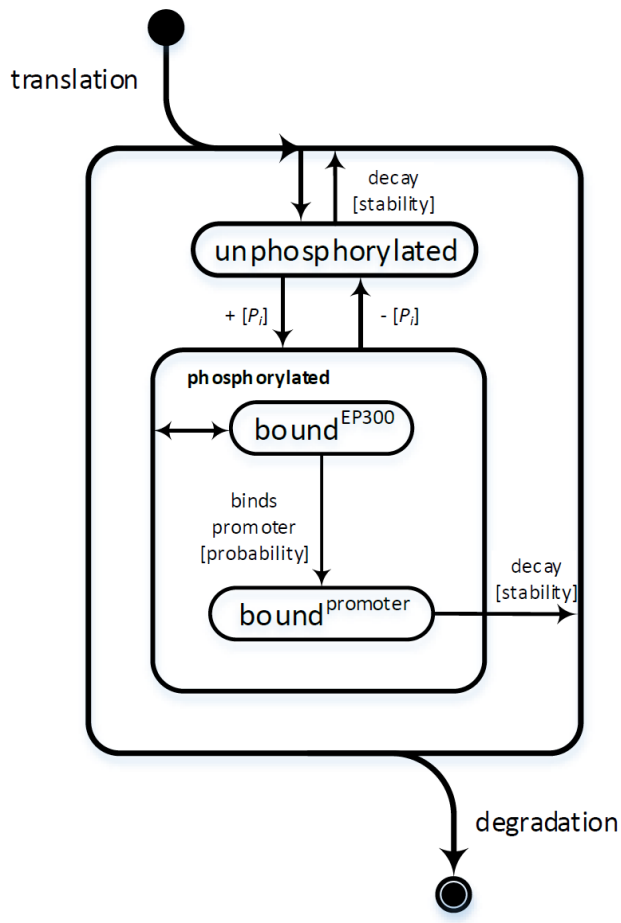

(b) Protein CREB state diagram

Figure 4.6: State diagrams of the domain model for EP300 and CREB protein with supporting evidence in Tables 4.8 and 4.9, respectively. Upon the activation of CREB phosphorylation, it is translocated to the nucleus where it can bind EP300 in order for them to elicit their function as a EP300-pCREB complex by binding to the promoter. After a transcriptional event is triggered, the complex is degraded. CREB binding capacity to EP300 is regulated by its phosphorylation state.

Table 4.8: Evidence supporting the domain state diagram for EP300 protein

Domain model – *state* diagram – EP300 protein		
State	**Associated transition**	**Evidence**
free	translation	Lackner et al. (2007)
	degradation	Schwanhäusser et al. (2011)
bound^{CREB}	binds pCREB [proximity]	Mayr and Montminy (2001)
bound^{promoter}	binds promoter [probability]	Vo et al. (2005)
	degradation	Schwanhäusser et al. (2011)

Table 4.9: Evidence supporting the domain state diagram for CREB protein

Domain model – *state* diagram – CREB protein		
State	**Associated transition**	**Evidence**
unphosphorylated	translation	Lackner et al. (2007)
	degradation	Schwanhäusser et al. (2011)
	$-$ [P$_i$]	Bito et al. (1996)
phosphorylated – bound^{EP300}	$+$ [P$_i$]	Mayr and Montminy (2001)
phosphorylated – bound^{promoter}	binds promoter [probability]	Vo et al. (2005)
	degradation	Schwanhäusser et al. (2011)

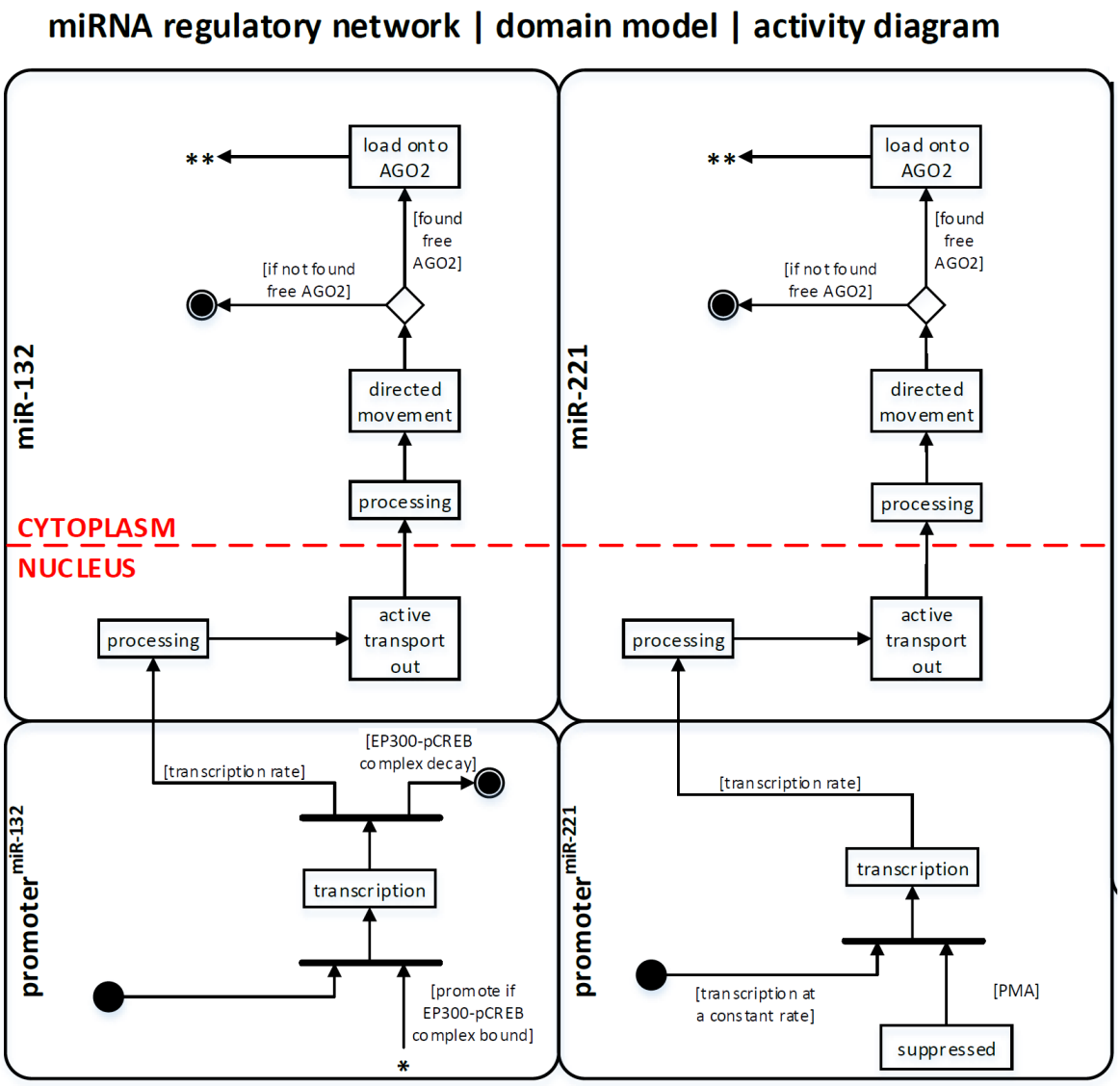

Figure 4.7: Combined activity diagram of the domain model for all interacting components in the model. The aim of the combined activity diagram was to demonstrate how the activities of the domain model components propagate, capturing the activity localisation to either the nucleus or the cytoplasm. Asterisks indicate a continuation point of an activity at another location with the equivalent number of asterisks. The evidence for the activities is already explained and presented in the above domain state diagrams; additional evidence of all molecular movement is justified within Section 4.2.1. Part 1 (next page extends figure to the right).

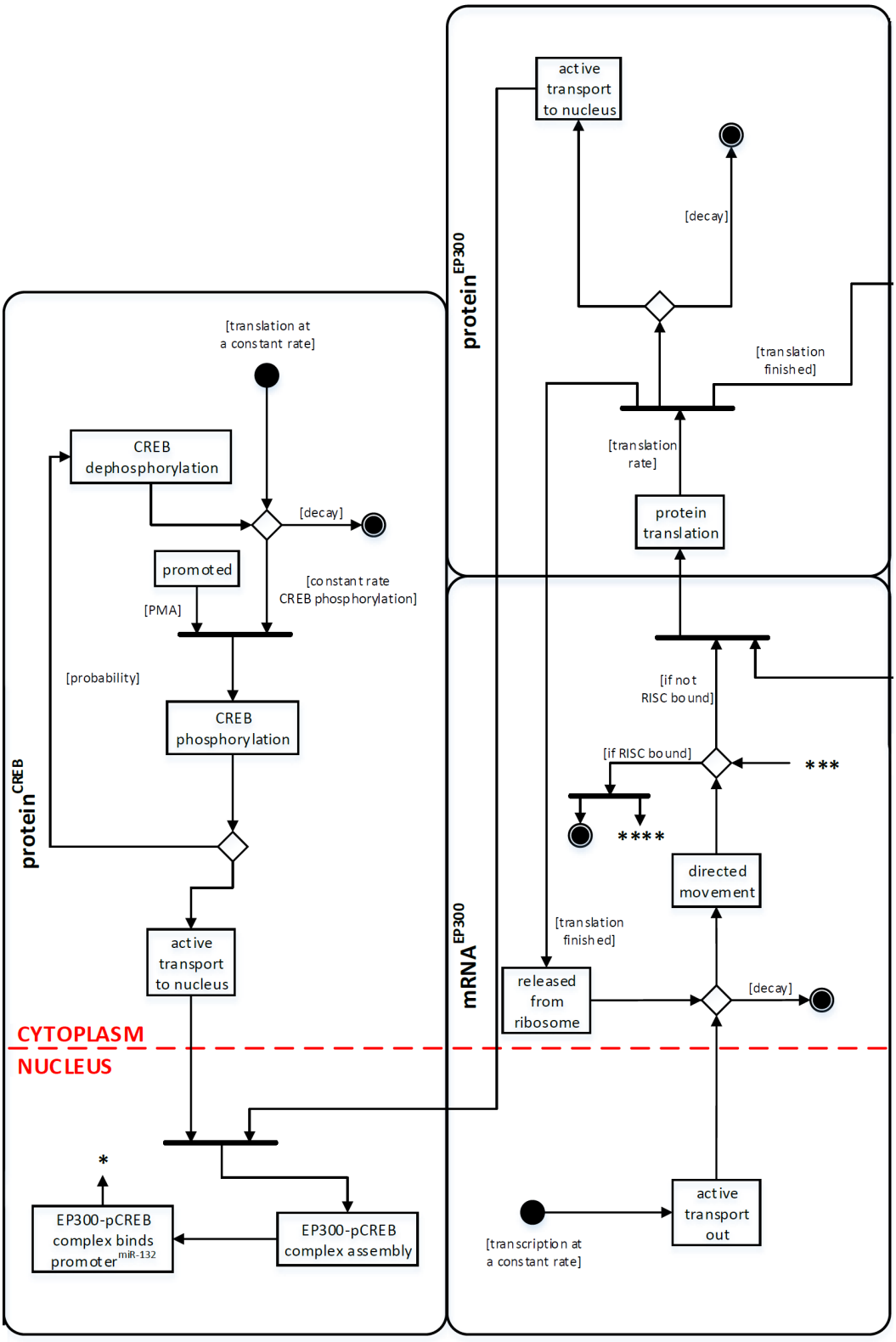

Figure 4.8: Combined activity diagram of the domain model for all interacting components in the model. Part 2 (next page extends figure to the right, previous page extends the figure to the left).

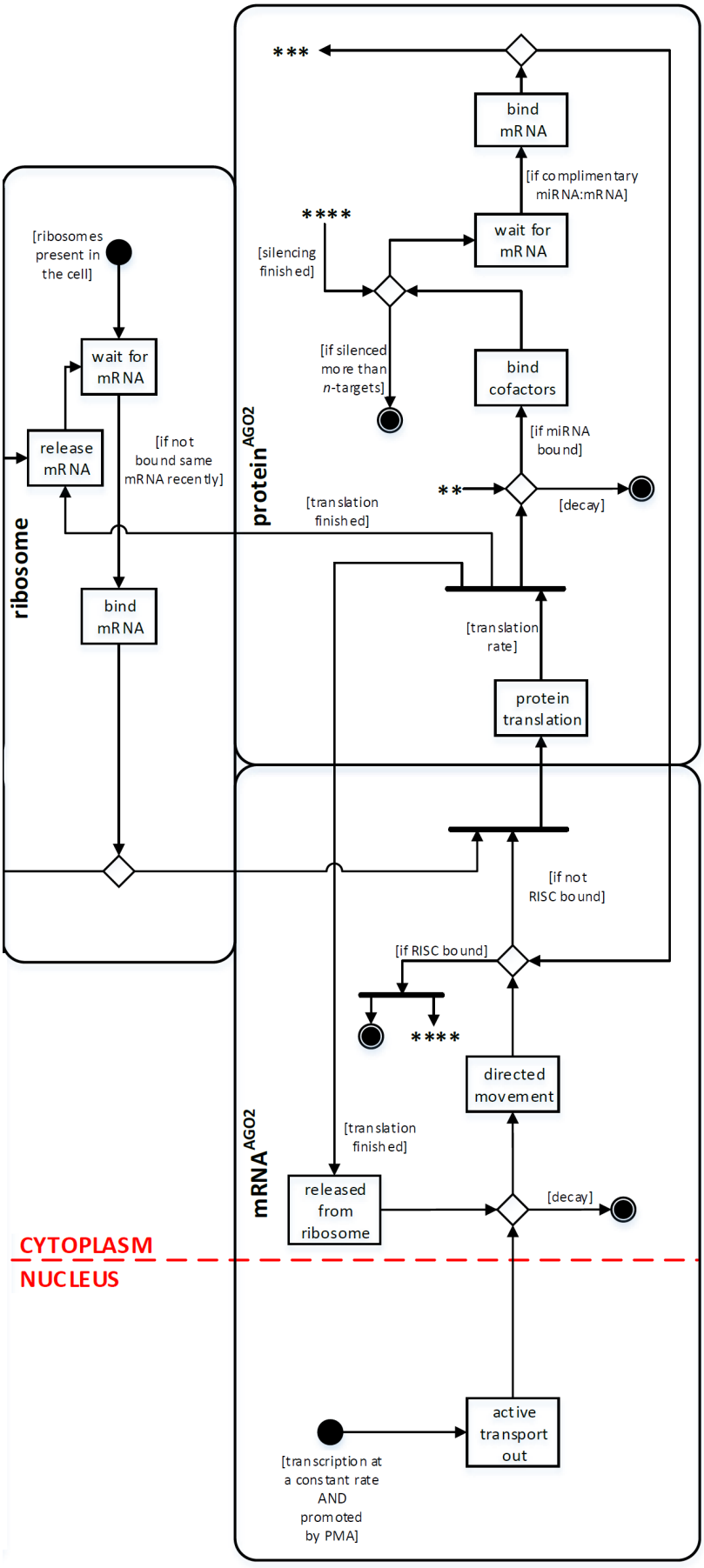

Figure 4.9: Combined activity diagram of the domain model for all interacting components in the model. Part 3 (previous page extends figure to the left).

4.2 Platform model

The domain model determined the scope of the model, capturing the necessary components and their behaviour for describing miR-132 mediated silencing of AGO2 and EP300. However, the domain model does not provide the specification for creating an executable model. Instead, the developed platform model builds on the domain model specifying the implementation strategy for each of the components within the domain model (development process described in Section 2.2). The *state* (Figures 4.10-4.13) and *activity* (Figures 4.14-4.20) diagrams detail the implemented states of each of the components and their activities. The differences between the domain and platform model assumption as reflected by the *state* and *activity* diagrams are summarised in Table 4.10. Additional justifications for the implementation decisions are described in detail in the Supporting evidence section below.

Table 4.10: Summary of changes made from the domain to the platform model (continued on the next page).

Component	Domain	Platform	Justification
AGO2 protein	AGO2 activity is affected by its phosphorylation	AGO2 is constantly active	[Domain expert assumption] The post-translational modification affecting AGO2 activity adds unnecessary complexity to the model that would not be traceable.
	mRNA unbound AGO2-miRNA complex can degrade	AGO2-miRNA complex can also be degraded subsequently after mRNA silencing	[Domain expert assumption] The AGO2-miRNA complex, from a simulation perspective, does not need to enter an mRNA free state in order to degrade; therefore a second exit point for the complex was introduced.
	AGO2 protein is available for miR-132/221 binding	A small proportion of AGO2 protein is available for miR-132/221 binding	[Domain expert assumption; Janas et al. (2012)] The limited abundance of AGO2 in the cells is scaled down in the model proportionally to the miR-132/221 fraction of the total miRNA pool in LECs (Lagos et al., 2010); this also reduces CPU time.
	AGO2-miR-132 complexes are available to silence mRNAs	A small proportion of AGO2-miR-132 complexes can silence mRNAs	[Wanet et al. (2012)] Many targets have been identified for miR-132, therefore only a proportion of these can target the 2 simulated targets captured in the model.
EP300 protein	All of EP300 is available to bind pCREB	A small proportion of EP300 is available to bind pCREB	[Franceschini et al. (2013), STRING database] In cells, although full populations of both EP300 and CREB are present, only a fraction of those associate together into a complex. The proportion has been estimated and scaled down to reduce EP300 proteins explicitly simulated in the model.
CREB protein	CREB is in very high abundance in cells	Only 100 CREB molecules are included in the model	[Domain expert assumption] CREB protein abundance is estimated to not be limiting (Schwanhäusser et al., 2011), therefore to reduce computational time it has been abstracted to a small population of recycled proteins.

Component	Domain	Platform	Justification
Ribosome	Ribosome synthesis and degradation is possible	Ribosomes are instantiated at the start of the simulation and not removed	[Domain expert assumption; Duncan and Hershey (1983)] The amount of ribosomes in the model is sufficient to allow for noncompetitve mRNA association with the ribosomes, which would be the case in proliferating cells for most protein coding genes. Decay/synthesis of new ribosomes adds unnecessary complexity to the model.
Promoter	miR-132 transcription is triggered upon EP300-pCREB complex binding	miR-132 transcription is triggered with a low probability following the EP300-pCREB complex binding event	[Zhang et al. (2005)] EP300-pCREB complexes activate transcription of many other genes, and therefore the abundance of these complexes activating miR-132 transcription has been scaled down in the model.
mRNAs	mRNA binds a ribosome based on its proximity to the ribosome	Newly transcribed mRNAs are transported to cytoplasmic foci where they can enter translation	[Takahashi et al. (2011)] Overlooked in the planning of the domain model, to incorporate a time delay on the silencing of mRNAs and allow possible localisation of silencing activity, cytoplasmic foci were introduced as mRNA localisation points.
	Equal probability of silencing for AGO2 and EP300	Differential probability of silencing for AGO2 and EP300	[Domain expert assumption] Although the silencing efficiency of AGO2 and EP300 by miR-132 are not exactly measured, it is assumed based on energy of the miRNA-target duplex and luciferase activity reporter assay (Section 3.3), the model implements the possibility of differential probability of silencing for explorative experimentation.
miRNAs	miRNAs can degrade only when not bound to AGO2	miRNAs can degrade when bound or not bound by AGO2	[Domain expert assumption] miRNAs not bound to AGO2 have a shortened lifespan, however the lifespan of a miRNA is dependent on its association with AGO2 for a limited period of time; the increased stability of miRNA is implemented as function of its association with AGO2, a calibrated stability constant, and its unbound lifespan. Decay of the miRNA can therefore occur even when bound to AGO2 for a prolonged period of time to avoid persistent miRNA accumulation.

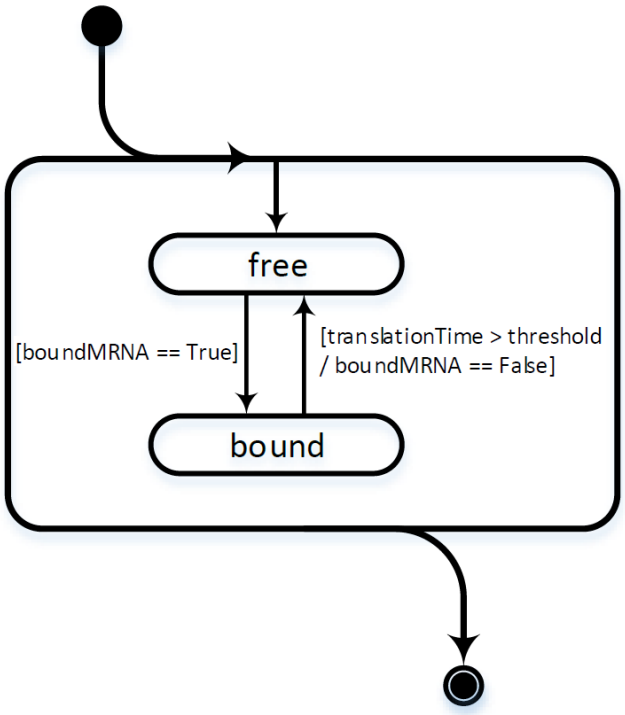

(a) ribosome platform state diagram

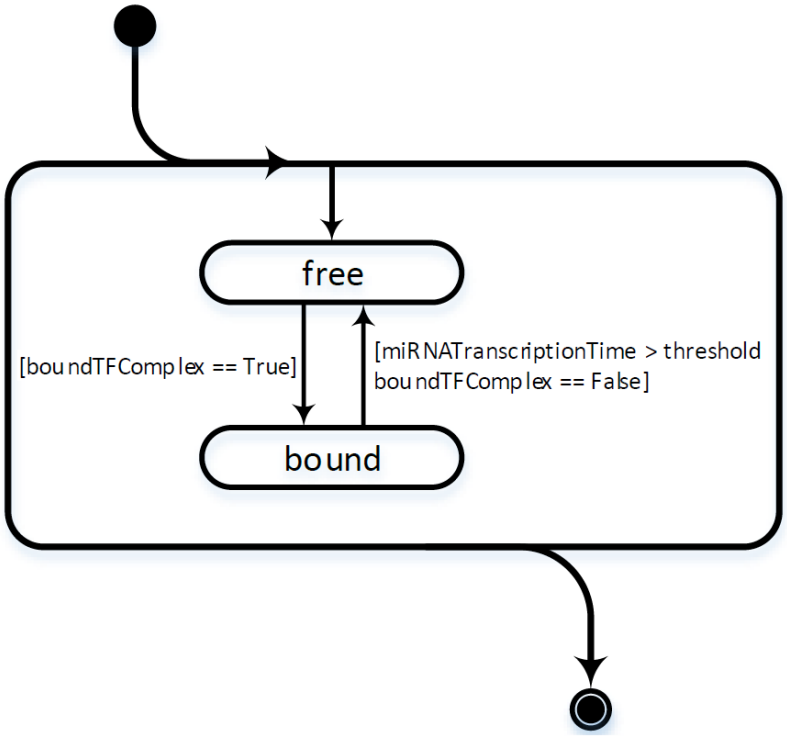

(b) promoter platform state diagram

Figure 4.10: State diagrams of the platform model for ribosome and promoter.

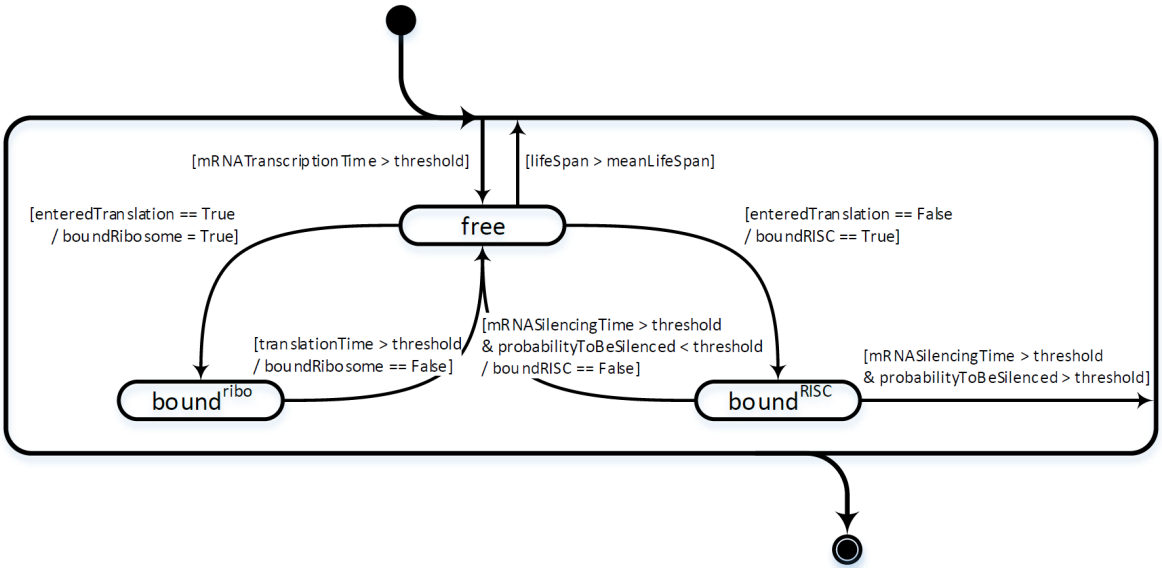

(a) mRNAs state diagram

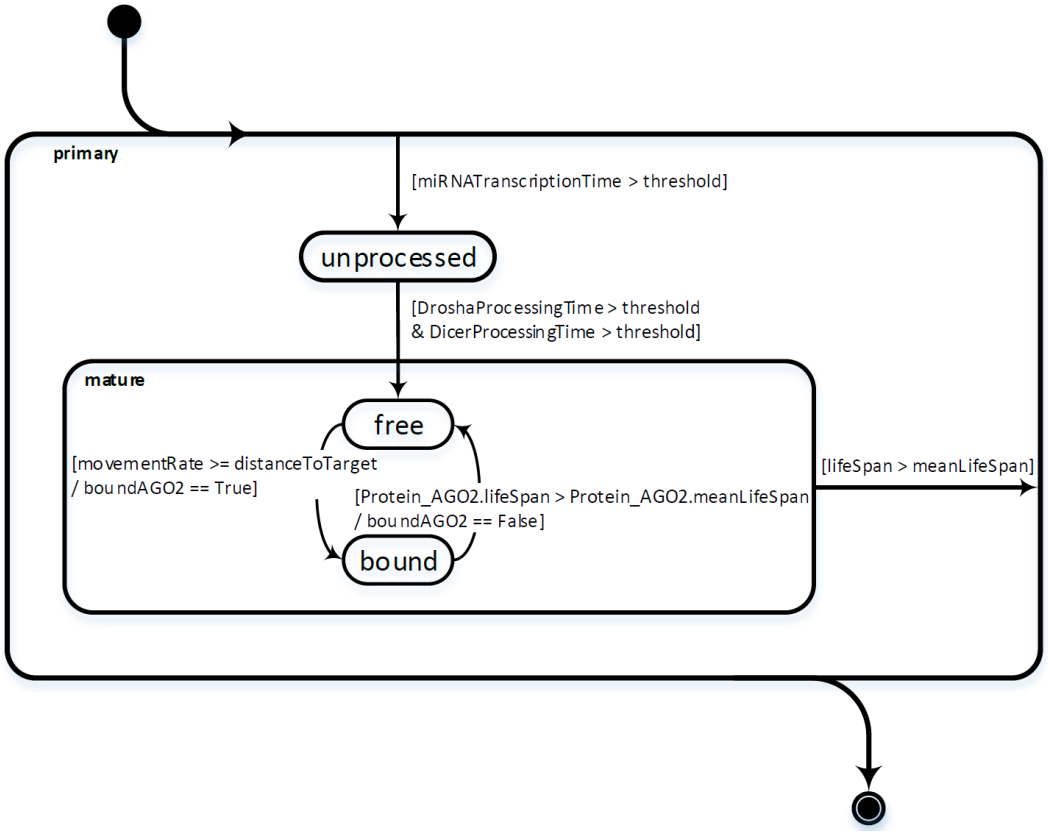

(b) miRNAs platform state diagram.

Figure 4.11: State diagrams of the platform model for *AGO2* mRNA and *EP300* mRNA, miR-132 and miR-221.

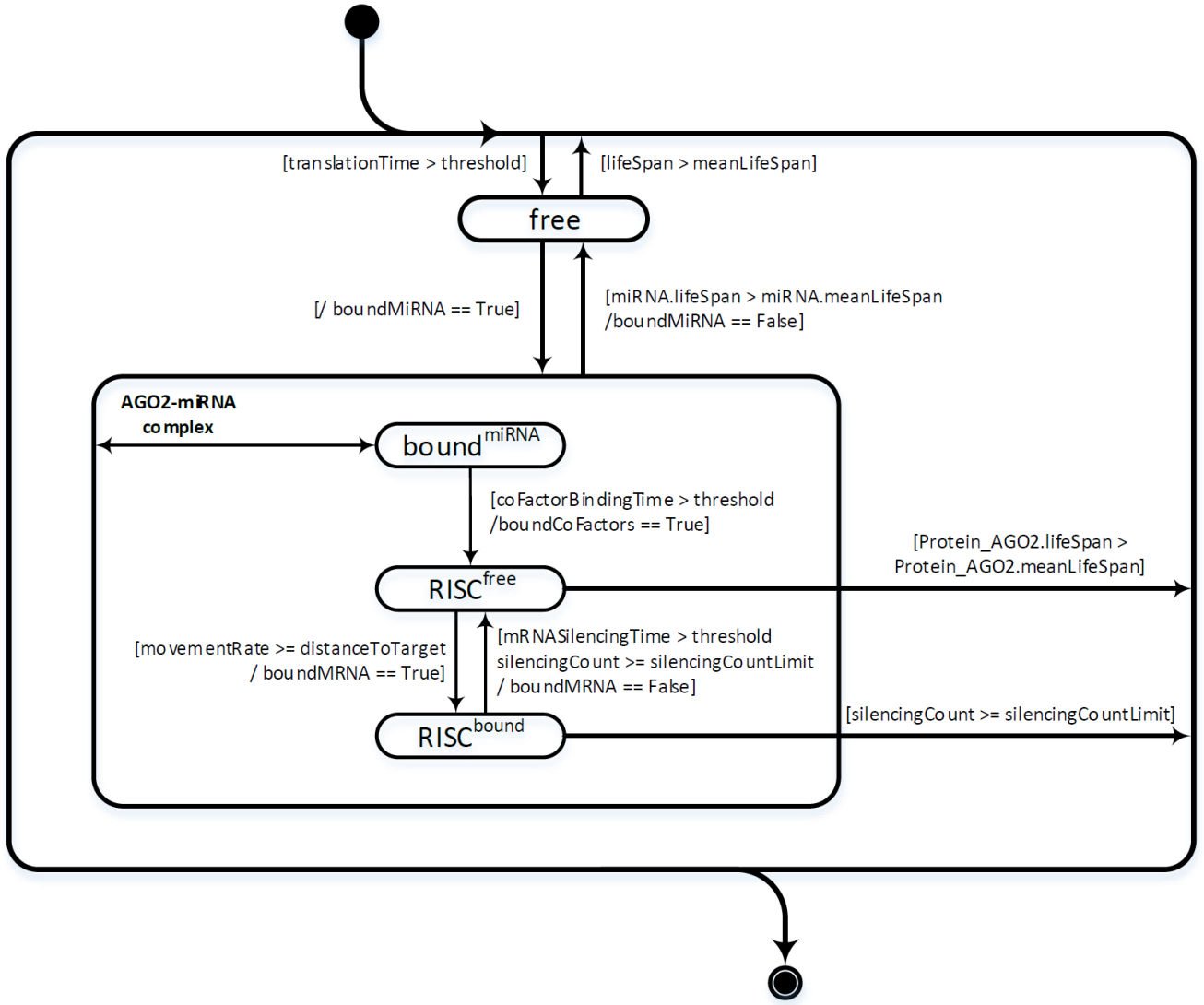

Figure 4.12: State diagram of the platform model for AGO2 protein.

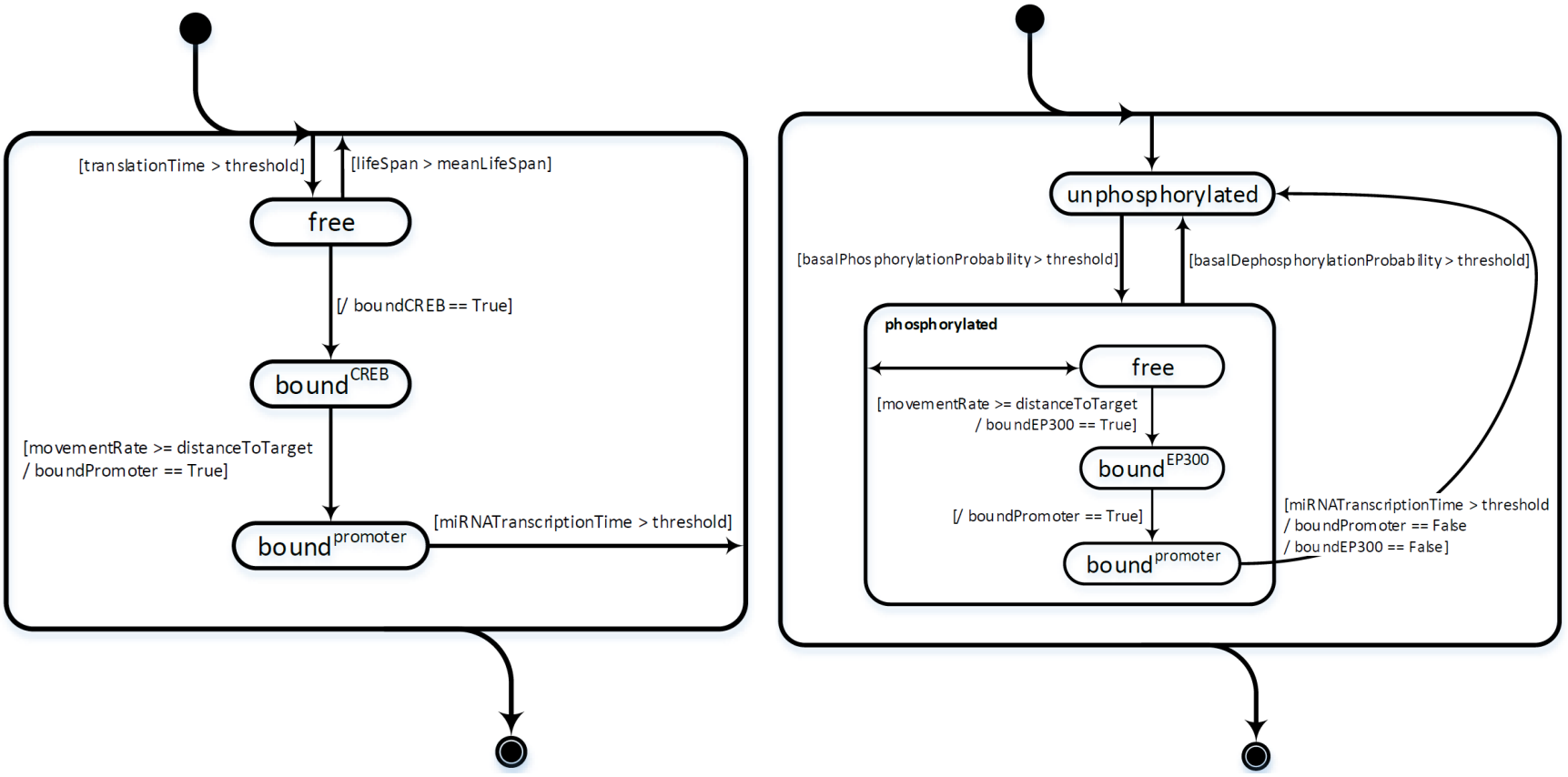

(a) Protein EP300 platform state diagram

(b) Protein CREB platform state diagram

Figure 4.13: State diagrams of the platform model for EP300 protein and CREB protein.

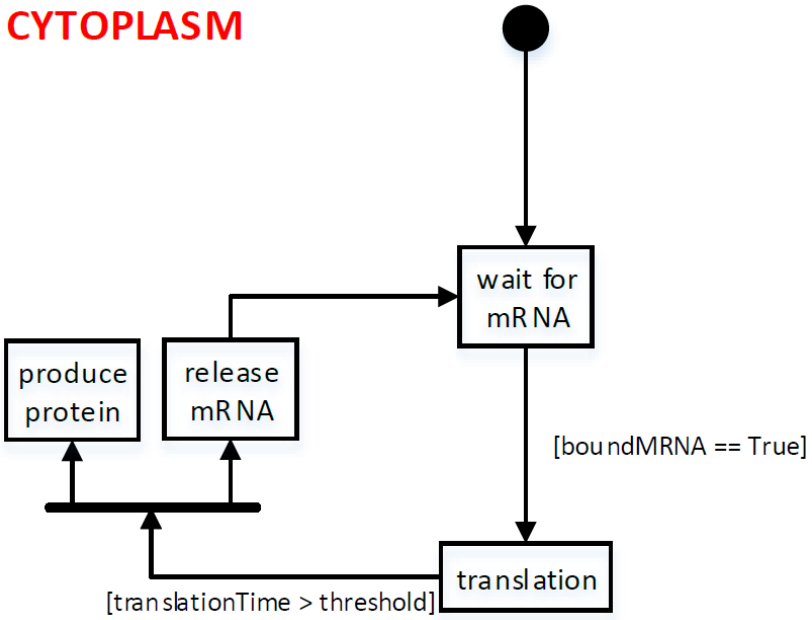

Figure 4.14: Activity diagram of the platform model for ribosome. The ribosome functions to translate mRNA into protein, as evident from its main activity. It is a stationary agent resident in the cytoplasm, which waits for an mRNA binding event to perform its function.

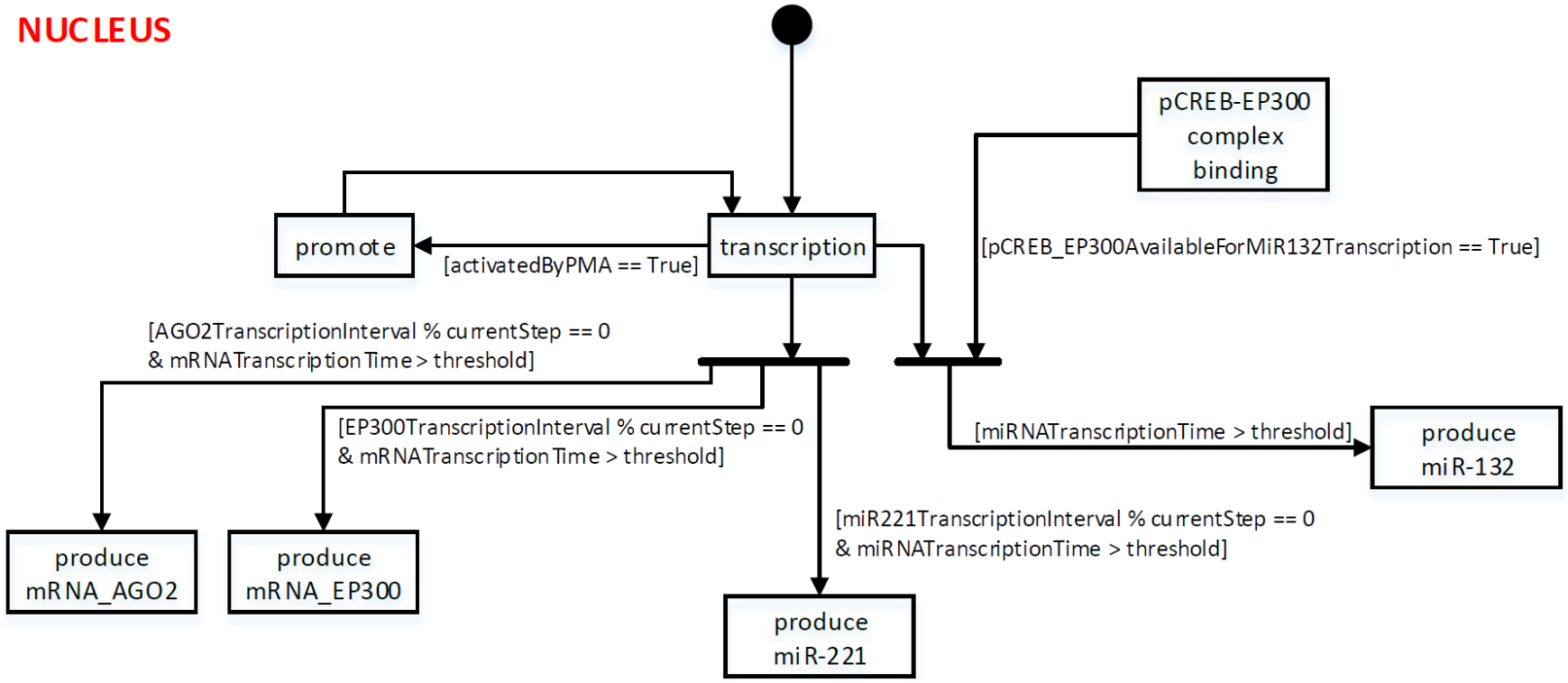

Figure 4.15: Activity diagram of the platform model for promoter. The promoter, a unique stationary agent resident in the nucleus, it functions to produce *AGO2* and *EP300* mRNA, and miR-221; miR-132 is produced in response to pCREB-EP300 complex binding with a certain probability (in Table 4.10, under Promoter). The transcriptional activity for AGO2 and miR-221 is directly affected during PMA activation.

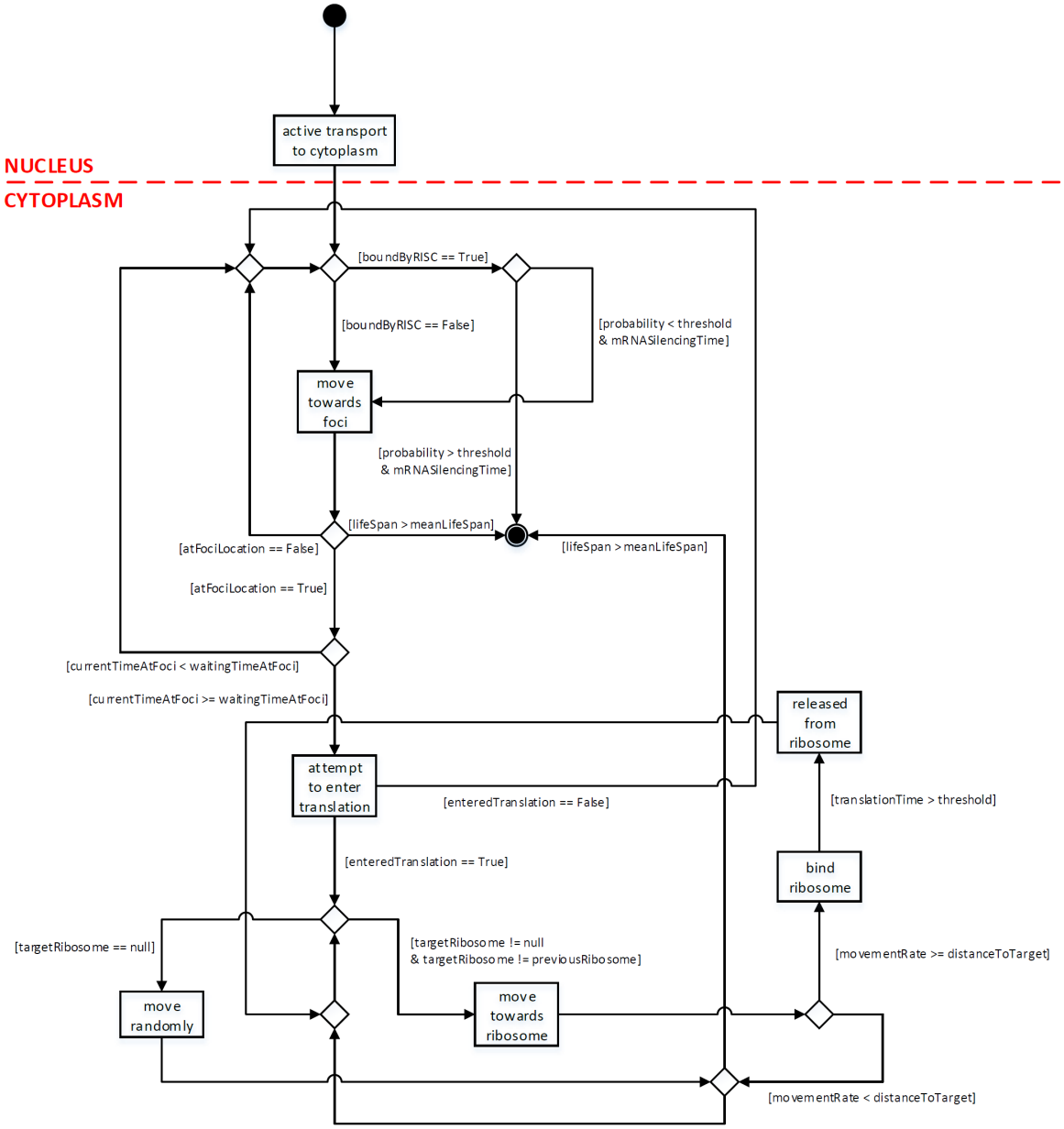

Figure 4.16: Activity diagrams of the platform model for *AGO2* mRNA and *EP300* mRNA. The mRNAs are both actively translocated to the cytoplasm after transcription, where they will move towards a location in the cytoplasm; there, at the cytoplasmic foci, a decision is made to either enter translation or remain stored at that location (in Table 4.10, under mRNA). Translating mRNAs cannot be targeted by miR-132 in this model, as most miRNAs have been found to be weakly associated with polysomes (Molotski and Soen, 2012).

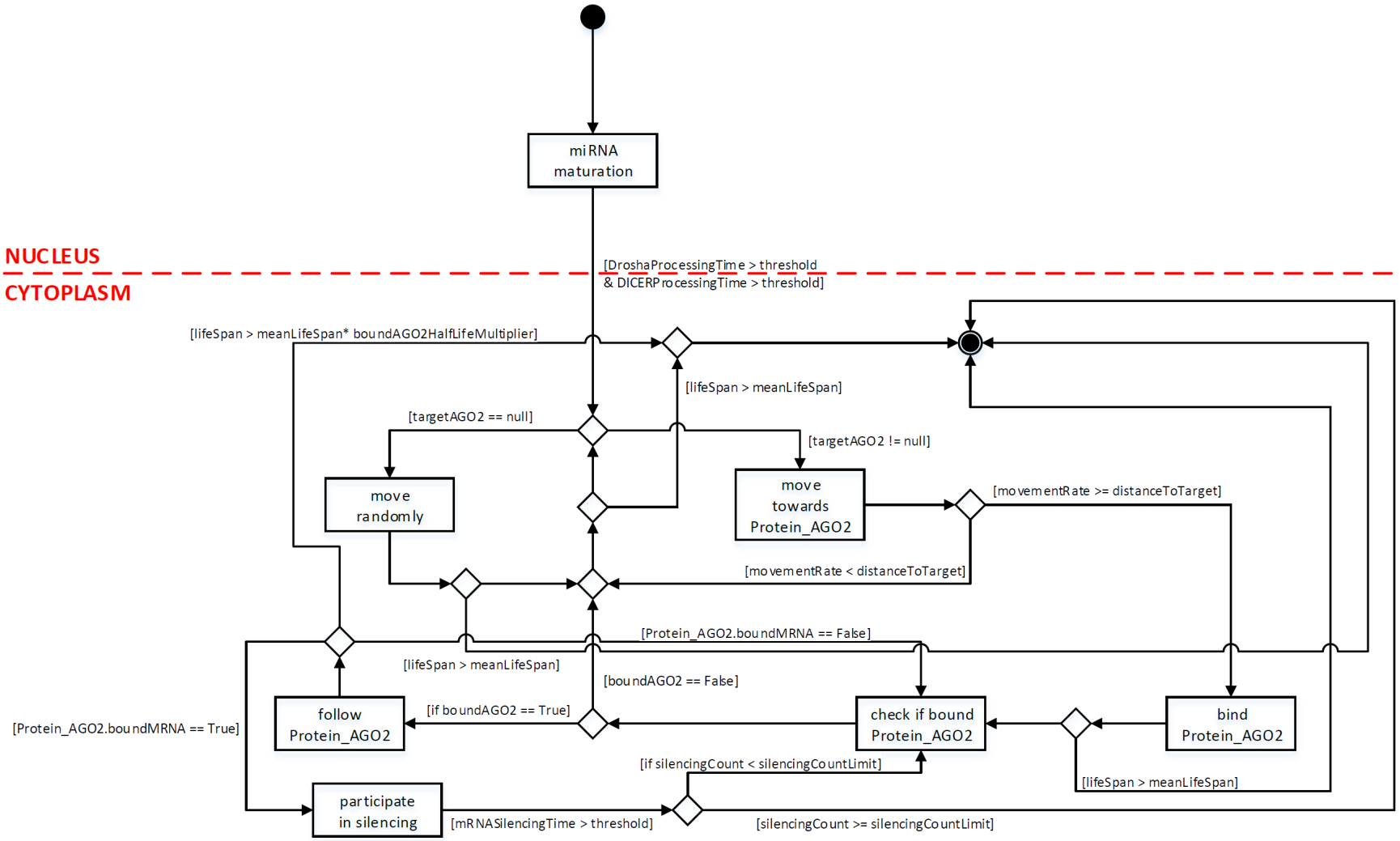

Figure 4.17: Activity diagrams of the platform model for miR-132 and miR-221. Both miRNAs have the same functional activity, however only miR-132 can participate in silencing targets in this model. Both miRNAs are produces as part of a canonical miRNA biogenesis process, and are loaded onto available AGO2 proteins as soon as possible.

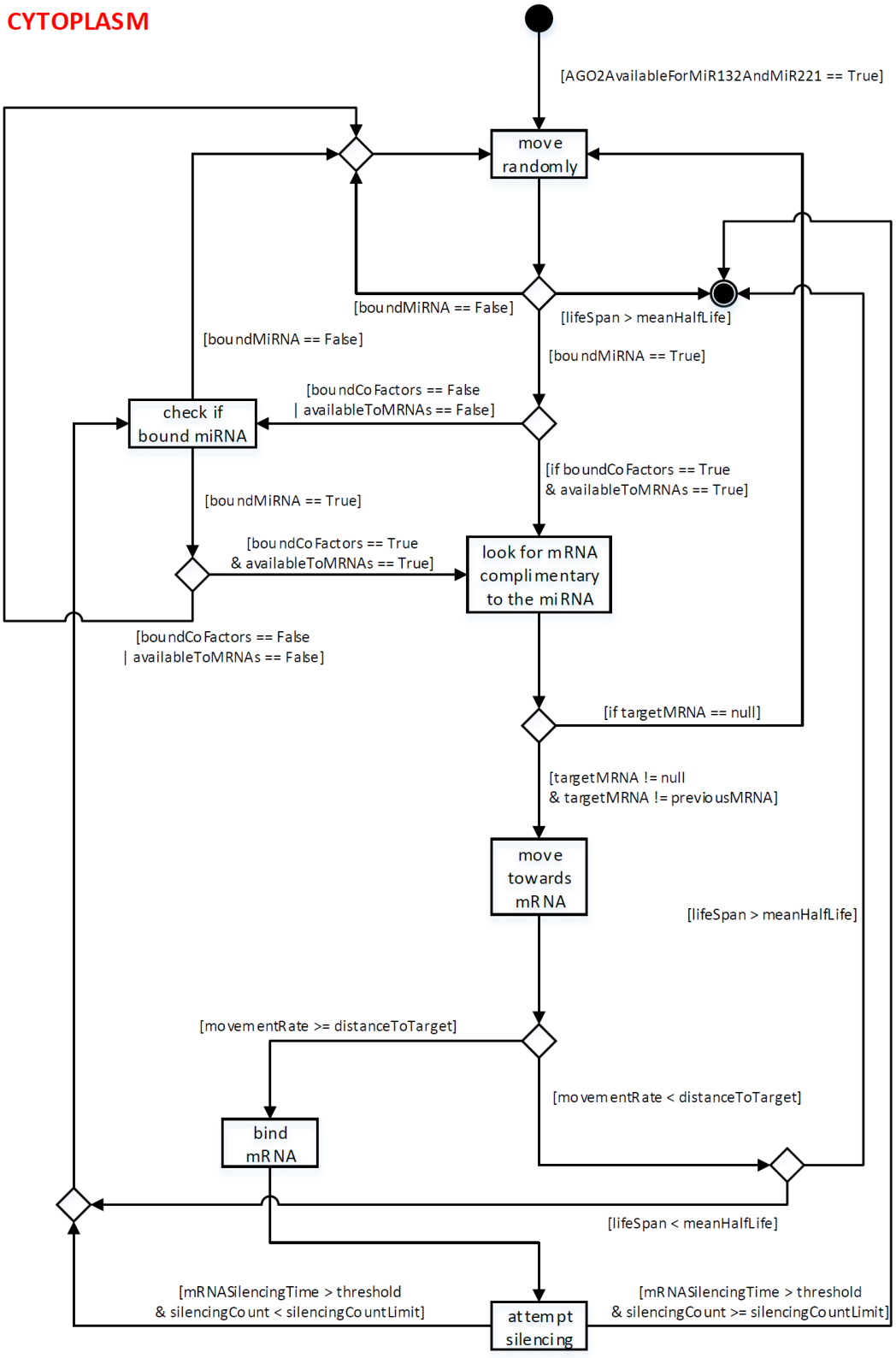

Figure 4.18: Activity diagram of the platform model for AGO2 protein. AGO2 functions as the silencing unit in the model – in complex with miR-132 it is will locate and bind a non-translating mRNA in order to attempt silencing, depending on the mRNA target (differential silencing efficiency).

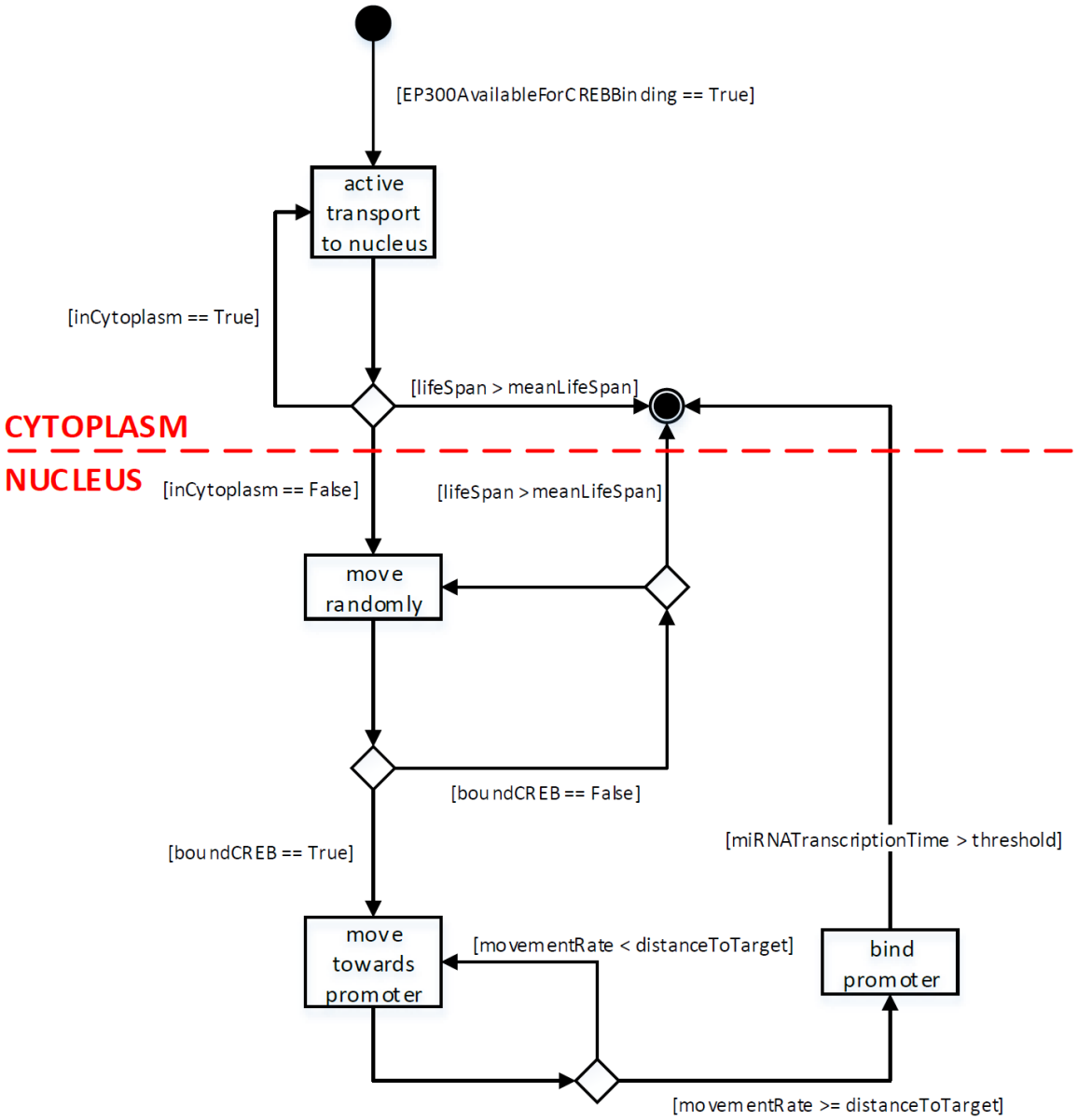

Figure 4.19: Activity diagram of the platform model for EP300 protein. EP300 main activity is to act as a co-transcriptional activator in the model by binding the active form of CREB, pCREB, and triggering miR-132 transcription upon the association with the promoter. It is translated into a protein in the cytoplasm, after which is is actively transported to the nucleus, where the majority of EP300 resides.

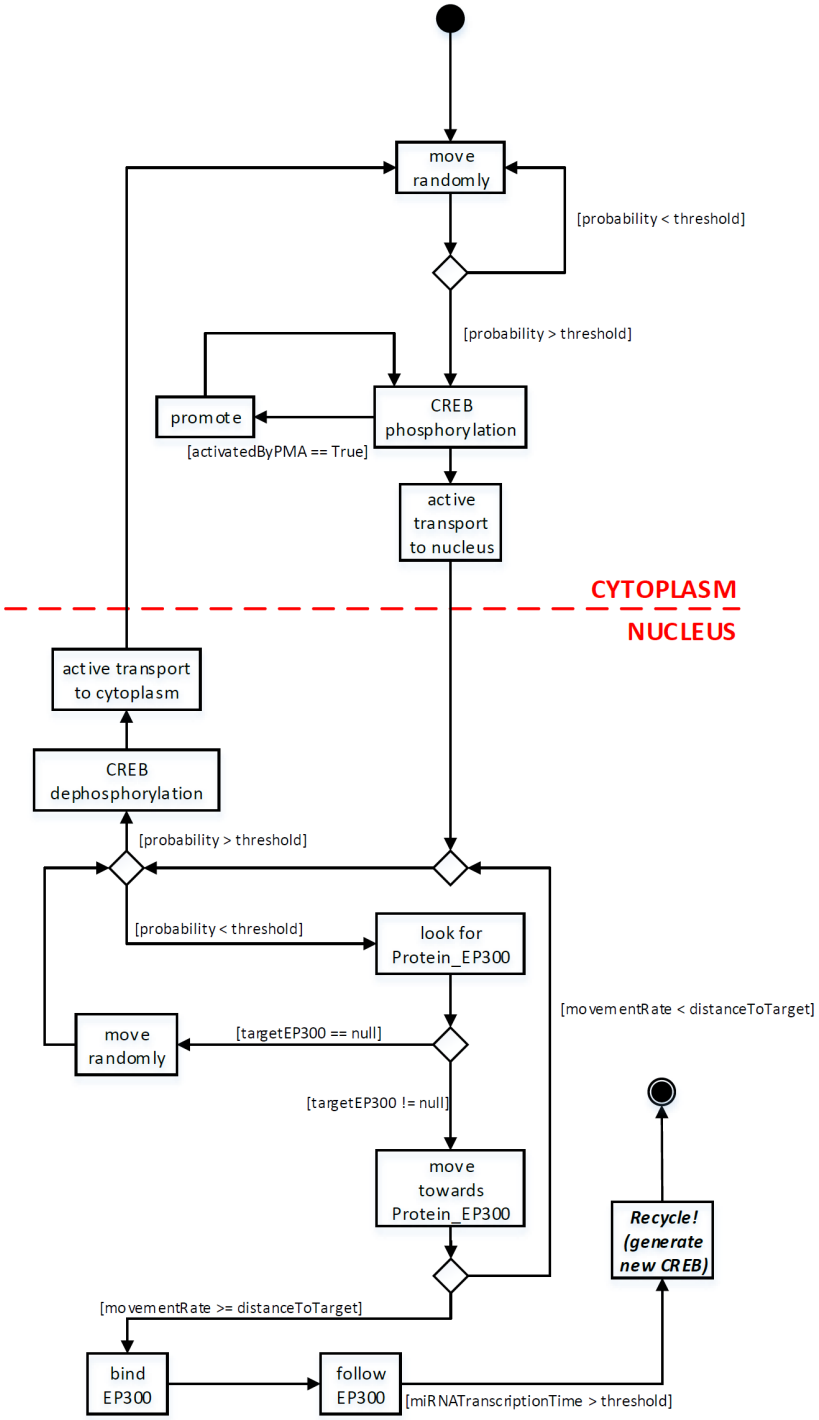

Figure 4.20: Activity diagram of the platform model for CREB protein. CREB is the only protein in the model that is not produced as a result of translation, but rather used as a recycled functional unit - upon its function as part of the EP300-pCREB complex triggering miR-132 transcription, it is removed from the simulation and replaced in the cytoplasm in its native, inactive form. The active, phosphorylated form of CREB, is targeted to the nucleus. A cell activated by PMA promotes the phosphorylation of CREB, increasing the potential for EP300 association in the nucleus to activate miR-132 transcription.

4.2.1 Supporting evidence

The assumptions that are made during the domain model planning propagate to the platform model, where more assumptions and implementation decisions are executed. In order to ensure that the model is representative of the problem domain, the documentation of each relevant model development step and decision is vital, and must be captured in a traceable explicit manner. In addition to the Parametrisation section and evidence provided to support the domain and platform models, some of the model specific justifications could not be categorised and presented under *class* and *activity* diagrams. This additional evidence supporting implementation decisions for the miR-132 silencing model is presented below:

space dimensionality The model is implemented in 2-D space. Although the LECs in the *in vitro* model system have a third axis, it makes up $<$10% of the cell diameter (see Table 4.11, cytoplasmDiameter). We consider 2-D space as a sufficient representation of the molecular motion without the implementation of collision dynamics.

space compartmentalisation The model implements a cell with borders that contains a cytoplasm and a nucleus. There is a 3rd type of compartment, *cytoplasmic foci*, which are single-point coordinate locations within the cytoplasm. The involved mobile components do not require a more complex compartmentalisation structure of the cell in this model.

space shape The space environment is implemented as a square. The implication of the space shape is unknown. The LECs have a stretched out cell shape with several protrusions around the cell.

molecule size The molecules have no size measure in the model, as we are not considering collision or any other function that is relevant to molecular size or shape.

nucleus size The size of the cell nucleus has been estimated with a nucleus to cytoplasm ratio approximately 1:3 for LECs (Podgrabinska et al., 2002).

movement direction Some components undergo *random movement* unless following a canonical process such activation or transport, in which case they will perform *random-*

directed movement (with a 180°random vector).

movement velocity The represented molecules cover a range of molecular weights, however most of the movement in the cell will occur in a random-directed fashion. In order to not lose the emergence of molecular interactions, the model simulates every second of *real* time, where large molecular components will travel at a similar slow rate (Wang et al., 2000).

simulation resolution As mentioned above, each step of the simulation represents one second of *real* time. This is sufficient resolution to capture the emergence of silencing events which occur on a longer time scale than 1 second.

ribosome mobility Ribosomes mobility is abstracted - the ribosomes are stationary units that mRNAs will travel to in a semi-directional manner.

mRNA storage Transcribed and spliced mRNAs would normally enter the cycle of translation, get stored or silenced. The model abstracts the storage by keeping the newly synthesised mRNAs at a cytoplasmic focus, where the mRNA will spend a set amount of time (*waitingTimeAtFoci*). Entry into translation is given by the *probabilityToEnterTranslation* parameter which is based on the translating mRNA percentage estimated for cells (Lackner et al., 2007).

translation rate Translation of a single mRNA occurs faster than the maximum synthesis rate in the model. However, the common translation in polysomes allows for translation rates to be much higher, assuming multiple ribosomes available to translate the mRNA molecule. Additionally, the model translation rates and transcription rates for the mRNAs have been calibrated to match the protein production rate per mRNA molecule during its lifespan.

cytoplasmic foci Cytoplasmic foci serve the purpose of mRNA storage and localisation. These abstract locations in space given by two coordinates allow for mRNAs to be kept in a region where mRNA silencing can occur. There are approximately 10 large cytosplasmic foci visible in the cell (Takahashi et al., 2011).

transcription rate The rate at which mRNAs and miRNAs are transcribed have been estimated directly through calibration. The transcription rate must ensure that the level of mRNA molecules present in the simulation is representative of the low mRNA copy numbers recorded by Schwanhäusser et al. (2011), given the appropriate lifespan, balanced by the effect of silencing.

silencing efficiency The binding of a miRNA to its target mRNA is not a fully efficient process, therefore the model implements a probability of silencing a single mRNA (*AGO2ProbabilityToBeSilenced*, *EP300ProbabilityToBeSilenced*). This probability represents the sum effect of a miRNA-mRNA association and dissociation and has been estimated based on Figure 3.3 and subsequent calibration.

miRNA maturation Determined by *DroshaProcessingTime* and *DICERProcessingTime*, the maturation of a miRNA follows the canonical pathway (Figure 1.1). The model allows for increasing the time delay between miRNA transcription and maturation, however for the purpose of the model the rate is considered to be negligable.

mRNA silencing time Upon miRNA-mRNA association, several proteins need to be recruited to perform silencing (Figure 1.4). The duration of this process has not been estimated, but this model incorporates this as an additional parameter *mRNASilencingTime* to investigate this value and its impact on the model system.

RISC recycling It has been suggested that RISC complexes (miRNA-AGO2 protein bound complexes) could be potentially recycled to perform silencing of more than one mRNA molecule. The exact stoichiometry has not been determined to our knowledge, and this model incorporates this additional parameter *silencingCountLimit* with the aim to investigate its impact on the model system.

phosphorylation and dephosphorylation CREB is phosphorylated in the cytoplasm, which signals its translocation to the nucleus, where it has a chance to encounter a phosphotase, lose its phosphorylated state and be exported to the cytoplasm. During normal cell function the level of phosphorylated CREB is low. The two parameters that govern CREB phosphorylation are *basalPhosphorylationProbability* and *basalDephos-*

phorylationProbability - both abstracted values estimated based on calibration – determine the chance of a single CREB molecule to undergo phosphorylation or dephosphorylation depending on its state and location.

4.2.2 Parametrisation

Every computational model requires a set of parameters that represent the biological system and can be used to make *in silico* predictions. The parameters displayed in the tables below are included in the simulation with presented evidence. The information sources combine inputs from data presented in Chapter 3 and published literature, pointing out parameters for which data is unavailable and the parameter values that are abstracted representations of biological phenomena. In some instances of Tables 4.11-4.12 the ”Source” is provided, but ”N/A” (i.e. Not Available) estimate is given – this indicates that the source was used in the calibration process but does not provide direct evidence for the estimate. The calibration of the parameters was carried subsequent to model implementation as described in Section 2.2.3.

Table 4.11: Parameter values for the current calibrated model baseline (as measured at 48 hours from the start of the simulation), the estimated biological range and source of information. (*) denotes that the value has been scaled according to the requirements of the platform model

Parameter	Unit	Calibrated value	Estimated value	Source / Note
cytoplasmDiameter	$10^{-1}\,\mu m$	300	250 x 150 x 20	estimated from Fig A.2
nucleusToCytoplasmRatio	a.u.	4	3	Podgrabinska et al. (2002)
ribosomeCount	a.u.	300*	surplus	Duncan and Hershey (1983)
minFociCount	a.u.	5	approx. 10	Takahashi et al. (2011)
maxFociCount	a.u.	10		
proteinCREBCount	a.u.	100*	>50000	Schwanhäusser et al. (2011)
miR132Count	a.u.	90	80-120	Lagos et al. (2010)
miR221Count	a.u.	5100	4500-6000	
mRNAEP300Count	a.u.	38	~20	Schwanhäusser et al. (2011)
mRNAAGO2Count	a.u.	39	~20	Schwanhäusser et al. (2011)
proteinEP300Count	a.u.	1050*	8000-15000	Schwanhäusser et al. (2011)
proteinAGO2Count	a.u.	420*	15000-30000	Janas et al. (2012)
miR132RISCCount	a.u.	40*	N/A	no estimate available
miR221RISCCount	a.u.	380*	N/A	
pCREBCount	a.u.	3*	<5%	estimated from Fig 3.10a
pCREB_EP300AvailableForMiR132Transcription	a.u.	100 (out of 1000)	<10%	Zhang et al. (2005)
miRNATranscriptionTime	s	20	$100\,nt\,s^{-1}$	Saini et al. (2007)
mRNATranscriptionTime	s	500		Ardehali and Lis (2009)
miR221TranscriptionInterval	s	5	N/A	Schwanhäusser et al. (2011)
EP300TranscriptionInterval	s	250	N/A	Schwanhäusser et al. (2011)
AGO2TranscriptionInterval	s	500	N/A	Schwanhäusser et al. (2011)
miR221PMAEffectTranscriptionMultiplier	a.u.	0.2	N/A	abstracted value

Table 4.12: Parameter values for the calibrated model baseline (as measured at 48 hours from the start of the simulation), the estimated biological range and source of information

Parameter	Unit	Calibrated value	Biological value	Source / Note
AGO2TranslationTime	s	50	10 to 20 $\mathrm{aa\,s^{-1}}$	Lackner et al. (2007)
EP300TranslationTime	s	50		
EP300AvailableForCREBBinding	a.u.	100 (out of 1000)	~10%	Franceschini et al. (2013)
AGO2AvailableForMiR132AndMiR221	a.u.	15 (out of 1000)	<2%	Janas et al. (2012)
miRNAMovementRate	$10^{-1}\,\mu\mathrm{m\,s^{-1}}$	10	<20	Wang et al. (2000)
DroshaProcessingTime	s	1	1	Ota et al. (2013)
DICERProcessingTime	s	1	1	Faller et al. (2010)
miRNAMeanLifeSpan	sec	36000	<86400	Winter and Diederichs (2011)
boundAGO2LifeSpanMultiplier	a.u.	2.0	>1.0	
mRNAMovementRate	$10^{-1}\,\mu\mathrm{m\,s^{-1}}$	10	<20	Wang et al. (2000)
waitingTimeAtFoci	s	60	N/A	no estimate available
probabilityToEnterTranslation	a.u.	60 (out of 100)	60-80%	Lackner et al. (2007)
AGO2ProbabilityToBeSilenced	a.u.	60	40%	estimated from Figure 3.3
AGO2mRNAMeanLifeSpan	s	21600	<25200	Schwanhäusser et al. (2011)
EP300ProbabilityToBeSilenced	a.u.	80	60%	estimated from Figure 3.3
EP300mRNAMeanLifeSpan	s	10800	<18000	Schwanhäusser et al. (2011)
proteinMovementRate	$10^{-1}\,\mu\mathrm{m\,s^{-1}}$	10	<20	Wang et al. (2000)
AGO2ProteinMeanLifeSpan	s	54000	46800-93600	Weinmann et al. (2009)
miR132RISCAvailableToMRNAs	a.u.	100 (out of 1000)	<10%	Wanet et al. (2012)
coFactorBindingTime	s	15	N/A	no estimate available
mRNASilencingTime	s	20	N/A	
silencingCountLimit	a.u.	3	N/A	Stalder et al. (2013)
EP300ProteinMeanLifeSpan	s	25200	54000-144000	Schwanhäusser et al. (2011)
basalPhosphorylationProbability	a.u.	3 (out of 10000)	N/A	abstracted value
basalDephosphorylationProbability	a.u.	40 (out of 10000)	N/A	

4.3 Executable model

The components described in the platform model were implemented using and ABM environment, where each component was defined as an agent class (inheritance diagram in Figure B.1). Agents like miRNAs and mRNAs share a lot of common parameters and functionality in this model: the mRNA and miRNA class were made as abstract classes, with specific miRNAs (miR-132, miR-221) and mRNAs (AGO2 and EP300 mRNA) implemented as independent agent classes inheriting from the parent classes, sharing much of the functionality. Proteins, on the other hand, share little common functionality and most of the movement and binding behaviour was implemented for each protein agent class (CREB, EP300, AGO2 proteins). The implementation and testing of the model is described under Section 2.2.2. Example outputs are available in the appendix

4.4 Calibration

The process of manual model calibration has been previously described by Read (2011). The rationale behind calibration is described in Section 2.2.3.3. The initial parameters used in the model prior to calibration do not necessarily give the appropriate outcome for all simulation measures. The model contains a range of implemented biological features and functionality required for the minimal representation of miR-132 mediated silencing of AGO2 and EP300, however it does not incorporate all known functionality of the miR-132 silencing network. Therefore, abstracted values that have not been biologically determined have been used as part of the model, and need to be calibrated alongside biological parameters in order to provide simulation outcomes as close to the supported measured biological data as possible.

The molecular abundances were used to calibrate the model (Table 4.11, -*Count* suffix parameters), with the biggest focus on miR-132 expression and abundance. The model, once calibrated, should be able to function as a silencing network where miR-132 in complex with AGO2 protein should be able to regulate the expression of EP300 and AGO2 through the suppression of their corresponding mRNA molecules (Figure 4.1).

4.4.1 Aleatory uncertainty analysis

Every simulation run of a stochastic simulation is different, provided that the *seed* value passed to the RNG is different (see Section 2.2.3 for more details). There are two types of uncertainty that can be considered in a simulation: aleatory and epistemic (Kiureghian and Ditlevsen, 2009). Epistemic uncertainty arises due to the lack of available data or unconsidered knowledge; following the CoSMoS process (Section 2.2), the development of the domain and platform model explicitly considers any gaps in knowledge and data, minimising the impact from epistemic uncertainty. Aleatory uncertainty which arises due to the implicit randomness of the stochastic behaviour as a result of agent-agent interactions in an ABM can be estimated by performing an aleatory uncertainty analysis of the model

(described in Section 2.2.3).

The first analysis method provided by *spartan* is the aleatory analysis (Alden et al., 2013), which essentially determines the number of simulation runs necessary to reduce the noise of the model output that is due to the stochastic nature of the simulation. For a biologist, this value (number of replicate simulations) would be equivalent to the amount of replicates needed to be performed of the same experiment given the same experimental setup and methodology, which would yield results with a certain error range. Until enough experimental replicates are performed, it is not possible to perform rigorous statistical analysis of the data set to determine the significance of the biological outcomes.

The aleatory analysis of miR-132 silencing model has been performed (Figure 4.21), showing the deviation (or in other words the uncertainty) of the measures given a certain number of simulation replicates. The measures presented are the agent counts of each of the molecules (e.g. AGO2 protein) and some of the complexes (e.g. RISC-miR-132). The Vargha-Delaney A-test was used to demonstrate the magnitude of the effect, which determined that after 100 simulation runs, the overall difference between the simulation outcomes would be approximately 5% (Figure 4.21). It is possible to reduce the uncertainty of the simulation by performing additional runs - with 200 replicates per simulation parameter set the difference between each outcome is consistently less than 5%. However, increased amount of runs requires increased execution time on a computing cluster, which is not always possible as mentioned in the following two techniques. Therefore, 100 replicate runs was used for each experimental condition for all purposes of the *in silico* simulation.

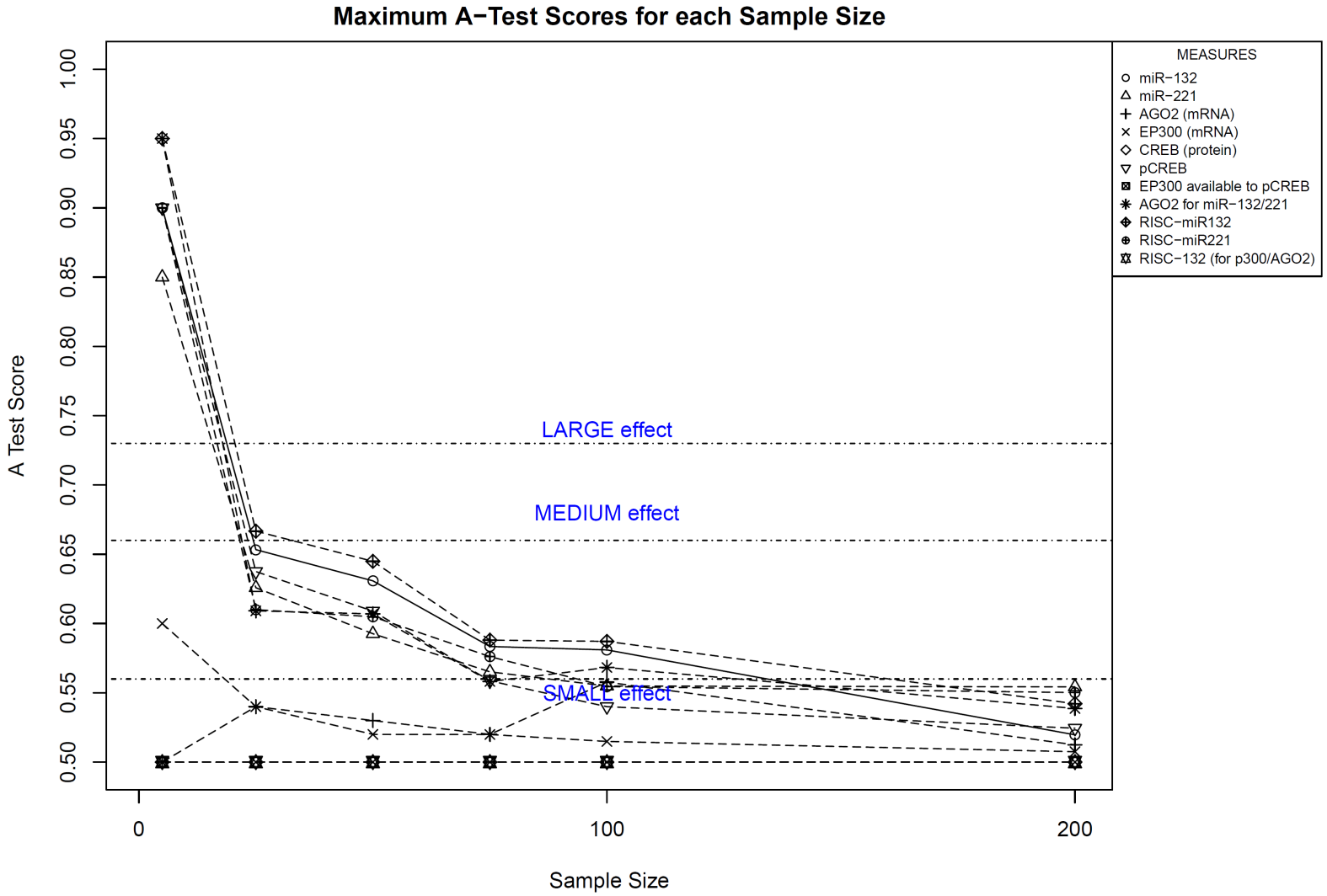

Figure 4.21: The aleatory analysis of the miR-132 silencing model displaying the uncertainty of each of the measures depending on the simulation runs performed for a single parameter set.

4.4.2 Single parameter perturbation

Single parameter perturbation effect is determined using the OAT analysis technique. The technique was used as one of the first analysis methods to investigate how dozens of parameters, when altered individually within a specified range, would affect the outcome of molecular abundance. Several rounds of OAT analysis was performed to look at different parameters and investigate the differences in outcome measures after readjusting some of the parameters as a result of the first OAT analysis.

The model contains over 50 parameters of which 25 were considered in the final round of calibration that showed higher sensitivity in response to change within its biologically accepted range of values (Table 4.11-4.12), each producing a summary graph demonstrating the magnitude effect of changing each individual parameter (Figure 4.22) and the individual breakdown of how each measure was affected as a result of this perturbation (Figure 4.23). Given 10 measures per a single parameter perturbation summary graph and approximately 25 parameters the final OAT analysis run, the included examples demonstrate the principle involved in the use of this analysis method to investigate system perturbation by a single parameter. Overall, 3 rounds of OAT analysis were performed in order to understand the sensitivity of each parameter in the simulation to an increasingly higher level of detail, narrowing down the range of parameter values that would create a baseline behaviour as described in the expected behaviours diagram (Figure 4.1).

One of the key parameters governing miR-132 transcription is the pCREB-EP300 complex availability. This parameter is an abstracted value, indicating how many pCREB-EP300 complexes are used up to produce a transcript of miR-132. Upon binding the promoter, each complex has a 10% chance to produce a miR-132. The stoichiometry of how many miR-132 transcriptional events occur as a result of a single complex binding is not known and therefore the abstracted value can incorporate that for investigating this biological question. As an example, increasing pCREB-EP300 availability to produce miR-132, as a net effect increases miR-132 abundance (Figure 4.23a and mildly impacts on miR-221 abundance (Fig-

ure 4.23b). The change in miRNA expression has downstream effects on how many each of the miRNAs is loaded onto AGO2 protein to form the functional RISC (Figure 4.23). Each of the outcome measures needed to be considered when calibrating the model as changing some parameters within certain ranges had a different magnitude of effect on the molecule abundance – changing pCREB-EP300 complex availability affects miR-132 abundance to a greater extent than the abundance of miR-221. These and hundreds of other graphs produced as a result of OAT analysis provided useful information that allowed stepwise manual model calibration.

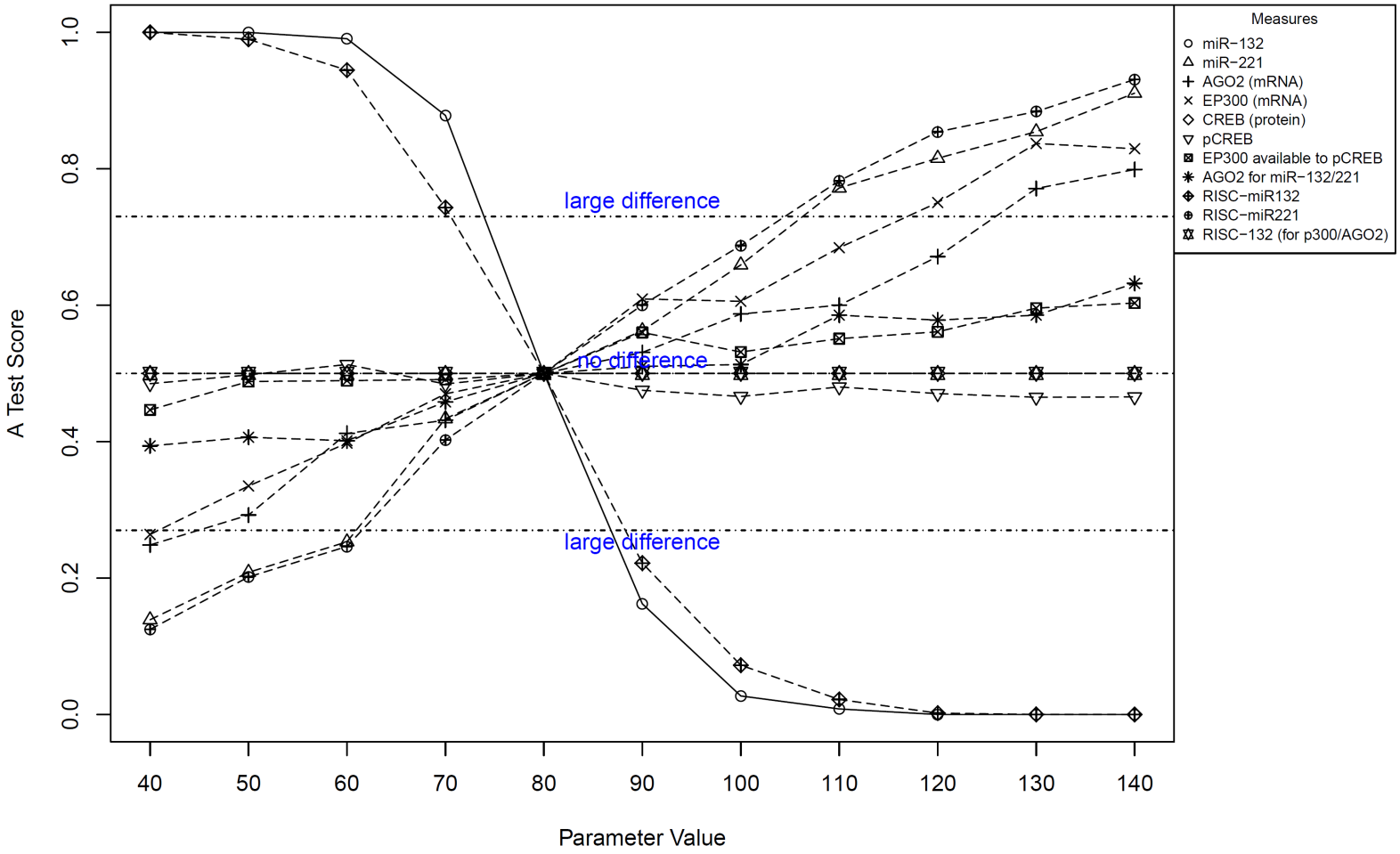

Figure 4.22: An example OAT analysis plot displaying how the pCREB-EP300 complex availability affects the outcome of several other parameters during the early stages of model calibration. The parameter value is a fraction of the complexes measured out of 1000 (i.e. parameter value 100 is equivalent to 10% of pCREB-EP300 availble for miR-132 transcription).

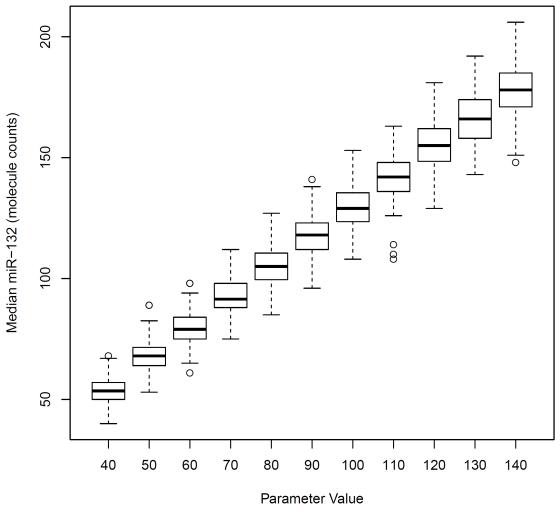

(a) miR-132 expression when altering pCREB-EP300 complex availability to transcribe miR-132

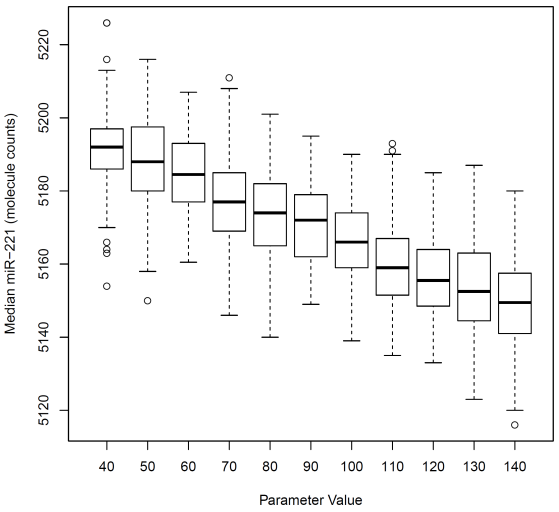

(b) miR-221 expression when altering pCREB-EP300 complex availability to transcribe miR-132

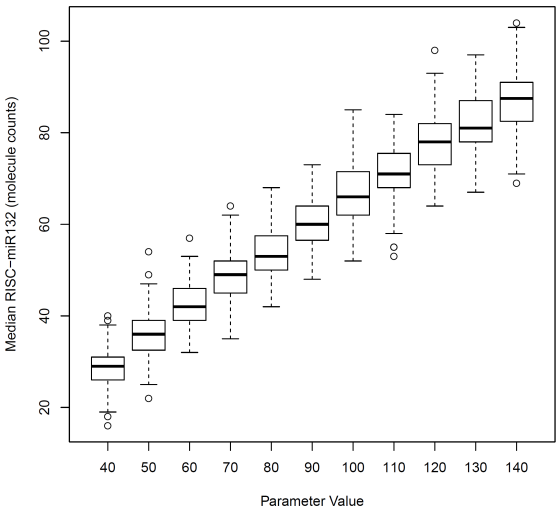

(c) Abundance of AGO2 protein loaded with miR-132 when altering pCREB-EP300 complex availability to transcribe miR-132

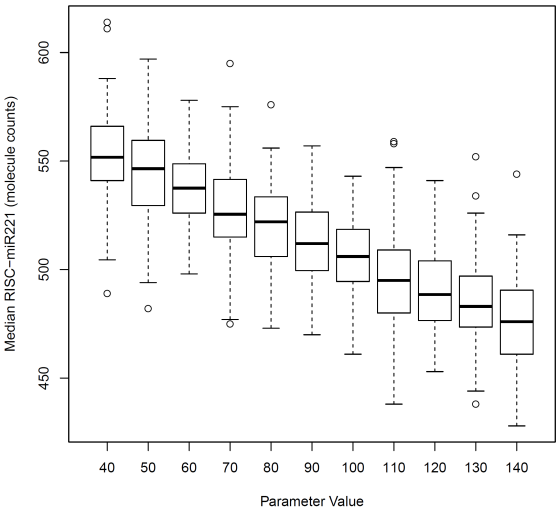

(d) Abundance of AGO2 protein loaded with miR-221 when altering pCREB-EP300 complex availability to transcribe miR-132

Figure 4.23: Increasing the transcription complex availability to transcribe miR-132 increases miR-132 loaded RISC count and decrease the RISC count loaded with miR-221, altering the abundance of individual miRNAs in a similar manner.

4.4.3 Global analysis of parameter space

Unlike the OAT analysis, the global analysis of parameter space allows for the identification of the affect of each parameter on the outcome measures during multiple system pertur-

bations. Global analysis was performed using the LHC sampling technique (Alden et al., 2013), during which 200 parameter files were generated, each with altered parameter values. The LHC sampling method alters multiple parameters simultaneously in order to cover most of the parameter space within the 200 parameter sample files. As pointed out earlier in the Aleatory uncertainty analysis section above, 100 replicate runs needed to be used for each parameter set. This meant that the LHC analysis technique required a grand total of 20 000 simulation runs. Depending on the parameter file setup of the analysis run, each individual simulation run can take up anything between minutes to hours of CPU time. Therefore a LHC involving 100 replicates across 200 different parameter files can only be achieved within a reasonable time scale through distributed computing.

The miR-132 silencing model global parameter analysis was conducted on the C2D2 cluster at York University with a sum CPU time of approximately 60 000 hours, distributed across 320 nodes, completed in just over a week of *real* time. The summary of the LHC analysis for the miR-132 silencing model is provided in Tables 4.13-4.14. The results of the LHC display the partial rank correlation coefficient (PRCC) for each parameter-outcome measure pair, showing both positive and negative effects of each parameter on the outcome measures. Parameters that are more likely to affect the outcome measure have a higher absolute value PRCC. The LHC analysis was most useful for investigating and appreciating the compound effects of altering parameters within the simulation, and greatly benefited the calibration process.

Table 4.13: LHC results summary (part 1). Values are displayed for p-value <0.05 threshold and for PRCC absolute value 0.3 or above.

Parameter / Agent Count	miR-132	miR-221	AGO2 mRNA	EP300 mRNA	pCREB
AGO2AvailableForMiR132AndMiR221		0.41			
AGO2mRNAMeanLifeSpan			0.89		
AGO2ProbabilityToBeSilenced			-0.32		
AGO2ProteinMeanLifeSpan					
AGO2TranscriptionInterval			-0.67		
AGO2TranslationTime		-0.31			
basalDephosphorylationProbability					-0.54
basalPhosphorylationProbability	0.59				0.93
boundAGO2LifeSpanMultiplier	0.30				
EP300AvailableForCREBBinding	0.39				
EP300mRNAMeanLifeSpan	0.56			0.85	-0.33
EP300ProbabilityToBeSilenced					
EP300ProteinMeanLifeSpan					
EP300TranscriptionInterval				-0.50	
EP300TranslationTime	-0.57				0.40
miR132RISCAvailableToMRNAs	-0.41		-0.49	-0.54	
miR221TranscriptionInterval		-0.92			
miRNAMeanLifeSpan	0.54	0.92			
miRNAMovementRate					
mRNASilencingTime					
pCREB_EP300AvailableForMiR132Transcription	0.42				
probabilityToEnterTranslation					
silencingCountLimit			-0.44	-0.50	
waitingTimeAtFoci					

Table 4.14: LHC results summary (part 2). Values are displayed for p-value <0.05 threshold and for PRCC absolute value 0.3 or above.

Parameter / Agent Count	RISC-miR-132	RISC-miR-221	EP300 protein	AGO2 protein
AGO2AvailableForMiR132AndMiR221	0.58	0.88		0.89
AGO2mRNAMeanLifeSpan	0.39	0.73		0.74
AGO2ProbabilityToBeSilenced				
AGO2ProteinMeanLifeSpan				
AGO2TranscriptionInterval		-0.45		-0.48
AGO2TranslationTime	-0.33	-0.74		-0.75
basalDephosphorylationProbability				
basalPhosphorylationProbability	0.43		-0.67	
boundAGO2LifeSpanMultiplier				
EP300AvailableForCREBBinding			0.52	
EP300mRNAMeanLifeSpan	0.39		0.66	
EP300ProbabilityToBeSilenced				
EP300ProteinMeanLifeSpan				
EP300TranscriptionInterval			-0.35	
EP300TranslationTime	-0.45		-0.76	
miR132RISCAvailableToMRNAs	-0.45	-0.34	-0.39	-0.39
miR221TranscriptionInterval				
miRNAMeanLifeSpan	0.46			
miRNAMovementRate				
mRNASilencingTime				
pCREB_EP300AvailableForMiR132Transcription				
probabilityToEnterTranslation				
silencingCountLimit		-0.35	-0.34	-0.37
waitingTimeAtFoci				

4.5 Baseline model

The result of calibration is an established baseline model which is considered representative of the biological phenomena as described by the domain model. Figures 4.24 and 4.25 present the first 72 hours of the baseline model compared to an enhanced miR-132 expression model[2], displaying the mean abundance of agents (or agent complexes) as recorded every 10 seconds of the simulation.

The abundance of the agents reaches a steady-state like behaviour by 48 hours of the simulation. The 48 hour time point is used to estimate the abundance of molecules in the model presented in the parametrisation Tables 4.11-4.12. Whilst some agents such as miR-221 and *AGO2* mRNA have a small deviation from the mean, most of the measures display approximately a 10% deviation from the mean value, which is comparable to the variation that can be measured by molecular biology techniques for a population of cells (such as demonstrated in Chapter 3). Here, we can consider each simulation replicate an independent cell with its unique profile of expression, where most of the cells will exhibit a regular pattern of expression closest to the mean.

As mentioned above, Figures 4.24 and 4.25 compare how molecular abundance differs between a baseline model (*red line, blue area*) and a system where pCREB-EP300 complex availability for miR-132 transcription has been enhanced 4-fold (*teal line, green area*). The baseline model is representative of a LEC, whereas the expression of miR-132 in some cells may be elevated (e.g. neurons); even the 4-fold change in miR-132 expression (Figure 4.24a) has global systemic effects, most prominently on RISC loading (Figures 4.24c and 4.24d) and consequently on AGO2 and EP300 mRNA and protein abundance (Figure 4.25). The increased deviation from the mean suggests that net effect of increased miR-132 abundance disrupts the regular protein expression and ”patterns” the protein synthesis and abundance by intercepting mRNAs through the action of miRNA mediated silencing. These effects

[2]a simulation, where the parameter governing miR-132 expression as a result of pCREB-EP300 transcriptional activation is changed to allow for increased miR-132 expression

propagate to functional transcription (pCREB-EP300) and silencing (RISC-132) complexes and could feed back on the miR-132 function. The increase in RISC loading with increased miR-132 expression (Figure 4.24a) despite the decrease in EP300 and AGO2 mRNA and protein abundance (Figure 4.25) suggests that the silencing efficiency of miR-132 targets is increased in an enhanced model of miR-132 expression, where miR-132 increases its competitiveness for AGO2 loading (Figure 4.24c) by outcompeting miR-221 (Figure 4.24d).

The current baseline model adequately represents the biological problem domain allowing to investigate the impact of miR-132 driven regulation of AGO2 and EP300, and the dynamics of miRNA-mediated gene silencing.

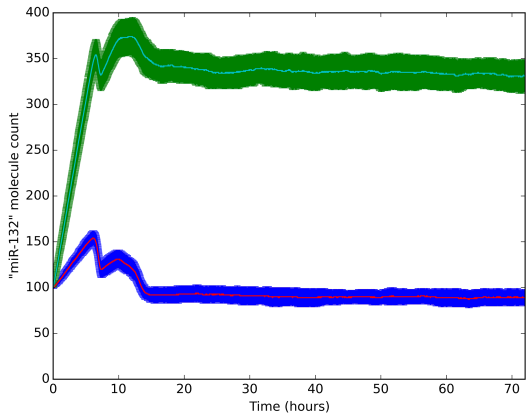

(a) expression of miR-132

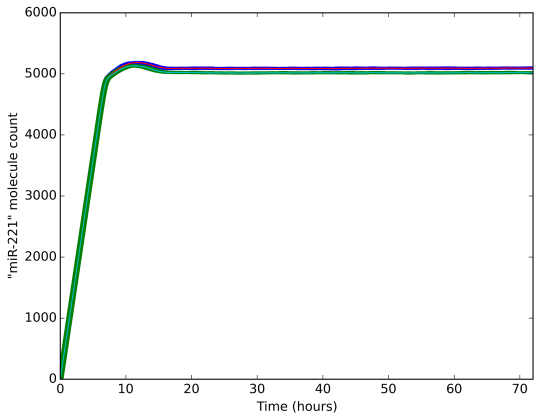

(b) expression of miR-221

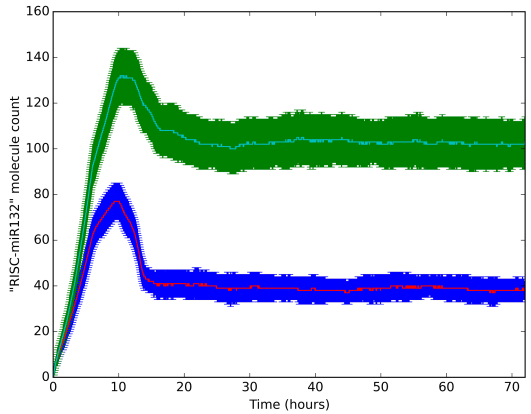

(c) abundance of miR-132 loaded RISC

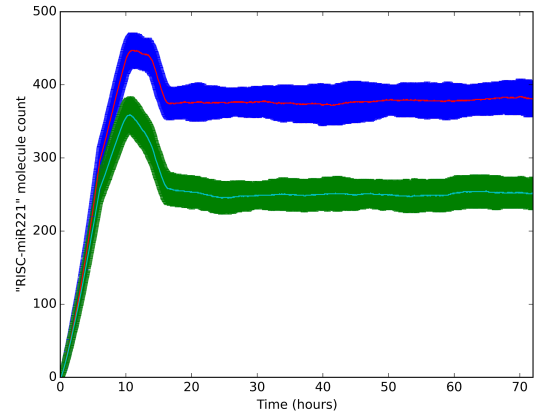

(d) abundance of miR-221 loaded RISC

Figure 4.24: Baseline expression of agents (mean - *red line*, standard deviation - *blue area*) compared to miR-132 enhanced expression effect on the expression system due to enhanced pCREB-EP300 complex availability (mean - *teal line*, standard deviation - *green area*) over 72 hours.

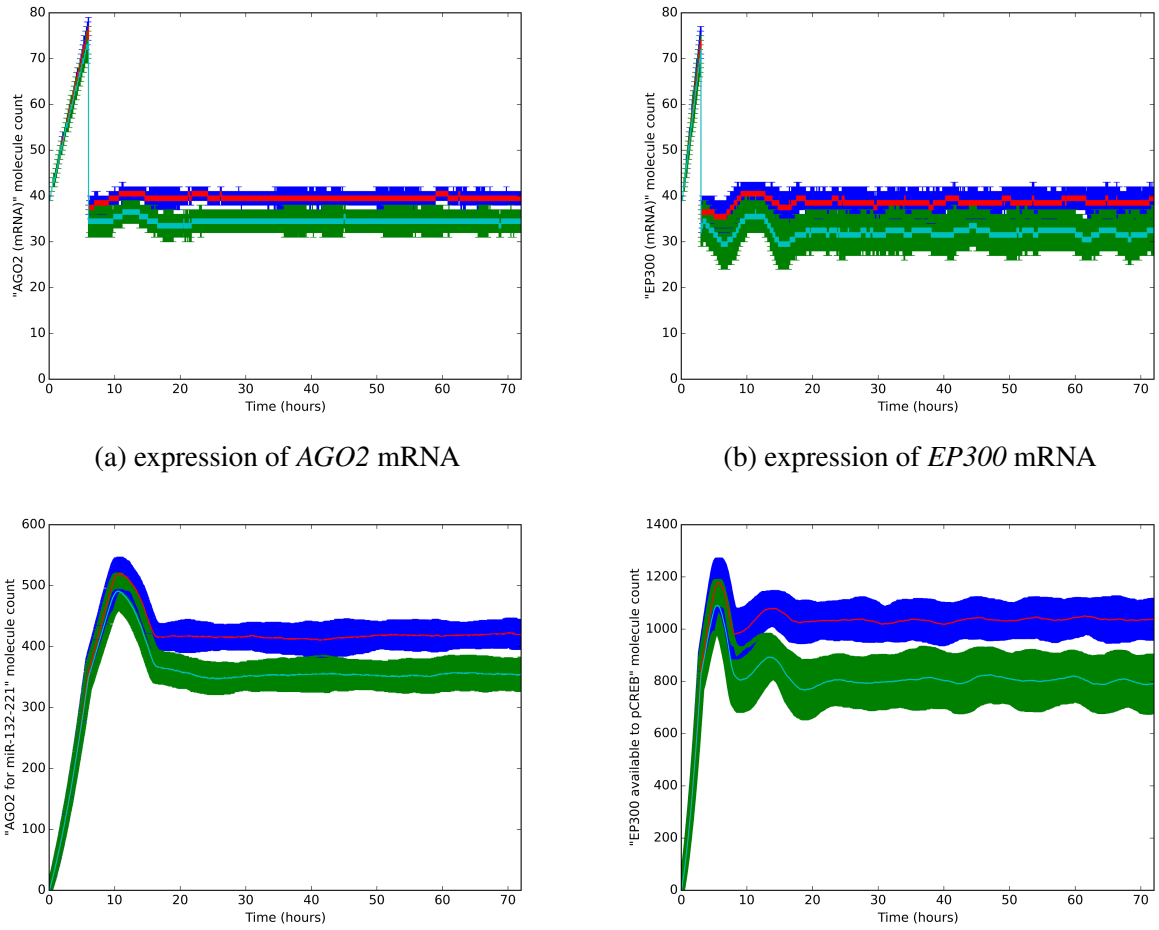

(a) expression of *AGO2* mRNA

(b) expression of *EP300* mRNA

(c) abundance of AGO2 protein available to miRNA

(d) abundance of EP300 protein available to pCREB

Figure 4.25: Baseline expression of agents (mean - *red line*, standard deviation - *blue area*) compared to miR-132 enhanced expression effect on the expression system due to enhanced pCREB-EP300 complex availability (mean - *teal line*, standard deviation - *green area*) over 72 hours.

4.6 Discussion – the miR-132 silencing model development

Aside from the work mentioned by Pedrioli et al. (2010), the miR-132 silencing model is the first miRNA-regulatory network model developed as an ABM. In addition to the benefits of capturing the regulatory network as an ABM (described in Section 1.3.2), the model ABM offers several novel perspectives of investigating miRNA-mediated gene regulation:

1. Captures the activity of low abundance entities (i.e. miR-132, *AGO2* and *EP300* mRNAs) and the dynamics of miR-132 self-regulation through a double-feedback loop with AGO2 and EP300

2. Implements 2D space, providing the potential to investigate role of AGO2 localisation and its contribution to miRNA-mediated silencing

3. Implements two explicit miRNA-mediated silencing control points: the recycling of RISC (re-use of a RISC for silencing several miRNAs) and the differential target mRNA silencing potential (probability to be silenced specific to each mRNA)

The model represents a regulatory feedback loop where miR-132 is the key regulator of its own transcription and required for controlling the level of silencing by targeting *AGO2* mRNA. This model is built based on LEC expression data, however, the principles developed for capturing miRNA mediated gene silencing can apply to other miRNA-mRNA regulatory circuits.

4.6.1 Reflecting on the development process

The model development process employed the CoSMoS process (Andrews et al., 2010a,b) as a framework for developing a model of biology, in this case the miR-132 mediated silencing network in LECs. The process offered two main useful elements: (1) the separation of the biological domain, the domain to be modelled, the implementation strategy, and the

interpretation and analysis of the *in silico* simulation results and (2) the transparency of capturing and presenting the model at each stage.

As the first stage of this thesis involved hands-on molecular biology approaches investigating the biological system captured in the model, the initial stages of domain development were the least time consuming. Since the problem domain was also well-established within the wet-lab experimental period investigating miR-132 regulation of AGO2, the development of the platform model also took up a little amount of time. Most effort was required in understanding how to capture the domain and platform diagrams using a formalised UML, and the calibration of the model. The process of implementation of the model is discussed in the section below.

4.6.2 Reflecting on Repast Simphony

Repast Simphony (North et al., 2013) was developed as an agent-based modelling environment in Java, but also offers a High Performance Computing framework in C. The Repast Simphony offered a much smaller learning curve and a wide variety of built-in functionality that was useful and common in agent-based systems. The application itself has several interfaces to other popular packages, like SPSS or R, offers live-rendered graphs without impacting on execution speeds, with all functionality available via the GUI.

Despite its appeal as a highly integrated ABM environment with top-level functionality, there were several drawbacks with this system design. Several features were counter intuitive and the batch submission system did not function properly. Here is a list of problems that were encountered with Repast Simphony prior to any modifications:

1. Repast Simphony is tightly linked to the GUI
2. The GUI is the only access point for starting a Batch run
3. The Batch run setup GUI is intuitive, but lacks a way of customising the number of replicates

4. The Batch run deployment system did not correctly use/identify the Sun Grid Engine on the remote machine when given the remote address

5. The Batch run setup GUI lacks a way of setting a random *seed* explicitly in the simulation (see next point)

6. The *seed* is provided within the parameter XML file and specified to produce a random *seed* each time a simulation is started. However, a new *seed* is generated and used by the RNG within the simulation when a *RandomHelper* module is invoked

7. The online documentation provides no supporting information for executing a single run of a Repast Simphony model without the GUI

8. Repast Simphony is ”bulky” - there are over 30 *jar* libraries packaged (over 50 MB) when compiling the simulation into an executable, most of them not used by the model but checked for on Repast Simphony runtime

9. Repast Simphony’s produced executable is an installer, not an executable simulation file. There is no documentation or instructions of building an executable *jar* of the simulation

10. Repast Simphony’s simulation trigger module RepastMain or RepastBatchMain only takes 2 parameters: the optional parameter input file location and the required scenario directory location. The output is managed by a separate module and an XML configuration file

11. Repast Simphony has poor backwards and forwards compatibility. Repast Simphony model created in version 2.1 does not compile into an executable *jar* due to several packages merged/made obsolete from version 2.1 to 2.2. Similar problem occurs when trying to build an executable of a model created in Repast Simphony version 2.2 in a version 2.1 environment

All of the aforementioned problems encountered when developing using Repast Simphony have been worked around for the purpose of this thesis and the miR-132 silencing model. However, the Repast Simphony framework can currently be considered as an unsuitable choice for scientific development of ABMs, with the GUI providing little to no support for creating reproducible simulation runs.

4.6.3 Reflecting on the baseline model

The current miR-132 silencing model is considered to be calibrated to a baseline behaviour. Although all the calibrated parameter values are within or close to their biological values (Tables 4.11-4.12), it is likely that several calibrated baselines with similar behaviour exist. The caveat of manual calibration means that only one of several solutions can be observed and established. Calibrating the simulation to a baseline model behaviour remains a laborious task, with an automatic calibration methodology in high demand. An attempt has been made to address the issues and possibilities of automatic calibration of biological ABMs (Read et al., 2013), but has not been easily adoptable to any other model to date.

There are several parameters such as *PMAEffectModifiers*, which determine the propagation of PMA-activity in the simulation on various agents, that have not been calibrated as part of the baseline model. Instead, the PMA activation of the cells is implemented and presented in the following chapter - Explorative simulation of miR-132 activity and function *in silico*.

Chapter 5

Explorative simulation of miR-132 activity and function *in silico*

The miR-132 silencing model (Chapter 4) was developed in order to investigate the miR-132 mediated regulation of AGO2 and EP300 in cultured LECs (Chapter 3). The model was calibrated to achieve a steady-state like behaviour of LECs *in vitro* (Section 4.4). In order to investigate how miR-132 mediated regulation propagates its effects on AGO2 and EP300 abundance and function in the model, the following Chapter describes the implementation of LEC activation. *In vitro*, the activating agent was PMA (Section 3.4), which drove several processes as depicted in the expected behaviour diagram (Figure 4.1). The activation of the LECs *in silico* was carried out 48 hours (172800 iterations) from the start of the simulation once the baseline behaviour had been achieved, simulating the activated state and the regulation of the model components during 48 hours of PMA activation (Section 5.2). In a cell, the increased expression of miR-132 during LEC activation by PMA acts as a constant regulator of its targets. Two of these are investigated in a closed regulatory network – EP300 and AGO2. But are both of them necessary to allow the cell to function? This raises the problem of importance of miR-132 mediated regulation, which is later explored *in silico* by making AGO2 a non-targeted mRNA molecule (Sections 5.2.3 and 5.2.4).

5.1 PMA activation

PMA induced activation of LECs showed an effect on multiple measures (Section 3.11). The function of PMA in the miR-132 silencing model was to induce CREB phosphorylation as seen in Figure 3.10, and account for the additional PMA induced regulatory effects on *AGO2* mRNA and miR-221 levels. PMA itself cannot directly bind to any of the aforementioned agents to elicit an agent-agent interaction and response. Instead, it is implemented as a model-wide state parameter, *activatedByPMA*, which results in the increased phosphorylation probability of the CREB protein and changes to transcription rates of *AGO2* mRNA and miR-221. The abstraction of PMA to a model-wide state parameter is justified for several reasons: its effect of inducing miR-132 across a wide range of concentrations (Figure 3.9) is saturated at the concentration ($25\,\mathrm{nM}$) used for all experimental conditions, and the upstream protein kinase cascades that result in PMA induced effects are not implemented and therefore its concentration distribution in space within the context of this model would not be relevant.

The gathered biological data (Section 3.4) was used as the determinant of how the PMA treatment of LECs affects CREB protein phosphorylation and *AGO2* mRNA and miR-221 abundance over a course of 24 hours. Unlike biological data, which has data available at discrete time points of LEC activation, the model simulates continuous data recording absolute quantities of molecules every 10 seconds of real time. This means that the PMA-driven activation of the agents in the simulation needed to be approximated using a suitable function that would fit the agents' expression and activation profiles as found in the *in vitro* data. Moreover, several assumptions had to be made regarding the effect of PMA and how it affected *AGO2* mRNA and miR-221 abundance, and CREB phosphorylation:

CREB protein During PMA activation, the CREB protein phosphorylation is rapidly increased as a consequence of upstream kinase activity (Figure 3.10). The model aims to identify if by altering the phosphorylation probability parameter of the agent, *phosphorylationProbability*, it is possible to achieve a CREB phosphorylation profile com-

parable to that in LECs during PMA activation.

miR-221 During PMA activation, the transcription rate of other genes is downregulated, including miR-221, resulting in an decreased expression of the miR-221. The model abstracts this observation by altering the promoter agent basal transcription rate parameter, *miR221TranscriptionInterval*, predicting that it is possible to achieve the miR-221 abundance comparable that in LECs during PMA activation.

AGO2 *mRNA* During PMA activation, the transcription rate of many genes is upregulated, including *AGO2*, resulting in an increased expression of the AGO2 mRNA and protein. The model abstracts this observation by altering the promoter agent basal transcription rate, *AGO2TranscriptionInterval*, predicting that it is possible to achieve the mRNA and protein abundances comparable to those in LECs during PMA activation.

In vitro the activation of LECs by PMA can be observed within 15 minutes from the treatment start: the phosphorylation of CREB rapidly escalates, with modest up- and downregulation of *AGO2* mRNA and miR-221 expression. PMA has longer lasting effects, resulting in a gradual decline in the activation profile. This activation can be approximated by a function with a positively (right) skewed distribution. The Gompertz probability density[1] function was taken as the basis for the PMA activation function used in the simulation. The PMA activation function was used to compute the parameter-altering modification y necessary for each iteration from the start of the PMA treatment x. The PMA activation function was defined as

$$f(y) = b\eta e^{bx} e^{\eta} e^{-\eta e^{bx}} \tag{5.1}$$

where $b > 0$ determines the scale and $\eta > 0$ determines the shape of the function, and e refers to the Euler's number. The purpose of the activation function was to mimic the resulting relative activity and abundance of the above mentioned molecules. The activation

[1] continuous probability distribution, more commonly applied in risk assessment and demography

functions variables b and η were adjusted manually (Table 5.1) to give an approximate fit to the available data points in Figure 5.1.

Table 5.1: Variable values b and η used for generating the profile of the PMA activation functions for each of the affected parameters.

Altered parameter	b	η	Plot
phosphorylationProbability	0.32	3.75	Figure 5.1a
miR221TranscriptionInterval	0.32	2.1	Figure 5.1b
AGO2TranscriptionInterval	0.13	3.7	Figure 5.1c

The activation function was implemented to modify the transcription rates of miR-221 and *AGO2* mRNA, as well as CREB phosphorylation. Provided the assumptions regarding the PMA effects in the simulation were correct, the relative activation function should provide *in silico* experimental data comparable to the *in vitro* biological data.

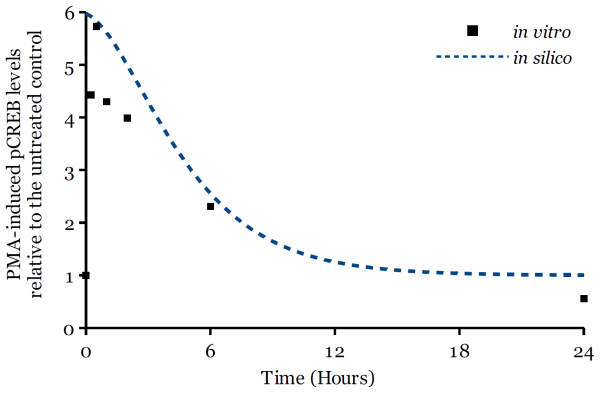

(a) The activation function altering the pCREB phosphorylation probability parameter *phosphorylationProbability*.

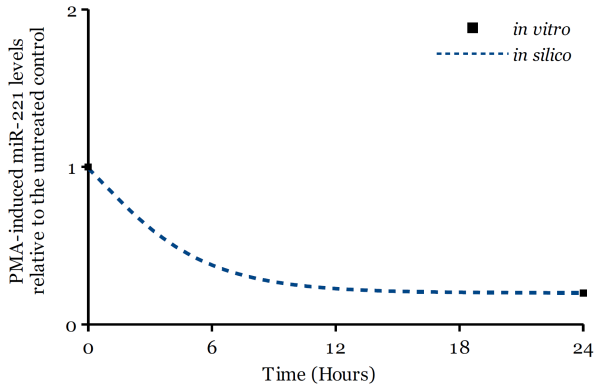

(b) The activation function altering the miR-221 transcription interval parameter *miR221TranscriptionInterval*.

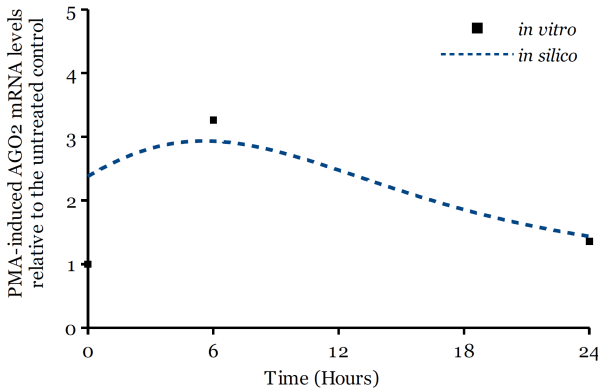

(c) The activation function altering the AGO2 *mRNA* transcription interval parameter *AGO2TranscriptionInterval*.

Figure 5.1: Implemented PMA treatment activation functions for CREB phosphorylation, miR-221 and *AGO2* mRNA (dashed continuous line) following the *in vitro* LEC data (single averaged data points) over a 24 hour time course.

5.2 Experimentation *in silico* during PMA-activity

The *in vitro* effect of PMA on most components included in the simulation was only measured up to 24 hours from the treatment, with few experimental data points recorded at earlier time points. The simulation of PMA activation presented in this section demonstrates how miR-132 is able to regulate EP300 and AGO2 in LECs with baseline miR-132 expression compared to enhanced expression of miR-132 (Figure 4.24a) and explores how PMA induced perturbation of the miR-132 regulatory network alters miRNA-mediated target regulation, namely AGO2 and EP300.

5.2.1 Baseline LEC stimulation

During regular LEC activity, untreated cells maintain a low level of CREB phosphorylation. In this *in silico* experiment, PMA functionality is activated at 48 hours, resulting in an increased CREB phosphorylation level (Figure 5.2a). The increased pCREB level allows for more miR-132 to be produced (Figure 5.2b), transcriptionally activated by the the pCREB-EP300 complex association. The increase in CREB phosphorylation together with the increase in miR-132 regulatory activity on *EP300* mRNA (Figure 5.2c) results in a rapid decline of EP300 protein (Figure 5.2e). Since PMA activation results in an increased AGO2 *mRNA* expression (Figure 5.1c) by ~3 fold, the mRNA copy number for AGO2 is increased during the early hours of PMA activation (Figure 5.2d) from ~40 molecules to ~100 molecules during the peak of PMA activation (2.5 fold change). The increase in *AGO2* mRNA is closely followed by the increase in AGO2 protein (Figure 5.2f) from ~420 molecules to ~1000 molecules during the peak of PMA activation (2.5 fold change).

AGO2 mRNA and protein levels return to baseline abundance after 48 hours of PMA treatment – ~40 and ~420 molecules, respectively. However, miR-132 abundance (~1.2 fold above pre-treatment level) remains at an elevated level of expression, up from 40 molecules pre-treatment to 60 molecules post-treatment (Figure 5.2b). This coincides with an in-

creased miR-132 bound AGO2 count, ~1.2 fold above pre-treatment level (Figure C.2c). Both miR-132 and miR-221 are competitors for AGO2 protein loading to form a RISC complex (AGO2 protein scaled proportionally to miRNA abundance in the cell, based on the 1:10 ratio; see evidence in Table 4.10). Since miR-221 expression is reduced during PMA activation by ~60% (Figure C.2b), and miR-221 loaded RISC baseline abundance is restored after 48 hours of PMA treatment to the baseline value of 380 molecules (Figure C.2d), it is likely that increased miR-132 bound AGO2 count is due to the drop in the expression of its competitor – miR-221. RISC-loaded miR-132 has an increased lifespan (given by the *boundAGO2LifeSpanMultiplier*) and therefore the abundance of miR-132 can remain above baseline for a prolonged period of time, keeping *EP300* mRNA and protein expression below baseline (Figures 5.2c and 5.2e).

Overall, the simulation results of PMA activation qualitatively reproduce the behaviour presented in the Domain model - expected behaviour diagram and the PMA activation data recorded for *in vitro* LECs (Figure 3.11). However, the miR-132 relative abundance during PMA activation *in silico* is only ~3 fold upregulated, compared to the ~5 fold upregulation recorded *in vitro* data (Figure 3.11a). Moreover, the relative increased abundance level of miR-132 after 24 hours of PMA treatment *in silico* is upregulated by ~1.2 fold, lower than in the *in vitro* data where miR-132 levels are maintained over 4 fold after 24 hours of PMA treatment. Based on this result, and the work that demonstrated that at least a 4 fold miR-132 induction in LECs is necessary to show a small but significant change in miR-132 mediated AGO2 regulation of activated LECs (Figure 3.13d), the following *in silico* experiments use an enhanced miR-132 transcription rate (enhanced miR-132 expression baseline of ~380 molecules, up from ~100 molecules at LEC baseline (Lagos et al., 2010)). The model parameters have been previously calibrated to the baseline behaviour of the regulatory network, where the molecular abundances qualitatively resemble the abundances seen in LECs (Tables 4.11 and 4.12). Increasing the amount of miR-132 in the model by altering the *pCREB_EP300AvailableForMiR132Transcription* parameter, the new miR-132 expression

profile represents a scenario where higher miR-132 expression would regulate its molecular targets consistent with the expected behaviours diagram (Figure 4.1). This allows the model to explore the regulatory outcomes on the miR-132/AGO2/EP300 regulatory network when the activated cell miR-132 abundance reaches a higher level of expression necessary for target regulation.

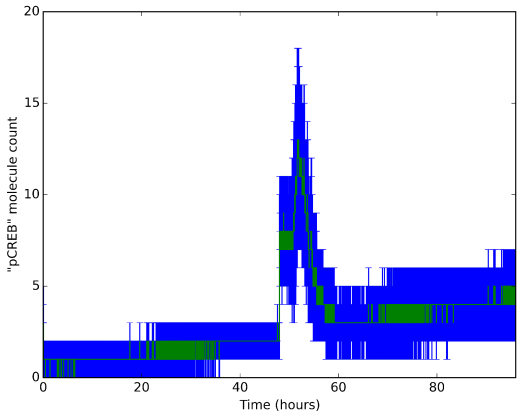

(a) % of phosphorylated CREB

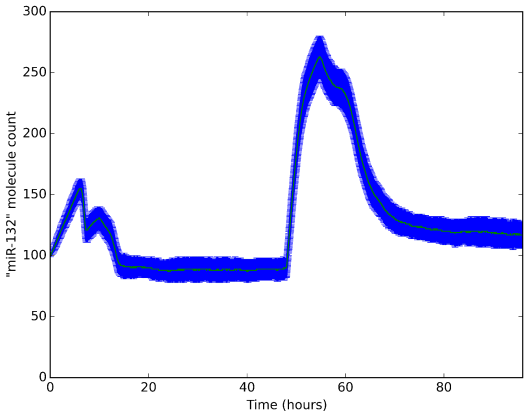

(b) absolute miR-132 count

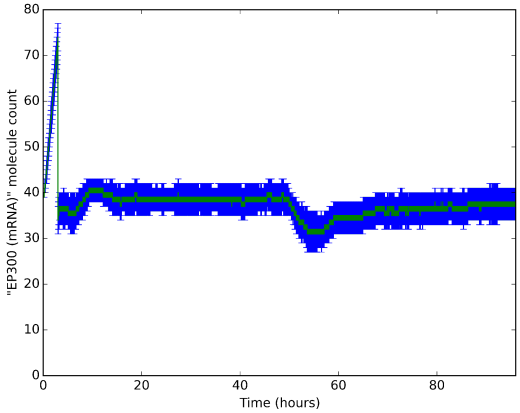

(c) absolute EP300 *mRNA* count

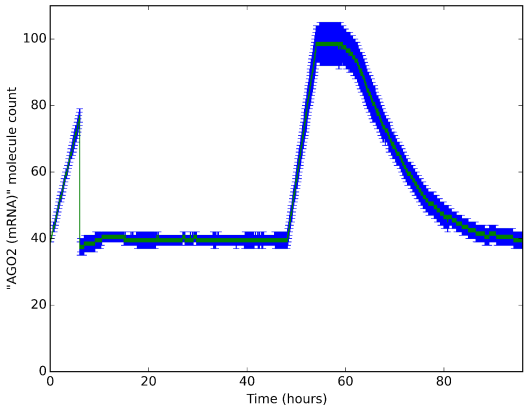

(d) absolute AGO2 *mRNA* count

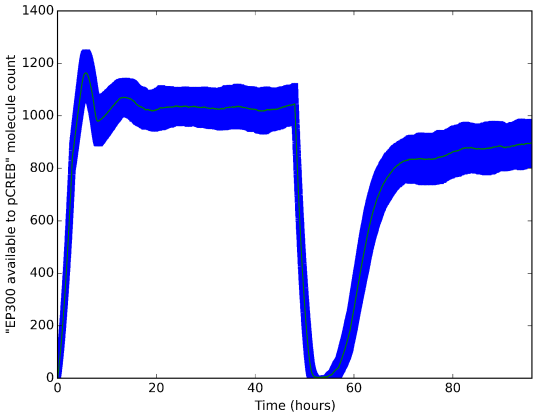

(e) absolute EP300 protein count

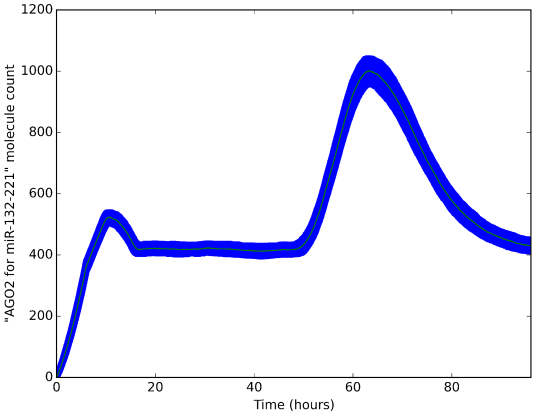

(f) absolute AGO2 protein count

Figure 5.2: Simulation of miR-132 mediated silencing of AGO2 and EP300 in LECs during PMA-activation, presenting the molecular abundance baseline in LECs and baseline perturbation during PMA treatment. The treatment is initiated at 48 hours after the simulation start time. The mean (*green line*) and standard deviation (*blue area*) is calculated based on 100 replicate simulation runs.

5.2.2 miR-132 enhanced transcription

The initial model baseline was calibrated to the molecular abundances recorded in LECs. Since the PMA treatment did not result in a miR-132 induction that was observed *in vitro*, an enhanced miR-132 expression regime was proposed to study the regulatory effects of miR-132 mediated target regulation. In order to determine the systemic effect of altering the *pCREB_EP300AvailableForMiR132Transcription* parameter, the baseline miR-132 model and miR-132 enhanced expression model needed to be compared.

The increased miR-132 transcriptional activity showed no effect on the CREB phosphorylation profile (Figure 5.3a). The new miR-132 baseline expression was enhanced by ~4-fold (Figure 5.3b). Both mRNAs and protein in the enhanced miR-132 transcriptional activity experiment have a lowered baseline expression, reduced by ~10% for AGO2 and ~20% for EP300 levels (Figure 5.3). Finally, EP300 protein levels recover slower: ~80% of the original baseline is restored by 48 hours after PMA treatment in miR-132 enhanced expression model, compared to 24 hours after PMA treatment in the miR-132 baseline model (Figure 5.2e).

Despite the 4-fold increase in miR-132 baseline in the enhanced miR-132 transcription model, the qualitative results represented the behaviour described in Domain model - expected behaviour diagram; miR-132 upregulation peaked at 900 molecules (Figure 5.3b) – 9 fold higher than the original untreated miR-132 baseline molecule abundance (Figure 4.24a), and remained at 500 molecules after 24 hours of PMA treatment – 5 fold higher than the original untreated miR-132 baseline molecule abundance. At this level of miR-132 abundance, it is expected to have functionally significant effects on target regulation and cell biology as demonstrated in Figure 3.13d and Lagos et al. (2010); Anand et al. (2010). The following sections explore the role of functional levels of miR-132 abundance on the regulation of AGO2 and EP300 using the miR-132 enhanced expression model.

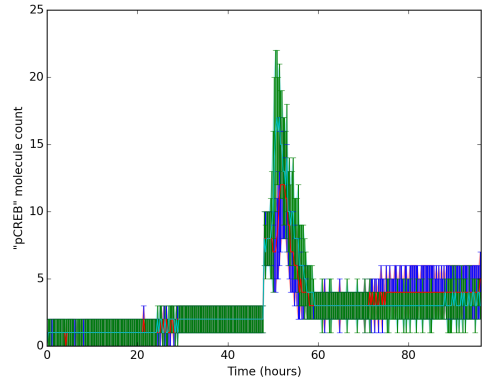

(a) % of phosphorylated CREB

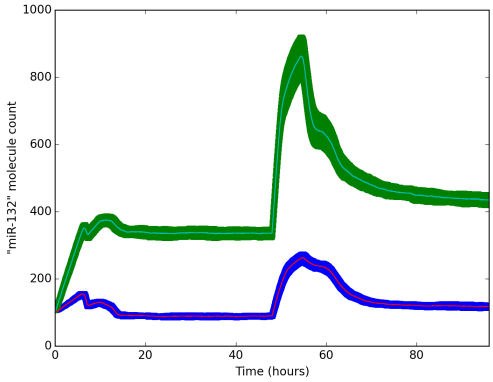

(b) absolute miR-132 count

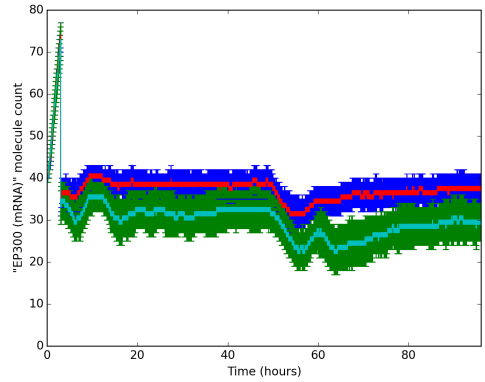

(c) absolute EP300 *mRNA* count

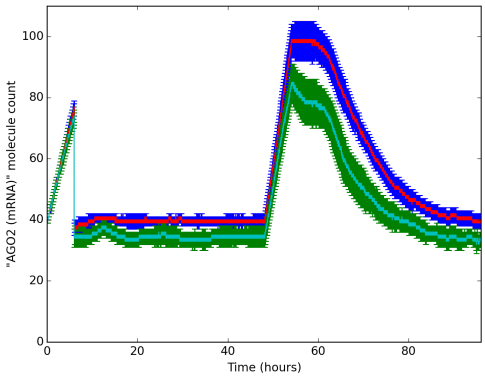

(d) absolute AGO2 *mRNA* count

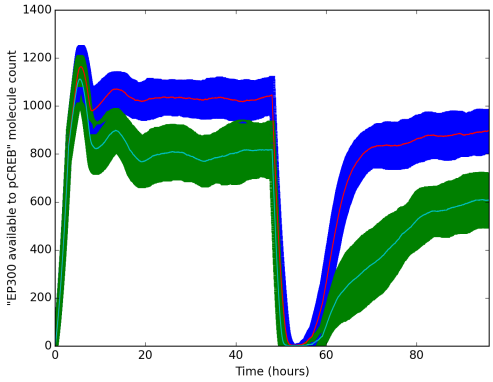

(e) absolute EP300 protein count

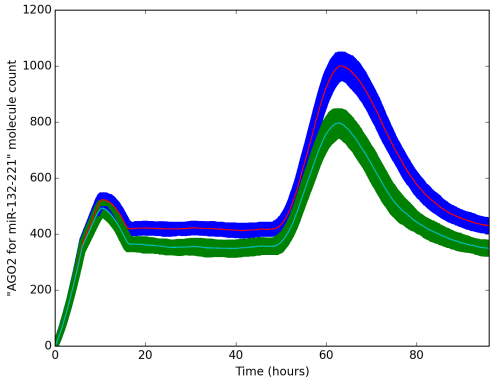

(f) absolute AGO2 protein count

Figure 5.3: Simulation of miR-132 mediated silencing of AGO2 and EP300 in LECs during PMA-activation with enhanced miR-132 transcription activity (mean - *teal line*, standard deviation - *green area*) compared to baseline PMA-activation (mean - *red line*, standard deviation - *blue area*), calculated based on 100 replicate simulation runs. The treatment is initiated at 48 hours after the simulation start time. The impact of the differences is measured by the K-S test in Table C.1.

5.2.3 Non-regulated *AGO2* mRNA

Using the enhanced miR-132 expression baseline model, *AGO2* mRNA is hypothesised to not be a target of miR-132. The implications of the loss of a miR-132 target, AGO2, is explored further in the *in silico* model.

Similar to previous *in silico* experiments, the CREB phosphorylation profile remained mostly unchanged, with a strong activation curve during the first hour of PMA activation and a gradual decline in phosphorylation levels (Figure 5.4a). However, the expression of miR-132 during PMA activation differed in shape and the deviation from the mean (Figure 5.4b). This effect could be linked to the fluctuating levels of *EP300* mRNA (Figure 5.4c) and protein (Figure 5.4e) expression – the former under the regulation of miR-132 and the latter required for miR-132 production. The pre-treatment baseline of the EP300 protein (Figure 5.4e) was highly unstable, and the EP300 protein levels could not be restored within 48 hours after PMA treatment.

By disrupting the regulatory function of miR-132 to target *AGO2* mRNA, the regulatory profile of miR-132 changed, leading to unstable regulation of EP300. This suggests that there is a balance between miRNA-mRNA ratios which are necessary to maintain a stable steady state for a robust miRNA-mediated regulatory response. Similar functionality would be expected if the other miR-132 target in the model, EP300, was not targeted by miR-132, explored further in the following section.

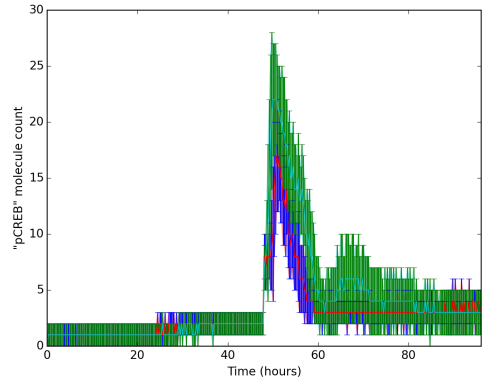

(a) % of phosphorylated CREB

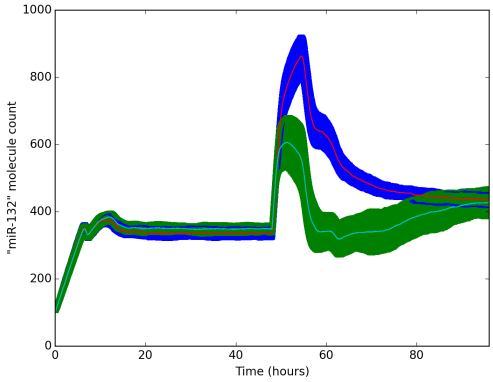

(b) absolute miR-132 count

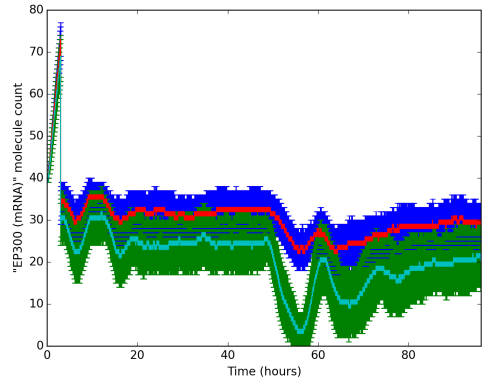

(c) absolute EP300 *mRNA* count

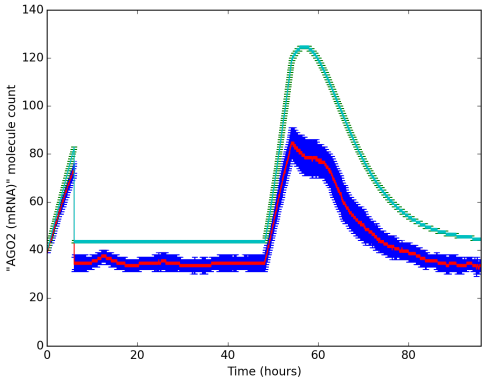

(d) absolute AGO2 *mRNA* count

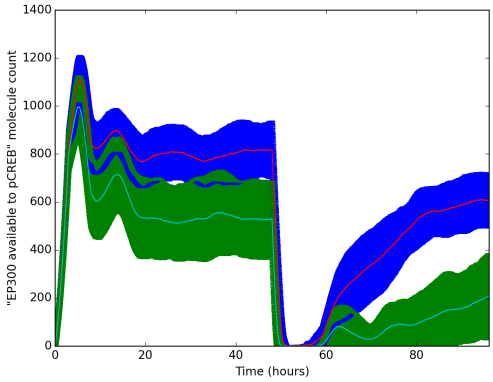

(e) absolute EP300 protein count

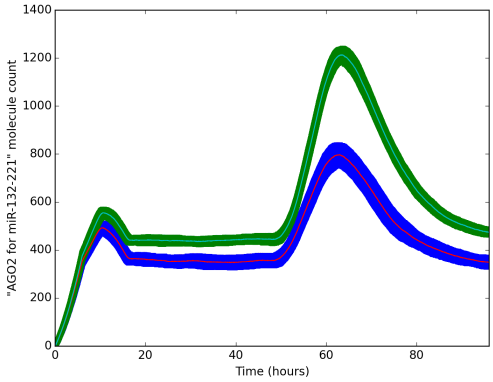

(f) absolute AGO2 protein count

Figure 5.4: Simulation of miR-132 mediated silencing of AGO2 and EP300 in LECs during PMA-activation with enhanced miR-132 transcription activity comparing a condition where AGO2 can (mean - *red line*, standard deviation - *blue area*) or cannot (mean - *teal line*, standard deviation - *green area*) be targeted by miR-132, calculated based on 100 replicate simulation runs. The treatment is initiated at 48 hours after the simulation start time. The impact of the differences is measured by the K-S test in Table C.2.

5.2.4 Non-regulated *EP300* mRNA

Similar to the experiment where AGO2 could not be target by miR-132, the next step was to investigate why EP300 would be an important target for miR-132, allowing to appreciate its role in this regulatory network. Unlike the non-regulated AGO2 experiment, in the non-regulated EP300 experiment the phosphorylation of CREB was upregulated 2-3 fold (Figure 5.5a). Since the pCREB-EP300 is necessary for the transcriptional activation of miR-132 production, the non-targeted *EP300* mRNA resulted in a ~50% higher abundance of the EP300 mRNA and protein (Figures 5.5c). The ~50% increased abundance of EP300 protein did not increase the baseline expression of miR-132 (Figure 5.5b), however during stimulation with PMA the expression of miR-132 was upregulated ~4-fold during the peak of its expression, up from ~3-fold compared to the control. Interestingly, AGO2 mRNA (Figure 5.5d) and protein (Figure 5.5f) abundance was downregulated ~40%, possibly due to the increased amount of miR-132 to *AGO2* mRNA ratio, despite the ~20% reduced AGO2 bound miR-132 count (Figure C.5c).

Like previous results where AGO2 was not targeted by miR-132, by making EP300 not a target of miR-132, the regulation of both EP300 and AGO2 are disrupted. Importantly, the baseline of miR-132 during non-stimulated conditions were unaffected during this mode of regulation, however during PMA-induced LEC activation this resulted in an increase in miR-132 abundance. Although AGO2 is involved in the regulation of miRNA abundance (Diederichs and Haber, 2007), the reduced AGO2 mRNA and protein expression when EP300 could not be targeted by miR-132 did not lead to a reduced pre- and 24h post-PMA treatment abundance of miR-132 (Figure C.5a) or miR-221 (Figure C.5b).

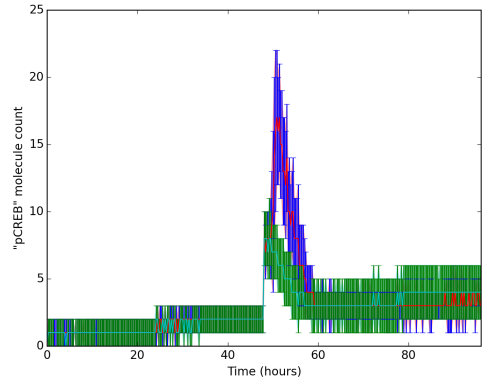

(a) % of phosphorylated CREB

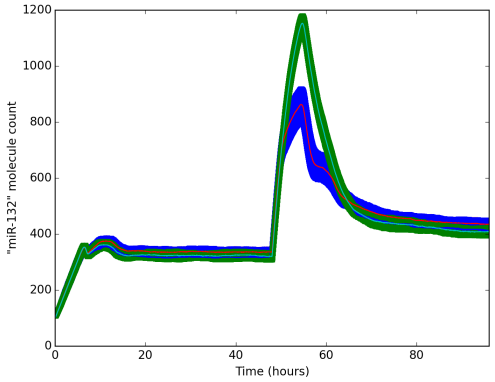

(b) absolute miR-132 count

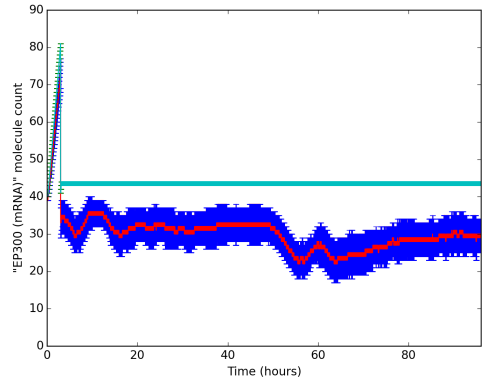

(c) absolute EP300 *mRNA* count

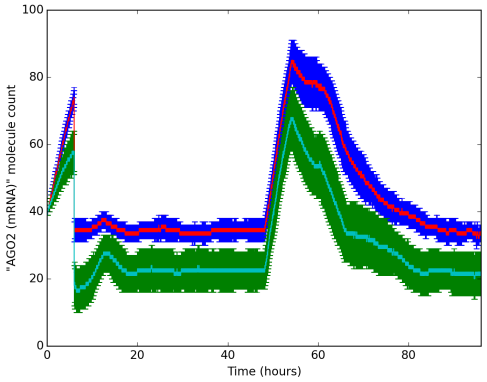

(d) absolute AGO2 *mRNA* count

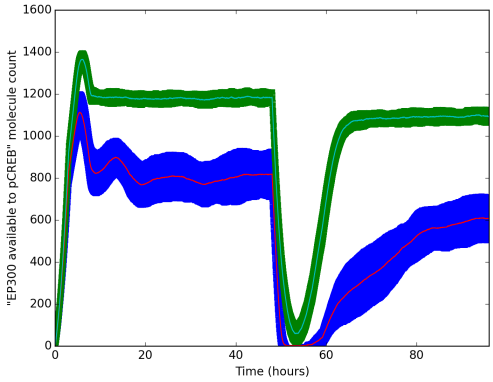

(e) absolute EP300 protein count

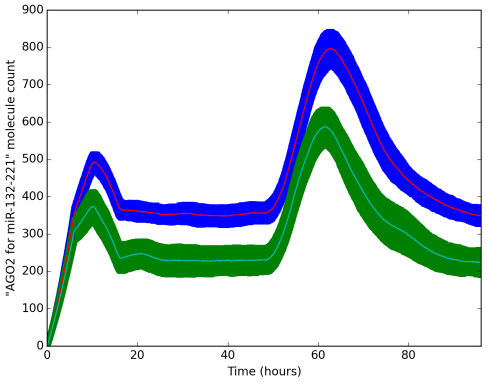

(f) absolute AGO2 protein count

Figure 5.5: Simulation of miR-132 mediated silencing of AGO2 and EP300 in LECs during PMA-activation with enhanced miR-132 transcription activity comparing a condition where EP300 can (mean - *red line*, standard deviation - *blue area*) or cannot (mean - *teal line*, standard deviation - *green area*) be targeted by miR-132, calculated based on 100 replicate simulation runs. The treatment is initiated at 48 hours after the simulation start time. The impact of the differences is measured by the K-S test in Table C.3.

5.3 Discussion

5.3.1 Simulating miR-132 expression in response to PMA treatment

The activation of miR-132 transcription in the model was abstracted, allowing a single pCREB-EP300 complex association event to trigger a single miR-132 transcriptional event. In the case of the LEC baseline with PMA treatment (Figure 5.2), miR-132 expression reached only a ~3-fold upregulation of miR-132 abundance. Since the level of miR-132 remained above the PMA activation baseline, the abundance of EP300 protein was maintained below the PMA activation baseline. Although this was an expected outcome, the regulatory potential of miR-132 would have been higher given a stronger miR-132 relative expression increase in response to PMA activation, leading to a more gradual recovery of EP300 protein expression. The smaller than expected (Figure 4.1; supporting data Figure 3.11a) increase in miR-132 expression suggests that some element of the domain model needs re-evaluation.

The smaller than expected relative change in miR-132 abundance may be due to a missing component in the domain model, most likely to do with how transcriptional activation operates upon transcription factor binding. For example, it is possible that miR-132 production should be more enhanced upon pCREB-EP300 complex binding to the promoter. The stoichiometry of pCREB-EP300 to produced miR-132 transcriptional events is undetermined with no available data to date, and would be necessary to adjust this parameter of the simulation. However, in a recent attempt to investigate transcription factor driven promoter activation, Rybakova et al. (2015) predicted that the burst-transcription of mRNAs could be as fast as 10 mRNAs per a single transcriptional activation cycle[2]. During this time, covalent modifications to chromatin components and DNA occur that regulate progression of transcription (Reid et al., 2009). Therefore, it is likely that the pCREB-EP300 potential to activate miR-132 transcription could be reviewed in the domain model. Since the aim of the model was not to address how transcription is activated for miR-132, but rather investigate

[2]in this context, a cycle consists of transcription factor binding, complex maturation, possible chromatin remodelling (e.g. acetylation by EP300) and eventually, complex disassembly

how CREB activation in complex with EP300 can regulate miR-132 mediated regulation of gene expression, it would be sufficient to abstract the activation mechanism by calibrating the parameter (*pCREB_EP300AvailableForMiR132Transcription*) responsible for miR-132 transcription upon the binding of the pCREB-EP300 complex. It is also possible, that during cell activation by PMA, EP300 activity is redistributed (together with Polymerase II) to potently activate transcription of other genes (Byun et al., 2009), such as the miR-132/212 locus. On the other hand, by performing native chromatin immunoprecipitation (Cosseau and Grunau, 2011) at various time points of miR-132 activation collecting information about pCREB-EP300 association with the promoter region, and comparing it to the resulting pri-miR-132 levels, it would be possible to better estimate this parameter to benefit the miR-132 silencing model.

5.3.2 miR-132 controlled recovery of EP300 activity

The low expression of miR-132 as found in LECs can be considered as functionally inactive. During cell activation in LECs, miR-132 has been shown to mediate the innate immune response (Lagos et al., 2010), where miR-132 expression was upregulated ~10-fold. The phosphorylation of CREB occurs in response to the PMA treatment, and the EP300 protein in complex with phosphorylated CREB protein is needed for the transcriptional activation of miR-132. From the presented explorative simulations (section 5.2), it is evident that EP300 protein abundance is depleted during the first hours of PMA-induced cell activation, and that the recovery of EP300 protein abundance depends on the miR-132 expression profile and abundance. The drop in EP300 protein expression has been previously demonstrated to be a result of signalling through the MAPK signalling cascade (Sánchez-Molina et al., 2006; Jeong et al., 2013), which is also activated during PMA stimulation, targeting EP300 for degradation.

In the miR-132 silencing model, the initial depletion of EP300 may be attributed to its co-activatory role to initiate transcription, including the transcription of pri-miR-132 (Vo

et al., 2005), and the recovery of EP300 protein to baseline abundance is halted by the presence of miR-132 loaded RISC, as demonstrated in the loss of miR-132 function experiment to regulate EP300 recovery in Figure 5.5. Although there is no EP300 that is degraded in the model, only a fraction of it is used to bind CREB, a proportion of which is used to transcribe pri-miR-132 transcription (exact parameters available in Tables 4.11 and 4.12; rationale for implementation in Table 4.10). Overall, the effect of EP300 regulation during cell activation can function as a temporal switch to prevent the subsequent reactivation of EP300 activity whilst the pCREB abundance is still high during the several hours after PMA treatment (Figure 3.10). From the immunological perspective, limiting pCREB-EP300 re-activation of EP300 after the initial cell activation through miR-132 modulates the strength of the immune response (Lagos et al., 2010), and would in general impact on EP300 function, e.g. lymphocyte development (Kasper et al., 2006).

5.3.3 AGO2 regulation by miR-132 during cell activation

In the explorative simulation (Figure 5.4) it was demonstrated that when miR-132 is unable to target AGO2, this impacts on EP300 protein abundance and miR-132 expression profile during activation. The silencing potential of miR-132 measured as the abundance of miR-132 RISC, was unaffected (Figure C.4c). However, the impact of miR-132 RISC silencing was fully directed at EP300 mRNA due to the lack of an additional miR-132 target. Since miR-132 and EP300 are controlling each other through a negative feedback loop, by removing the ability of miR-132 to regulate AGO2 (a positive regulator of miR-132), this created an unstable regulation between miR-132 and EP300. These results can be attributed to the combined effect of several observations:

1. Lack of AGO2 regulation by miR-132 results in an increased *AGO2* mRNA and protein abundance

2. Increased AGO2 protein abundance allows for more miR-132 to bind and form functional RISC to target *EP300* mRNA

3. miR-132 bound AGO2 count is sustained overall (peaks at ~300 molecules, sustains ~150 molecules at 48 hours after PMA treatment) during the PMA activation (Figure C.3c) compared to the enhanced miR-132 expression baseline (Figure C.4c), suggesting that miR-132 silencing activity is unchanged but more effective at silencing EP300

The latter, third observation, is likely due to the increased ratio of miR-132 and *EP300* mRNA, which is a consequence of the second observation. A similar effect has been previously observed that the miRNA-mRNA ratio would affect protein expression, where increasing abundance of miRNA target sites for the same proportion of the miRNA would dilute the suppressive effect of the miRNA (Poliseno et al., 2010). Complementing this principle, where overexpression of miRNA target sites can act as an effective inhibitor of miRNA function has been previously demonstrated as a novel technology for miRNA functional inhibition, termed "miRNA sponges" (Ebert et al., 2007).

Simulating miR-132 mediated gene regulation without additional miR-132 target mRNAs (AGO2^{-UTR}), miR-132 was unable to control and maintain a steady expression level of EP300, causing the expression of EP300 to remain below 200 molecules after 48 hours of PMA treatment, down by 60% from the pre-PMA treatment abundance (Figure 5.4). Although only two miR-132 targets – AGO2 and EP300 – are represented in this model, this poses regulatory constraints on the miRNA network: miR-132 functions to maintain steady state expression levels of several targets (including others mentioned in Section 1.2.5.3), requiring the presence of two or more targets in order to avoid an unstable regulatory interaction. In addition, many miRNAs form self-regulatory feedback loops with their targets (Bosia et al., 2012). Therefore, during cell activation – the established steady state expression of EP300 and AGO2 under the control of miR-132 may be an essential feature for LECs: at steady-state when miR-132 expression is low, the targets of miR-132 are be-

low miR-132 regulatory threshold, however, during perturbation when miR-132 abundance is increased above its regulatory threshold, it is able to restore the steady state levels of its targets over a 2 day time scale. This way, miR-132 confers robustness on the biological system during normal and changing gene expression by regulating AGO2 and EP300 simultaneously. Such regulation is necessary for normal physiological functioning of biological processes, where miRNAs buffer noise of target regulation (Herranz and Cohen, 2010) by being involved in the regulation of multiple targets. Expanding the model to incorporate several other targets of miR-132 would allow to investigate the different thresholds during which miR-132, in activated cells, would function to control a broader gene regulatory network.

Chapter 6

Discussion and future work

6.1 Summary

The work presented in this thesis identified AGO2 as a novel target of miR-132, and described several experimental designs investigating AGO2 and miR-132 regulation in the context of a negative feedback loop. Based on these findings, we developed an ABM capturing the regulatory feedback between two miR-132 targets - AGO2 and EP300 - allowing to further investigate the dynamics of miR-132 mediated regulation in activated LECs. The key findings of this work are:

1. **Established that mammalian AGO2 is a conserved miR-132 target (Chapter 3)**
    - miR-132 directly interacts with AGO2 3'UTR (Section 3.2)
    - miR-132 *seed* sequence determines the specificity for AGO2 association and suppression (Section 3.2)
    - AGO2 is regulated at mRNA and protein level by miR-132 (Section 3.3)
    - The regulation of miR-132 *in vivo* does not show apparent effects on its targets' abundances: AGO2 and RASA1 show no difference in protein expression between wild type and miR-132 double knockout mice (Section 3.9)

2. **Demonstrated that miR-132 can be transcriptionally induced in LECs by PMA through the activation of pCREB (Chapter 3)**

    - PMA rapidly induces the phosphorylation of CREB within the first 2 hours after treatment (Section 3.4)
    - pCREB binds the promoter to induce pri-miR-132 transcription, which is sustained around 24 hours, dependent on levels of available pCREB (Section 3.4)
    - Inhibition of the endogenously induced miR-132 increases AGO2 protein expression (Section 3.5.2)

3. **Demonstrated that AGO2 protein abundance regulated by miR-132 affects the abundance of other miRNAs in LECs (Chapter 3)**

    - The loss of AGO2 during miR-132 overexpression leads to a loss in mature miRNA levels (Section 3.3)
    - The loss of mature miR-126 during miR-132 overexpression can be partially rescued by AGO2^{-UTR} overexpression (Section 3.6.3)

4. **Showed that an ABM model describing miR-132 regulation in a two-target feedback loop qualitatively reproduces the expected behaviour of the captured problem domain (Chapter 4)**

5. **Demonstrated that the effect of LEC activation by PMA perturbs the function of miR-132 mediated silencing of AGO2 and EP300 regulation *in silico* (Chapter 5)**

    - The simulation of LEC activation suggested that other mechanisms may be at play in the induction of miR-132 transcription (Section 5.2)
    - Simulation during miR-132 enhanced expression during PMA-induced LEC activation suggested a function for miR-132 in the stable recovery of EP300 protein expression (Section 5.2.2)

- Target (dis-)regulation experiments revealed a possible role for miR-132 targets during LEC activation in maintaining a robust miRNA-mediated target regulatory response (Section 5.2.3-5.2.4)

The regulatory capacity of miR-132 during LEC activation by PMA appeared as mild, with several other effects (rapid depletion of EP300 during CREB activation, AGO2 transcriptional upregulation by PMA, miR-221 abundance decrease after PMA treatment) feeding into the regulatory network that was under the control of miR-132. The *in vitro* experimental system in Chapter 3 was further investigated using an ABM (Chapter 4), in order to dissect the regulatory properties of this network and further the knowledge in miRNA-mediated control of gene targets (Chapter 5). Although the model was designed and calibrated to describe the regulation of miR-132 and its two targets – AGO2 and EP300 – in LECs, it is possible to extend, modify and calibrate the model to accommodate other targets or investigate a different miRNA network with different cell baseline expression levels of its constituents.

6.2 AGO2 expression is necessary, but not sufficient, for the prolonged expression of miR-132

Winter and Diederichs (2011) demonstrated that affecting the abundance of AGO1, AGO2 and AGO4 through overexpression or knockdown positively correlated with miRNA abundance. Based on this observation, Chapter 3 detailed how different expression levels of AGO2 correlated with miRNA abundance. Importantly, experiments with LECs *in vitro* demonstrated that alongside of several measured miRNAs, including miR-132, AGO2 protein was also upregulated as a result of PMA treatment, where AGO2 protein reached peak expression (up to ~1.5-fold) during the first 6 hours after treatment, and returned to a steady state expression after 24 hours. Knowing that miRNAs can stabilise AGO2 protein abundance by forming a miRNA-AGO2 complex (Martinez and Gregory, 2013), the PMA-induced cell activation could explain some of the increased AGO2 abundance as a result of possible global miRNA upregulation (Lu et al., 2010). Followed up by measuring *AGO2* mRNA levels, suggesting that AGO2 was transcriptionally induced, making transcription the dominant cause for AGO2 protein upregulation (Figure 3.11). The resulting phenotype was an increased AGO2 abundance that was maintained only during the first 24 hours after PMA treatment.

It has been previously reported that miR-132 can be transcriptionally induced during cell activation (Vo et al., 2005; Remenyi et al., 2010). In this work the PMA treatment resulted in a 5-6-fold increase of mature miR-132 abundance. The primary transcript of miR-132 returned to baseline expression by 24 hours after its transcriptional induction by PMA. The abundance of miR-132 was maintained for a prolonged period of time, still 4-fold above its baseline expression. Although miR-132 could be stabilised by the increased AGO2 expression (Winter and Diederichs, 2011) during PMA induction, AGO2 cannot be the sole contributor towards miR-132 increased abundance reaching as far as 48 hours after PMA treatment. Since miR-132 half-life was estimated to be 9-10 hours (Nahid et al.,

2013), and AGO2 protein expression returned to baseline 24 hours post-PMA treatment, it is possible that more factors are at play in stabilising the abundance of miR-132. Interestingly, Edbauer et al. (2010) showed that the Fragile X Mental Retardation Protein (FMRP) is able to stabilise the abundance of miR-132 by direct association. Moreover, the activity of FMRP is regulated by phosphorylation mediated by Extracellular Signal Regulated Kinase (ERK)/p70 Ribosomal Protein S6 Kinase 1 (S6K1) signalling, where in its phosphorylated state it has been found with stalled polyribosomes (Ceman et al., 2003), binding miRNAs directly and reducing their binding affinity for DICER (Cheever and Ceman, 2009). Tested by the *in silico* model (Chapter 5), PMA-induction of AGO2 and miR-132 was insufficient to explain the prolonged stability of miR-132 abundance. As hypothesised from the *in vitro* experiments and Winter and Diederichs (2011), the expectation that AGO2 would be able to stabilise miR-132 expression and maintain its abundance above steady-state expression 3-4-fold was not met. This reinforced the idea that AGO2 alone is not fully responsible for the increased abundance of miR-132 after 24 hours from PMA treatment.

The loading of miRNAs onto AGO family proteins is likely to be competitive due to the low AGO:miRNA ratio (1:10) (Janas et al., 2012). This provides the opportunity for the cell during its activation to upregulate AGO2 expression in order to accommodate the needed functionality from miR-132 by simultaneously producing the guide strands (i.e. miR-132) as well as effector proteins (i.e. AGO2) (Figure 6.1). Such a regulatory feature would favour enhanced regulation of miR-132 targets during early hours of a viral infection (Lagos et al., 2010) or increase endothelial cell angiogenic potential (Anand et al., 2010). Cell activation through B-cell signalling has revealed miR-132 as a regulator of SRY (Sex Determining Region Y)-Box 4 (Sox4), affecting B-cell development (Mehta et al., 2015a); additionally, Mehta et al. (2015b) found that miR-132 is upregulated in hematopoietic stem cells (HSCs), necessary for appropriate hematopoietic function and development, targeting an ageing related transcription factor, FOXO3. Aside from the function of miR-132 in cell development and immunity, a large proportion of confirmed miR-132 targets are linked to the regulation of

gene expression programmes: transcriptional regulation through EP300 (Hasan et al., 2001), chromatin remodelling through the regulation of Ep300, Mecp2, Jarid1a (Alvarez-Saavedra et al., 2011) and Silent Mating Type Information Regulation 2 Homolog 1 (SIRT1) (Yamakuchi, 2012), and controlling *tau* mRNA splicing (Smith et al., 2011). With a broad repertoire of targets, the sustained expression of miR-132 would ensure a gradual recovery of its target gene expression after cell activation as proposed from the *in silico* modelling experiments (Chapter 5).

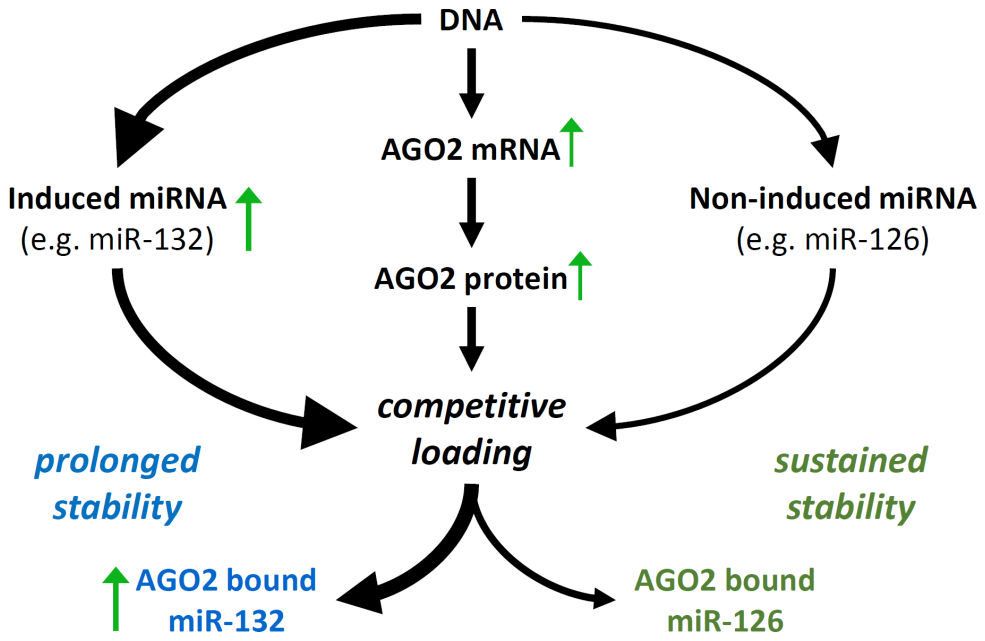

Figure 6.1: A proposed model for the role of AGO2 upregulation during LEC activation. Within the first few hours of PMA treatment the expression of PMA-inducible miRNAs is increased (e.g. miR-132), whereas the abundance of other miRNAs is unaffected (e.g. miR-126). In order to accommodate the increase in miR-132 expression and allow it to form functional complexes, new AGO2 needs to be synthesised with an increased rate during the first 24 hours of PMA-induced transcriptional activation. Since the abundance of AGO2 protein is more than 10 times lower than the abundance of miRNAs, the loading of newly produced miRNAs is subject to competitive AGO2 loading. As a net effect, the induced miR-132 remains in high abundance in the cell after 24 hours from PMA treatment, whilst the expression of miR-126 is maintained at a steady state.

6.3 Fine-tuning confers robustness to miRNA function, and consequently to gene expression

One of the most common functional denominators of miRNAs is their potential to regulate a broad range of genes, yet rarely exceeding more than a 2-fold change during a regulatory effect on a single gene target (Baek et al., 2008). This observation has suggested that miRNAs maintain protein expression levels by continuously fine-tuning a wide range of targets, similar to the regulation of miR-132 on AGO2 during the inhibition of miR-132 in activated LECs (Section 3.5.2). Despite their general role in mildly regulating target gene expression, it is known that during a cellular activation event (Taganov et al., 2006; Lagos et al., 2010), even low-expressed miRNAs are increased in abundance, in this case, to regulate the inflammatory response preventing the overproduction of cytokines. This suggests that miRNAs are predominantly acting to buffer gene expression for such activation events, and have been described as fine-tuners of gene expression (Stark et al., 2005; Herranz and Cohen, 2010; Bosia et al., 2012).

With almost 1 in 20 genes encoding for a miRNA in animals (Bartel, 2004; Berezikov et al., 2005), this makes them one of the most abundant and conserved functional elements in the genome. Unlike transcription factors, miRNAs can actively modulate protein expression at a post-transcriptional level. Although most miRNAs inhibit protein expression, it has been suggested that some miRNAs can positively regulate target gene expression through promoter activation (Place et al., 2008). However, miRNA-induced positive regulation of target genes has been described as a possible artefact of experimental setups where miRNA-regulated networks are affected through off-target miRNA displacement, resulting in apparent target derepression (Nyayanit and Gadgil, 2015). The latter argument relies on the more recently described view, the competing endogenous RNA (ceRNA) hypothesis (Salmena et al., 2011), based on the earlier work by Poliseno et al. (2010) and Cesana et al. (2011). In such a system, each miRNA is sequestered by the potential target sites accessible in the

cell; with an increasing target-to-miRNA ratio, the ceRNA effect has potentially large-scale effects on gene expression programmes. Computational modelling of a ceRNA network demonstrated the effects of ceRNA regulation during equilibrium and non-equilibrium conditions (Bosia et al., 2013), investigating how ceRNAs function at threshold concentrations of their potential shared targets.

Challenging the ceRNA hypothesis, Denzler et al. (2014) perform a series of experiments with miR-122 expressed in hepatocytes, in an attempt to experimentally establish the necessary threshold when the ceRNA effect becomes apparent. The level of miR-122 was reduced in the experiments from the natural abundance of 1.2×10^5 molecules per cell to as low as 1% of total miR-122 abundance (1.2×10^3 molecules per cell); using the range of miR-122 expression levels they demonstrated that in order for miR-122 mediated target regulation to be affected by the ceRNA effect, it would require 1.5×10^5 added target sites per cell; this would physiologically be an unlikely event, therefore, their findings demonstrating that mRNA target site increase sequestering miRNAs to derepress other mRNAs is also – unlikely. However, in the context of LECs, where expression of miR-132 at basal expression is 1×10^2 , this may not be the case – LEC activation which is characterised by an increased expression of miR-132 reaches a level of expression close to 5×10^2 Considering that the abundance of most mRNAs (Schwanhäusser et al., 2011) is in the low 2-digit range, the fluctuation of miR-132 levels, as well as increase in transcription of some mRNAs (e.g. AGO2 Adams et al. (2009)) during cell activation can have regulatory effects coherent with the ceRNA hypothesis. This is due to the baseline ratio of total miR-132 target sites: mRNAs that can be targeted in LECs, provided as many as ~10 unique targets in a 2-digit range that would present accessible sites for miR-132 interaction, would have a close to 1:1 ratio of miRNA-to-target. At this threshold level, the fluctuating levels of miR-132 and its targets as a consequence of transcriptional activation, mRNA turnover and silencing, are likely to have dynamic regulatory potential that support the ceRNA hypothesis (discussed below). The baseline expression of the overexpressed sites in the work by Denzler et al. (2014) was

far too high to be able to draw comparisons of the resulting effect between miRNA to target ratios, where in most of the experimental conditions the initial target site abundance was several magnitudes above the physiological level for low-expressed miRNAs. In addition, their experimental system did not consider low expressed miRNA regulatory properties in the context of activation, where the ratio of miRNA to mRNA target sites can be lower than one, using only a highly abundant miR-122 as the core of their findings.

Building on the ceRNA hypothesis, the miR-132 silencing model (Chapter 5) describes how a non-target AGO2 or EP300 disrupts the regulation of the other target. It is worth noting, that the model currently only includes 2 targets. Nevertheless, the titrating effect of miR-132 by a single remaining target when the other target is unavailable causes the regulatory feedback between miR-132 and one of the active targets to be disrupted. This effect is more pronounced when AGO2 is not targeted by miR-132. The implications of this regulatory disruption and change in baseline expression of miR-132 and AGO2/EP300 have not been yet investigated. The work presented in Chapter 5 compliments the hypothesis that ceRNA regulation is an important mechanism for the function of miRNA regulatory networks. The regulatory effect of the ceRNA hypothesis might be prevalent with small miRNA to target ratios, thresholds of which could be investigated with a range of endogenous low-abundant miRNAs during cell activation.

6.4 AGO2 loading during LEC activation

During PMA induction both AGO2 mRNA and protein was above baseline during the first 24 hours, however the expression of miR-132 remained 4-fold above baseline even 48 hours post-PMA treatment. In order to address the cause for the increased stability of miR-132, it would be worth investigating the following:

- Determine the localisation of miR-132 during PMA induction by immunoflorescence, in the attempt to identify its associated partners for binding and the compartments

in the cell where miR-132 resides shortly after cytoplasmic processing, including the relocalisation and phosphorylation of AGO2 that would indicate increased silencing activity (Zeng et al., 2008)

- The half-life of miR-132 may be increased when it is associated with AGO2, as suggested by Winter and Diederichs (2011). However, AGO2 expression returns to baseline within 24 hours after PMA treatment. The hypothesis would be that during the early time points of PMA treatment the induced AGO2 expression alongside the increased miR-132 expression allows miR-132 to compete for AGO2 loading more effectively, resulting in an accumulation of miR-132 bound AGO2 after 24 hours. Immunoprecipitation of AGO2 complexes compared to the total mature miR-132 pool would allow investigating into whether more miR-132 is bound to AGO2 despite the restored levels of AGO2 24 hours post-PMA activation.

- It is possible that AGO1 is also induced during PMA treatment, providing more RNA-binding proteins for miR-132 during processing. A qRT-PCR and western blot comparing AGO1 and AGO2 expression over a time course would address this hypothesis.

- FMRP phosphorylation and relocalisation could also affect miR-132 stability by its association with miR-132 directly (Edbauer et al., 2010)

- If not all of mature miR-132 during LEC activation is used up shortly after its processing, it would result in a reduced regulation of miR-132 targets. Therefore, another likely scenario is that miR-132/AGO2 complexes are stabilised and can be recycled to perform several silencing events of multiple mRNA copies. An *in silico* experiment using the miR-132 silencing model could be a starting point for investigate this hypothesis, as RISC recycling has already been implemented.

Understanding the reason behind the prolonged stability of miR-132 would reveal how AGO2 protein expression relates to miRNA functional potential during cell activation, i.e.

the central role of AGO2 loading following miRNA biogenesis, and how it relates to miR-132 function in endothelial cells (Anand et al., 2010; Lagos et al., 2010). The current model that attempts to address this was presented in Figure 6.1.

6.5 Reflection on the development of an agent-based model development on an intracellular scale integrated with experimental data acquisition

Intracellular molecular interaction models using agent-based technology have existed for over a decade (González et al., 2003; Pogson et al., 2006; Fredrick et al., 2013; Williams, 2014). Due to the large abundance of some of the molecular components present in cells, the advancement in computer processing and availability of computing clusters, it has become possible to execute models with thousands of agents representing molecular interactions inside the cell.

One of the biggest challenges of developing a computational model, including the miR-132 silencing model, was calibration of the parameters. Although few parameters govern the behaviour of each individual agent that represent a biological molecule, 9 types of agents were considered essential for describing miRNA mediated silencing in the context of LEC activation. Importantly, the few necessary parameters describing mRNA transcription rates and life spans of mRNA and protein molecules were difficult to obtain, having to rely on experiments from a combination of sources. Although copy numbers of miR-132 and miR-221 were obtained from the same biological system (i.e. HDLECs), with miR-132 being the central regulatory component of the network, other agent abundances were taken from similar cell types, which may not necessarily represent the same protein or mRNA stability as found in LECs. Inevitably, the calibration of model parameters was necessary to compensate for possible deviations of biological parameters from their true value in LECs,

and to reproduce the qualitative behaviour of miRNA mediated regulation due to justifiable parameter abstractions.

As a consequence of the many requirements imposed by model parametrisation, the integrated approach to investigate miR-132 regulatory properties of its targets could benefit from *ab initio* domain model planning strategy: the first few months of the project would involve the capturing the initial problem domain, which typically would involve the presence of a subject matter expert. Importantly, this would allow to determine what experiments would be needed to provide support for the model described in the problem domain, and effectively support transitions between model development and experimental data acquisition.

6.6 Expansion of the miRNA-regulatory network

During the development of the miR-132 silencing model, the experimental data gathered in Chapter 3 enabled calibration and investigation of the miR-132 regulatory network with two of its targets – AGO2 and EP300. Although both targets formed a negative feedback loop with miR-132, they were distinct in the functional impact of their regulation (regulation of self-transcription *vs* regulation of silencing capacity). Moreover, the rate of transcription of each of the target mRNAs was different, as well as the targeting efficiency of miR-132 between the two target mRNAs. To date, no other agent-based model involving a miRNA regulatory network has been published aside from the one available resource found online by Ripoli et al. (2009), making this study of particular interest for investigating the dynamics of miRNA mediated regulation in a system with low abundance of the most essential molecules - miRNAs and their target mRNAs.

Coherent with the ceRNA hypothesis, the model captures some of the key behaviours of a ceRNA system: a single miRNA is capable of regulating multiple targets with distinct transcription/translation dynamics, functional impact on the abundance of miR-132, and with distinct affinities for interacting with target mRNAs. The model itself can be extended

to address the biological domain problem of miR-132 stability by investigating:

- The cause behind the loss of miR-132 abundance in the model compared to the *in vitro* data 24 hours post-PMA treatment. The experiments are described in the Section above, and would contribute to the accuracy of the PMA-induced functional readout of the model.

- The expression of miR-132 expression as a result CREB phosphorylation as the amplitude of upregulation of miR-132 *in silico* is lower than in the corresponding *in vitro* experiments. In order to test if the understanding of pCREB induced miR-132 transcriptional activation is representative of the real world domain, it may be interesting to alter the simulation by allowing more miR-132 transcripts to be produced per pCREB-EP300 complex binding event, which would require model recalibration. Alternatively, identifying the stoichiometry of the pCREB-EP300 complex to pri-miR-132 ratio would be useful information in completing the domain knowledge of miR-132 transcriptional induction.

- Addition of a PMA positively responsive miRNA agent, such as miR-146a, and predict the impact of miR-132 and miR-146a simultaneous regulation during LEC activation as a measure of NF-κB downstream signalling. Rather than using a decoy miRNA which is downregulated after PMA induced LEC activation (i.e. miR-221), a miRNA that is positively regulated and in similar abundance to miR-132 in LECs (i.e. miR-146a, Figure 3.14) would provide novel insight into the dynamics of a 2-miRNA interaction regulatory network.

- Investigation and incorporation of expression data of additional miR-132 targets would provide further work and suggest testable hypothesis to support the ceRNA hypothesis (Salmena et al., 2011; Bosia et al., 2013)

- The addition of P-body (currently represented by *Foci* in the model) localisation functionality for AGO2, by implementing its functional role after possible post-translational

modification (Zeng et al., 2008); this would require time-lapse imaging data of AGO2 (and phospho-AGO2 at S387) redistribution during cell activation

Given the time available it was not possible to test some of the model predictions in order to fulfil the systems biology cycle (Kitano, 2002). However, the findings presented in this Chapter suggested several experiments that benefit the biological domain as a result of the *in silico* exploration of miR-132 regulation of AGO2 and EP300 in a closed two-target gene regulatory network.

6.7 Conclusion

The integrated approach combining wet-lab molecular techniques with computational modelling presented in this thesis benefited the understanding of miRNA-mediated silencing, yet challenges remain in the development of models capturing the complexity of biological systems. Utilising the integrated approach to dissect miRNA-mediated regulation within a network of interacting molecules, the work demonstrated the functional relevance of miR-132 mediated regulation of a novel target, AGO2, and a previously validated target, EP300. Together with the experimental data, the predictions and observations made from agent-based modelling of the miR-132 regulatory network in the context of cell activation provide new avenues to be explored in the domain of miRNA-mediated gene regulation.

Appendices

Appendix A

Biological data

A.1 EP300 antibody optimisation

The EP300 protein is a 300 kDa protein that can be detected by the mouse-monoclonal Abcam 3G230 antibody. According to the manufacturer's instructions, it has cross-reactivity with human and rat species, and is suitable for western blotting.

Based on performed western blots, the antibody detects a band at 300 kDA, but longer exposures and re-use of the antibody for subsequent western blot membranes increases the signal to noise ratio. Overall, the antibody detects the EP300 target in LECs and HeLa when it is the first probed target on a fresh PVDF membrane.

Several configurations of the antibody dilution and buffer were tested in HeLas (Figure A.1). EP300 was detected most clearly when using a 1:500 primary antibody in 5% PBS/T-milk, with PBS/T as the washing buffer, and 1:5000 mouse-IgG PBS/T secondary antibody. The incubation periods and the protocol for staining is described in section 2.1.3.6. Due to the cost of using a EP300 as a 2nd positive control for miR-132 regulation after the optimisation, only RASA1 was continued to be used as the only positive control for miR-132 regulation events.

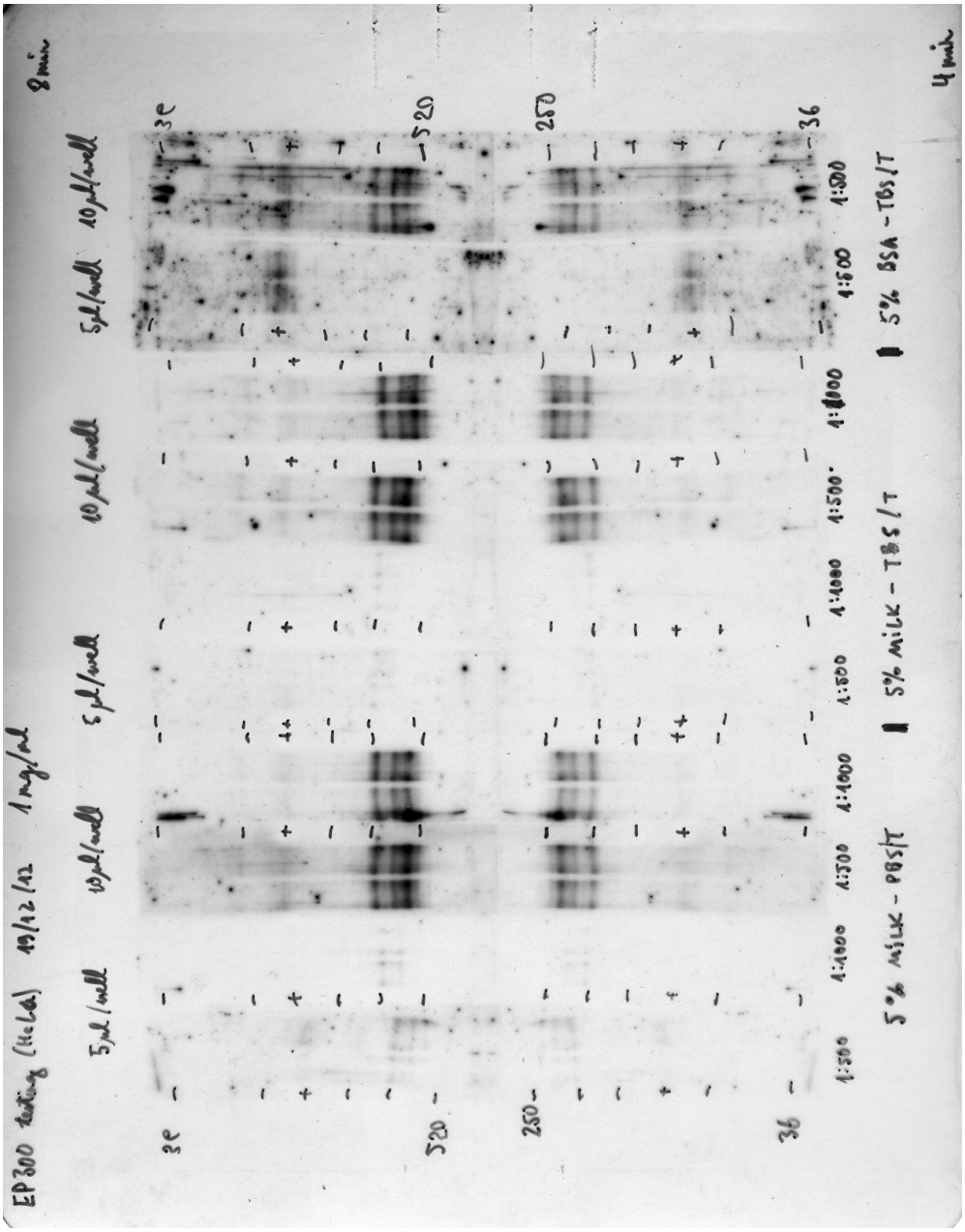

Figure A.1: EP300 antibody optimisation using HeLa lysates: comparison of 3 buffers (5% milk-PBS/T, 5% milk-TBS/T, 5% BSA-PBS/T) used in the preparation of the primary antibody with either 1:500 or 1:1000 concentration. Test lanes for each condition were loaded with 5 or $10\,\mu g\,\mu l^{-1}$ of protein lysate. Image displays a 4 minute and an 8 minute exposure of the hyperfilm to the ECL-treated membrane. Note: the predicted band in HeLas runs just below the 250 kDa marker.

A.2 HDLEC morphology

PMA induces a morphological change in HDLECs. This can be attributed to the cell activation, where the endothelial cells perform their role in angiogenesis and become more elongated, as well as actively proliferating (Figure 3.25a). After 24 hours of PMA treatment activated endothelial cells appear elongated, with miR-132 inhibition showing no apparent effects on cell morphology (Figure A.2).

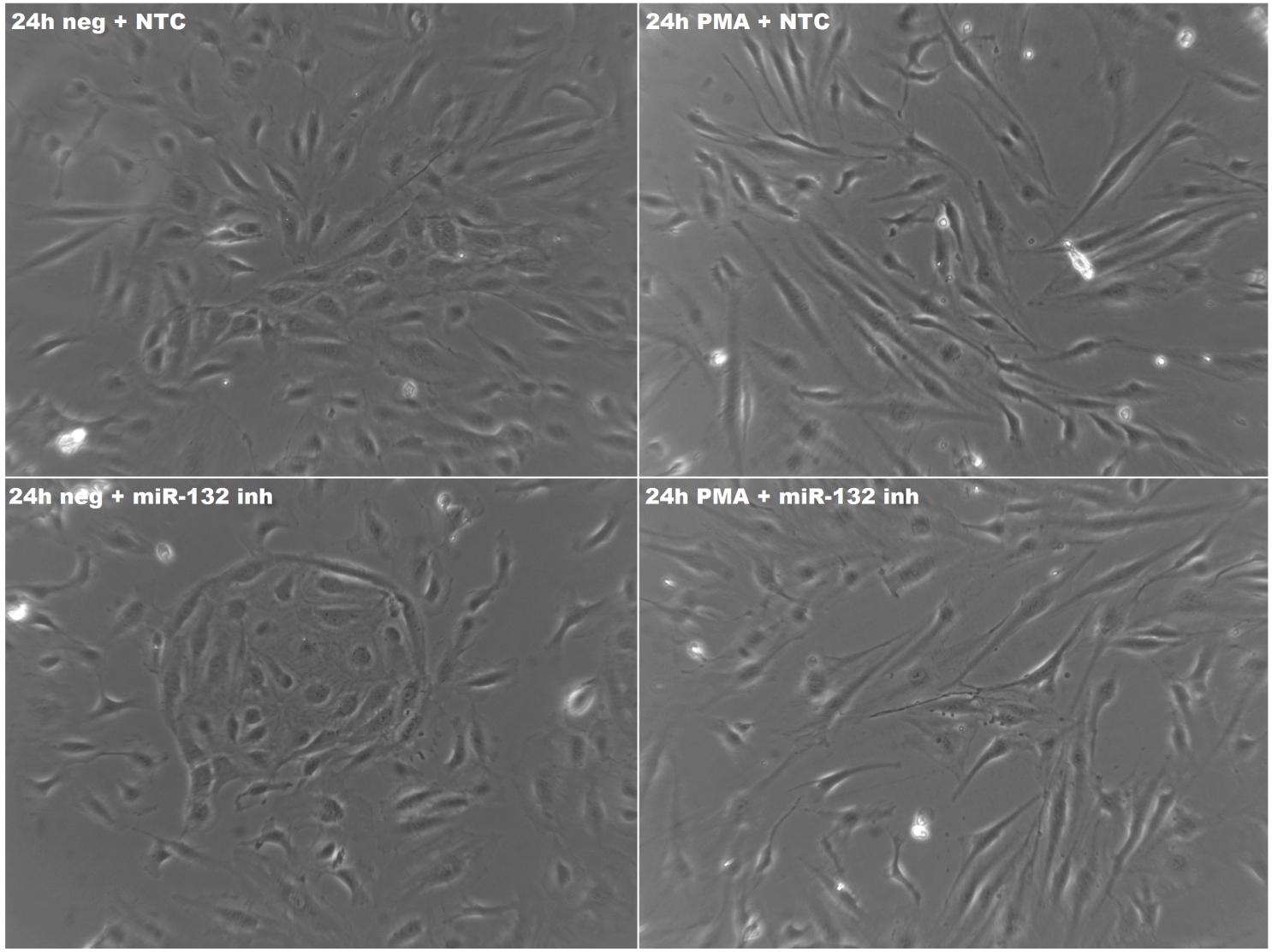

Figure A.2: Morphology of miR-132 inhibited LECs 24 hours after PMA treatment.

A.3 Expression by experimental replicate

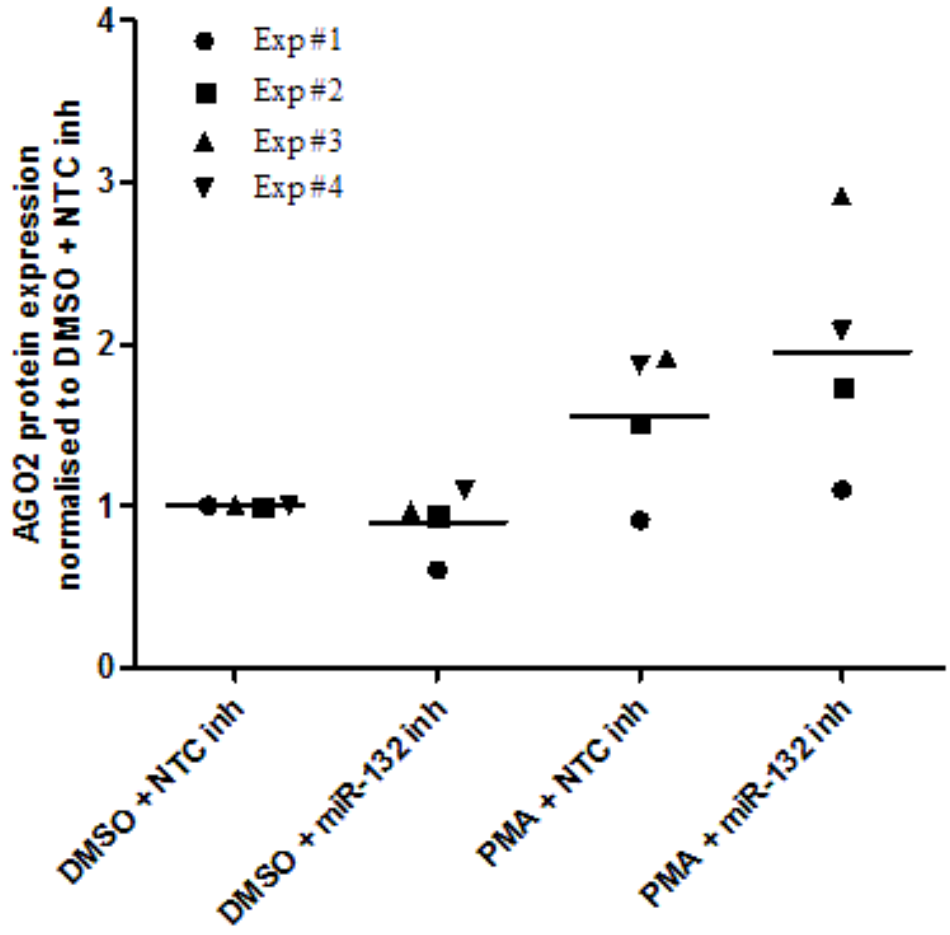

Figure A.3: Inhibition (LNA) of miR-132 in PMA-activated LECs: relative expression of AGO2 protein broken down by experimental replicate. Although there is a trend, where miR-132 inhibition of PMA-activated LECs derepresses AGO2 protein expression, it does not reach statistical significance (Figure(3.13d) ($n = 3$).

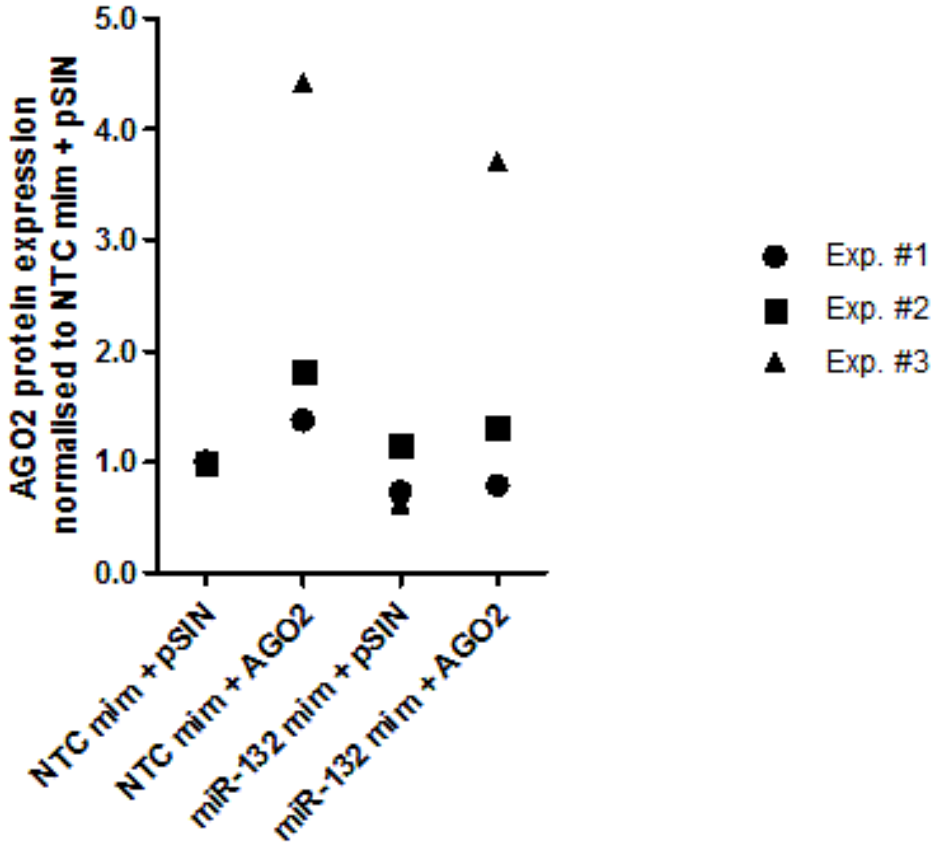

Figure A.4: Overexpression of miR-132 mimics for 30 hours followed by AGO2^{-UTR} lentiviral overexpression for 24 hours: relative expression of AGO2 protein broken down by experimental replicate. Although there is a trend, where miR-132 overexpression suppresses AGO2 protein expression during AGO2^{-UTR} overexpression, it does not reach statistical significance (Figure 3.20d) ($n = 3$).

Appendix B

Model development

B.1 Class inheritance

The class inheritance diagram (Figure B.1) for agent classes is presented below. Agents like miRNAs and mRNAs share a lot of common parameters and functionality for the purpose of this model. The mRNA class and miRNA class was made an abstract class, with specific miRNAs (miR-132, miR-221) and mRNAs (*AGO2* and *EP300* mRNA) as agent classes. Proteins, on the other hand share little common functionality and most of the movement and binding behaviour was implemented for each protein agent class (CREB, EP300, AGO2 proteins).

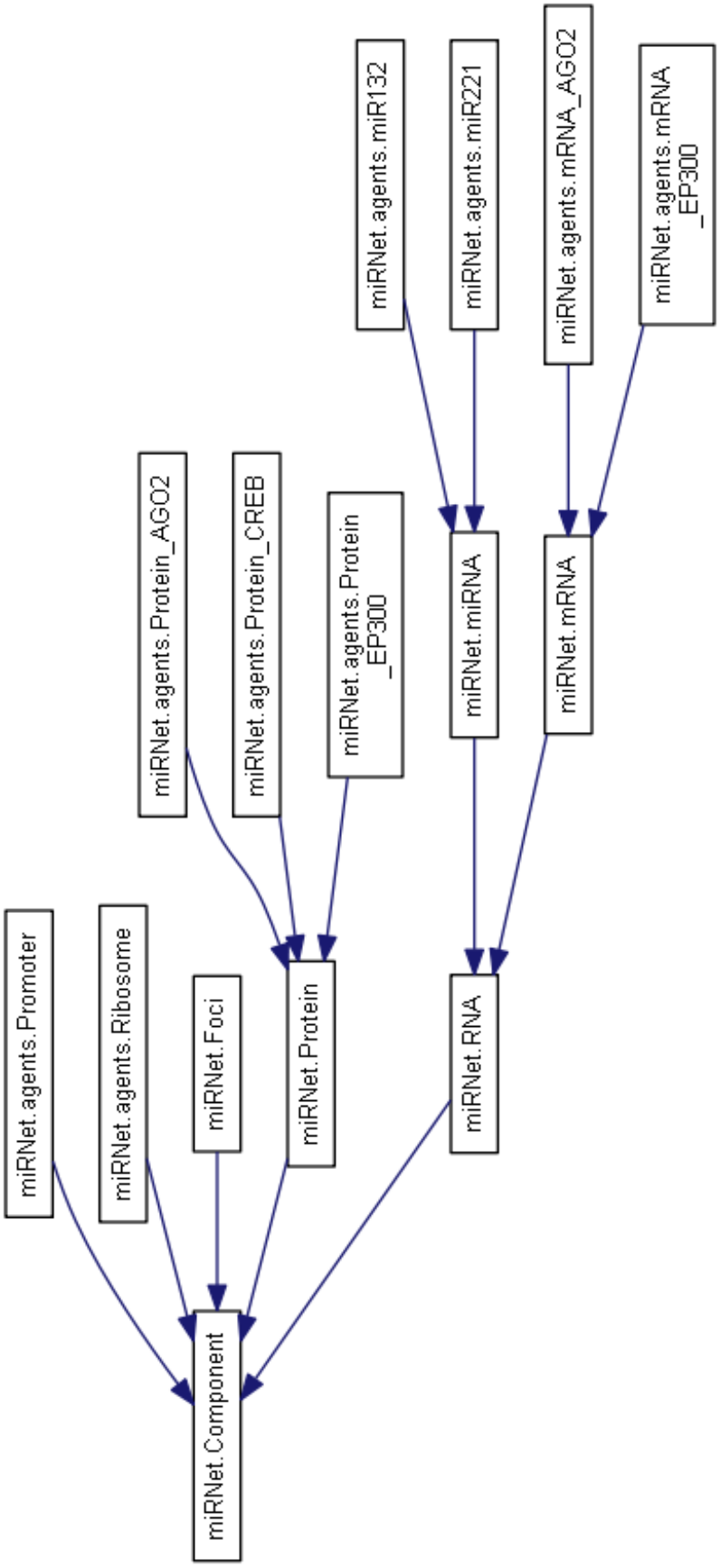

Figure B.1: Class inheritance diagram for the active agents in the simulation.

Appendix C

Simulation results

C.1 Visual model output of the miR-132 silencing model

Several screenshots of the visual output of the model are shown in Figure C.1. The simulation starts in a state where equilibrium has not been reached. In the 1st iteration (Figure C.1a) the mRNAs and 100 molecules of miR-132 are present in the cell, localised to the nucleus, with ribosomes placed randomly outside of the nucleus (the red square indicates the approximate region of the nucleus). On the 100th iteration (Figure C.1b) most of the mRNAs have localised to cytoplasmic foci (circled in red as the approximate localisation) where they are temporarily stored and will enter translation over a period of time by binding to a ribosome. By the 1000th iteration (Figure C.1c), some EP300 mRNA has been translated into protein and has localised to the nucleus, allowing it to bind CREB within the nucleus to initiate miR-132 transcription at the promoter. In addition, more miR-221 has been produced, along-side the translated AGO2 protein. Some of the AGO2 protein has formed complexes with miR-132 and miR-221 (green or red triangle over a red square, respectively), that should be visible at a finer zoom of the digital copy of the thesis. Finally, the 10000th iteration shows that the model becomes soon saturated with agents for visual display (Figure C.1d), but allows the distinguishing of the nucleus from the cytoplasm through the localisation of miR-221 (yellow triangle) in the cytoplasm and EP300 protein in the nucleus (teal circle).

Note: the simulation images displayed are zoomed in to enhance the details of the simulation functionality and agent localisation; the displayed is not the full size of the cell representation.

(a) 1st iteration of the simulation

(b) 100th iteration of the simulation

(c) 1000th iteration of the simulation

(d) 10000th iteration of the simulation

Figure C.1: Model output at the start of the simulation, at the 100th, 1000th and 10000th iteration. Figure legend: light green triangle - miR-132, yellow triangle - miR-221, blue circle - EP300 mRNA, orange circle - AGO2 mRNA, pink cross - ribosome, white square - promoter/transcription site, teal square - cytoplasmic foci, dark green circle - CREB protein, teal triangle - EP300 protein, red square - AGO2 protein.

C.2 RISC loading – baseline

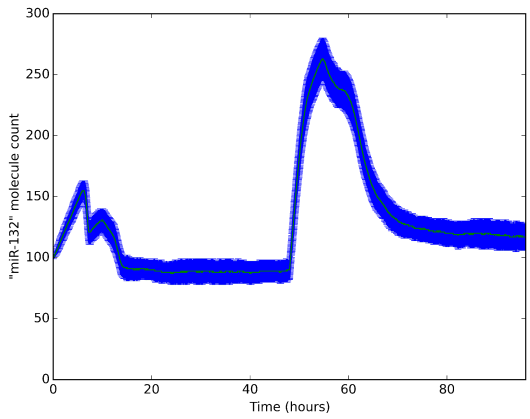

(a) absolute miR-132 count

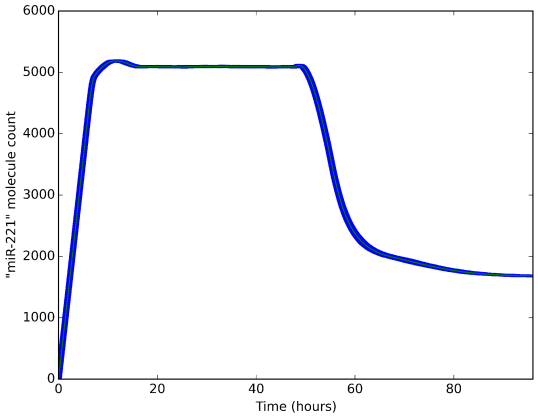

(b) absolute miR-221 count

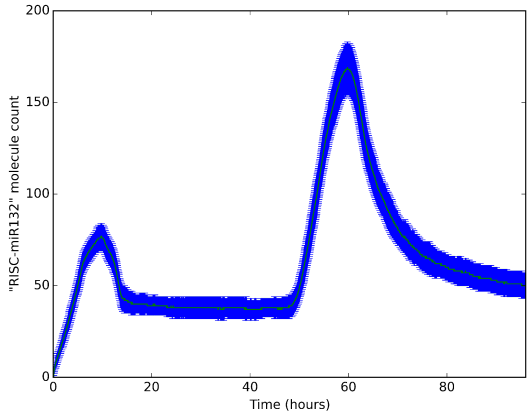

(c) absolute AGO2 bound miR-132 count

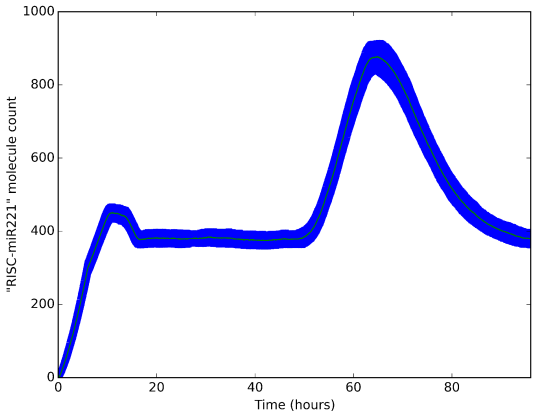

(d) absolute AGO2 bound miR-221 count

Figure C.2: RISC loading distribution during miR-132 mediated silencing of AGO2 and EP300 in PMA-activated LECs, presenting the molecular abundance baseline in LECs and baseline perturbation during PMA treatment. The treatment is initiated at 48 hours after the simulation start time. The mean (*green line*) and standard deviation (*blue area*) is calculated based on 100 replicate simulation runs.

C.3 RISC loading – during enhanced miR-132 expression

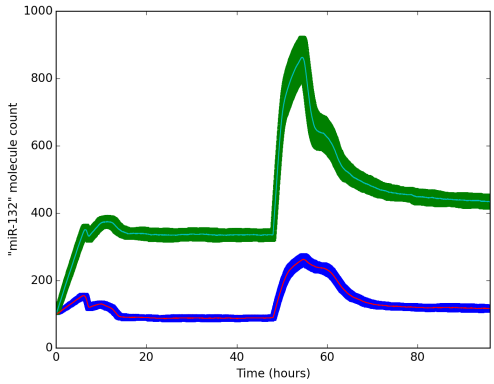

(a) absolute miR-132 count

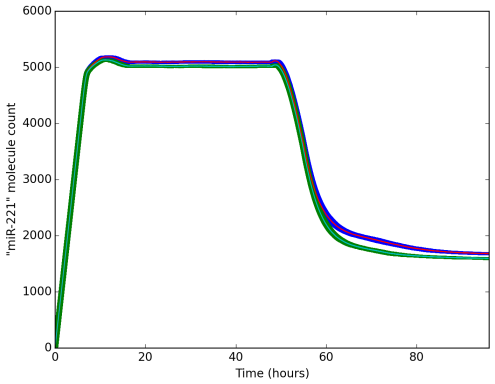

(b) absolute miR-221 count

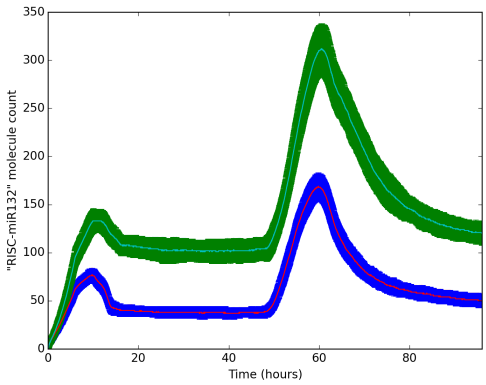

(c) absolute AGO2 bound miR-132 count

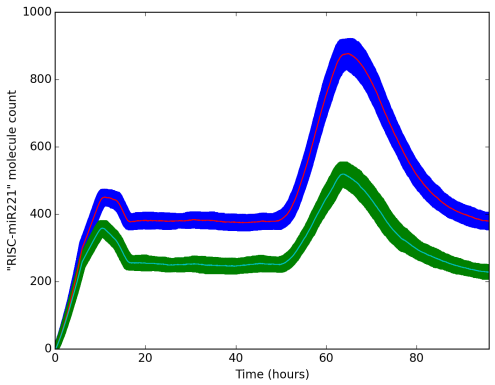

(d) absolute AGO2 bound miR-221 count

Figure C.3: RISC loading distribution during miR-132 mediated silencing of AGO2 and EP300 in PMA-activated LECs with enhanced miR-132 transcription activity (mean - *teal line*, standard deviation - *green area*) compared to baseline PMA activation (mean - *red line*, standard deviation - *blue area*), calculated based on 100 replicate simulation runs. The treatment is initiated at 48 hours after the simulation start time.

C.4 RISC loading – during enhanced miR-132 expression with a non-regulated *AGO2* mRNA

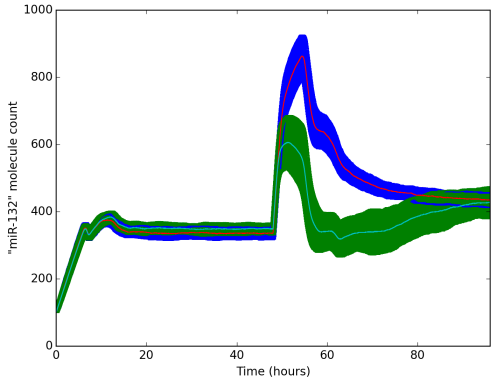

(a) absolute miR-132 count

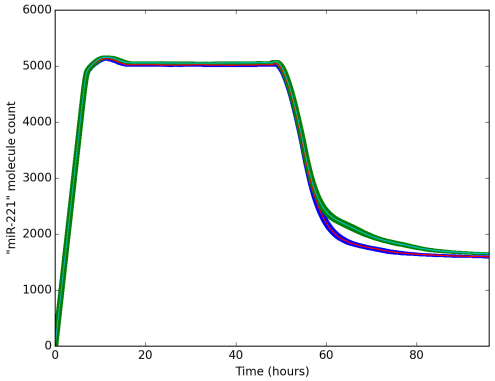

(b) absolute miR-221 count

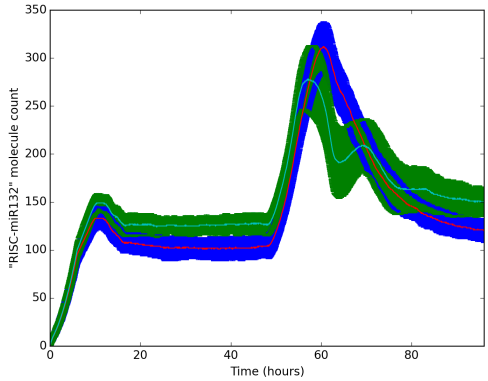

(c) absolute AGO2 bound miR-132 count

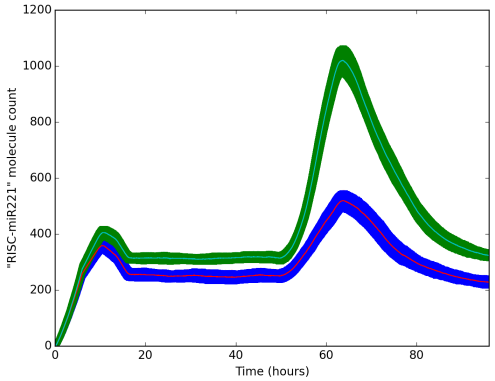

(d) absolute AGO2 bound miR-221 count

Figure C.4: RISC loading distribution during miR-132 mediated silencing of AGO2 and EP300 in PMA-activated LECs with enhanced miR-132 transcription activity where AGO2 can (mean - *red line*, standard deviation - *blue area*) or cannot (mean - *teal line*, standard deviation - *green area*) be targeted by miR-132, calculated based on 100 replicate simulation runs. The treatment is initiated at 48 hours after the simulation start time.

C.5 RISC loading – during enhanced miR-132 expression with a non-regulated *EP300* mRNA

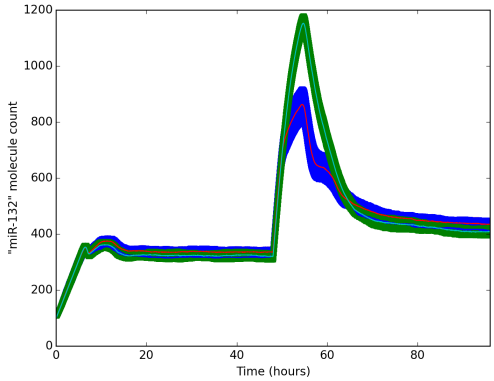

(a) absolute miR-132 count

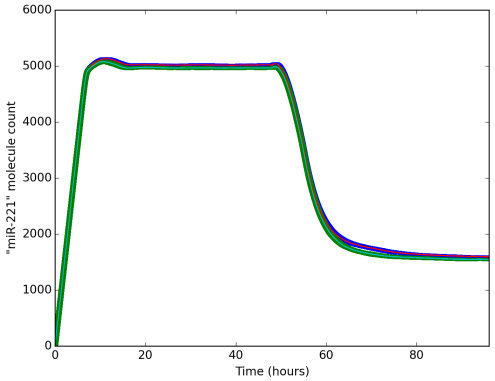

(b) absolute miR-221 count

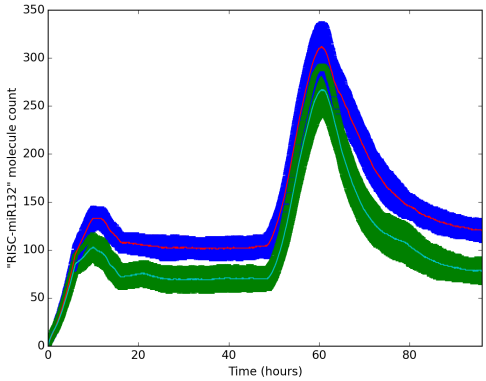

(c) absolute AGO2 bound miR-132 count

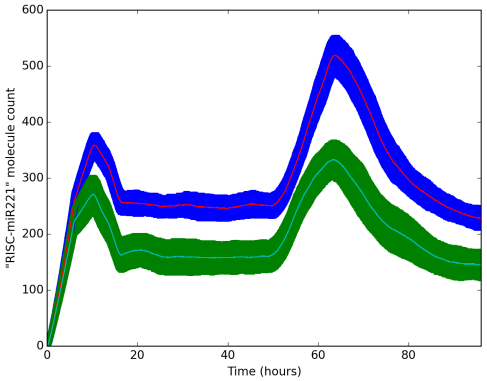

(d) absolute AGO2 bound miR-221 count

Figure C.5: RISC loading distribution during miR-132 mediated silencing of AGO2 and EP300 in PMA-activated LECs with enhanced miR-132 transcription activity where EP300 can (mean - *red line*, standard deviation - *blue area*) or cannot (mean - *teal line*, standard deviation - *green area*) be targeted by miR-132, calculated based on 100 replicate simulation runs. The treatment is initiated at 48 hours after the simulation start time.

C.6 Two-sample Kolmogorov-Smirnov tests

The K-S test was used to compare the probability distributions of the simulations for results presented in Chapter 5. Since the data from the simulation is continuous (recorded over time) and one-dimensional (e.g. a single agent abundance), and the response to PMA treatment creates an effect that propagates over time, K-S statistical test was considered to be an appropriate way to measure the differences between continuous distributions. The comparison was drawn between PMA-activated conditions, starting from the PMA treatment and lasting 48 hours. The cumulative distributions of 100 replicate runs for each measure (e.g. miR-132 abundance) were compared, and the K-S statistic and p-values presented in Tables C.1-C.3. As it is evident, all differences observed were found statistically different from each other (p-value < 0.001), however the K-S statistic reveals how different the two experimental conditions were (ranging from $0...1$, where 1 indicates a large difference and 0 suggests a small difference between the distributions of two conditions). The K-S test was carried out in Python using the *SciPy* package contained *stats* module, *ks_2samp* function[1].

Table C.1: Comparison of the PMA treatment effect between the abundances of different molecules or complexes in the baseline miR-132 model *versus* a model with enhanced miR-132 expression (Figure 5.3).

LEC baseline compared to enhanced baseline		
KS statistic	**p-value**	**Measure**
1.000	0.000	miR-132
0.394	0.000	miR-221
0.303	0.000	AGO2 mRNA
0.629	0.000	EP300 mRNA
0.083	0.000	pCREB
0.578	0.000	EP300 available to pCREB
0.303	0.000	AGO2 for miR-132/221
0.720	0.000	RISC-miR132
0.591	0.000	RISC-miR221

[1] http://docs.scipy.org/doc/scipy-0.14.0/reference/generated/scipy.stats.ks_2samp.html

Table C.2: Comparison of the PMA treatment effect between the abundances of different molecules or complexes in the model with enhanced miR-132 expression where AGO2 can or cannot be regulated by miR-132 (Figure 5.4).

Enhanced baseline with AGO2 compared to AGO2^{-UTR}		
K-S statistic	**p-value**	**Measure**
0.542	0.000	miR-132
0.325	0.000	miR-221
0.472	0.000	AGO2 mRNA
0.534	0.000	EP300 mRNA
0.160	0.000	pCREB
0.517	0.000	EP300 available to pCREB
0.424	0.000	AGO2 for miR-132/221
0.221	0.000	RISC-miR132
0.454	0.000	RISC-miR221

Table C.3: Comparison of the PMA treatment effect between the abundances of different molecules or complexes in the model with enhanced miR-132 expression where EP300 can or cannot be regulated by miR-132 (Figure 5.5).

Enhanced baseline with EP300 compared to EP300^{-UTR}		
KS statistic	**p-value**	**Measure**
0.212	0.000	miR-132
0.334	0.000	miR-221
0.464	0.000	AGO2 mRNA
0.999	0.000	EP300 mRNA
0.070	0.000	pCREB
0.740	0.000	EP300 available to pCREB
0.478	0.000	AGO2 for miR-132/221
0.412	0.000	RISC-miR132
0.505	0.000	RISC-miR221

Abbreviations

ABM agent-based model

AChE Acetylcholinesterase

AGO Argonaute

AMPK1 5'-AMP-activated Protein Kinase Catalytic Subunit α-1

ANG1 Angiopoietin 1

ANG2 Angiopoietin 2

APS ammonium persulfate

ATP adenosine triphosphate

BDNF Brain-Derived Neutrophic Factor

BSA bovine serum albumin

Btg2 B-cell Translocation Gene 2

ceRNA competing endogenous RNA

CoSMoS Complex Systems Modelling and Simulation

CPU central processing unit

CREB cAMP-Response Element Binding protein

DGCR8 DiGeorge Syndrome Critical Region 8

DMEM Dulbecco's Modified Eagle Medium

DMSO dimethyl sulfoxide

EDTA ethylenediaminetetraacetic acid

EGFR Epidermal Growth Factor Receptor

Ep300 E1A-associated Protein p300

ERK Extracellular Signal Regulated Kinase

EXP1 Exportin 1

EXP5 Exportin 5

FCS fetal calf serum

FMRP Fragile X Mental Retardation Protein

FOXO3 Forkhead Box O3

GO Gene Ontology

GTP guanosine triphosphate

GUI Graphical User Interface

HDLEC Human Dermal Lymphatic Endothelial Cell

HFF Human Foreskin Fibroblast

HPRT Hypoxanthine Phosphoribosyltransferase

HSC hematopoietic stem cell

HSP90 Heat Shock Protein 90

IL22 Interleukin 22

IL6 Interleukin 6

Jarid1a Lysine (K)-Specific Demethylase 5A

K-S Kolmogorov-Smirnov

LBK1 Liver Kinase B1

LEC Lymphatic Endothelial Cell

LHC *Latin Hypercube*

LPS lipopolysaccharide

LYVE1 Lymphatic Vessel Endothelial Hyaluronan Receptor

MAPK Mitogen-Activated Protein Kinase

Mecp2 Methyl CpG Binding Protein 2

miRNA microRNA

OAT *one-at-a-time*

ODE Ordinary Differential Equation

p250GAP Rho GTPase Activating Protein 32

PACT Protein Activator of PKR

Paip2 Polyadenylate-binding Protein-Interacting Protein 2

PBS phosphate-buffered saline

PDE Partial Differential Equation

PDPN Podoplanin

Per1 Period Circadian Clock 1

PMA phorbol myristate acetate

PRCC partial rank correlation coefficient

pre-miR precursor miRNA

pri-miR primary miRNA

PROX1 Prospero Homeobox protein 1

PTEN Phosphatase and Tensin Homolog

PVDF polyvinylidene fluoride

qRT-PCR quantitative reverse transcription polymerase chain reaction

RBP RNA-binding protein

RIPA radio-immunoprecipitation assay

RISC RNA-induced silencing complex

RNG Random Number Generator

S.E.M. standard error margin

S6K1 p70 Ribosomal Protein S6 Kinase 1

SCN suprachiasmatic nucleus

SDE Stochastic Differential Equation

SDS sodium dodecyl sulphate

SDS-PAGE SDS-polyacrylamide gel electrophoresis

siRNA small interfering RNA

SIRT1 Silent Mating Type Information Regulation 2 Homolog 1

Sox4 SRY (Sex Determining Region Y)-Box 4

SP1 Specificity Protein 1

SPRED1 Sprouty-Related, EVH1 Domain Containing 1

TIE2 Tyrosine kinase with Ig and EGF homology domains-2

TRBP TAR RNA Binding Protein

TSS transcriptional start site

UML Unified Modeling Language

UTR untranslated region

VEGF Vascular Endothelial Growth Factor

VEGFC Vascular Endothelial Growth Factor C

VEGFR1 Vascular Endothelial Growth Factor Receptor 1

VEGFR3 Vascular Endothelial Growth Factor Receptor 3

YCIL York Computational Immunology Lab

References

E Acerbi, J Decraene, and A Gouaillard. Computational reconstruction of biochemical networks. In *Information Fusion (FUSION), 2012 15th International Conference on*, pages 1134–1141. IEEE, 2012.

Brian D. Adams, Kevin P. Claffey, and Bruce A. White. Argonaute-2 expression is regulated by epidermal growth factor receptor and mitogen-activated protein kinase signaling and correlates with a transformed phenotype in breast cancer cells. *Endocrinology*, 150(1): 14–23, 2009.

Kieran Alden, Jon Timmis, Paul S. Andrews, Henrique Veiga-Fernandes, and Mark C. Coles. Pairing experimentation and computational modeling to understand the role of tissue inducer cells in the development of lymphoid organs. *Frontiers in Immunology*, 3, 2012.

Kieran Alden, Mark Read, Jon Timmis, Paul S. Andrews, Henrique Veiga-Fernandes, and Mark Coles. Spartan: A Comprehensive Tool for Understanding Uncertainty in Simulations of Biological Systems. *PLoS Computational Biology*, 9(2), 2013.

Kari Alitalo. The lymphatic vasculature in disease. *Nature Medicine*, 17(11):1371–1380, 2011.

Yael Altuvia, Pablo Landgraf, Gila Lithwick, Naama Elefant, Sébastien Pfeffer, Alexei Aravin, Michael J. Brownstein, Thomas Tuschl, and Hanah Margalit. Clustering and conservation patterns of human microRNAs. *Nucleic Acids Research*, 33(8):2697–2706, 2005.

Matías Alvarez-Saavedra, Ghadi Antoun, Akiko Yanagiya, Reynaldo Oliva-Hernandez, Daniel Cornejo-Palma, Carolina Perez-Iratxeta, Nahum Sonenberg, and Hai Ying M Cheng. miRNA-132 orchestrates chromatin remodeling and translational control of the circadian clock. *Human Molecular Genetics*, 20(4):731–751, 2011.

Rui Alves, Fernando Antunes, and Armindo Salvador. Tools for kinetic modeling of biochemical networks. *Nature Biotechnology*, 24(6):667–672, 2006.

Gary An, Qi Mi, Joyeeta Dutta-Moscato, and Yoram Vodovotz. Agent-based models in translational systems biology. *Wiley Interdisciplinary Reviews: Systems Biology and Medicine*, 1(2):159–171, 2009.

Sudarshan Anand, Bharat K Majeti, Lisette M Acevedo, Eric A Murphy, Rajesh Mukthavaram, Lea Scheppke, Miller Huang, David J Shields, Jeffrey N Lindquist, Philip E Lapinski, Philip D King, Sara M Weis, and David A Cheresh. MicroRNA-132-mediated loss of p120RasGAP activates the endothelium to facilitate pathological angiogenesis. *Nature Medicine*, 16(8):909–914, 2010.

Paul S. Andrews, Fiona A. C. Polack, and Adam T. Sampson. The CoSMoS Process, Version 0.1: A Process for the Modelling and Simulation of Complex Systems. *ICECCS 2010*, pages 276–285, 2010a.

Paul S. Andrews, Susan Stepney, Tim Hoverd, Fiona A. C. Polack, Adam T. Sampson, and Jon Timmis. CoSMoS process, models, and metamodels. *CoSMoS 2011*, pages 1–14, 2010b.

M Behfar Ardehali and John T Lis. Tracking rates of transcription and splicing in vivo. *Nature Structural & Molecular Biology*, 16(11):1123–1124, 2009.

M Ashburner, C A Ball, J A Blake, D Botstein, H Butler, J M Cherry, A P Davis, K Dolinski, S S Dwight, J T Eppig, M A Harris, D P Hill, L Issel-Tarver, A Kasarskis, S Lewis, J C Matese, J E Richardson, M Ringwald, G M Rubin, and G Sherlock. Gene ontology: tool

for the unification of biology. The Gene Ontology Consortium. *Nature Genetics*, 25(1): 25–29, 2000.

Miriam Ragle Aure, Sandra Jernstrom, Marit Krohn, Hans Kristian Moen Vollan, Eldri U Due, Einar Rodland, Rolf Karesen, Prahlad Ram, Yiling Lu, Gordon B Mills, Kristine Kleivi Sahlberg, Anne-Lise Borresen-Dale, Ole Christian Lingjaerde, and Vessela N Kristensen. Integrated analysis reveals microRNA networks coordinately expressed with key proteins in breast cancer. *Genome Medicine*, 7(1):21, 2015.

Michael J Axtell, Jakub O Westholm, and Eric C Lai. Vive la différence: biogenesis and evolution of microRNAs in plants and animals. *Genome Biology*, 12(4):221, 2011.

Mohammad Azimi, Evgeny Bulat, Karsten Weis, and Mohammad R K Mofrad. An agent-based model for mRNA export through the nuclear pore complex. *Molecular Biology of the Cell*, 25(22):3643–3653, 2014.

Joshua E. Babiarz, J. Graham Ruby, Yangming Wang, David P. Bartel, and Robert Blelloch. Mouse ES cells express endogenous shRNAs, siRNAs, and other microprocessor-independent, dicer-dependent small RNAs. *Genes and Development*, 22(20):2773–2785, 2008.

Daehyun Baek, Judit Villén, Chanseok Shin, Fernando D Camargo, Steven P Gygi, and David P Bartel. The impact of microRNAs on protein output. *Nature*, 455(7209):64–71, 2008.

Suneale Banerji, Jian Ni, Shu Xia Wang, Steven Clasper, Jeffrey Su, Raija Tammi, Margaret Jones, and David G. Jackson. LYVE-1, a new homologue of the CD44 glycoprotein, is a lymph-specific receptor for hyaluronan. *Journal of Cell Biology*, 144(4):789–801, 1999.

David P. Bartel. MicroRNAs: Genomics, Biogenesis, Mechanism, and Function. *Cell*, 116 (2):281–297, 2004.

David P Bartel. MicroRNA Target Recognition and Regulatory Functions. *Cell*, 136(2): 215–233, 2009.

Isabelle Behm-Ansmant, Jan Rehwinkel, Tobias Doerks, Alexander Stark, Peer Bork, and Elisa Izaurralde. mRNA degradation by miRNAs and GW182 requires both CCR4:NOT deadenylase and DCP1:DCP2 decapping complexes. *Genes and Development*, 20(14): 1885–1898, 2006.

Eugene Berezikov, Victor Guryev, José Van De Belt, Erno Wienholds, R. H A Plasterk, and Edwin Cuppen. Phylogenetic shadowing and computational identification of human microRNA genes. *Cell*, 120(1):21–24, 2005.

Emily Bernstein, Sang Yong Kim, Michelle A Carmell, Elizabeth P Murchison, Heather Alcorn, Mamie Z Li, Alea A Mills, Stephen J Elledge, Kathryn V Anderson, and Gregory J Hannon. Dicer is essential for mouse development. *Nature Genetics*, 35(3):215–217, 2003.

Doron Betel, Manda Wilson, Aaron Gabow, Debora S. Marks, and Chris Sander. The microRNA.org resource: Targets and expression. *Nucleic Acids Research*, 36, 2008.

Haruhiko Bito, Karl Deisseroth, and Richard W. Tsien. CREB phosphorylation and dephosphorylation: A Ca2+- and stimulus duration-dependent switch for hippocampal gene expression. *Cell*, 87(7):1203–1214, 1996.

Markus T Bohnsack, Kevin Czaplinski, and Dirk Gorlich. Exportin 5 is a RanGTP-dependent dsRNA-binding protein that mediates nuclear export of pre-miRNAs. *RNA*, 10(2):185–191, 2004.

Glen M Borchert, William Lanier, and Beverly L Davidson. RNA polymerase III transcribes human microRNAs. *Nature Structural & Molecular Biology*, 13(12):1097–1101, 2006.

Carla Bosia, Matteo Osella, Mariama El Baroudi, Davide Corà, and Michele Caselle. Gene

autoregulation via intronic microRNAs and its functions. *BMC Systems Biology*, 6(1): 131, 2012.

Carla Bosia, Andrea Pagnani, and Riccardo Zecchina. Modelling Competing Endogenous RNA Networks. *PLoS ONE*, 8(6), 2013.

Andrew D Bosson, Jesse R Zamudio, and Phillip A Sharp. Endogenous miRNA and target concentrations determine susceptibility to potential ceRNA competition. *Molecular Cell*, 56(3):347–359, 2014.

Joerg E. Braun, Eric Huntzinger, Maria Fauser, and Elisa Izaurralde. GW182 proteins directly recruit cytoplasmic deadenylase complexes to miRNA targets. *Molecular Cell*, 44 (1):120–133, 2011.

S Breiteneder-Geleff, A Soleiman, R Horvat, G Amann, H Kowalski, and D Kerjaschki. Podoplanin–a specific marker for lymphatic endothelium expressed in angiosarcoma. *Verhandlungen der Deutschen Gesellschaft fur Pathologie*, 83:270–275, 1999.

Jung S Byun, Madeline M Wong, Wenwu Cui, Gila Idelman, Quentin Li, Adriana De Siervi, Sven Bilke, Cynthia M Haggerty, Audrey Player, Yong Hong Wang, Michael J Thirman, Joseph J Kaberlein, Constantinos Petrovas, Richard A Koup, Dan Longo, Keiko Ozato, and Kevin Gardner. Dynamic bookmarking of primary response genes by p300 and RNA polymerase II complexes. *Proceedings of the National Academy of Sciences of the United States of America*, 106(46):19286–19291, 2009.

Stephanie Ceman, William T. O'Donnell, Matt Reed, Stephana Patton, Jan Pohl, and Stephen T. Warren. Phosphorylation influences the translation state of FMRP-associated polyribosomes. *Human Molecular Genetics*, 12(24):3295–3305, 2003.

Marcella Cesana, Davide Cacchiarelli, Ivano Legnini, Tiziana Santini, Olga Sthandier, Mauro Chinappi, Anna Tramontano, and Irene Bozzoni. A long noncoding RNA con-

trols muscle differentiation by functioning as a competing endogenous RNA. *Cell*, 147 (2):358–369, 2011.

Anne Cheever and Stephanie Ceman. Phosphorylation of FMRP inhibits association with Dicer. *RNA*, 15(3):362–366, 2009.

Sihem Cheloufi, Camila O Dos Santos, Mark M W Chong, and Gregory J Hannon. A dicer-independent miRNA biogenesis pathway that requires Ago catalysis. *Nature*, 465(7298): 584–589, 2010.

Yun Chen and David H. Gorski. Regulation of angiogenesis through a microRNA (miR-130a) that down-regulates antiangiogenic homeobox genes GAX and HOXA5. *Blood*, 111(3):1217–1226, 2008.

Hai Ying M Cheng, Joseph W. Papp, Olga Varlamova, Heather Dziema, Brandon Russell, John P. Curfman, Takanobu Nakazawa, Kimiko Shimizu, Hitoshi Okamura, Soren Impey, and Karl Obrietan. microRNA Modulation of Circadian-Clock Period and Entrainment. *Neuron*, 54(5):813–829, 2007.

Mark M W Chong, Guoan Zhang, Sihem Cheloufi, Thomas A. Neubert, Gregory J. Hannon, and Dan R. Littman. Canonical and alternate functions of the microRNA biogenesis machinery. *Genes and Development*, 24(17):1951–1960, 2010.

Daniel Cifuentes, Huiling Xue, David W Taylor, Heather Patnode, Yuichiro Mishima, Sihem Cheloufi, Enbo Ma, Shrikant Mane, Gregory J Hannon, Nathan D Lawson, Scot A Wolfe, and Antonio J Giraldez. A novel miRNA processing pathway independent of Dicer requires Argonaute2 catalytic activity. *Science*, 328(5986):1694–1698, 2010.

C Clarke, M Henry, P Doolan, S Kelly, S Aherne, N Sanchez, P Kelly, P Kinsella, L Breen, S F Madden, L Zhang, M Leonard, M Clynes, P Meleady, and N Barron. Integrated miRNA, mRNA and protein expression analysis reveals the role of post-transcriptional regulation in controlling CHO cell growth rate. *BMC Genomics*, 13:656, 2012.

David L. Corcoran, Kusum V. Pandit, Ben Gordon, Arindam Bhattacharjee, Naftali Kaminski, and Panayiotis V. Benos. Features of mammalian microRNA promoters emerge from polymerase II chromatin immunoprecipitation data. *PLoS ONE*, 4(4), 2009.

Céline Cosseau and Christoph Grunau. Native chromatin immunoprecipitation. *Methods in Molecular Biology*, 791:195–212, 2011.

Jacques B de Kok, Rian W Roelofs, Belinda A Giesendorf, Jeroen L Pennings, Erwin T Waas, Ton Feuth, Dorine W Swinkels, and Paul N Span. Normalization of gene expression measurements in tumor tissues: comparison of 13 endogenous control genes. *Laboratory investigation; a journal of technical methods and pathology*, 85(1):154–159, 2005.

Rémy Denzler, Vikram Agarwal, Joanna Stefano, David P. Bartel, and Markus Stoffel. Assessing the ceRNA Hypothesis with Quantitative Measurements of miRNA and Target Abundance. *Molecular Cell*, 54(5):766–776, 2014.

Michael Dews, Asal Homayouni, Duonan Yu, Danielle Murphy, Cinzia Sevignani, Erik Wentzel, Emma E Furth, William M Lee, Greg H Enders, Joshua T Mendell, and Andrei Thomas-Tikhonenko. Augmentation of tumor angiogenesis by a Myc-activated microRNA cluster. *Nature Genetics*, 38(9):1060–1065, 2006.

Sven Diederichs and Daniel A. Haber. Dual Role for Argonautes in MicroRNA Processing and Posttranscriptional Regulation of MicroRNA Expression. *Cell*, 131(6):1097–1108, 2007.

Min Ding, Jiang Li, Yong Yu, Hui Liu, Zi Yan, Jinghan Wang, and Qijun Qian. Integrated analysis of miRNA, gene, and pathway regulatory networks in hepatic cancer stem cells. *Journal of Translational Medicine*, 13:259, 2015.

R Duncan and J W Hershey. Identification and quantitation of levels of protein synthe-

sis initiation factors in crude HeLa cell lysates by two-dimensional polyacrylamide gel electrophoresis. *The Journal of Biological Chemistry*, 258(11):7228–7235, 1983.

Samantha L. Eaton, Sarah L. Roche, Maica Llavero Hurtado, Karla J. Oldknow, Colin Farquharson, Thomas H. Gillingwater, and Thomas M. Wishart. Total Protein Analysis as a Reliable Loading Control for Quantitative Fluorescent Western Blotting. *PLoS ONE*, 8 (8), 2013.

Margaret S. Ebert and Phillip A. Sharp. Roles for MicroRNAs in conferring robustness to biological processes. *Cell*, 149(3):505–524, 2012.

Margaret S Ebert, Joel R Neilson, and Phillip A Sharp. MicroRNA sponges: competitive inhibitors of small RNAs in mammalian cells. *Nature Methods*, 4(9):721–726, 2007.

Faeza Ebrahimi, Vinod Gopalan, Robert Anthony Smith, and Alfred King Yin Lam. MiR-126 in human cancers: Clinical roles and current perspectives. *Experimental and Molecular Pathology*, 96(1):98–107, 2014.

Eclipse Foundation. JVM Monitor, Eclipse IDE plugin. 2012. URL `http://jvmmonitor.org/`.

Dieter Edbauer, Joel R. Neilson, Kelly A. Foster, Chi Fong Wang, Daniel P. Seeburg, Matthew N. Batterton, Tomoko Tada, Bridget M. Dolan, Phillip A. Sharp, and Morgan Sheng. Regulation of Synaptic Structure and Function by FMRP-Associated MicroRNAs miR-125b and miR-132. *Neuron*, 65(3):373–384, 2010.

Stephen W Eichhorn, Huili Guo, Sean E McGeary, Ricard A Rodriguez-Mias, Chanseok Shin, Daehyun Baek, Shu-hao Hsu, Kalpana Ghoshal, Judit Villén, and David P Bartel. mRNA Destabilization Is the Dominant Effect of Mammalian MicroRNAs by the Time Substantial Repression Ensues. *Molecular Cell*, 56(1):104–115, 2014.

Elad Elkayam, Claus D. Kuhn, Ante Tocilj, Astrid D. Haase, Emily M. Greene, Gregory J.

Hannon, and Leemor Joshua-Tor. The structure of human argonaute-2 in complex with miR-20a. *Cell*, 150(1):100–110, 2012.

Ana Eulalio, Isabelle Behm-Ansmant, Daniel Schweizer, and Elisa Izaurralde. P-body formation is a consequence, not the cause, of RNA-mediated gene silencing. *Molecular and Cellular Biology*, 27(11):3970–3981, 2007.

Ana Eulalio, Eric Huntzinger, and Elisa Izaurralde. GW182 interaction with Argonaute is essential for miRNA-mediated translational repression and mRNA decay. *Nature Structural & Molecular Biology*, 15(4):346–353, 2008.

Marc R Fabian and Nahum Sonenberg. The mechanics of miRNA-mediated gene silencing: a look under the hood of miRISC. *Nature Structural & Molecular Biology*, 19(6):586–593, 2012.

Christopher R. Faehnle, Elad Elkayam, Astrid D. Haase, Gregory J. Hannon, and Leemor Joshua-Tor. The Making of a Slicer: Activation of Human Argonaute-1. *Cell Reports*, 3 (6):1901–1909, 2013.

Michael Faller, Daniel Toso, Michio Matsunaga, Ivo Atanasov, Rachel Senturia, Yanqiu Chen, Z Hong Zhou, and Feng Guo. DGCR8 recognizes primary transcripts of microRNAs through highly cooperative binding and formation of higher-order structures. *RNA*, 16(8):1570–1583, 2010.

Stephen Fasciano, Amanda Kaufman, and Rekha C. Patel. Expression of PACT is regulated by Sp1 transcription factor. *Gene*, 388:74–82, 2007.

Jason E. Fish, Massimo M. Santoro, Sarah U. Morton, Sangho Yu, Ru Fang Yeh, Joshua D. Wythe, Kathryn N. Ivey, Benoit G. Bruneau, Didier Y R Stainier, and Deepak Srivastava. miR-126 Regulates Angiogenic Signaling and Vascular Integrity. *Developmental Cell*, 15 (2):272–284, 2008.

Joshua J Forman, Aster Legesse-Miller, and Hilary A Coller. A search for conserved sequences in coding regions reveals that the let-7 microRNA targets Dicer within its coding sequence. *Proceedings of the National Academy of Sciences of the United States of America*, 105(39):14879–14884, 2008.

Andrea Franceschini, Damian Szklarczyk, Sune Frankild, Michael Kuhn, Milan Simonovic, Alexander Roth, Jianyi Lin, Pablo Minguez, Peer Bork, Christian Von Mering, and Lars J. Jensen. STRING v9.1: Protein-protein interaction networks, with increased coverage and integration. *Nucleic Acids Research*, 41, 2013.

Neil D Fredrick, John a Berges, Benjamin S Twining, Daliangelis Nuñez Milland, and Ferdi L Hellweger. Exploring Mechanisms of Intracellular P Heterogeneity in Cultured Phytoplankton using Agent Based Modeling. *Applied and environmental microbiology*, 79(14):4359–68, 2013.

Robin C. Friedman, Kyle Kai How Farh, Christopher B. Burge, and David P. Bartel. Most mammalian mRNAs are conserved targets of microRNAs. *Genome Research*, 19(1):92–105, 2009.

Dimos Gaidatzis, Erik van Nimwegen, Jean Hausser, and Mihaela Zavolan. Inference of miRNA targets using evolutionary conservation and pathway analysis. *BMC Bioinformatics*, 8, 2007.

Vincenzo Alessandro Gennarino, Giovanni D'Angelo, Gopuraja Dharmalingam, Serena Fernandez, Giorgio Russolillo, Remo Sanges, Margherita Mutarelli, Vincenzo Belcastro, Andrea Ballabio, Pasquale Verde, Marco Sardiello, and Sandro Banfi. Identification of microRNA-regulated gene networks by expression analysis of target genes. *Genome Research*, 22(6):1163–1172, 2012.

Derrick Gibbings, Serge Mostowy, Florence Jay, Yannick Schwab, Pascale Cossart, and

Olivier Voinnet. Selective autophagy degrades DICER and AGO2 and regulates miRNA activity. *Nature Cell Biology*, 14(12):1314–21, 2012.

Daniel T. Gillespie. Exact stochastic simulation of coupled chemical reactions. *The Journal of Physical Chemistry*, 81(25):2340–2361, 1977.

Jakub Godlewski, Michal O. Nowicki, Agnieszka Bronisz, Gerard Nuovo, Jeff Palatini, Michael De Lay, James Van Brocklyn, Michael C. Ostrowski, E. Antonio Chiocca, and Sean E. Lawler. MicroRNA-451 Regulates LKB1/AMPK Signaling and Allows Adaptation to Metabolic Stress in Glioma Cells. *Molecular Cell*, 37(5):620–632, 2010.

G A Gonzalez and M R Montminy. Cyclic AMP stimulates somatostatin gene transcription by phosphorylation of CREB at serine 133. *Cell*, 59(4):675–680, 1989.

Pedro Pablo González, Maura Cárdenas, David Camacho, Armando Franyuti, Octavio Rosas, and Jaime Lagúnez-Otero. Cellulat: An agent-based intracellular signalling model. In *BioSystems*, volume 68, pages 171–185, 2003.

Richard I Gregory, Kai-Ping Yan, Govindasamy Amuthan, Thimmaiah Chendrimada, Behzad Doratotaj, Neil Cooch, and Ramin Shiekhattar. The Microprocessor complex mediates the genesis of microRNAs. *Nature*, 432(7014):235–240, 2004.

Isao Hamaguchi, Tohru Morisada, Masaki Azuma, Kyoko Murakami, Madoka Kuramitsu, Takuo Mizukami, Kazuyuki Ohbo, Kazunari Yamaguchi, Yuichi Oike, Daniel J. Dumont, and Toshio Suda. Loss of Tie2 receptor compromises embryonic stem cell-derived endothelial but not hematopoietic cell survival. *Blood*, 107(3):1207–1213, 2006.

Jinju Han, Yoontae Lee, Kyu Hyun Yeom, Young Kook Kim, Hua Jin, and V. Narry Kim. The Drosha-DGCR8 complex in primary microRNA processing. *Genes and Development*, 18(24):3016–3027, 2004.

Jinju Han, Jakob S. Pedersen, S. Chul Kwon, Cassandra D. Belair, Young Kook Kim, Kyu Hyeon Yeom, Woo Young Yang, David Haussler, Robert Blelloch, and V. Narry

Kim. Posttranscriptional Crossregulation between Drosha and DGCR8. *Cell*, 136(1): 75–84, 2009.

S Hasan, P O Hassa, R Imhof, and M O Hottiger. Transcription coactivator p300 binds PCNA and may have a role in DNA repair synthesis. *Nature*, 410(6826):387–391, 2001.

Jean Hausser, Philipp Berninger, Christoph Rodak, Yvonne Jantscher, Stefan Wirth, and Mihaela Zavolan. MirZ: An integrated microRNA expression atlas and target prediction resource. *Nucleic Acids Research*, 37, 2009.

Jon C. Helton. Uncertainty and sensitivity analysis for models of complex systems. *Computational Methods in Transport: Verification and Validation*, 1, 2008.

Inha Heo, Chirlmin Joo, Jun Cho, Minju Ha, Jinju Han, and V. Narry Kim. Lin28 Mediates the Terminal Uridylation of let-7 Precursor MicroRNA. *Molecular Cell*, 32(2):276–284, 2008.

Héctor Herranz and Stephen M. Cohen. MicroRNAs and gene regulatory networks: Managing the impact of noise in biological systems. *Genes and Development*, 24(13):1339–1344, 2010.

Hai Yang Hu, Zheng Yan, Ying Xu, Hao Hu, Corinna Menzel, Yan Hong Zhou, Wei Chen, and Philipp Khaitovich. Sequence features associated with microRNA strand selection in humans and flies. *BMC Genomics*, 10:413, 2009.

Zhong Hua, Qing Lv, Wenbin Ye, Chung Kwun Amy Wong, Guoping Cai, Dayong Gu, Yanhong Ji, Chen Zhao, Jifeng Wang, Burton B. Yang, and Yaou Zhang. Mirna-directed regulation of VEGF and other angiogenic under hypoxia. *PLoS ONE*, 1(1), 2006.

Eric Huntzinger and Elisa Izaurralde. Gene silencing by microRNAs: contributions of translational repression and mRNA decay. *Nature Reviews. Genetics*, 12(2):99–110, 2011.

Soren Impey, Monika Davare, Adam Lasiek, Dale Fortin, Hideaki Ando, Olga Varlamova, Karl Obrietan, Thomas R. Soderling, Richard H. Goodman, and Gary A. Wayman. An activity-induced microRNA controls dendritic spine formation by regulating Rac1-PAK signaling. *Molecular and Cellular Neuroscience*, 43(1):146–156, 2010.

M. M. Janas, B. Wang, A. S. Harris, M. Aguiar, J. M. Shaffer, Y. V. B. K. Subrahmanyam, M. A. Behlke, K. W. Wucherpfennig, S. P. Gygi, E. Gagnon, and C. D. Novina. Alternative RISC assembly: Binding and repression of microRNA-mRNA duplexes by human Ago proteins. *RNA*, 18(11):2041–2055, 2012.

Min Jae Jeong, Eui Jun Kim, Eun Ah Cho, Sang Kyu Ye, Gyeong Hoon Kang, and Yong Sung Juhnn. CAMP signalling decreases p300 protein levels by promoting its ubiquitin/proteasome dependent degradation via Epac and p38 MAPK in lung cancer cells. *FEBS Letters*, 587(9):1373–1378, 2013.

Louise A. Johnson and David G. Jackson. Inflammation-induced secretion of CCL21 in lymphatic endothelium is a key regulator of integrinmediated dendritic cell transmigration. *International Immunology*, 22(10):839–849, 2010.

Minoru Kanehisa, Susumu Goto, Yoko Sato, Masayuki Kawashima, Miho Furumichi, and Mao Tanabe. Data, information, knowledge and principle: Back to metabolism in KEGG. *Nucleic Acids Research*, 42, 2014.

Marika J Karkkainen, Paula Haiko, Kirsi Sainio, Juha Partanen, Jussi Taipale, Tatiana V Petrova, Michael Jeltsch, David G Jackson, Marja Talikka, Heikki Rauvala, Christer Betsholtz, and Kari Alitalo. Vascular endothelial growth factor C is required for sprouting of the first lymphatic vessels from embryonic veins. *Nature Immunology*, 5(1):74–80, 2004.

Lawryn H Kasper, Tomofusa Fukuyama, Michelle A Biesen, Fayçal Boussouar, Caili Tong, Antoine de Pauw, Peter J Murray, Jan M A van Deursen, and Paul K Brindle. Conditional

knockout mice reveal distinct functions for the global transcriptional coactivators CBP and p300 in T-cell development. *Molecular and Cellular Biology*, 26(3):789–809, 2006.

Tomoko Kawamata, Hervé Seitz, and Yukihide Tomari. Structural determinants of miRNAs for RISC loading and slicer-independent unwinding. *Nature Structural & Molecular Biology*, 16(9):953–960, 2009.

Jan Kazenwadel, Michael Z. Michael, and Natasha L. Harvey. Prox1 expression is negatively regulated by miR-181 in endothelial cells. *Blood*, 116(13):2395–2401, 2010.

Nancy Kedersha and Paul Anderson. Mammalian Stress Granules and Processing Bodies. *Methods in Enzymology*, 431:61–81, 2007.

Michael Kertesz, Nicola Iovino, Ulrich Unnerstall, Ulrike Gaul, and Eran Segal. The role of site accessibility in microRNA target recognition. *Nature Genetics*, 39(10):1278–1284, 2007.

Salim Khan, Ravi Makkena, Foster McGeary, Keith Decker, William Gillis, and Carl Schmidt. A multi-agent system for the quantitative simulation of biological networks. In *AAMAS '03: Proceedings of the second international joint conference on Autonomous agents and multiagent systems*, pages 385–392, 2003.

Hiroaki Kitano. Computational systems biology. *Nature*, 420(6912):206–210, 2002.

Armen Der Kiureghian and Ove Ditlevsen. Aleatory or epistemic? Does it matter? *Structural Safety*, 31(2):105–112, 2009.

Ana Kozomara and Sam Griffiths-Jones. MiRBase: Annotating high confidence microRNAs using deep sequencing data. *Nucleic Acids Research*, 42, 2014.

Azra Krek, Dominic Grün, Matthew N Poy, Rachel Wolf, Lauren Rosenberg, Eric J Epstein, Philip MacMenamin, Isabelle da Piedade, Kristin C Gunsalus, Markus Stoffel, and

Nikolaus Rajewsky. Combinatorial microRNA target predictions. *Nature Genetics*, 37 (5):495–500, 2005.

Angelika Kuehbacher, Carmen Urbich, Andreas M. Zeiher, and Stefanie Dimmeler. Role of Dicer and Drosha for endothelial microRNA expression and angiogenesis. *Circulation Research*, 101(1):59–68, 2007.

Daniel H. Lackner, Traude H. Beilharz, Samuel Marguerat, Juan Mata, Stephen Watt, Falk Schubert, Thomas Preiss, and Jürg Bähler. A Network of Multiple Regulatory Layers Shapes Gene Expression in Fission Yeast. *Molecular Cell*, 26(1):145–155, 2007.

D L Lafontaine and D Tollervey. The function and synthesis of ribosomes. *Nature Reviews. Molecular cell biology*, 2(7):514–520, 2001.

Dimitris Lagos, Richard James Vart, Fiona Gratrix, Samantha Jane Westrop, Victoria Emuss, Ping-Pui Wong, Rebecca Robey, Nesrina Imami, Mark Bower, Frances Gotch, and Chris Boshoff. Toll-like receptor 4 mediates innate immunity to Kaposi sarcoma herpesvirus. *Cell Host & Microbe*, 4(5):470–83, 2008.

Dimitris Lagos, Gabriel Pollara, Stephen Henderson, Fiona Gratrix, Martin Fabani, Richard S B Milne, Frances Gotch, and Chris Boshoff. miR-132 regulates antiviral innate immunity through suppression of the p300 transcriptional co-activator. *Nature Cell Biology*, 12 (5):513–9, 2010.

M Lagos-Quintana, R Rauhut, W Lendeckel, and T Tuschl. Identification of novel genes coding for small expressed RNAs. *Science*, 294(5543):853–858, 2001.

N C Lau, L P Lim, E G Weinstein, and D P Bartel. An abundant class of tiny RNAs with probable regulatory roles in Caenorhabditis elegans. *Science*, 294(5543):858–862, 2001.

Carlos le Sage, Remco Nagel, David A Egan, Mariette Schrier, Elly Mesman, Annunziato Mangiola, Corrado Anile, Giulio Maira, Neri Mercatelli, Silvia Anna Ciafrè, Maria Giulia

Farace, and Reuven Agami. Regulation of the p27(Kip1) tumor suppressor by miR-221 and miR-222 promotes cancer cell proliferation. *The EMBO Journal*, 26(15):3699–3708, 2007.

Eun Joo Lee, Myungwon Baek, Yuriy Gusev, Daniel J Brackett, Gerard J Nuovo, and Thomas D Schmittgen. Systematic evaluation of microRNA processing patterns in tissues, cell lines, and tumors. *RNA*, 14(1):35–42, 2008.

H. Y. Lee and J. A. Doudna. TRBP alters human precursor microRNA processing in vitro. *RNA*, 18(11):2012–2019, 2012.

Ho Young Lee, Kaihong Zhou, Alison Marie Smith, Cameron L. Noland, and Jennifer A. Doudna. Differential roles of human Dicer-binding proteins TRBP and PACT in small RNA processing. *Nucleic Acids Research*, 41(13):6568–6576, 2013.

R C Lee and V Ambros. An extensive class of small RNAs in Caenorhabditis elegans. *Science*, 294(5543):862–864, 2001.

R. C. Lee, R. L. Feinbaum, and V. Ambros. The C. elegans heterochronic gene lin-4 encodes small RNAs with antisense complementarity to lin-14. *Cell*, 75(5):843–854, 1993.

Yoontae Lee, Kipyoung Jeon, Jun Tae Lee, Sunyoung Kim, and V. Narry Kim. MicroRNA maturation: Stepwise processing and subcellular localization. *EMBO Journal*, 21(17): 4663–4670, 2002.

Yoontae Lee, Chiyoung Ahn, Jinju Han, Hyounjeong Choi, Jaekwang Kim, Jeongbin Yim, Junho Lee, Patrick Provost, Olof Rå dmark, Sunyoung Kim, and V Narry Kim. The nuclear RNase III Drosha initiates microRNA processing. *Nature*, 425(6956):415–419, 2003.

Yoontae Lee, Minju Kim, Jinju Han, Kyu-Hyun Yeom, Sanghyuk Lee, Sung Hee Baek, and V Narry Kim. MicroRNA genes are transcribed by RNA polymerase II. *The EMBO Journal*, 23(20):4051–4060, 2004.

German Leonov, Kunal Shah, Daniel Yee, Jon Timmis, Tyson V. Sharp, and Dimitris Lagos. Suppression of AGO2 by miR-132 as a determinant of miRNA-mediated silencing in human primary endothelial cells. *Int. J. Biochem. Cell Biol.*, 69:75–84, 2015.

Benjamin P. Lewis, Christopher B. Burge, and David P. Bartel. Conserved seed pairing, often flanked by adenosines, indicates that thousands of human genes are microRNA targets. *Cell*, 120(1):15–20, 2005.

Zhiguang Li, Taichun Qin, Kejian Wang, Michael Hackenberg, Jian Yan, Yuan Gao, Li-Rong Yu, Leming Shi, Zhenqiang Su, and Tao Chen. Integrated microRNA, mRNA, and protein expression profiling reveals microRNA regulatory networks in rat kidney treated with a carcinogenic dose of aristolochic acid. *BMC Genomics*, 16:365, 2015.

Jidong Liu, Michelle A Carmell, Fabiola V Rivas, Carolyn G Marsden, J Michael Thomson, Ji-Joon Song, Scott M Hammond, Leemor Joshua-Tor, and Gregory J Hannon. Argonaute2 is the catalytic engine of mammalian RNAi. *Science*, 305(5689):1437–1441, 2004.

Zuhong Lu, Wei Wang, Dequang Zhou, Xiaolong Shi, Chao Tang, Xueying Xie, Jing Tu, and Qinyu Ge. Global Egr1-miRNAs binding analysis in PMA-induced K562 cells using ChIP-Seq. *Journal of Biomedicine and Biotechnology*, 2010.

Elsebet Lund, Michael D. Sheets, Susanne Blaser Imboden, and James E. Dahlberg. Limiting ago protein restricts RNAi and microRNA biogenesis during early development in Xenopus laevis. *Genes and Development*, 25(11):1121–1131, 2011.

Stephen T Magill, Xiaolu A Cambronne, Bryan W Luikart, Daniel T Lioy, Barbara H Leighton, Gary L Westbrook, Gail Mandel, and Richard H Goodman. microRNA-132 regulates dendritic growth and arborization of newborn neurons in the adult hippocampus. *Proceedings of the National Academy of Sciences of the United States of America*, 107(47):20382–20387, 2010.

P C Maisonpierre, C Suri, P F Jones, S Bartunkova, S J Wiegand, C Radziejewski, D Compton, J McClain, T H Aldrich, N Papadopoulos, T J Daly, S Davis, T N Sato, and G D Yancopoulos. Angiopoietin-2, a natural antagonist for Tie2 that disrupts in vivo angiogenesis. *Science*, 277(5322):55–60, 1997.

Natalia J Martinez and Richard I Gregory. Argonaute2 expression is post-transcriptionally coupled to microRNA abundance. *RNA*, 19(5):605–12, 2013.

Makoto Matsumoto and Takuji Nishimura. Mersenne twister: a 623-dimensionally equidistributed uniform pseudo-random number generator. *ACM Transactions on Modeling and Computer Simulation*, 8(1):3–30, 1998.

B Mayr and M Montminy. Transcriptional regulation by the phosphorylation-dependent factor CREB. *Nature Reviews. Molecular cell biology*, 2(8):599–609, 2001.

Arnav Mehta, Mati Mann, Jimmy L Zhao, Georgi K Marinov, Devdoot Majumdar, Yvette Garcia-Flores, Xiaomi Du, Erdem Erikci, Kamal Chowdhury, and David Baltimore. The microRNA-212/132 cluster regulates B cell development by targeting Sox4. *The Journal of Experimental Medicine*, 2015a.

Arnav Mehta, Jimmy L. Zhao, Nikita Sinha, Georgi K. Marinov, Mati Mann, Monika S. Kowalczyk, Rachel P. Galimidi, Xiaomi Du, Erdem Erikci, Aviv Regev, Kamal Chowdhury, and David Baltimore. The MicroRNA-132 and MicroRNA-212 Cluster Regulates Hematopoietic Stem Cell Maintenance and Survival with Age by Buffering FOXO3 Expression. *Immunity*, 42(6):1021–1032, 2015b.

Gunter Meister. Argonaute proteins: functional insights and emerging roles. *Nature Reviews. Genetics*, 14(7):447–59, 2013.

Gunter Meister, Markus Landthaler, Agnieszka Patkaniowska, Yair Dorsett, Grace Teng, and Thomas Tuschl. Human Argonaute2 mediates RNA cleavage targeted by miRNAs and siRNAs. *Molecular Cell*, 15(2):185–197, 2004.

Fanyin Meng, Roger Henson, Hania Wehbe-Janek, Kalpana Ghoshal, Samson T. Jacob, and Tushar Patel. MicroRNA-21 Regulates Expression of the PTEN Tumor Suppressor Gene in Human Hepatocellular Cancer. *Gastroenterology*, 133(2):647–658, 2007.

Kevin C. Miranda, Tien Huynh, Yvonne Tay, Yen Sin Ang, Wai Leong Tam, Andrew M. Thomson, Bing Lim, and Isidore Rigoutsos. A Pattern-Based Method for the Identification of MicroRNA Binding Sites and Their Corresponding Heteroduplexes. *Cell*, 126(6): 1203–1217, 2006.

N. Molotski and Y. Soen. Differential association of microRNAs with polysomes reflects distinct strengths of interactions with their mRNA targets. *RNA*, 18(9):1612–1623, 2012.

R Montesano and L Orci. Phorbol esters induce angiogenesis in vitro from large-vessel endothelial cells. *Journal of Cellular Physiology*, 130(2):284–291, 1987.

John W J Moore, Daniel Moyo, Lynette Beattie, Paul S Andrews, Jon Timmis, and Paul M Kaye. Functional complexity of the Leishmania granuloma and the potential of in silico modeling. *Frontiers in Immunology*, 4:35, 2013.

Tohru Morisada, Yuichi Oike, Yoshihiro Yamada, Takashi Urano, Masaki Akao, Yoshiaki Kubota, Hiromitsu Maekawa, Yoshishige Kimura, Masako Ohmura, Takeshi Miyamoto, Shiro Nozawa, Gou Young Koh, Kari Alitalo, and Toshio Suda. Angiopoietin-1 promotes LYVE-1-positive lymphatic vessel formation. *Blood*, 105(12):4649–4656, 2005.

Shankar Mukherji, Margaret S Ebert, Grace X Y Zheng, John S Tsang, Phillip A Sharp, and Alexander van Oudenaarden. MicroRNAs can generate thresholds in target gene expression. *Nature Genetics*, 43(9):854–859, 2011.

Elizabeth P Murchison, Janet F Partridge, Oliver H Tam, Sihem Cheloufi, and Gregory J Hannon. Characterization of Dicer-deficient murine embryonic stem cells. *Proceedings of the National Academy of Sciences of the United States of America*, 102(34):12135–12140, 2005.

Md A Nahid, Bing Yao, Paul R Dominguez-Gutierrez, Lakshmyya Kesavalu, Minoru Satoh, and Edward K L Chan. Regulation of TLR2-mediated tolerance and cross-tolerance through IRAK4 modulation by miR-132 and miR-212. *Journal of Immunology*, 190(3): 1250–63, 2013.

Takahisa Nakamura, Ryan C Kunz, Cai Zhang, Taishi Kimura, Celvie L Yuan, Brenna Baccaro, Yuka Namiki, Steven P Gygi, and Gokhan S Hotamisligil. A critical role for PKR complexes with TRBP in Immunometabolic regulation and eIF2alpha phosphorylation in obesity. *Cell Reports*, 11(2):295–307, 2015.

Petr V. Nazarov, Susanne E. Reinsbach, Arnaud Muller, Nathalie Nicot, Demetra Philippidou, Laurent Vallar, and Stephanie Kreis. Interplay of microRNAs, transcription factors and target genes: Linking dynamic expression changes to function. *Nucleic Acids Research*, 41(5):2817–2831, 2013.

Martin A Newman, J Michael Thomson, and Scott M Hammond. Lin-28 interaction with the Let-7 precursor loop mediates regulated microRNA processing. *RNA*, 14(8):1539–1549, 2008.

Stefania Nicoli, Carl Philipp Knyphausen, Lihua J. Zhu, Abirami Lakshmanan, and Nathan D. Lawson. MiR-221 Is Required for Endothelial Tip Cell Behaviors during Vascular Development. *Developmental Cell*, 22(2):418–429, 2012.

Nijiro Nohata, Toyoyuki Hanazawa, Hideki Enokida, and Naohiko Seki. microRNA-1/133a and microRNA-206/133b clusters: Dysregulation and functional roles in human cancers. *Oncotarget*, 3(1):9–21, 2012.

Michael J. North, Nicholson T. Collier, and Jerry R. Vos. Experiences creating three implementations of the repast agent modeling toolkit. *ACM Transactions on Modeling and Computer Simulation*, 16:1–25, 2006.

Michael J North, Nicholson T Collier, Jonathan Ozik, Eric R Tatara, Charles M Macal, Mark Bragen, and Pam Sydelko. Complex adaptive systems modeling with Repast Simphony. *Complex Adaptive Systems Modeling*, 1(1):3, 2013.

D Nyayanit and C. J. Gadgil. Mathematical modeling of combinatorial regulation suggests that apparent positive regulation of targets by miRNA could be an artifact resulting from competition for mRNA. *RNA*, 21(3):307–319, 2015.

Susanna Obad, Camila O dos Santos, Andreas Petri, Markus Heidenblad, Oliver Broom, Cristian Ruse, Cexiong Fu, Morten Lindow, Jan Stenvang, Ellen Marie Straarup, Henrik Frydenlund Hansen, Troels Koch, Darryl Pappin, Gregory J Hannon, and Sakari Kauppinen. Silencing of microRNA families by seed-targeting tiny LNAs. *Nature Genetics*, 43(4):371–378, 2011.

Benedikt Obermayer and Erel Levine. Exploring the miRNA regulatory network using evolutionary correlations. *PLoS Computational Biology*, 10(10), 2014.

Dónal O'Carroll, Ingrid Mecklenbrauker, Partha Pratim Das, Angela Santana, Ulrich Koenig, Anton J. Enright, Eric A. Miska, and Alexander Tarakhovsky. A Slicer-independent role for Argonaute 2 in hematopoiesis and the microRNA pathway. *Genes and Development*, 21(16):1999–2004, 2007.

Chimari Okada, Eiki Yamashita, Soo Jae Lee, Satoshi Shibata, Jun Katahira, Atsushi Nakagawa, Yoshihiro Yoneda, and Tomitake Tsukihara. A high-resolution structure of the pre-microRNA nuclear export machinery. *Science*, 326(5957):1275–1279, 2009.

Katsutomo Okamura, Akira Ishizuka, Haruhiko Siomi, and Mikiko C. Siomi. Distinct roles for Argonaute proteins in small RNA-directed RNA cleavage pathways. *Genes and Development*, 18(14):1655–1666, 2004.

Katsutomo Okamura, Joshua W. Hagen, Hong Duan, David M. Tyler, and Eric C. Lai. The

Mirtron Pathway Generates microRNA-Class Regulatory RNAs in Drosophila. *Cell*, 130 (1):89–100, 2007.

A K Olsson, A Dimberg, J Kreuger, and L Claesson-Welsh. VEGF receptor signalling - in control of vascular function. *Nature Reviews. Molecular cell biology*, 7(5):359–371, 2006.

Hiromitsu Ota, Masayuki Sakurai, Ravi Gupta, Louis Valente, Bjorn Erik Wulff, Kentaro Ariyoshi, Hisashi Iizasa, Ramana V. Davuluri, and Kazuko Nishikura. ADAR1 forms a complex with dicer to promote MicroRNA processing and RNA-induced gene silencing. *Cell*, 153(3):575–589, 2013.

Fatih Ozsolak, Laura L. Poling, Zhengxin Wang, Hui Liu, X. Shirley Liu, Robert G. Roeder, Xinmin Zhang, Jun S. Song, and David E. Fisher. Chromatin structure analyses identify miRNA promoters. *Genes and Development*, 22(22):3172–3183, 2008.

Mei-Ren Pan, Tsung-Ming Chang, Hui-Chiu Chang, Jen-Liang Su, Hsei-Wei Wang, and Wen-Chun Hung. Sumoylation of Prox1 controls its ability to induce VEGFR3 expression and lymphatic phenotypes in endothelial cells. *Journal of Cell Science*, 122:3358–3364, 2009.

Francesco Pappalardo, Ivan Martinez Forero, Marzio Pennisi, Asis Palazon, Ignacio Melero, and Santo Motta. Simb16: Modeling induced immune system response against B16-melanoma. *PLoS ONE*, 6(10), 2011.

Zain Paroo, Xuecheng Ye, She Chen, and Qinghua Liu. Phosphorylation of the Human MicroRNA-Generating Complex Mediates MAPK/Erk Signaling. *Cell*, 139(1):112–122, 2009.

Deena M Leslie Pedrioli, Terhi Karpanen, Vasilios Dabouras, Giorgia Jurisic, Glenn van de Hoek, Jay W Shin, Daniela Marino, Roland E Kälin, Sebastian Leidel, Paolo Cinelli, Stefan Schulte-Merker, André W Brändli, and Michael Detmar. miR-31 functions as

a negative regulator of lymphatic vascular lineage-specific differentiation in vitro and vascular development in vivo. *Molecular and Cellular Biology*, 30(14):3620–3634, 2010.

Michael Petersen and Jesper Wengel. LNA: A versatile tool for therapeutics and genomics. *Trends in Biotechnology*, 21(2):74–81, 2003.

Sebastian Petri, Anne Dueck, Gerhard Lehmann, Nicholas Putz, Sabine Rudel, Elisabeth Kremmer, and Gunter Meister. Increased siRNA duplex stability correlates with reduced off-target and elevated on-target effects. *RNA*, 17(4):737–749, 2011.

Xianghua Piao, Xue Zhang, Ligang Wu, and Joel G Belasco. CCR4-NOT deadenylates mRNA associated with RNA-induced silencing complexes in human cells. *Molecular and Cellular Biology*, 30(6):1486–1494, 2010.

Robert F Place, Long-Cheng Li, Deepa Pookot, Emily J Noonan, and Rajvir Dahiya. MicroRNA-373 induces expression of genes with complementary promoter sequences. *Proceedings of the National Academy of Sciences of the United States of America*, 105 (5):1608–1613, 2008.

Simona Podgrabinska, Pascal Braun, Paula Velasco, Bryan Kloos, Michael S Pepper, and Mihaela Skobe. Molecular characterization of lymphatic endothelial cells. *Proceedings of the National Academy of Sciences of the United States of America*, 99(25):16069–16074, 2002.

Mark Pogson, Rod Smallwood, Eva Qwarnstrom, and Mike Holcombe. Formal agent-based modelling of intracellular chemical interactions. *BioSystems*, 85(1):37–45, 2006.

Laura Poliseno, Andrea Tuccoli, Laura Mariani, Monica Evangelista, Lorenzo Citti, Keith Woods, Alberto Mercatanti, Scott Hammond, and Giuseppe Rainaldi. MicroRNAs modulate the angiogenic properties of HUVECs. *Blood*, 108(9):3068–3071, 2006.

Laura Poliseno, Leonardo Salmena, Jiangwen Zhang, Brett Carver, William J Haveman,

and Pier Paolo Pandolfi. A coding-independent function of gene and pseudogene mRNAs regulates tumour biology. *Nature*, 465(7301):1033–1038, 2010.

Yijun Qi, Ahmet M. Denli, and Gregory J. Hannon. Biochemical specialization within Arabidopsis RNA silencing pathways. *Molecular Cell*, 19(3):421–428, 2005.

Tim A. Rand, Sean Petersen, Fenghe Du, and Xiaodong Wang. Argonaute2 cleaves the anti-guide strand of siRNA during RISC activation. *Cell*, 123(4):621–629, 2005.

Mark Read, Paul S. Andrews, Jon Timmis, and Vipin Kumar. Techniques for grounding agent-based simulations in the real domain: a case study in experimental autoimmune encephalomyelitis. *Mathematical and Computer Modelling of Dynamical Systems*, 18 (1):67–86, 2012.

Mark Read, Magnus Tripp, Hannah Leonova, Louis M Rose, and Jon Timmis. Automated calibration of agent-based immunological simulations. In *Advances in Artificial Life, ECAL*, pages 874–875, 2013.

Mark Norman Read. *Statistical and Modelling Techniques to Build Con dence in the Investigation of Immunology through Agent-Based Simulation*. PhD thesis, University of York, 2011.

Marc Rehmsmeier, Peter Steffen, Matthias Hochsmann, and Robert Giegerich. Fast and effective prediction of microRNA/target duplexes. *RNA*, 10(10):1507–1517, 2004.

Jan Rehwinkel, Isabelle Behm-Ansmant, David Gatfield, and Elisa Izaurralde. A crucial role for GW182 and the DCP1:DCP2 decapping complex in miRNA-mediated gene silencing. *RNA*, 11(11):1640–1647, 2005.

David W Reid and Christopher V Nicchitta. Diversity and selectivity in mRNA translation on the endoplasmic reticulum. *Nature Reviews. Molecular cell biology*, 16(4):221–231, 2015.

George Reid, Rozenn Gallais, and Raphaël Métivier. Marking time: The dynamic role of chromatin and covalent modification in transcription. *International Journal of Biochemistry and Cell Biology*, 41(1):155–163, 2009.

Judit Remenyi, Christopher J Hunter, Christian Cole, Hideaki Ando, Soren Impey, Claire E Monk, Kirsty J Martin, Geoffrey J Barton, Gyorgy Hutvagner, and J Simon C Arthur. Regulation of the miR-212/132 locus by MSK1 and CREB in response to neurotrophins. *The Biochemical Journal*, 428(2):281–291, 2010.

P Reusch, B Barleon, K Weindel, G Martiny-Baron, A Godde, G Siemeister, and D Marme. Identification of a soluble form of the angiopoietin receptor TIE-2 released from endothelial cells and present in human blood. *Angiogenesis*, 4(2):123–131, 2001.

Andrea Ripoli, Alberto Mercatanti, and Giuseppe Rainaldi. An agent-based model of microRNA-mediated gene regulation: simulation and interpretation of observational data, 2009. URL `http://bioinformatics.hsanmartino.it/bits_library/library/00387.pdf`.

Julian C. Roberts, Richard B. Warren, Christopher E M Griffiths, and Kehinde Ross. Expression of microRNA-184 in keratinocytes represses argonaute 2. *Journal of Cellular Physiology*, 228(12):2314–2323, 2013.

J Graham Ruby, Calvin H Jan, and David P Bartel. Intronic microRNA precursors that bypass Drosha processing. *Nature*, 448(7149):83–86, 2007.

Vera M. Ruda, Rohit Chandwani, Alfica Sehgal, Roman L. Bogorad, Akin Akinc, Klaus Charisse, Alexander Tarakhovsky, Tatiana I. Novobrantseva, and Victor Koteliansky. The roles of individual mammalian argonautes in RNA interference in vivo. *PLoS ONE*, 9(7), 2014.

Sabine Rüdel, Yanli Wang, René Lenobel, Roman Körner, He Hsuan Hsiao, Henning

Urlaub, Dinshaw Patel, and Gunter Meister. Phosphorylation of human Argonaute proteins affects small RNA binding. *Nucleic Acids Research*, 39(6):2330–2343, 2011.

Katja N Rybakova, Frank J Bruggeman, Aleksandra Tomaszewska, Martijn J Moné, Carsten Carlberg, and Hans V Westerhoff. Multiplex Eukaryotic Transcription (In)activation: Timing, Bursting and Cycling of a Ratchet Clock Mechanism. *PLoS Computational Biology*, 11(4), 2015.

Céline Sabatel, Ludovic Malvaux, Nicolas Bovy, Christophe Deroanne, Vincent Lambert, Maria Luz Alvarez Gonzalez, Alain Colige, Jean Marie Rakic, Agnès Noël, Joseph A. Martial, and Ingrid Struman. MicroRNA-21 exhibits antiangiogenic function by targeting RhoB expression in endothelial cells. *PLoS ONE*, 6(2), 2011.

På l Sæ trom, Bret S E Heale, Ola Snø ve, Lars Aagaard, Jessica Alluin, and John J. Rossi. Distance constraints between microRNA target sites dictate efficacy and cooperativity. *Nucleic Acids Research*, 35(7):2333–2342, 2007.

Harpreet Kaur Saini, Sam Griffiths-Jones, and Anton James Enright. Genomic analysis of human microRNA transcripts. *Proceedings of the National Academy of Sciences of the United States of America*, 104(45):17719–17724, 2007.

Leonardo Salmena, Laura Poliseno, Yvonne Tay, Lev Kats, and Pier Paolo Pandolfi. A ceRNA hypothesis: The rosetta stone of a hidden RNA language? *Cell*, 146(3):353–358, 2011.

Sara Sánchez-Molina, José Luis Oliva, Susana García-Vargas, Ester Valls, José M Rojas, and Marian A Martínez-Balbás. The histone acetyltransferases CBP/p300 are degraded in NIH 3T3 cells by activation of Ras signalling pathway. *The Biochemical Journal*, 398 (2):215–224, 2006.

Nicole T Schirle and Ian J MacRae. The crystal structure of human Argonaute2. *Science*, 336(6084):1037–40, 2012.

Ulf Schmitz, Xin Lai, Felix Winter, Olaf Wolkenhauer, Julio Vera, and Shailendra K. Gupta. Cooperative gene regulation by microRNA pairs and their identification using a computational workflow. *Nucleic Acids Research*, 42(12):7539–7552, 2014.

Tina A. Schuetz, Stefan Becker, Andreas Mang, Alina Toma, and Thorsten M. Buzug. A computational multiscale model of glioblastoma growth: Regulation of cell migration and proliferation via microRNA-451, LKB1 and AMPK. In *Proceedings of the Annual International Conference of the IEEE Engineering in Medicine and Biology Society, EMBS*, pages 6620–6623, 2012.

Björn Schwanhäusser, Dorothea Busse, Na Li, Gunnar Dittmar, Johannes Schuchhardt, Jana Wolf, Wei Chen, and Matthias Selbach. Global quantification of mammalian gene expression control. *Nature*, 473(7347):337–342, 2011.

Debarka Sengupta and Sanghamitra Bandyopadhyay. Topological patterns in microRNA-gene regulatory network: studies in colorectal and breast cancer. *Molecular BioSystems*, pages 1360–1371, 2013.

Iftach Shaked, Ari Meerson, Yochai Wolf, Ran Avni, David Greenberg, Adi Gilboa-Geffen, and Hermona Soreq. MicroRNA-132 Potentiates Cholinergic Anti-Inflammatory Signaling by Targeting Acetylcholinesterase. *Immunity*, 31(6):965–973, 2009.

Reut Shalgi, Daniel Lieber, Moshe Oren, and Yitzhak Pilpel. Global and local architecture of the mammalian microRNA-transcription factor regulatory network. *PLoS Computational Biology*, 3(7):1291–1304, 2007.

Harprit Singh, Tania M. Hansen, Nisha Patel, and Nicholas P J Brindle. The molecular balance between receptor tyrosine kinases Tie1 and Tie2 is dynamically controlled by VEGF and TNFα and regulates angiopoietin signalling. *PLoS ONE*, 7(1), 2012.

Mikiko C Siomi and Haruhiko Siomi. Characterization of endogenous human Argonautes

and their miRNA partners in RNA silencing. *Nucleic acids symposium series (2004)*, (52):59–60, 2008.

Pascal Y. Smith, Charlotte Delay, Johanne Girard, Marie Amé lie Papon, Emmanuel Planel, Nicolas Sergeant, Luc Buée, and Sébastien S. Hébert. MicroRNA-132 loss is associated with tau exon 10 inclusion in progressive supranuclear palsy. *Human Molecular Genetics*, 20(20):4016–4024, 2011.

Sree N Sreenath, Kwang-Hyun Cho, and Peter Wellstead. Modelling the dynamics of signalling pathways. *Essays in biochemistry*, 45:1–28, 2008.

Lukas Stalder, Wolf Heusermann, Lena Sokol, Dominic Trojer, Joel Wirz, Justin Hean, Anja Fritzsche, Florian Aeschimann, Vera Pfanzagl, Pascal Basselet, Jan Weiler, Martin Hintersteiner, David V Morrissey, and Nicole C Meisner-Kober. The rough endoplasmatic reticulum is a central nucleation site of siRNA-mediated RNA silencing. *The EMBO Journal*, pages 1115–27, 2013.

Alexander Stark, Julius Brennecke, Natascha Bushati, Robert B. Russell, and Stephen M. Cohen. Animal microRNAs confer robustness to gene expression and have a significant impact on 3'UTR evolution. *Cell*, 123(6):1133–1146, 2005.

Jan Stenvang, Andreas Petri, Morten Lindow, Susanna Obad, and Sakari Kauppinen. Inhibition of microRNA function by antimiR oligonucleotides. *Silence*, 3(1):1, 2012.

Hong Su, Melanie I. Trombly, Jian Chen, and Xiaozhong Wang. Essential and overlapping functions for mammalian argonautes in microRNA silencing. *Genes and Development*, 23(3):304–317, 2009.

Konstantin D Taganov, Mark P Boldin, Kuang-Jung Chang, and David Baltimore. NF-kappaB-dependent induction of microRNA miR-146, an inhibitor targeted to signaling proteins of innate immune responses. *Proceedings of the National Academy of Sciences of the United States of America*, 103(33):12481–12486, 2006.

Shinya Takahashi, Kyoko Sakurai, Arisa Ebihara, Hiroaki Kajiho, Kota Saito, Kenji Kontani, Hiroshi Nishina, and Toshiaki Katada. RhoA activation participates in rearrangement of processing bodies and release of nucleated AU-rich mRNAs. *Nucleic Acids Research*, 39(8):3446–3457, 2011.

Xiaoli Tang, Ming Li, Lynne Tucker, and Bharat Ramratnam. Glycogen synthase kinase 3 beta (GSK3) phosphorylates the RNAase III enzyme Drosha at S300 and S302. *PLoS ONE*, 6(6), 2011.

Sudhir G. Tattikota, Thomas Rathjen, Sarah J. McAnulty, Hans Hermann Wessels, Ildem Akerman, Martijn Van De Bunt, Jean Hausser, Jonathan L S Esguerra, Anne Musahl, Amit K. Pandey, Xintian You, Wei Chen, Pedro L. Herrera, Paul R. Johnson, Donal O'Carroll, Lena Eliasson, Mihaela Zavolan, Anna L. Gloyn, Jorge Ferrer, Ruby Shalom-Feuerstein, Daniel Aberdam, and Matthew N. Poy. Argonaute2 mediates compensatory expansion of the pancreatic β cell. *Cell Metabolism*, 19(1):122–134, 2014.

Daniel W. Thomson, Cameron P. Bracken, Jan M. Szubert, and Gregory J. Goodall. On Measuring miRNAs after Transient Transfection of Mimics or Antisense Inhibitors. *PLoS ONE*, 8(1), 2013.

Thomas Thum, Paolo Galuppo, Christian Wolf, Jan Fiedler, Susanne Kneitz, Linda W. Van Laake, Pieter A. Doevendans, Christine L. Mummery, Jürgen Borlak, Axel Haverich, Carina Gross, Stefan Engelhardt, Georg Ertl, and Johann Bauersachs. MicroRNAs in the human heart: A clue to fetal gene reprogramming in heart failure. *Circulation*, 116(3): 258–267, 2007.

Shogo Tokumaru, Motoshi Suzuki, Hideki Yamada, Masato Nagino, and Takashi Takahashi. let-7 regulates Dicer expression and constitutes a negative feedback loop. *Carcinogenesis*, 29(11):2073–2077, 2008.

Linus Torvalds and Junio Hamano. Git. 2005. URL `http://git-scm.com/`.

Akihisa Tsutsumi, Tomoko Kawamata, Natsuko Izumi, Hervé Seitz, and Yukihide Tomari. Recognition of the pre-miRNA structure by Drosophila Dicer-1. *Nature Structural & Molecular Biology*, 18(10):1153–1158, 2011.

Ahmet Ucar, Shashi K. Gupta, Jan Fiedler, Erdem Erikci, Michal Kardasinski, Sandor Batkai, Seema Dangwal, Regalla Kumarswamy, Claudia Bang, Angelika Holzmann, Janet Remke, Massimiliano Caprio, Claudia Jentzsch, Stefan Engelhardt, Sabine Geisendorf, Carolina Glas, Thomas G. Hofmann, Michelle Nessling, Karsten Richter, Mario Schiffer, Lucie Carrier, L. Christian Napp, Johann Bauersachs, Kamal Chowdhury, and Thomas Thum. The miRNA-212/132 family regulates both cardiac hypertrophy and cardiomyocyte autophagy. *Nature Communications*, 3:1078, 2012.

Paul N. Valdmanis, Shuo Gu, Nina Schüermann, Praveen Sethupathy, Dirk Grimm, and Mark A. Kay. Expression determinants of mammalian argonaute proteins in mediating gene silencing. *Nucleic Acids Research*, 40(8):3704–3713, 2012.

Dimitri van Heesch. Generate documentation from source code. 2012. URL `http://www.stack.nl/~dimitri/doxygen/`.

W Vanden Berghe, K De Bosscher, E Boone, S Plaisance, and G Haegeman. The nuclear factor-kappaB engages CBP/p300 and histone acetyltransferase activity for transcriptional activation of the interleukin-6 gene promoter. *Journal of Biological Chemistry*, 274(45):32091–8, 1999.

Andras Vargha and Harold D. Delaney. A Critique and Improvement of the CL Common Language Effect Size Statistics of McGraw and Wong. *Journal of Educational and Behavioral Statistics*, 25(2):101–132, 2000.

Tanja Veikkola, Lotta Jussila, Taija Makinen, Terhi Karpanen, Michael Jeltsch, Tatiana V. Petrova, Hajime Kubo, Gavin Thurston, Donald M. McDonald, Marc G. Achen, Steven A. Stacker, and Kari Alitalo. Signalling via vascular endothelial growth factor receptor-3 is

sufficient for lymphangiogenesis in transgenic mice. *EMBO Journal*, 20(6):1223–1231, 2001.

Ngan Vo, Matthew E Klein, Olga Varlamova, David M Keller, Tadashi Yamamoto, Richard H Goodman, and Soren Impey. A cAMP-response element binding protein-induced microRNA regulates neuronal morphogenesis. *Proceedings of the National Academy of Sciences of the United States of America*, 102(45):16426–16431, 2005.

Anaïs Wanet, Aurélie Tacheny, Thierry Arnould, and Patricia Renard. MiR-212/132 expression and functions: Within and beyond the neuronal compartment. *Nucleic Acids Research*, 40(11):4742–4753, 2012.

L Wang, C L Ho, D Sun, R K Liem, and A Brown. Rapid movement of axonal neurofilaments interrupted by prolonged pauses. *Nature Cell Biology*, 2(3):137–141, 2000.

Shusheng Wang, Arin B. Aurora, Brett A. Johnson, Xiaoxia Qi, John McAnally, Joseph A. Hill, James A. Richardson, Rhonda Bassel-Duby, and Eric N. Olson. The Endothelial-Specific MicroRNA miR-126 Governs Vascular Integrity and Angiogenesis. *Developmental Cell*, 15(2):261–271, 2008.

Ting Wang, Jin Gu, and Yanda Li. Inferring the perturbed microRNA regulatory networks from gene expression data using a network propagation based method. *BMC Bioinformatics*, 15(1):255, 2014.

Yangming Wang, Rostislav Medvid, Collin Melton, Rudolf Jaenisch, and Robert Blelloch. DGCR8 is essential for microRNA biogenesis and silencing of embryonic stem cell self-renewal. *Nature Genetics*, 39(3):380–385, 2007.

Gary A Wayman, Monika Davare, Hideaki Ando, Dale Fortin, Olga Varlamova, Hai-Ying M Cheng, Daniel Marks, Karl Obrietan, Thomas R Soderling, Richard H Goodman, and Soren Impey. An activity-regulated microRNA controls dendritic plasticity by down-

regulating p250GAP. *Proceedings of the National Academy of Sciences of the United States of America*, 105(26):9093–9098, 2008.

Michael Weber, Ana M Sotoca, Peter Kupfer, Reinhard Guthke, and Everardus J van Zoelen. Dynamic modelling of microRNA regulation during mesenchymal stem cell differentiation. *BMC Systems Biology*, 7:124, 2013.

Liang Meng Wee, C. Fabián Flores-Jasso, William E. Salomon, and Phillip D. Zamore. Argonaute divides Its RNA guide into domains with distinct functions and RNA-binding properties. *Cell*, 151(5):1055–1067, 2012.

Lasse Weinmann, Julia Höck, Tomi Ivacevic, Thomas Ohrt, Jörg Mütze, Petra Schwille, Elisabeth Kremmer, Vladimir Benes, Henning Urlaub, and Gunter Meister. Importin 8 Is a Gene Silencing Factor that Targets Argonaute Proteins to Distinct mRNAs. *Cell*, 136 (3):496–507, 2009.

Jeffrey T. Wigle and Guillermo Oliver. Prox1 function is required for the development of the murine lymphatic system. *Cell*, 98(6):769–778, 1999.

Richard Alun Williams. *An Agent-Based Model of the IL-1 Stimulated Nuclear Factor-kappa B Signalling Pathway*. PhD thesis, 2014.

Julia Winter and Sven Diederichs. Argonaute proteins regulate microRNA stability: Increased microRNA abundance by Argonaute proteins is due to microRNA stabilization. *RNA Biology*, 8(6):1149–1157, 2011.

O Wolkenhauer, S N Sreenath, P Wellstead, M Ullah, and K-H Cho. A systems- and signal-oriented approach to intracellular dynamics. *Biochemical Society Transactions*, 33:507–515, 2005.

C. Wu, J. So, B. N. Davis-Dusenbery, H. H. Qi, D. B. Bloch, Y. Shi, G. Lagna, and A. Hata. Hypoxia Potentiates MicroRNA-Mediated Gene Silencing through Posttransla-

tional Modification of Argonaute2. *Molecular and Cellular Biology*, 31(23):4760–4774, 2011.

Mingyi Xie, Mingfeng Li, Anna Vilborg, Nara Lee, Mei Di Shu, Valeria Yartseva, Nenad Šestan, and Joan A. Steitz. Mammalian 5-capped microRNA precursors that generate a single microRNA. *Cell*, 155(7):1568–1580, 2013.

Munekazu Yamakuchi. MicroRNA regulation of SIRT1. *Frontiers in Physiology*, 2012.

Zhong Yao, Julia Petschnigg, Robin Ketteler, and Igor Stagljar. Application guide for omics approaches to cell signaling. *Nature Chemical Biology*, 11(6):387–397, 2015.

Mayuko Yoda, Tomoko Kawamata, Zain Paroo, Xuecheng Ye, Shintaro Iwasaki, Qinghua Liu, and Yukihide Tomari. ATP-dependent human RISC assembly pathways. *Nature Structural & Molecular Biology*, 17(1):17–23, 2010.

Mayuko Yoda, Daniel Cifuentes, Natsuko Izumi, Yuriko Sakaguchi, Tsutomu Suzuki, Antonio J. Giraldez, and Yukihide Tomari. Poly(A)-specific ribonuclease mediates 3'-end trimming of argonaute2-cleaved precursor micrornas. *Cell Reports*, 5(3):715–726, 2013.

Dong Yue, Hui Liu, and Yufei Huang. Survey of Computational Algorithms for MicroRNA Target Prediction. *Current Genomics*, 10(7):478–492, 2009.

Yan Zeng, Heidi Sankala, Xiaoxiao Zhang, and Paul R Graves. Phosphorylation of Argonaute 2 at serine-387 facilitates its localization to processing bodies. *The Biochemical Journal*, 413(3):429–436, 2008.

J Zhang, H Jin, H Liu, S Lv, B Wang, R Wang, M Ding, Y Yang, L Li, S Fu, D Xie, M Wu, W Zhou, and Q Qian. MiRNA-99a directly regulates AGO2 through translational repression in hepatocellular carcinoma. *Oncogenesis*, 3, 2014a.

X Zhang, D T Odom, S H Koo, M D Conkright, G Canettieri, J Best, H Chen, R Jenner, E Herbolsheimer, E Jacobsen, S Kadam, J R Ecker, B Emerson, J B Hogenesch, T Unter-

man, R A Young, and M Montminy. Genome-wide analysis of cAMP-response element binding protein occupancy, phosphorylation, and target gene activation in human tissues. *Proceedings of the National Academy of Sciences of the United States of America*, 102 (12):4459–4464, 2005.

Yanqiong Zhang, Xiaodong Guo, Lu Xiong, Lingxiang Yu, Zhiwei Li, Qiuyan Guo, Zhiyan Li, Boan Li, and Na Lin. Comprehensive analysis of microRNA-regulated protein interaction network reveals the tumor suppressive role of microRNA-149 in human hepatocellular carcinoma via targeting AKT-mTOR pathway. *Molecular Cancer*, 13:253, 2014b.

Dinghai Zheng, Nader Ezzeddine, Chyi Ying A Chen, Wenmiao Zhu, Xiangwei He, and Ann Bin Shyu. Deadenylation is prerequisite for P-body formation and mRNA decay in mammalian cells. *Journal of Cell Biology*, 182(1):89–101, 2008.

Wei Zheng, Harri Nurmi, Sila Appak, Amélie Sabine, Esther Bovay, Emilia A. Korhonen, Fabrizio Orsenigo, Marja Lohela, Gabriela D'Amico, Tanja Holopainen, Ching Ching Leow, Elisabetta Dejana, Tatiana V. Petrova, Hellmut G. Augustin, and Kari Alitalo. Angiopoietin 2 regulates the transformation and integrity of lymphatic endothelial cell junctions. *Genes and Development*, 28(14):1592–1603, 2014.

Ni Zhu, Dongze Zhang, Haoping Xie, Zhe Zhou, Huyan Chen, Tiantian Hu, Yuan Bai, Yuan Shen, Wenjun Yuan, Qing Jing, and Yongwen Qin. Endothelial-specific intron-derived miR-126 is down-regulated in human breast cancer and targets both VEGFA and PIK3R2. *Molecular and Cellular Biochemistry*, 351(1-2):157–164, 2011.

Andrei Zinovyev, Nadya Morozova, Alexander N. Gorban, and Annick Harel-Belan. Mathematical modeling of microRNA-mediated mechanisms of translation repression. *Advances in Experimental Medicine and Biology*, 774:189–224, 2013.